UNIVERSITY OF THESSALY

SCHOOL OF ENGINEERING

DEPARTMENT OF MECHANICAL ENGINEERING

PhD Thesis

DESIGN AND DEVELOPMENT OF A FUEL CELL SYSTEM (PEM TYPE) – WATER ELECTROLYSIS TYPE PEM: PREPARATION AND CHARACTERIZATION OF LOW COST ELECTROCATALYSTS

by

TZORBATZOGLOU E. FOTINI

Submitted in partial fulfillment of the

Requirements for the

Degree of Doctor of Philosophy in the

Department of Mechanical Engineering of the

University of Thessaly

2015

PhD Examination Committee:

Supervisor: Dr. Tsiakaras Panagiotis

                        Professor, Department of Mechanical Engineering,

                        University of Thessaly

Examiner: Dr. Bebelis Symeon

                        Associate Professor, Department of Chemical Engineering,

                        University of Patras

Examiner: Dr. Neophytides Stylianos

                        Research Director, Institute of Chemical Engineering and High Temperature

                        Processes (ICE/HT)

Examiner: Dr. Andritsos Nikolaos

                        Professor, Department of Mechanical Engineering,

                        University of Thessaly

Examiner: Dr. Stamatelos Tassos

                        Professor, Department of Mechanical Engineering,

                        University of Thessaly

Examiner: Dr. Stapountzis Herricos

                        Associate Professor, Department of Mechanical Engineering,

                        University of Thessaly

Examiner: Dr. Stamatis Tassos

                        Associate Professor, Department of Mechanical Engineering,

                        University of Thessaly

Acknowlegments

The PhD research was carried out in the Alternative Energy Conversion Systems Laboratory of the Department of Mechanical engineering. Reached the end of this long and hard journey, I would like to express my gratitude to my thesis supervisor, Professor Tsiakaras Panagiotis for his vision in proposing such an interesting PhD theme. During the present study we made many challenging discussions, with many ups and down moments, leading to a fruitful strategic conduction of the thesis. In all aspects, I am grateful and I feel the necessity to express my gratitude to him. I would also like to thank for their time and their useful advices the members of the examination committee: Prof. Symeon Bebelis and Dr. Stylianos Neophytides (also members of the advisory committee), as well as Prof. Andritsos Nikolaos, Prof. Stamatelos Anastasios, Prof. Stapountzis Erikos and Prof. Stamatis Anastasios.

I am thankful also to Laboratory's Alternative Conversion Systems Research Group for their support and help regarding the completion of my dissertation. More precisely, I would like firstly to thank, Dr. Sotiria Kontou for her support and encouragement. I would like to thank Dr. Antonios Seretis, Efthymia Karampogia, Dr. Nicoletta Sachinidou and Katerina Kourenta for their interesting and rewarding suggestions. Finally, during the thesis I received invaluable help from my colleague and friend Dr. Brouzgou Angeliki, who I am indebted i had the pleasure to work with.

During my PhD study, life would be much more difficult without the support and companionship of good friends that I had Aspasia Chatzipasxali, Annia Kordatou and Tsousi Xara. Finally, I owe the deepest gratitude to my beloved family, for their support and continuous encouragement during my PhD, specially my father, Vangeli, my mother Ntina and as well as to my brother George. Last, but not least, I would like to give the

most special thanks and my endless love to my husband, Nikos, for being incredible supportive of me over all the PhD long and hard journey.

At this part I would like to thank the Research Committee of University of Thessaly in Greece, especially Apostolis Zisis, Kourti Xrysoula and Papaoikonomou Katerina for having a very nice collaboration.

Volos, May 2015

Short curriculum Vitae
(fotinitzo@gmail.com)

Fotini Tzorbatzoglou - _Personal information:_ She was born in Larisa, Greece on 17th June 1984.

Studies: She studied Mechanical Engineering at the Department of Mechanical Engineering of the University of Western Macedonia, Greece, 2008. In 2011 she acquired the Postgraduate Specialization Diploma: "State-of-the-Art Design and Analysis Methods in Industry" in the Energy Systems, Industrial Processes and Pollution-Abatement Technologies Division of the Department of Mechanical Engineering at the University of Thessaly (ME-UTH), Greece. On 2011 she won a scholarship by the European Union (European Social Fund – ESF) and Greek national funds through the Operational Program "Education and Lifelong Learning" of the National Strategic Reference Framework (NSRF) - Research Funding Program: Heracleitus II, to perform her PhD research studies in the Laboratory of Alternative Energy Conversion Systems of the Dept. of ME-UTH and it is expected to defend her PhD on May 2015.

Languages: She fluently speaks and writes English (Certificate of Proficiency in English, from the Michigan University).

Research interests: are focused in the fields of i) solid state electrochemistry, ii) low temperature Fuel Cells iii) Design and development of novel catalytic and electrocatalytic processes.

Professional experience: F. Tzorbatzoglou has two-year experience as Mechanical Engineer in photovoltaic systems and alternative energy conversion systems.

Publications in refereed Journals

- F. Tzorbatzoglou, A. Brouzgou, P. Tsiakaras, *Electrocatalytic activity of Vulcan-XC-72 supported Pd, Rh and PdxRhy toward HOR and ORR,* Applied Catalysis B: Environmental, Volumes 174–175, (2015), 203–211.

- F. Tzorbatzoglou, A. Brouzgou, P. Tsiakaras, *Hydrogen oxidation and Oxygen reduction reactions over Pd_xIr_y electrocatalysts for PEMFC application,* submitted to Applied Catalysis B: Environmental.

- K. Wang, Z. Pan, F. Tzorbatzoglou, Y. Zhang, Y. Wang, P. Tsiakaras and S. Song, *An investigation of WC stability during the preparation of Pt@WC/OMC via a pulse microwave assisted polyol method,* Applied Catalysis B: Environmental, 166, (2015) 224–230.

- X. Yuan, D. Yuan, F. Zeng, W. Zou, F. Tzorbatzoglou, P. Tsiakaras and Y. Wang, *Preparation of graphitic mesoporous carbon for the simultaneous detection of hydroquinone and catechol,* Applied Catalysis B: Environmental, 129, (2013) 367–374.

- A. Stamatis, C.Vinni, D. Bakalis, F. Tzorbatzoglou and P.Tsiakaras, *Exergy Analysis of an Intermediate Temperature Solid Oxide Fuel Cell-Gas Turbine Hybrid System Fed with Ethanol,* Energies 2012, 4268-4287.

Conferences

- *'Production of cheap energy applying very low Pt-loading electrocatalyst (Pd$_{99}$Pt/Vulcan-XC-72) as anode for H$_2$-proton exchange membrane fuel cells'*, **F. Tzorbatzoglou,** A. Brougou and P. Tsiakaras Second International Conference on "Energy, Sustainability and Climate Change" ESCC 2015, Crete, Greece, June 21-27, 2015.

- *'Hydrogen oxidation and oxygen reduction over Pd$_x$Ir$_y$/Vulcan-XC72 binary electrocatalysts: the effect of ratio (Pd:Ir)*, F. Tzorbatzoglou, A. Brouzgou, P. Tsiakaras, Organizing Committee of BIT's 4th Annual World Congress of Advanced Materials-2015 (WCAM-2015), May 27-29, 2015, Chongqing, China.

- *'Pd$_x$Rh$_y$ Bimetallic Electrocatalysts for Hydrogen Oxidation Reaction (HOR)'*, **F. Tzorbatzoglou**, A. Brouzgou, S.Song and P. Tsiakaras, 10th International Green Energy Conference (IGEC-X), May 24-27, 2015, Taichung, Taiwan.

- *A review of the most efficient low-Pt and Pt-free electrocatalysts for hydrogen PEMFCs,* **F. Tzorbatzoglou,** A. Brouzgou, and P. Tsiakaras, Proceedings of EFC2013, Fifth European Fuel Cell Technology & Applications Conference - Piero Lunghi Conference, December 11-13, 2013, Rome, Italy.

- *'Electrocatalysts for fuel cells fed with hydrogen: Current status, challenges and perspectives'*, **F. Tzorbatzoglou** and P. Tsiakaras, 1st Environmental Conference Thessaly September 8-10, 2012, Skiathos, Greece.

- *'Electro-oxidation of ethanol and its intermediate products: a two-step sequence of efficient PtSn@Rh/C synthesis.'*, S. Song, A. Brouzgou, **F. Tzorbatzoglou,** P. Tsiakaras, Proceedings of Conference Grove Fuel Cell 2012, 11-12 April, Germany, Berlin.

- *Low temperature production of hydrogen through ethanol catalytic decomposition over commercial copper chromite*, A. Vinci, A. Brouzgou, K. Papagerides, **F. Tzorbaztoglou**, S. Cavallaro, P. Tsiakaras, Cat4Bio Conference Advances in Catalysis for Biomass Valorization, 2012, 8-11 July, Thessaloniki, Greece.

- *'Direct alcohol fuel cells: Challenges and future trends'*, A. Brouzgou, **F. Tzorbatzoglou,** P. Tsiakaras, Proceedings of the 2011 3rd International Youth Conference on Energetics, IYCE 2011

DESIGN AND DEVELOPMENT OF A FUEL CELL SYSTEM (PEM TYPE) – WATER ELECTROLYSIS TYPE PEM: PREPARATION AND CHARACTERIZATION OF LOW COST ELECTROCATALYSTS

Abstract

In today's world, the demand for clean and sustainable energy sources has become a strong driving force in continuing economic development, and thus as well in the improvement of human living conditions. Proton exchange membrane (PEM) fuel cells, as clean energy-converting devices, have drawn a great deal of attention in recent years due to their high efficiency, high energy density, and low or zero emissions. In these systems, hydrogen is considered as the preferred fuel in virtue of its high activity and environmental benignity. Fuel cell is considered as one of the most promising products of 21st Century, as it can compete, in terms of efficiency, with batteries, internal combustion engines and other conventional power supply technologies. However, the major barrier to the widespread use of fuel cells is their a) high cost and b) low reliability/durability. This high cost of the catalyst is due to the extensively adopted platinum (Pt) based nanomaterials for the desirable PEMFC performance with high activity and high stability. The limited resources of platinum are the major factors in these challenges, increasing the interest of the scientific community towards the exploration of Pt-free electrocatalysts.

The last decade, a severe number of research groups world-widely have focused on the investigation of electrocatalysts with small amount of Pt or without Pt, for both the hydrogen oxidation reaction (HOR) and the oxygen reduction reaction (ORR). With the exception of

Pt, the electrocatalytic activity of palladium (Pd) is one of the highest among the pure metals for both HOR and ORR. This, combined with the fact that the cost of Pd is about the half of Pt, makes it an attractive alternative [20].

In the present Ph.D thesis, literature review was conducted in order to identify the most efficient and studied electrocatalysts for proton exchange membrane fuel cells fed with hydrogen. The first step of design and development of fuel cells is the recognition of the most active electrocatalysts towards anode and cathode reaction. To this purpose, in the present work binary Pd-based electrocatalysts were investigated as anode and cathode electrocatalysts for HOR and ORR, respectively. More precisely, Pd_xRh_y (20 wt%)/ Vulcan XV-72, Pd_xIr_y (20 wt%)/Vulcan XC-72, Pd_xPt_y (20 wt%)/Vulcan XC-72 and PdPt@WC/OMC are studied as anode and cathode materials for PEMFCs.

For the preparation of the examined electrocatalysts a modified-microwave assisted polyol method was used. Preparation method is a very important parameter for catalysts' preparation as it affects their properties (lattice parameter, diameter of nanoparticles, catalysts dispersion on the support). The modified microwave assisted polyol method was chosen because of the following remarkable advantages: i) rapid volumetric heating, ii) higher reaction rate and selectivity, iii) shorter reaction time and iv) higher yield of the product compared to the conventional heating methods. As a result, the microwave heating makes the fast preparation of nanomaterials possible, leading to relative low cost, energy saving and high efficiency for materials production, thus advancing rapidly towards their practical applications. Therefore, the use of microwave heating is more popular in scientific world.

The physicochemical characterization of electrocatalysts was conducted by X-ray Diffraction (XRD) and Transmission Electron Microscopy (TEM). The X-ray Diffraction

(XRD) measurements were carried out with the aid of a D/Max-IIIA (Rigaku Co., Japan) employing Cu Kα (λ = 0.15406 nm) as the radiation source at 40 kV and 40 mA. Catalysts were investigated by TEM using a Philips CM12 microscope (resolution 0.2 nm), provided with high resolution camera, at an accelerating voltage of 120 kV. The electrochemical characterization was carried out with the Cyclic Voltammetry (CV), Rotating Disk Electrode Technique (RDE) and Chronoamperometry techniques (CA). At the end a chapter summarizes the scientific results of the examined electrocatalysts in the framework of the present PhD dissertation. At the same time some outlooks for further continuation of this research are provided.

Thereafter, a PEM made of Nafion 212, with $Pd_{97}Pt_3/C$, $Pd_{98}Pt_2/C$ loading $0.5mgPtcm^{-2}$ as an anode and Pt loading $0.5mgPtcm^{-2}$ as a cathode, was used. The performance of the MEA was evaluated, using serpentine flow channels with total surface area = $5cm^2$ (2.24x2.24) of Fuel Cell Technologies, Inc. company. Polarization studies were conducted at various cell temperatures with humidified hydrogen and oxygen gas reactants. Cyclic voltammetry and rotating disk electrode studies were also carried out to estimate the electrochemical active surface area and to characterize the electrocatalyst for the Hydrogen Oxidation Reaction (HOR) and Oxygen Reduction Reaction (ORR). Impedance measurements were carried out using a Materials M 520 frequency response analyser (AMEL) coupled to 7050 AMEL electrochemical station.

Hydrogen in molecular form can be produced from many different sources and in many different ways. In the second part of this work, we discuss about one of the main sources used for the production of hydrogen. Electrolysis is the reverse of the hydrogen oxidation reaction in a fuel cell. This reaction takes place in a unit called an electrolyzer. Electrolyzers

can be small, appliance-size equipment and well-suited for small-scale distributed hydrogen production. However, electrolyzers are facing the main problem that fuel cells faced with. Their prohibitive cost which comes mainly from the use of noble metals as electrocatalysts, postpones applications in the industry. Many concerns are related to the high costs of catalysts used, based on Ir and Pt black with high metal loading. It is suggested that capital costs could be reduced by reducing the loading and/or substituting the expensive noble materials used for the fabrication of catalyst layers. In this thesis we study the efficiency and the electrocatalytic activity of different PdRh and PdIr nanostructures prepared via a modified pulse-microwave assisted polyol method, in 0.5 mol L^{-1} H_2SO_4 toward hydrogen evolution reaction (HER). The results show that incorporation of Ir and Rh in Pd as a binder in construction of the electrode, improve the electrocatalytic behavior of palladium for proton reduction.

Σχεδιασμός και ανάπτυξη συστήματος κυψελίδας καυσίμου (τύπου pem) – κυψελίδας ηλεκτρόλυσης νερού (τύπου pem): παρασκευή και χαρακτηρισμός νέων ηλεκτροκαταλυτικών υλικών χαμηλού κόστους

Περίληψη

Τα τελευταία χρόνια, η απαίτηση για καθαρές και βιώσιμες πηγές ενέργειας έχει γίνει μια ισχυρή κινητήριος δύναμη για τη συνέχιση της οικονομικής ανάπτυξης καθώς επίσης και για τη βελτίωση των συνθηκών διαβίωσης του ανθρώπου. Για το λόγο αυτό η παγκόσμια ερευνητική κοινότητα έχει στρέψει το ενδιαφέρον της στην ανάπτυξη νέων συστημάτων μετατροπής ενέργειας, όπως είναι οι κυψέλες καυσίμου πολυμερικής μεμβράνης (PEM), δηλαδή μεμβράνες ανταλλαγής πρωτονίων, στοχεύοντας σε υψηλότερες ενεργειακές αποδόσεις και χαμηλές ή μηδενικές εκπομπές καυσίμου. Στις κυψέλες καυσίμου τύπου PEM, το προτιμώμενο καύσιμο θεωρείται το καύσιμο του υδρογόνου, λόγω της υψηλότερης απόδοσης τους (έως 70%), Οι κυψέλες καυσίμου θεωρούνται από τα πιο ελπιδοφόρα συστήματα μετατροπής της ενέργειας του $21^{ου}$ αιώνα, καθώς μπορούν να ανταγωνιστούν, από την άποψη της αποτελεσματικότητας, με τις μπαταρίες, τους κινητήρες εσωτερικής καύσης και τα ηλεκτρικά δίκτυα. Ωστόσο, το μεγάλο μειονέκτημα και ο βασικός λόγος που περιορίζεται η μαζική εμπορευματοποίηση των συστημάτων αυτών είναι το υψηλό τους κόστος. Το υψηλό κόστος οφείλεται κυρίως στην υψηλή τιμή και στα λίγα αποθέματα της πλατίνας (λευκόχρυσος Pt), η οποία μέχρι σήμερα θεωρείται ο αποδοτικότερος και σταθερότερος καταλύτης των κυψελίδων καυσίμου. Έτσι η επιστημονική κοινότητα, καθώς και ο στόχος της παρούσας διδακτορικής διατριβής είναι η ανάπτυξη νέων καταλυτών μικρής (μg_{Pt}) ή μηδενικής περιεκτικότητας σε λευκόχρυσο, επιλύοντας ως έναν βαθμό το πρόβλημα κόστους.

Την τελευταία δεκαετία, ένας σοβαρός αριθμός ερευνητικών ομάδων παγκοσμίως επικεντρώθηκαν στην έρευνα των ηλεκτροκαταλυτών με μικρή ποσότητα Pt ή χωρίς Pt, τόσο για την αντίδραση της οξείδωσης του υδρογόνου (HOR) όσο και για την αντίδραση αναγωγής του οξυγόνου (ORR). Με εξαίρεση την πλατίνα, η ηλεκτροκαταλυτική δραστηριότητα του παλλαδίου (Pd) είναι μια από τις υψηλότερες μεταξύ των καθαρών μετάλλων και για την HOR και την ORR. Αυτό, σε συνδυασμό με το γεγονός ότι το κόστος του παλλαδίου είναι περίπου το ήμισυ του κόστους της πλατίνας, μας το καθιστά μια ελκυστική εναλλακτική λύση.

Στην παρούσα διδακτορική διατριβή, διεξήχθη βιβλιογραφική ανασκόπηση με σκοπό να προσδιοριστούν οι πιο αποτελεσματικοί ηλεκτροκαταλύτες για τις κυψέλες καυσίμου πολυμερικής μεμβράνης τροφοδοσίας υδρογόνου. Το πρώτο βήμα του σχεδιασμού και της ανάπτυξης των κυψελών καυσίμου είναι η αναγνώριση των πιο δραστήριων ηλεκτροκαταλυτών ως προς την αντίδραση της ανόδου και της καθόδου. Για το σκοπό αυτό, στην παρούσα εργασία, διμεταλλικοί ηλεκτροκαταλύτες που έχουν ως βάση το παλλάδιο (Pd-based) κατασκευάστηκαν και εξετάστηκαν ως ανοδικοί και καθοδικοί ηλεκτροκαταλύτες, για HOR και ORR, αντίστοιχα. Πιο συγκεκριμένα, μια σειρά διμεταλλικών καταλυτών Pd_xRh_y/ Vulcan XC-72, Pd_xIr_y / Vulcan XC-72 με ατομική αναλογία (x,y = 3:1, 1:1, 1:3) και PdPt (97:3, 98:2, 99:1) μελετήθηκαν ως ανοδικοί και καθοδικοί καταλύτες για PEMFCs.

Για την παρασκευή των εξεταζόμενων ηλεκτροκαταλυτών χρησιμοποιήθηκε η μέθοδος σύνθεσης πολυόλης με παλμικά μικροκύματα. Η μέθοδος παρασκευής είναι μια πολύ σημαντική παράμετρος για την απόδοση των καταλυτών, καθώς επηρεάζει τις ιδιότητές τους (παράμετρος πλέγμα, διάμετρος των νανοσωματιδίων). Τα αξιοσημείωτα πλεονεκτήματα της

μέθοδου της πολυόλης με τη βοήθεια μικροκυμάτων είναι τα εξής: i) η ταχεία ογκομετρική θέρμανση ii) η υψηλότερη ταχύτητα και εκλεκτικότητα αντίδρασης iii) λιγότερος χρόνος αντίδρασης και ίν) υψηλότερη απόδοση του προϊόντος σε σύγκριση με τις συμβατικές μεθόδους θέρμανσης. Ως αποτέλεσμα, η θέρμανση με μικροκύματα καθιστά γρήγορη την παρασκευή νάνο-υλικών με σχετικά χαμηλό κόστος εξοικονόμηση ενέργειας, με μεγαλύτερη απόδοση προϊόντος και με τη δυνατότητα περισσότερων πρακτικών εφαρμογών. Για τους παραπάνω λόγους η μέθοδος σύνθεσης πολυόλης με τη βοήθεια παλμικών μικροκυμάτων είναι η πιο διαδεδομένη στην επιστημονική κοινότητα.

Οι φυσικοχημικοί χαρακτηρισμοί των παρασκευασθέντων καταλυτών έγιναν με χρήση των τεχνικών της περίθλασης ακτίνων X (XRD) και της ηλεκτρονικής μικροσκοπίας διέλευσης (TEM). Τα φάσματα περίθλασης ακτίνων X ελήφθησαν με χρήση περιθλασίμετρου D/Max-IIIA (Rigaku Co., Japan) εξοπλισμένου με λάμπα Cu και φίλτρο Ni (ώστε να παρέχεται η ακτινοβολία Kα του Cu, λ=1.54056 nm). Οι μικρογραφίες των δειγμάτων με την τεχνική της ηλεκτρονικής μικροσκοπίας διέλευσης (Transmission Electron Microscopy - TEM) ελήφθησαν με ηλεκτρονικό μικροσκόπιο τύπου JEOL JEM-2010 (HR). Οι ηλεκτροχημικές μετρήσεις διεξήχθησαν με τον ηλεκτροχημικό σταθμό AMEL 5000 με την μέθοδο της κυκλικής βολταμετρίας (CV), ηλεκτρόδιο περιστρεφόμενου δίσκου (RDE) και την τεχνική χρονοαμπερομετρίας (CA). Στο τέλος κάθε κεφαλαίου συνοψίζονται τα επιστημονικά αποτελέσματα των εξεταζόμενων ηλεκτροκαταλυτών. Ταυτόχρονα, δίνονται κάποιες προοπτικές για περαιτέρω συνέχιση της έρευνας αυτής.

Για τον ηλεκτροχημικό χαρακτηρισμό των συστοιχιών άνοδος/ηλεκτρολύτης/κάθοδος (membrane electrode assembly, MEA) χρησιμοποιείται κυψέλη καυσίμου τύπου (PEM) (Εικόνα 2Α) με κανάλια ροής "σερπεντίνη" (Εικόνα 2Β) συνολικής επιφάνειας A=5cm^2

(2.24x2.24), της εταιρείας Fuel Cell Technologies, Inc. Το υδρογόνο τροφοδοτείται στην άνοδο και το οξυγόνο στην κάθοδο. Οι ροές της τροφοδοσίας ελέγχονται από ψηφιακά ροόμετρα μάζας (Brooks Instruments). Για λόγους ασφάλειας, αμέσως μετά την έξοδο από τα ροόμετρα έχουν τοποθετηθεί διοδικές βαλβίδες on/off στη ροή του υδρογόνου και του οξυγόνου. Στη συνέχεια οι ροές εισέρχονται στους κορεστές υγρασίας, όπου τα αντιδρώντα αέρια εμπλουτίζονται σε υδρατμούς και οδηγούνται προς την κυψέλη καυσίμου. Τα αέρια αντιδρώντα χρειάζεται να εμπλουτίζονται σε υδρατμούς πριν την είσοδο τους στην κυψέλη καυσίμου έτσι ώστε η μεμβράνη να ενυδατώνεται συνεχώς και να μην επηρεάζεται αρνητικά η αγωγιμότητά της. Το τμήμα των γραμμών τροφοδοσίας από την έξοδο των κορεστών μέχρι την είσοδο της ανόδου και της καθόδου θερμαίνεται. Η θερμοκρασία των συγκεκριμένων γραμμών δεν πρέπει να έχει μεγάλη απόκλιση ($\pm 5^{o}C$) από τη θερμοκρασία της κυψέλης καυσίμου, καθώς μπορεί να προκληθεί συμπύκνωση των υδρατμών στο εσωτερικό της κυψέλης και να παρατηρηθούν φαινόμενα πλημμύρισης (flooding). Οι ηλεκτροχημικές μετρήσεις λαμβάνουν χώρα με τη βοήθεια ηλεκτροχημικού σταθμού (AMEL 7050) και τα δεδομένα καταγράφονται σε υπολογιστή αυτόματα.

Το υδρογόνο μπορεί να παρασκευαστεί με πολλούς και διάφορους τρόπους, όπως για παράδειγμα από την πυρηνική ενέργεια μέσω θερμικής αποσύνθεσης του νερού ή από την ηλιακή ενέργεια μέσω ηλεκτρόλυσης του νερού και έχει προταθεί από την επιστημονική κοινότητα σαν το πιο πιθανό καύσιμο του μέλλοντος λόγω των σημαντικών ιδιοτήτων του σε αντικατάσταση των παραγώγων του πετρελαίου, καυσίμων του σήμερα. Στο δεύτερο μέρος της εργασίας αυτής, συζητούμε για μία από τις κύριες πηγές που χρησιμοποιούνται για την παραγωγή του υδρογόνου. Η ηλεκτρόλυση του νερού είναι η αντίστροφη διαδικασία της αντίδρασης οξείδωσης του υδρογόνου σε ένα κελί καυσίμου. Κατά την ηλεκτρόλυση του

νερού, το νερό διασπάται στα βασικά στοιχεία, υδρογόνο και οξυγόνο, με την παροχή ηλεκτρικού ρεύματος. Η απαιτούμενη ηλεκτρική ενέργεια μπορεί να προέλθει από οποιαδήποτε ανανεώσιμη πηγή ενέργειας. Ένα από τα πλεονεκτήματα αυτής της μεθόδου είναι η υψηλής καθαρότητας υδρογόνο που παράγεται. Επίσης, το παραγόμενο οξυγόνο μπορεί να αξιοποιηθεί για βιομηχανική η άλλη χρήση.

Μια συσκευή ηλεκτρόλυσης μπορεί να είναι μικρή σε μέγεθος και κατάλληλη για μικρής κλίμακας παραγωγή υδρογόνου. Ωστόσο, η μέθοδος της ηλεκτρόλυσης αντιμετωπίζει το βασικό πρόβλημα που αντιμετωπίζουν και οι κυψέλες καυσίμου. Το απαγορευτικό κόστος τους, το οποίο προέρχεται κυρίως από τη χρήση των πολύτιμων μετάλλων, αναβάλλει εφαρμογές στη βιομηχανία. Σε αυτό το κεφάλαιο μελετάται η αποτελεσματικότητα και η καταλυτική δράση ηλεκτροκαταλυτών μηδενικής περιεκτικότητας σε πλατίνα και με βάση το παλλάδιο, για την αντίδραση σχηματισμού υδρογόνου (HER) σε όξινο περιβάλλον.

1. Motivation & Background

The population growth, resource consumption and environmental degradation are the challenges the world faces today. The environment is threatened by the perils of global warming, climate change and energy crises. Energy plays an important role in many aspects of our lives. Energy production and use is interconnected with many other aspects of modern life, such as water consumption, use of goods and services, transportation, economic growth, land use, and population growth. Production and use of energy (most of which comes from fossil fuels) also contributes to climate change, accounting for more than 80% of greenhouse gas emissions. Moreover, the conventional power generation supply, based on fossil fuels, is limited and these fuels are expected to be fully depleted in the next years (40 - 100 years) [1]. Unless some immediate remedial measures are taken, things are only expected to get worse.

An alternative approach considers the use of renewable sources to produce and store the energy needed. Renewable sources such as hydroelectric power [2, 3], biomass [4], solar [5], wind [5], and geothermal energy [6] are now being investigated to produce mainly electricity, but is also being investigated the use of bio-fuels [7-9], such as bio-diesel [9, 10], bio-ethanol [11] or bio-methanol [12]. All these technologies have advantages and disadvantages, depending on the region and on the local peculiarities.

Fuel cell Technology is now going through a decisive phase, where important changes in the innovation process may be expected. Worldwide development efforts of large

companies and huge public support programs document the hope that the use of this technology will lead to the opening of a huge market potential as well as to solutions for transportation and the energy industry. The fuel cell technology is in fact linked to prospects of environmentally friendly drives in road transportation and more ecologically efficient and better performing heat and power supply plants. Fuel cells could power our cars, with hydrogen replacing the petroleum fuel that is used in most vehicles today. Many vehicle manufacturers are actively researching and developing transportation fuel cell technologies [13].

Fuel cells can power almost any portable device or machine that uses batteries. Unlike a typical battery, which eventually goes dead, a fuel cell continues to produce energy as long as fuel and oxidant are supplied. Laptop computers, cellular phones, video recorders, and hearing aids could be powered by portable fuel cells [14-16].

Additionally, they have strong benefits over conventional combustion-based technologies currently used in many power plants and cars. They produce much smaller quantities of greenhouse gases and none of the air pollutants that create smog and cause health problems. If pure hydrogen is used as a fuel, fuel cells emit only heat and water as a byproduct. Hydrogen-powered fuel cells are also far more energy efficient than traditional combustion technologies [17].

Despite the considerable advantages related with the use of fuel cells, they also show serious drawbacks. The major barrier to the widespread use of fuel cells is their high cost when compared with the available technologies and they cannot yet compete economically with more traditional energy technologies. Fuel cells systems are notoriously expensive due to their use of platinum material. Platinum is required for a fuel cell to generate electricity. This material makes up the catalysts that fuel cells use, which power electrochemical processes. Platinum is quite resistant to chemical corrosion and

has shown that it is the best material available for fuel cell catalysts of all kinds. The problem, however, is that platinum is both rare and expensive. The majority of the world's platinum comes from South Africa and access to this resource is not readily available. The expensive nature of platinum translates directly into higher costs when it comes to fuel cell technology.

The reason why platinum is today the most valuable of precious metals is because it is required in so many industrial applications. It is estimated that one-fifth of everything we use either contains platinum or requires platinum in its manufacture [18]. Among all the known modern uses of platinum, most of the annual production is consumed by two dominant categories - catalytic converters and fine jewelry. Together, these two applications consume more than 70% of the world's supply of platinum.

Platinum has been considered as the best catalyst for the electrochemical reactions that take place in the anode compartment of PEMFCs, but accounts for about 50% of the fuel cells cost [19]. To accelerate breakthroughs in PEMFCs' R&D and their sustainable commercialization, great effort has been devoted by a number of research groups world-wide in order to decrease the Platinum (Pt) loading [20].

With the exception of Pt, the electrocatalytic activity of Palladium (Pd) is one of the highest among the Hydrogen PEMFC. This, combined with the fact that the cost of Pd is lower than that of Pt, makes it an attractive alternative. In recent years, Pd-based catalysts have emerged as a potential alternative to Pt-catalysts for PEMFC applications, due to their lower cost, greater abundance and better resistance to CO-poisoning. For example, the replacement of Pt/C by PtPd/C with a 1:1 Pt:Pd atomic ratio, leads to a 35 wt. % of Pt reduction [21]. Nevertheless, critical challenges for Pd-based catalysts still remain in terms of their electrocatalytic activity and stability during hydrogen oxidation reactions [18]. The kinetic of the cathode ORR is relatively slow compared to that of the anode, releasing to a

large overpotential which contributes more in the total cell voltage. The challenge is to carefully replace the platinum loading in order to ensure good performance using non Pt or low Pt loading for catalysts. The first step of design and development of fuel cells is the recognition of the most active electrocatalysts towards anode and cathode reaction [22].

Following this direction, many alloys were studied using mainly Ru as the second metal and a third component such as W [23], Sn [23], Os, Pd [24], Au, Ag, Rh, or W_2C [25] to form binary and ternary alloys respectively. Another effective way to decrease Pt loading is the adoption of high specific surface area supports to enhance both Pt dispersion and utilization coefficient. To this purpose, novel carbon materials with special nano-scale surface structures have been developed, offering some advantages compared to the commonly and widely adopted XC-72R carbon black (Cabot Corp.) such as: higher surface area, higher conductivity, higher stability etc. As a result, through the above attempts the total Pt loading (anode + cathode) in H_2-PEMFCs the last decade has been dramatically reduced [26] and there is still room for further reduction.

The present PhD research, is devoted to the study of different platinum-free (PdRh and PdIr) and quasi zero-platinum (PdPt) nanostructures (prepared via a modified microwave-assisted polyol method) as anode and cathode electrocatalysts for hydrogen oxidation and oxygen reduction reactions. Cyclic voltammetry, rotating disk electrode and electrochemical impedance spectroscopy techniques were adopted to estimate the electrochemical active surface area and to characterize the electrocatalyst. For all measurements, the catalyst total loading was maintained at 11 μg cm^{-2}. Moreover, membrane electrode assemblies were constructed, with ultra low platinum electrocatalysts as anode and cathode, and their performance was measured by the aid of a single hydrogen proton exchange membrane fuel cell (H_2-PEMFC).

2. PhD Thesis Outline

The PhD thesis is consisted of two parts: i) the first and bigger one is devoted to fabrication and investigation of active low cost electrocatalysts towards anode and cathode reaction for Hydrogen PEMFC and ii) the second is devoted to PEM electrolysis, viable hydrogen production solution, by studying the electrochemical behavior of low cost electrocatalysts towards hydrogen evolution reaction (HER).

More precisely, the PhD thesis is classified into the following nine chapters:

Chapter 1: Motivation and Background

Chapter 2: The aim of Chapter 2 is a quick introduction at the basic elements of fuel cells, the main types of fuel cells and a brief discussion about the fuels used in fuel cells. In sequence a quick view of hydrogen production methods, storage methods and hydrogen uses are also discussed. Moreover, a brief historical overview of hydrogen proton exchange membrane fuel cells and the state-of-the-art of low Pt-loading anodes, low Pt-loading cathodes and platinum free electrocatalysts for Hydrogen PEMFC are also discussed.

Chapter 3: The experimental apparatus that were used to carry out the experimental measurements for the physicochemical and electrochemical characterization of the studied electrocatalysts are described in this chapter. At first stage their physicochemical characterization was conducted by the techniques of Transmitting Electrode Microscopy (TEM) and X-Ray Diffraction (XRD). Then, their electrochemical characterization towards hydrogen oxidation reaction (HOR) and oxygen reduction reaction (ORR) was conducted by the Cyclic Voltammetry (CV), Chronoamperometry and Rotating Disk Electrode (RDE) methods. Fuel cell performance was studied and examined by

electrochemical impedance spectroscopy (EIS), cyclic voltammetry (CV) and potentiodynamic (I-V) techniques.

Chapter 4: In this chapter carbon-supported (Vulcan XC-72) Pd, Rh, and PdxRhy (20wt.%, x:y=1:1, 3:1, 1:3) electrocatalysts are prepared according a modified pulse-microwave assisted polyol synthesis method and their hydrogen electrooxidation (HOR) and oxygen reduction (ORR) electrocatalytic activity is measured. The as-prepared electrocatalysts were physicochemically characterized by Transmission Electron Microscopy (TEM) and X-ray diffraction (XRD). Their electrochemical characterization is carried out by the aid of Cyclic Voltammetry (CV), Rotating Disk Electrode (RDE) and Chronoamperometry (CA) techniques.

Chapter 5: In chapter Pd_xIr_y supported on Vulcan XC-72 carbon (with x:y atomic ratios 3:1, 1:1, 1:3) are prepared by a modified microwave-assisted polyol method, physicochemically characterized and electrochemically studied both as anodes for Hydrogen Oxidation Reaction (HOR) and as cathodes for Oxygen Reduction Reaction (ORR) in acid media. The as prepared catalysts are characterized structurally by X-ray diffraction (XRD), morphologically by Transmission Electron Microscopy (TEM), while their electrocatalytic properties are evaluated by cyclic voltammetry (CV) and by rotating disk electrode (RDE).

Chapter 6: The tungsten carbide (WC) stability during the preparation of Pt@WC/OMC (Ordered Mesoporous Carbon) electrocatalysts, via a pulse microwave-assisted polyol method, is investigated by the aid of X-ray diffraction and thermogravimetric method. More precisely, OMC self-supported Tungsten Carbide (WC/OMC) is successfully synthesized by combing the hydrothermal process with a hard template method and its stability is step by step checked during the preparation process of the Pt@WC/OMC electrocatalyst by the pulse microwave-assisted polyol method.

Chapter 7: Very low-platinum electrocatalysts, $Pd_{97}Pt_3$/C, $Pd_{98}Pt_2$/C, $Pd_{99}Pt_1$/C and pure Pd/C are prepared and examined for the hydrogen oxidation (HOR) with the rotating electrode technique and in a single hydrogen proton exchange membrane fuel cell. The electrocatalysts are physicochemically characterized with techniques of X-ray diffraction (XRD) and transmission electron microscopy (TEM). Among the investigated electrocatalysts $Pd_{98}Pt_2$/C presented the highest electrocatalytic activity. Moreover, $Pd_{97}Pt_3$/C and $Pd_{98}Pt_2$/C electrocatalysts are examined as anode electrode in a single hydrogen proton exchange membrane fuel cell. Along with the temperature increased from 30 to 80°C, the power density increases.

Chapter 8: A brief summary of the fundamentals of water electrolysis and the available electrolyzers' technology are presented. Moreover, the fabrication and investigation the electrochemical behavior of cathode catalysts appropriate for medium- temperature proton exchange membrane (PEM) water electrolysis (WE) is shown. The electrochemical characterizations were performed using cyclic voltammetry (CV), linear sweep voltammetry (LSV) and electrochemical impedance spectroscopy (EIS).

Chapter 9: The Conclusions and future perspectives are summarized in this Chapter. A modified microwave assisted polyol method was chosen for the preparation of electrocatalysts, because the following remarkable advantages: i) rapid volumetric heating, ii) higher reaction rate and selectivity, iii) shorter reaction time and iv) higher yield of the product compared. Atomic ratios $PdRh_3$ and PdIr are suggested as anode electrocatalysts in fuel cells, while $PdRh_3$ and Pd_3Ir as cathode electrodes as they present the optimum electrocatalytic activity.

References

[1]   S. Shafiee, E. Topal. Energy Policy 37 (2009) 181-189.

[2]   C.P. Barros. Energy Economics 30 (2008) 59-75.

[3]   F.C. Menz. Energy Policy 33 (2005) 2398-2410.

[4]   A.L. Cowie, W. David Gardner. Biomass and Bioenergy 31 (2007) 601-607.

[5]   Varun, R. Prakash, I.K. Bhat. Renewable and Sustainable Energy Reviews 13 (2009) 2716-2721.

[6]   D.L. Gallup. Geothermics 38 (2009) 326-334.

[7]   A. Demirbas. Energy Conversion and Management 50 (2009) 2239-2249.

[8]   A. Murugesan, C. Umarani, R. Subramanian, N. Nedunchezhian. Renewable and Sustainable Energy Reviews 13 (2009) 653-662.

[9]   D. Subramaniam, A. Murugesan, A. Avinash, A. Kumaravel. Renewable and Sustainable Energy Reviews 22 (2013) 361-370.

[10]   M. Balat, H. Balat. Applied Energy 87 (2010) 1815-1835.

[11]   M. Balat, H. Balat. Applied Energy 86 (2009) 2273-2282.

[12]   K.A. Vogt, D.J. Vogt, T. Patel-Weynand, R. Upadhye, D. Edlund, R.L. Edmonds, J.C. Gordon, A.S. Suntana, R. Sigurdardottir, M. Miller, P.A. Roads, M.G. Andreu. Renewable Energy 34 (2009) 233-241.

[13]   K.R. Cooper, V. Ramani, J.M. Fenton, H.R. Kunz, Experimental Methods and Data Analysis for Polymer Electrolyte Fuel Cells, Scribner Associates, Southern Pines, N.C., 2005.

[14]   J. Ramírez-Salgado, M.A. Domínguez-Aguilar. Journal of Power Sources 186 (2009) 455-463.

[15]   P. Agnolucci. International Journal of Hydrogen Energy 32 (2007) 4319-4328.

[16]   C.A. Cottrell, S.E. Grasman, M. Thomas, K.B. Martin, J.W. Sheffield. International Journal of Hydrogen Energy 36 (2011) 7969-7975.

[17]   C. Song. Catalysis Today 77 (2002) 17-49.

[18]   Non-Noble Metal Fuel Cell catalysts, in: Z. Chen, J.-P. Dodelet, J. Zhang (Eds.), © 2014 Wiley-VCH GmbH & Co, 2014.

[19]   H.A. Gasteiger, S.S. Kocha, B. Sompalli, F.T. Wagner. Applied Catalysis B: Environmental 56 (2005) 9-35.

[20]   Platinum Today Available from: , http://www.platinum.matthey.com/prices/price-charts.

[21]   F. Alcaide, G. Álvarez, P.L. Cabot, O. Miguel, A. Querejeta. International Journal of Hydrogen Energy 35 (2010) 11634-11641.

[22]   A. Brouzgou, S.Q. Song, P. Tsiakaras. Applied Catalysis B: Environmental 127 (2012) 371-388.

[23]   M. Götz, H. Wendt. Electrochimica Acta 43 (1998) 3637-3644.

[24]   C. He, H.R. Kunz, J.M. Fenton. Journal of The Electrochemical Society 150 (2003) A1017-A1024.

[25]   R. Venkataraman, H.R. Kunz, J.M. Fenton. Journal of The Electrochemical Society 150 (2003) A278-A284.

[26]   Y. Wang, K.S. Chen, J. Mishler, S.C. Cho, X.C. Adroher. Applied Energy 88 (2011) 981-1007.

Hydrogen Fuel Cell systems – Theoretical background

Abstract

The aim of Chapter 2 is to provide a quick introduction to the basic elements of fuel cells, and a quick view to their historical background and their applications. In these systems, hydrogen is considered as the preferred fuel in virtue of its high activity and environmental benignity. The expense of rare metals such as platinum in a polymer electrolyte membrane fuel cell (PEMFC) is one of the most important barriers to the commercialization of fuel cells. The cost target of ~30 \$/kW (current Internal Combustion Engine's cost) that has been set for 2015 and can be met only if the maximum mass specific power density (max-MSPD) will be reduced to less than 200 mg of Pt_{total} per kW at cell voltages higher than 0.65 V (U.S. Department of Energy, DOE).

Contents

List of Figures

List of Tables

2.1   Introduction

Global warming occurs when gases like carbon dioxide and methane stay trapped in the earth's atmosphere. This carbon overload is caused mainly when we burn fossil fuels like coal, oil and gas or cut down and burn forests. There are many heat-trapping gases (from methane to water vapor), but CO_2 puts us at the greatest risk of irreversible changes if it continues to accumulate unabated in the atmosphere.

These gases are known as 'greenhouse gases' because of their capacity to retain heat and this effect is known as the greenhouse effect [1]. Originally, it was this effect that made the earth a habitable place or it would have been too cold to live in. However, retention of excess heat or the 'enhanced greenhouse effect' is a serious threat to the planet as it leads to an increase in global temperature which in turn is the cause of global climate change. Land degradation, air and water pollution, sea-level rise, flood of coastal areas and loss of biodiversity are only a few examples of the consequences of climate change.

It is now widely accepted that if are not taken concerted efforts to reduce greenhouse gas emissions (GHGs), it is possible that the levels of GHGs will triple by the year 2100. Resolving the problem of climate change requires multiple, long-term strategies that will demand enormous sustained effort, engaging the cooperation of both developed and developing countries. Currently, developed countries account for the larger share of greenhouse gas emissions, but developing country emissions continue to rise steadily. By the year 2025 emissions from developing countries are expected to represent 50% of the global total. This calls for immediate action globally.

The economic development of modern societies is crucially dependent on energy. Energy is vital for sustainable development. It is used to generate electricity for a variety of needs, among which are domestic needs, transport needs and industrial needs. The methods of production, supply and consumption of energy are key issues in sustainable

development because they strongly affect the local and global environment. However, the current methods of energy production are primarily by the use of fossil fuels. These methods of production are not sustainable in the long run and therefore do not contribute to sustainable development.

In the past, fossil energy sources could be used to solve world energy problems. However, fossil fuels cannot continue indefinitely as the principal energy sources due to the rapid increase of world energy demand and energy consumption. Fossil and nuclear fuel reserves are becoming increasingly limited and the world's energy future will have to include several renewable alternatives to these failing resources. As a consequence, investigations of alternative energy strategies have recently become important, particularly for future world stability. The most important property of alternative energy sources is their environmental compatibility. In line with this characteristic, hydrogen likely will become one of the most attractive energy carriers in the near future [2]. Much research, including experimental and theoretical studies, has recently been carried out on hydrogen energy [3].

Providing safe, environmentally friendly, and reliable energy supplies is essential for having a sustainable and high quality life, but they are subjected to social, political, environmental and economic challenges [4]. Fuel cells technology is seen as a viable clean air alternative to all applications of internal combustion engine and other conventional power supply technologies. In terms of greenhouse gas emissions, fuel cells offer a significant improvement over internal combustion engines. In addition, the future demand for portable electric power supplies is likely to exceed the capability of current battery technology [5]. Fuel cells can operate on hydrogen or a variety of gaseous and liquid hydrocarbons fuels.

2.2   Fuel Cells

Hydrogen is the most common fuel used in fuel cells and is also the least harmful to the environment. Fuel cells are electrical generation devices that utilize a chemical reaction to unleash a fuel's latent energy. They are clean and efficient energy sources for transportation, stationary, and distributed power.

In a typical fuel cell, gaseous fuels are fed continuously to the anode (negative electrode) compartment and an oxidant (i.e., oxygen from air) is fed continuously to the cathode (positive electrode) compartment; the electrochemical reactions take place at the electrodes to produce an electric current. The fuel processor is a critical component of a fuel cell power system and must be able to provide a clean H_2 or H_2-rich synthesis gas to the fuel cell stack for long term operation. In spite of the increasing technical and commercial importance of fuel cells, there are few books in which fuel processing technology is treated comprehensively. The majority of books over the years about fuel cells address fuel processing technologies only briefly; e.g., in a single section in a chapter.

A fuel cell, although having components and characteristics similar to those of a typical battery, differs in several respects. The battery is an energy storage device. The maximum energy available is determined by the amount of chemical reactant stored within the battery itself. The battery will cease to produce electrical energy when the chemical reactants are consumed (i.e., discharged). In a secondary battery, the reactants are regenerated by recharging, which involves putting energy into the battery from an external source. The fuel cell, on the other hand, is an energy conversion device that theoretically has the capability of producing electrical energy for as long as the fuel and oxidant are supplied to the electrodes. Both convert chemical energy directly into electricity. The difference is that in a battery the chemical energy has to be stored beforehand, while fuel cells only operate when it is supplied from external sources and

the energy produces continuously as the fuel is supplied to the anode. A fuel cell consists of two electrodes sandwiched around an electrolyte. Oxygen passes over one electrode and hydrogen over the other, generating electricity, water and heat.

The first developed fuel cells were alkaline. The principle of operation of the hydrogen-oxygen alkaline fuel cell is simply a reversal of the process of the electrolysis of water.

Principle of H$_2$-O$_2$ Fuel Cell (1969):

Hydrogen Electrode (anode reaction):	$2\,H_2 <=> 4\,H^+ + 4\,e^-$	**(2.1)**
	$4H^+ + 4OH^- <=> 4H_2O$	**(2.2)**
Oxygen electrode (cathode reaction):	$O_2 + 2H_2O + 4e^- <=> 4OH^-$	**(2.3)**
Overall Cell Reaction:	$2\,H_2 + O_2 <=> 2\,H_2O$	**(2.4)**

An oxygen molecule is adsorbed on the cathode's surface, where it picks up four electrons and combines with two of the water molecules present in the electrolyte, forming four hydroxyl ions. Two hydrogen molecules are adsorbed on the anode and are contemporaneously oxidized to hydrogen ions, which ultimately combine with the hydroxyl ions producing water and four electrons. If the process were perfectly reversible in the thermodynamic sense, the fuel cell would generate a voltage just equal to the required for the electrolysis, 1.23 V [6].

Since the fuel cell technology has been evolved and solid membranes replaced liquid-electrolytes the operation of hydrogen-oxygen fuel cell has been simplified according to the following reactions:

Principle of H$_2$-O$_2$ Fuel Cell (today):

Hydrogen Electrode (anode reaction):	$H_2 <=> 2H^+ + 2e^-$	**(2.5)**
Oxygen electrode (cathode reaction):	$1/2O_2 + 2H^+ + 2e^- <=> H_2O$	**(2.6)**
Overall Cell Reaction:	$H_2 + 1/2O_2 <=> H_2O$	**(2.7)**

Hydrogen gas is fed to the anode where it adsorbs onto the catalyst surface and oxygen from the air enters the fuel cell through the cathode. With the aid of a catalyst, the

hydrogen molecule splits into two protons and electrons, which take separate paths to the cathode. The proton passes through the electrolyte membrane and the electrons create a current that is utilized before it returns to the cathode. At the cathode, the electrons are reunited with the hydrogen and oxygen to form water. A schematic representation of a fuel cell with the reactant/product gases and the ion conduction flow directions through the cell is shown in Figure 2.1.
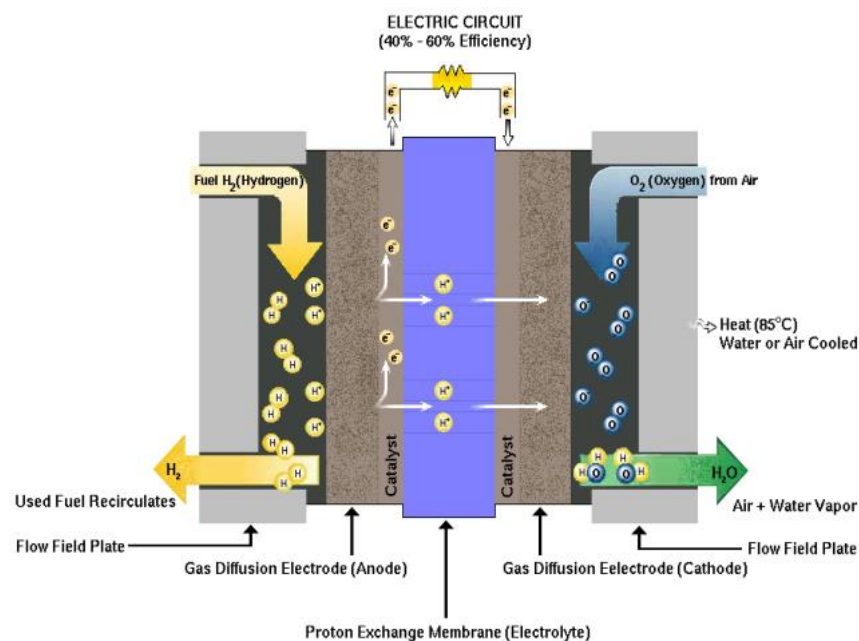

Figure 2.1: Schematic design of a proton exchange membrane fuel cell using hydrogen as fuel.

2.2.1 Different Types of Fuel Cells

Just like there are different types of internal combustion engines, there are also different types of fuel cells - choosing the most suitable fuel cell depends on the application. Designers and engineers need to consider many factors including; the operating temperature, the fuel type, the electrical efficiency, the amount of vibration, physical shock loading and of course, any size constraints.

Fuel cells can be grouped into high temperature and low temperature types. Low temperature fuel cells require a relatively pure supply of hydrogen as a fuel. This often

means that a fuel processor is required to convert or 'reform' the primary fuel (such as natural gas) into pure hydrogen. This process consumes additional energy and requires specialized equipment. High temperature fuel cells do not need this additional process because they can 'internally reform' the fuel at elevated temperatures, meaning it is not necessary to invest money in hydrogen infrastructure.

Different types of fuel cells are categorized by the type of electrolyte. Within each fuel cell type different companies are using different designs to tailor a fuel cell's performance for a given application. The main groups of fuel cells are listed below [7]:

- **Polymer Electrolyte Fuel Cell (PEFC) or Proton Exchange Membrane Fuel Cell (PEMFC):** Here, the electrolyte is a polymer ion exchange membrane that is very good at conducting protons often combined with an expensive platinum catalyst. These fuel cells are a good option for automotive and portable applications as they are best suited for fast start up and shut down situations.

- **Phosphoric Acid Fuel Cells (PAFCs):** In this fuel cell, concentrated phosphoric acid is used as the electrolyte. The design and power outputs make them suitable for buses and large stationary applications.

- **Alkaline Fuel Cells (AFCs):** The electrolyte is essentially a potassium hydroxide solution. These fuel cells are often used for expensive mission critical applications such as the USA space programs.

- **Molten Carbonate Fuel Cells (MOFCs):** These highly specialized fuel cells use a combination of high temperature alkali carbonates (sodium or potassium) as an electrolyte and can use a wide range of fuel types. MCFC are best suited to large stationary power applications.

- **Solid Oxide Fuel Cells (SOFCs):** With SOFCs, the electrolyte is a solid non-porous ceramic based metal oxide often Yttria doped Zirconia material. Because SOFCs

operate at high temperature, a wide range of fuels can be used without having to specially pre-treat the fuel.

Table 2.1: Characteristics of each type fuel cell

Type	Electrolyte	Fuel	Operating temperature	Typical applications
Proton Exchange Membrane Fuel Cells (PEMFCs)	Sulfonic acid incorporated into a solid membrane	Pure Hydrogen, Methanol	50-90^{0}C	Transport, mobile applications
Phosphoric Acid Fuel Cells (PAFCs)	Phosphoric acid	Pure Hydrogen	190-220^{0}C	Buses, trucks & large stationary applications
Solid Oxide Fuel Cells (SOFCs)	Ceramic, solid oxide, zirconia	Most hydrocarbon based fuels	450-1000^{0}C	Small (<1kW) to large (mW) stationary power generation
Molten Carbonate Fuel Cells (MCFCs)	Molten lithium carbonate	Most hydrocarbon based fuels	550-700^{0}C	Large stationary power generation
Alkaline Fuel Cells (AFCs)	Potassium hydroxide	Pure Hydrogen	150-200^{0}C	Space exploration, power generation

Different types of fuel cells operate at different temperatures. While PEMFC and AFC are generally called low temperature fuel cells and MCFC and SOFC being called high temperature fuel cells, the PAFC falls in between and can be called an intermediate temperature fuel cell.

2.2.2 Main advantages & disadvantages of Fuel Cells

Fuel cells systems are rapidly gaining worldwide attention as a feasible energy medium and power source for a variety of portable, stationary and mobile applications .Fuel cells offer significant benefits and have various advantages compared to conventional power sources, such as internal combustion engines or batteries.

a. Portable, transportation or stationary sectors

One of the characteristics of fuel cell systems is that their efficiency is nearly unaffected by size. This means that small, relatively high efficient power plants can be developed, thus avoiding the higher cost exposure associated with large plant

development. They can be used advantageously in the portable [8, 9], transportation or stationary sectors [8, 10]. Portable power solutions like cellular phones, video cameras, personal digital assistants (PDAs) or laptops, among others, are easily found everywhere. The portable power solutions face significant challenges such as to provide more power and power for longer periods of time. Fuel cells show some advantages comparing with the direct competitors: easy recharging, compactness, low noise and are easily scalable, being also able to produce different amounts of power. In the transportation sector, the fuel cells allow a new range of power use from scooters to trucks or other vehicles.

b. High efficiency

Fuel cells convert chemical energy directly into electricity without the combustion process. As a result, a fuel cell is not governed by thermodynamic laws, such as the Carnot efficiency ($\eta_c = 1-T_L/T_H$, where T_L and T_H the low and high temperature), associated with heat engines, currently used for power generation. Instead, the maximum energy or electrical work available is defined by the Gibbs energy (ΔG) of the reactants and products:

$$\eta_{rev}=\Delta G/\Delta H \qquad\qquad (2.8)$$

where η_{rev} is the reversible efficiency and ΔH is the enthalpy change of the electrochemical reaction. The maximum efficiency of a fuel cell is around 83% when it works reversibly. This ideal value decreases when the fuel cells starts to generate electrical power. Despite this efficiency reduction, the actual performance of fuel cells, $\eta_{rev} = 40-55\%$) is still very high compared to thermal conversion systems.

c. Low environmental impact

Fuel cell systems operate without pollution when run on pure hydrogen, the only by-product of the electrochemical reactions is water or CO_2 at very low concentrations. Moreover, the use of low temperatures avoids other side reactions involving pollution by products (nitrogen and sulphur oxides, etc). Another important advantage is the use of bio-alcohols. Methanol and ethanol can be used in the so-called Direct Methanol Fuel Cells or Direct Ethanol Fuel Cells (DMFCs, or DEFCs, respectively). Since alcohols can be obtained from renewable sources, this process of energy conversion is sustainable.

Despite the considerable advantages related with the use of fuel cells, they also show serious drawbacks. The major barrier to the widespread use of fuel cells is their high cost when compared with the available technologies. Additional limitations of fuel cells are related to their durability, room temperature compatibility and ability to produce good performances right after starting or restarting after a resting period. The use of the fuel cell technology is intimately related with the ability to develop technological solutions that minimize or solve these drawbacks

2.3 Fuels for Fuels Cells

For the past one hundred years, liquid hydrocarbon fuels have been a major driving force behind industrialized countries [11]. Product demand has increased at a phenomenal rate, and we have reached the point where the demand to the liquid hydrocarbon fuels culture is approaching and other fuel sources are being sought. As other sources and types of fuels are being sought, it is considered useful to include information on the various types of liquid fuels and the relevant chemical and physical properties of these fuels as a means of comparison to the fuels of the future.

Just as a regular fuel generates energy by combustion, a fuel cell is a device that generates electricity by a chemical reaction. In fact, a fuel cell is an electrochemical cell

that produces electricity through the reaction, triggered in the presence of an electrolyte, between the fuel (on the anode side) and an oxidant (on the cathode side). The reactants flow into the cell and the reaction products flow out of it, while the electrolyte remains within it and the reactions that produce electricity take place at the electrodes. Hydrogen or hydrogen-rich synthesis gas is the basic fuel for fuel cells. Unfortunately, the lack of available alternative sources of hydrogen dictates that the hydrogen (or hydrogen-rich synthesis gas) derives from hydrocarbon fuels. Depending on the application (stationary, central power, remote, auxiliary, transportation, military, etc.), there are a wide range of conventional fuels, such as natural gas, liquefied petroleum gas (LPG), light distillates, methanol, ethanol, dimethyl ether, naphtha, gasoline, kerosene, jet fuels, diesel, and biodiesel, that could be used in reforming processes to produce hydrogen (or hydrogen-rich synthesis gas) to power fuel cells [12].

Hydrocarbon fuels behave differently and in order to place fuel cells in the proper perspective, with some degree of detail, of the manufacture and properties of the common fuels as well as a description of various biofuels. This would not be an exhaustive treatment of all fuel properties, but only of those relevant to fuel processing for the purpose of providing hydrogen (or hydrogenrich synthesis gas) for fuel cells, e.g., aromatic content (which affects coking), olefin content, contaminant levels, additives, and boiling point range (which affects vaporization of the fuels in the fuel processor), all of which may affect the catalysts used for fuel processing [12].

2.3.1 Methanol

Among all possible fuels that can be used for feeding directly a fuel cell, methanol is the most studied due to its high electrochemical activity when compared with other liquid fuels such as ethanol or formic acid. Simultaneously, methanol is liquid at room temperature, has high energy density and is not expensive. Furthermore, methanol

production is not dependent on hydrogen generation processes because it can be obtained by steam reformation of natural gas or by wood distillation.

Historically, methanol (wood alcohol) was first produced by destructive distillation (pyrolysis) of wood. Biomethanol may be produced by gasification of organic materials to synthesis gas followed by conventional methanol synthesis. This was one of the older alternative fuels. It used to be used in vehicle concentrations as high as M85, but it is not commonly used in such high blends anymore because automakers are not developing methanol powered vehicle. Like Ethanol, Methanol is very good for blending with gasoline to replace the harmful octane enhancers.

Methanol, like ethanol, burns at lower temperatures than gasoline. Using methanol as a fuel in spark ignition engines can offer an increased thermal efficiency and increased power output (as compared to gasoline) due to its high octane rating (114) and high heat of vaporization. Methanol, an industrial chemical that can also be used as fuel, can be made from a wide variety of source materials. Viable feedstocks include agricultural products such as corn, sugarcane and switch grass, as well as other sources such as natural gas, coal, or municipal waste. Can even be produced using carbon dioxide emissions that would otherwise contribute to greenhouse gas.

Direct methanol fuel cells are regarded as promising electrochemical systems for directly converting the chemical energy of a fuel and an oxidant into electric energy in a wide range of the portable and transportation applications. A short list of their advantages may include, interalia, their suitability for applications where mass and volume constraints are stringent, the compatibility of liquid methanol for handling and storage in the existed gasoline infrastructure, and their ability for quick start-up and immediate response to consumer needs [13, 14].

2.3.2 Ethanol

Other fuels that are becoming more important to feed directly a fuel cell are ethanol (direct ethanol fuel cells – DEFC) [15]. Ethanol (C_2H_6O) ethyl alcohol, pure alcohol, grain alcohol, drinking alcohol) is a volatile, flammable, and colorless liquid. It is a psychoactive drug, best known as the type of alcohol found in alcoholic beverages and in thermometers. In common usage, it is often referred to simply as alcohol. Ethanol is considered to be attractive due to its low toxicity, natural availability, renewability and minimal pollutants emission. However, under similar operating conditions, the direct ethanol fuel cells performance is still much inferior to that of fuel cells fed with hydrogen or methanol. This happens essentially due to the slow reaction kinetics of the ethanol electro-oxidation.

Ethanol fuel is a gasoline alternative that is manufactured from the conversion of carbon based feed stocks such as sugar cane, sugar beets, switch grass, corn, and barley. In the dry milling process (production of bioethanol), the corn kernel or other starchy grain is ground into flour (meal) and processed without separating out the various component parts of the grain.

Direct ethanol fuel cells (DEFCs) have spurred more and more interest in recent years due to ethanol intrinsic advantages such as its low toxicity, renewability, and its easy production in great quantity by the fermentation from sugar-containing raw materials [16]. Furthermore, the high theoretical mass energy density (about 8.00 kWh/kg) [17] provides it with a potential candidate fuel for polymer electrolyte membrane fuel cells. When ethanol is used as the fuel, its desired reaction in DEFCs is the complete oxidation to CO_2 and water.

2.3.3 Biodiesel

Biodiesel is a fuel produced from biological source and is the generic name for fuels obtained by esterification of vegetable oil. Biodiesel can be used in a diesel engine without modification and is a clean burning alternative fuel produced from domestic, renewable resources. The fuel is a mixture of fatty acid alkyl esters made from vegetable oils, animal fats, or recycled greases.

Biodiesel is better for the environment because it is made from renewable resources and has lower emissions compared to petroleum diesel. It is less toxic than table salt and biodegrades as fast as sugar. Produced domestically with natural resources, its use decreases our dependence on imported fuel and contributes to our own economy. Biodiesel use also reduces greenhouse gas emissions. The carbon dioxide released in biodiesel combustion is offset by the carbon dioxide sequestered while growing the feedstock from which biodiesel is produced. Pure biodiesel (B100) use reduces carbon dioxide emissions by more than 75% compared to petroleum diesel. Using 20%biodiesel (B20) reduces carbon dioxide emissions by 15%.

2.3.4 Hydrogen

Hydrogen comes from the Greek words ''hydro'' and ''genes'' meaning ''water'' and ''generator''. Hydrogen is one of the main compounds of water and of all organic matter and it's widely spread not only in the Earth but also in the entire Universe. In the 20th century, hydrogen was extensively used in the manufacture of ammonia, methanol, gasoline and heating oil, as well as in such commodities as fertilizers, glass, refined metals, vitamins, cosmetics, semi-conductor circuits, lubricants, cleaners, margarine and rocket fuel. After 1974, many studies were conducted to investigate the uses for hydrogen energy and facilitate its penetration as an energy carrier. Subsequently, many industries

worldwide began developing and producing hydrogen, hydrogen-powered vehicles, hydrogen fuel cells, and other hydrogen-based technologies.

Hydrogen is not an energy source, but an energy carrier because it takes a great deal of energy to extract it from water. In nature, hydrogen is never found on its own; it is always combined into molecules with other elements, typically oxygen and carbon. Hydrogen can be extracted from virtually any hydrogen-containing compound, including both renewable and non-renewable resources. There are three hydrogen isotopes: i) protium, mass 1, found in more than 99,985% of the natural element, ii) deuterium, mass 2, found in nature in 0.015% approximately and iii) tritium, mass 3, which appears in small quantities in nature but can be artificially produced by various nuclear reactions.

Hydrogen obtained from dissociation of water with renewable energy, nuclear or the water-gas shift reaction in advanced gasification technologies provided with CO_2 capture and sequestration has been identified as one of the strategic technologies for an appealing, clean, abundant, safe and cost effective energy carrier for a low carbon economy. Hydrogen produced through renewable energy sources is an emissions-free way to carry clean energy. Hydrogen is most commonly generated from renewables with a device called electrolyzer, which uses electricity to separate water into hydrogen and oxygen. By converting renewable electricity into hydrogen, the intermittent power of wind and sunlight can be stored for long periods and used in a fuel cell for power at any time. It can be burned in internal combustion engines. Hydrogen Fuel Cells are being looked into as a way to provide power and research is being conducted on hydrogen as a possible major future fuel. For instance it can be converted to and from electricity from bio-fuels, from and into natural gas and diesel fuel, theoretically with no emissions of either CO_2 or toxic chemicals.

Several important properties of hydrogen are listed in Table 1. In comparison to air (see also Table 1), hydrogen exhibits 14-fold lower density, 3.8-fold higher speed of sound, and seven-fold higher thermal conductivity. These exceptional properties of hydrogen have useful applications: Its low density and high sonic speed are exploited in the supersonic tube vehicle (STV) concept, and its high thermal conductivity has been exploited by using hydrogen gas as a coolant for nuclear reactors so as to avoid radioactive contamination of the coolant.

Table 2.2: Properties of Hydrogen and Comparison with properties of Air

Property	Hydrogen	Air	Hydrogen Value / Air Value
Molecular Mass	2,016		
Boiling point, K	20		
Melting point, K	14		
Density (ρ), g/L	0,082	1,16	0,071
Viscosity (μ), μPa-s	9,0	18,6	0,48
Speed of sound, m/s (km/h)	1.310 (4.720)	346 (1.246)	3,8
Thermal conductivity, mW/m-K	187	26,2	7,1
[*]At pressure P = 100kPa and temperature T = 298-300K			

The greatest obstacle for the wide use of hydrogen as an energy carrier in our daily life is the generation and distribution of hydrogen. Although hydrogen can be produced in various ways, most of the hydrogen produced today comes from large chemical plants making its way to the final customer very long.
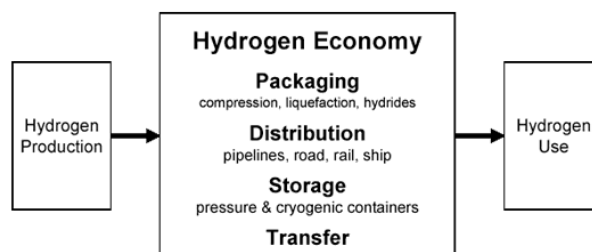

Figure 2.2: Schematic Representation.

Like any other product, hydrogen must be packaged, transported, stored and transferred, to bring it from production to final use (Figure 2.2). These standard product

processes require energy. In today's fossil energy economy, the energy lost between the well and the consumer is about 12% for oil and about 5% for gas.

2.4 Hydrogen Production

Hydrogen production is the family of industrial methods for generating hydrogen. Hydrogen in molecular form can be produced from many different sources and in many different ways. It can be produced from a wide of feedstocks and any hydrogen- rich material can serve as a possible fuel source for fuel cells. The vast majority of today's hydrogen is produced via steam reformation of natural gas (95% in the U.S., roughly 48% globally) but alternative sources such as biogas are growing in popularity. Many other methods are known including electrolysis and thermolysis.

2.4.1 Steam reforming

Fossil fuels are the dominant source of industrial hydrogen. Hydrogen can be generated from natural gas with approximately 80% efficiency or from other hydrocarbons to a varying degree of effiency. Specifically, bulk hydrogen is usually produced by the steam reforming of methane or natural gas. At high temperatures (700-1100°C), steam (H_2O) reacts with methane (CH_4) in an endothermic reaction to yield syngas.

$$CH_4 + H_2O \rightarrow CO + 3\,H_2 \qquad\qquad (2.9)$$

In a second stage, additional hydrogen is generated through the lower –temperature, exothermic, water gas shift reaction, performed at about 130°C:

$$CO + H_2O \rightarrow CO_2 + H_2 \qquad\qquad (2.10)$$

Essentially, the oxygen (O) atom is stripped from the additional water (steam) to oxidize CO to CO_2. This oxidation also provides energy to maintain the reaction. Additional heat required to drive the process is generally supplied by burning some portion of the methane.

Natural gas, the feedstock of choice for most of today's mass-produced hydrogen, contains methane (CH_4) that can be used to produce hydrogen via a thermal process known as steam-methane reformation. In steam-methane reforming, methane reacts with steam in the presence of a catalyst to produce hydrogen, carbon monoxide, and a relatively small amount of carbon dioxide. Steam reforming is endothermic, meaning heat must be supplied to the process for the reaction to proceed. The process is approximately 72% efficient. This type of reforming works similarly for other hydrocarbon fuels, combining the fuel with steam by vaporizing them together at high temperatures. Hydrogen is then separated out using membranes.

Another type of reformer is the partial oxidation (POX) reformer. Partial oxidation is a reforming process in which the fuel is partially combusted; it is exothermic and provides heat for other reactions in the reforming system (usually in combination with steam reforming). The oxygen fed into the system is sub-stoichiometric so that both CO and CO_2 are formed. Some CO_2 is emitted in the reforming process, but the emissions of NOX, SOX, particulates, and other smog producing agents are cut to zero.

2.4.2 Water Electrolysis

Electrolysis is the process of using electricity to split water into hydrogen and oxygen. Making hydrogen from water by electrolysis is one of the more energy-intensive methods. As long as the electricity comes from a clean source, electrolysis is a clean process, but it is associated with considerable losses. Electrolysis is the reverse of the hydrogen oxidation reaction in a fuel cell. This reaction takes place in a unit called an electrolyzer. Electrolyzers can be small, appliance-size equipment and well-suited for small-scale distributed hydrogen production. Research is also under way to examine larger-scale electrolysis that could be tied directly to renewable or other non-greenhouse gas emitting

electricity production. Hydrogen production at a wind farm generating electricity is an example of this. The overall electrolysis reaction is:

$$e^- + H_2O \rightarrow \frac{1}{2} O_2 + H_2 \qquad (2.11)$$

Hydrogen produced via electrolysis can result in zero greenhouse gas emissions, depending on the source of the electricity used [18]. The source of the required electricity including its cost and efficiency, as well as emissions resulting from electricity generation must be considered when evaluating the benefits of hydrogen production via electrolysis. In many regions of the country, today's power grid is not ideal for providing the electricity required for electrolysis because of the greenhouse gases released and the amount of energy required to generate electricity. Hydrogen production via electrolysis is being pursued for renewable (wind) and nuclear options. These pathways result in virtually zero GHG emissions and criteria pollutants.

Electrolysis technologies with reduced capital costs, enhanced system efficiency, and improved durability for distributed scale hydrogen production from electricity and water. When an electric current is introduced to water (H_2O), hydrogen and oxygen are separated, with hydrogen forming at the cathode and oxygen forming at the anode. Electricity can be provided from any source, but using solar and wind energy to electrolyze water provides the cleanest pathway to produce hydrogen. This model is being used in some hydrogen refueling stations and in renewable energy storage systems that utilize hydrogen.

2.4.3 Enzymes

Another method to generate hydrogen is with bacteria and algae. Cyanobacteria, an abundant single-celled organism, produce hydrogen through its normal metabolic function. Cyanobacteria can grow in the air or water, and contain enzymes that absorb

sunlight for energy and split the molecules of water, thus producing hydrogen. Since cyanobacteria take water and synthesize it to hydrogen, the waste emitted is more water, which becomes food for the next metabolism. Sodium borohydride ($NaBH_4$) is an inorganic compound that can dissolve in water in the absence of a base. Hydrogen can be generated through catalytic decomposition.

2.5 Storage and delivery

Hydrogen storage is a key enabling technology for the advancement of hydrogen and fuel cell power technologies in transportation, stationary, and portable applications. Hydrogen can be stored in materials, such as nanotubes [19], carbon fibers [20], metal hydrides and in a number of chemical compounds. Hydrogen stored in alcohols or hydrocarbons such as methanol or methane can be an option. Such alcohols and hydrocarbons are usually reformed into hydrogenrich synthesis gases by several methods, the main processes are catalytic steam reforming (CSR), partial oxidation (POX) and autothermal reforming (ATR).

Lower-cost, lighter-weight, and higher-density hydrogen storage is one of the key technologies needed for the introduction of hydrogen-based systems. Hydrogen can be stored as either a liquid or a gas. To store hydrogen in liquid form, hydrogen must be cooled to -423°F, requiring a tremendous amount of energy. Therefore, hydrogen produced in large quantities is usually pressurized as a gas then stored in caverns, gas fields, or mines before being piped to the consumer as natural gas is today. Researchers are examining an impressive array of storage options with support from the U.S. Department of Energy.

High-pressure tanks can be used to store hydrogen. Today, compressed hydrogen tanks for 5,000 psi (~35 MPa) and 10,000 psi (~70 MPa)] have been certified worldwide according to ISO 11439 (Europe), NGV-2 (U.S.), and approved by TUV (Germany) and

The High Pressure Gas Safety Institute of Japan (KHK). However, driving ranges for compressed tanks remain inadequate and the energy consumed to compress the hydrogen reduces the efficiency of this storage media. The weight and size of the tanks are also an impediment to this application.

Liquefied Hydrogen - The energy density of hydrogen can be improved by storing hydrogen in a liquid state. However, hydrogen losses become a concern and improved tank insulation is required to minimize losses from hydrogen boil-off. In addition, advances in liquefaction efficiencies are required to reduce the energy required to cool and liquefy hydrogen gas.

2.6 Hydrogen uses

Hydrogen is the lightest and most common element in the world. It is one of the components of water and vital to life. There are a lot of benefits that can be derived from using hydrogen as opposed to other chemical elements. It is widely used in many industries mainly because it causes for more sustainable form of energy.

2.6.1 Fueling

The element is often used as fuel because of its high calorific value. Combustion generates plenty of energy. Numerous transit systems around the world have conducted demonstration programs placing hydrogen fuel cell buses in operation that provide pollution-free, quiet urban public transportation. Hydrogen vehicle fueling stations may generate hydrogen on-site or receive deliveries of trucked-in hydrogen. In either case, the stations possess equipment to compress, store and dispense the hydrogen fuel. Compressing hydrogen gas to 350 (5,000 psi) or 700 bar (10,000 psi) reduces the volume, and the compressed gas is then stored onsite in high pressure or cryogenic tanks. A few sites store hydrogen in liquid form, which is converted to a gaseous state and compressed

before being dispensed. Researchers are also examining additional storage options, such as the use of advanced solid state materials and liquid materials.

On-board hydrogen storage is a challenge for automotive engineers, who are limited by size and weight constraints while seeking to meet the driving range of today's gas-fueled vehicles (300 or more miles per fueling). Several recent fuel cell vehicles have either met or exceeded this milestone with novel tank design. Researchers are examining an array of storage options with support from the U.S. Department of Energy (DOE). Today's fuel cell electric (FCEVs) use compressed hydrogen tanks or liquid hydrogen tanks. New technologies, such as metal hydrides and chemical hydrides may be come viable in the future. Another option is to store hydrogen-containing compounds, such as gasoline or methanol, onboard a vehicle and extracting the hydrogen using a fuel reformer.

Today, there are more than 100 hydrogen fueling stations operating around the world, with a fueling process that is swift (just minutes) and remarkably similar to filling up a tank with gasoline.

2.6.2 Industrial applications

Other uses of hydrogen are in the fertilizer and paint industries. It is also used in the food and chemical industries. Food industries use the element to make hydrogenated vegetable oils such as margarine and butter. In this procedure, vegetables oils are combined with hydrogen. By using nickel as a catalyst, solid fat substances are produced. In petrochemical industry, hydrogen is required for crude oil refinements.

Welding companies use the element for welding torches. These torches are utilized for steel melting. Hydrogen is required as a reducing agent in chemical industries. Chemical industries use them for metal extraction. For example, hydrogen is needed to treat mined tungsten to make them pure.

2.6.3 Chemical compounds

This element is used for producing several chemical compounds. Apart from ammonia, hydrogen can be harnessed in other ways. It can be used to make fertilizers, hydrochloric acis and an assortment of bases. The same element is required for methyl alcohol production. Methyl alcohol is used in inks, varnishes and paints. Hydrogen peroxide is another vital compound.

Hydrogen peroxide is used in many ways. First and foremost it is used for medication. It is included in most first aid kits. It is primarily used for treating wounds and cuts. Peroxide is also a toenail fungus disinfectant. Hydrogen peroxide can be diluted in water. It can kill bacteria and germs if used as whitewash. The same element can be used for teeth whitening and canker sores treatment.

2.7 Hydrogen PEM fuel cell

The development of highly active oxygen reduction electrocatalysts with enhanced durability remains still to be a critical challenge for a wider commercialization of hydrogen proton exchange membrane fuel cells (PEMFCs). The hydrogen proton exchange membrane fuel cell converts chemical Gibbs free energy directly into electrical energy with the single product of water. It is one of the promising technologies for low emission and noise energy production in different fields, for example in automotive or portable applications. The overall reaction of a hydrogen / oxygen PEM fuel cell is $2H_2 + O_2 => 2H_2O$. Figure 1 shows a schematic of a single cell (membrane electrode assembly, MEA) hydrogen / oxygen PEM fuel cell.
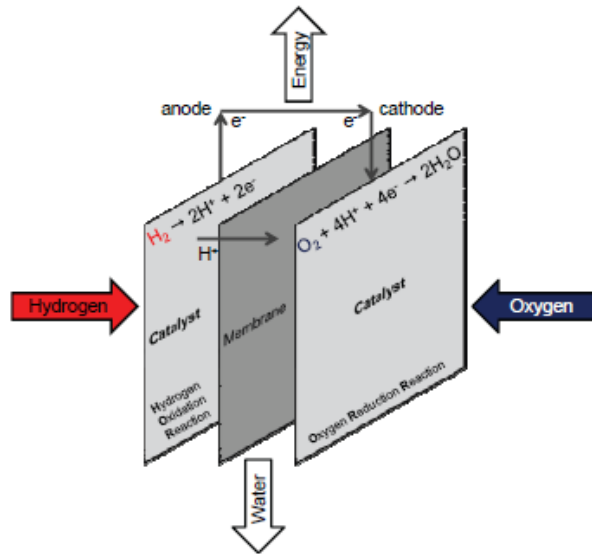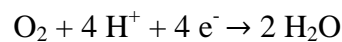
Figure 2.3: Schematic of a single cell (membrane electrode assembly, MEA) hydrogen /oxygen PEM fuel cell.

The oxygen reacts on the cathode side of the PEMFC with protons and electrons to form water according to the half-cell redox process

$$O_2 + 4\ H^+ + 4\ e^- \rightarrow 2\ H_2O$$

where the protons are supplied by the hydrogen splitting on the anodic side via membrane crossing [21]. This oxygen reduction reaction (ORR) on the cathodic side is a sluggish rate limiting reaction and therefore leads to significant cell voltage and overall efficiency losses in a PEMFC [22, 23].

2.7.1 Hydrogen PEM fuel cell electrocatalyst research targets

It is well known that PEMFC systems are intended to be used for transportation and portable applications as well as for stationary ones, mainly due to their low temperature operation and quick start-up. Fuel cell is considered as one of the most promising products of 21st Century, as it can compete, in terms of efficiency, with batteries, internal combustion engines and power grids. The challenge is whether fuel cell can be made with a reasonable price [24].

Whatever the case will be, Pt or Pt-based binary or ternary catalysts are still the well-known and commonly-adopted materials providing the highest activity for electrode reactions and lifetime stability. Nevertheless, the total Pt reserves in the world will be depleted if each vehicle, which is powered by a 75 kW fuel cell stack, needs approximately 75 g of Pt (~1 mg Pt/W) [25]. More precisely, one and a half billion cars will require more than 110,000 tons of Pt, which is far more than the world-wide estimated Pt reserves (~28,000 tons), in addition to the other applications of Pt in the area of catalysis, jewellery and so on. Therefore, in order to increase Pt's utilization coefficient and consequently decrease its content, the research and development has shot either to Pt-based electrocatalysts with low-Pt loading, which are usually dispersed on carbon supports with high specific surface area [26] or to non-Pt (Pt-free) electrocatalysts. Moreover, the cost target of ~30 \$/kW (current Internal Combustion Engine's cost) that has been set for 2015 and can be met only if the maximum mass specific power density (max-MSPD) will be reduced to less than 200 mg of Pt_{total} per kW (higher than $5mW\mu g_{Pt_{total}}^{-1}$) at cell voltages higher than 0.65 V (U.S. Department of Energy, DOE). This cost reduction could be achieved: (a) by increasing the power density to 0.8-0.9Wcm_{MEA}^{-2} at cell voltages >0.65 V, (b) by reducing mass transfer loss at higher current densities, and (c) by reducing Pt-loading in MEAs to < 150μgcm_{MEA}^{-2} [25].

In literature a lot of novel materials have been studied as anode and cathode electrocatalysts for (H_2-PEMFCs). Many different techniques have been adopted in order to reduce Pt loading in PEMFCs sputter deposition [27], hydrothermal method [28], electrospinning and chemical dealloying techniques [29, 30], thin film method [31, 32], ion beam assisted deposition (IBAD) method [33].

Fig.2.4 summarizes all the results reported in the International literature the last decade, concerning both low Pt anodes and low Pt cathodes. As it can be seen, the results

can be classified in three regions of maximum power density ($mWcm^{-2}$) a) higher than $30mW\mu g^{-1}_{Pt}$, b) between 5 - $30mW\mu g^{-1}_{Pt}$ and c) lower than $5mW\mu g^{-1}_{Pt}$. The reported maximum power density close to 906 $mWcm^{-2}$, has been reached by Pintauro *et al.*[30] over nanostructured fuel cell electrodes. More precisely they fabricated a MEA with both cathode and anode Pt loading of 114 $\mu gPtcm^{-2}$, by using electrospinning technique with superior catalyst utilization and long-term durability. Sung *et al.* achieved a maximum power density of 750 $mWcm^{-2}$ with a total Pt loading 32 $\mu g_{Pt}cm^{-2}$ by containing PdPt/C anode electrocatalyst and Pt/C cathode [34].
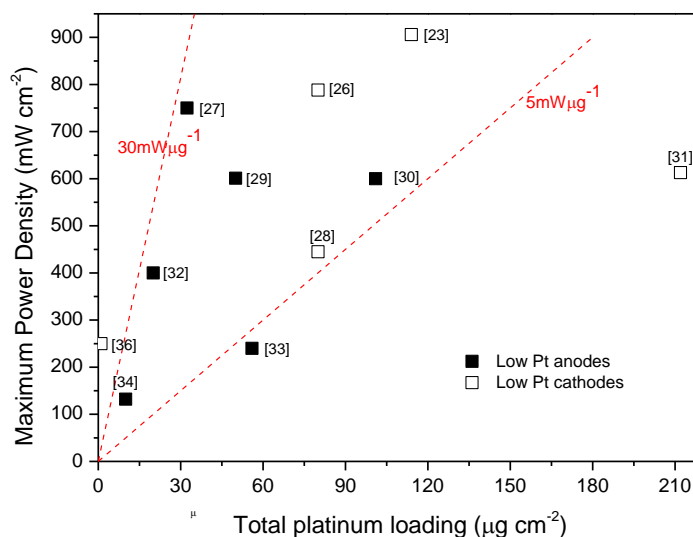
Figure 2.4: H₂-PEMFC operation results: Maximum Power Density (mW cm⁻²) dependency on total (anode + cathode) Pt loading (µg cm⁻²). In the brackets the reference number is reported.

A carbon supported PdPt catalyst with Pd:Pt atomic ratio of 19:1 was synthesized as anode by the sodium borohydride reduction method combined with freeze-drying. The Pt loading was only 5 at.%Pt (19:1 atomic ratio of Pd:Pt) indicating that Pd can successfully enhance the cell performance. As it is observed, despite the very low Pt loading, this electrocatalyst presented the highest power density values. Mukerjee *et al.* [33, 35] synthesized electrodes by direct metallization of non-catalyzed gas diffusion layers via the method of dual ion beam assisted deposition (IBAD), which performed a substantially high power density 788 and 445mW cm^{-2} by using a MEA with Pt loading of 80 $\mu g_{Pt}cm^{-2}$.

Using a modified thin-film method, Manthiram *et al.* [36] fabricated a MEA with 25 $\mu g_{Pt}cm^{-2}$ each electrode and achieved a power density of 601 mWcm^{-2}. Additionally, Antolini *et al.*[37] also achieved 600 mWcm^{-2} over electrodes prepared by replacing Pt/C with PdPt/C indicating that Pd-based catalysts can substitute conventional Pt catalysts in PEMFCs with only a slightly loss in cell performance.

Ultra-low platinum loading cathode electrocatalyst of $12\mu g_{Pt}cm^{-2}$ was fabricated using thin films of multiwall carbon nanotube supported Pt catalysts (Pt/MWNTs) [38]. As it can be seen (Fig.3) the peak power density, for a H$_2$-PEMFC's membrane electrode assembly loaded with $12\mu g_{Pt}$ cm^{-2} and tested at 70°C, was 613 mWcm^2. Brault *et al.*[39] fabricated ultra-low Pt content PEMFC electrodes (10μg cm^{-2} for anode and 10μg cm^{-2} for cathode) employing a method of carbon and platinum magnetron co-sputtering on a commercial E-Tek un-catalyzed gas diffusion layer, which presented high power density of 400 mWcm^{-2}, equivalent to a specific power of 20kW g_{Pt}^{-1}. Moreover, another attractive strategy to reduce precious metal loading, is making catalyst skins over nanoporous metal supports. Erlebacher *et al.*[40] fabricated platinum-plated nanoporous gold leaf (Pt-NPGL) MEA (carbon-free electrocatalyst), which exhibited maximum power density 250 mWcm^{-2}. By sputter-deposited Pt thin film layers onto different porous electrodes, Gruber *et al.*[41] reached 132 mWcm^{-2} over a very low total Pt amount of 10μg cm^{-2}.

More precisely, Fig. 2.5 depicts the results of the recently appeared investigations concerning different techniques that are used for the preparation of low platinum anodes and low platinum cathodes for H$_2$-PEMFC. A three step electrodeposition process has been adopted for the preparation of a PtFeNi catalyst [42] with an ultra-low Pt loading of 50 μgPtcm$^-$2, which exhibited good performance and stability. Mougenot *et al.[43]* prepared a MEA with an ultra-low Pt loading made by pure Pd anode and PdPt cathode,

deposited on commercial carbon woven web and carbon paper GDLs by plasma sputtering, that under fuel cell operation performed 250 mWcm^{-2}.
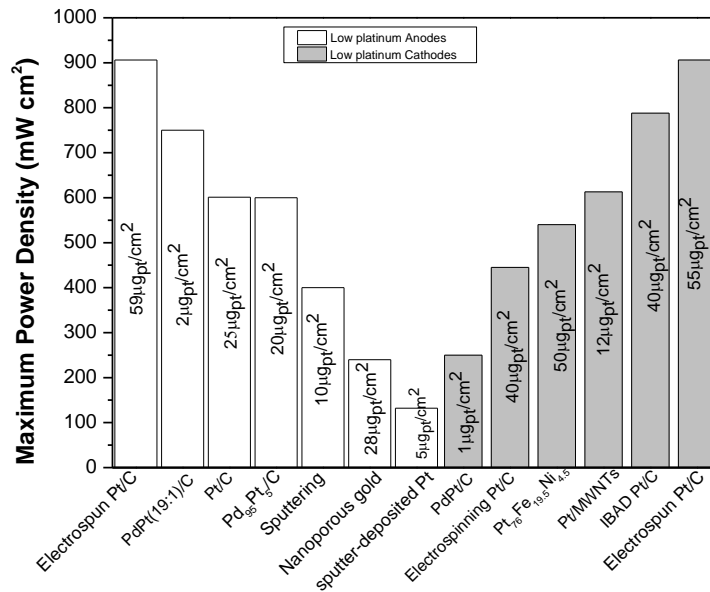

Figure 2.5: Maximum Power Density (mWcm^{-2}) dependency different Pt anodes and Pt cathodes. Inside the columns is reported the platinum amount (μgcm^{-2}) contained in each electrode.

As expected, using Pt-based binary or ternary catalyst and increasing Pt's utilization coefficient are the commonly methods for decreasing Pt content and providing the highest activity for electrode reactions and lifetime stability.

2.8 Platinum free electrocatalysts for Hydrogen PEMFC

2.8.1 Anodes

In recent years, considerable progress have been achieved in developing non-platinum electrodes, however there are few reports on H$_2$-PEMFCs with Pt-free anode catalysts. Even in these cases the cathode was loaded with Pt. A successful anode catalyst should combine high HOR activity with good long-term stability, a major challenge in the strongly acidic environment of the PEMFC anode. The last decade's efforts for the replacement of the expensive and scarce Pt by non-Pt electrocatalysts in PEMFC anodes is depicted in Fig. 2.5. As one can distinguish, the highest performance (Fig.2.4) for Pt-

free anode achieved by Jianxin Ma *et al.*[44]. They prepared highly dispersed non-platinum catalyst based on Ir and Ir-V nanoclusters for PEMFC anode via ethylene glycol method, which at 0.512V exhibited about 563mWcm^{-2}. This material is expecting to be very promising candidate as platinum alternative anode catalyst. Recently, Hyuk Chang *et al.*[45] over a Pd_3Au/WC catalyst achieved a performance of 238mWcm^{-2}, which was the second best value after that of iridium-vanadium alloy. Moreover, a strong interaction between PdNi alloys and WC in the case of PdNi/WC anode electrocatalyst for HOR caused a performance of 230mWcm^{-2} [46]. Jacobson *et al.* focused on transition metal sulfides (RuS_2/C) for HOR under fuel cell operation and they measured maximum power density value at 100 mWcm^{-2} which is the third better fuel cell performance at non –Pt anodes Fig. 2.6.
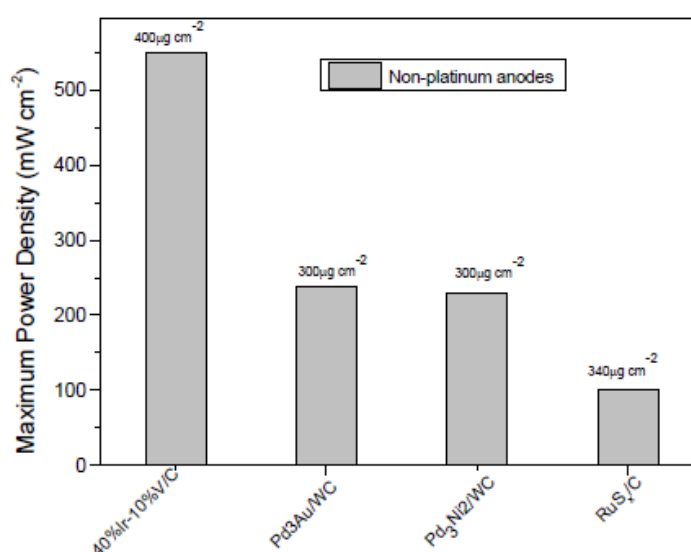
Figure 2.6: Maximum Power Density (mWcm^{-2}) over different Pt-free anodes.

2.8.2 Cathodes

The last decade, a large number of investigations have also been appeared regarding the replacement of Pt in fuel cells' cathodes, aimed at the enhancement of the activity towards ORR, which is much slower than HOR. The highest performance reported in the literature for non-platinum cathode in H_2-PEMFC, is 529 mWcm^{-2} achieved by B. N.

Popov *et al.*[47] over Co-Fe-N/C electrocatalyst, obtained through high-temperature pyrolysis of Co-Fe-N chelate complex on the support, followed by chemical leaching.

The maximum power density of 517 mWcm^{-2} obtained by 40% Ir–10% V/C as the cathode catalyst and 400 μgcm^{-2} Pt anode loading [48]. In the case that polyaniline [49] was used as both carbon and nitrogen precursor, the cell maximum power density reached the value of 380 mWcm^{-2}, the anode's Pt loading was 250 μgcm^{-2}. In a general overview of Fig. 2.6, comparison of the performances exhibited by Pt catalysts, the transition metals (binary and ternary) carbides, nitrides and oxynitrides exhibited remarkably equal or slightly better performance with the same loading of metal. The most common examined binary and ternary alloys are Pd-M (M = Ti [50], Ni [51], Co-Mo [52].
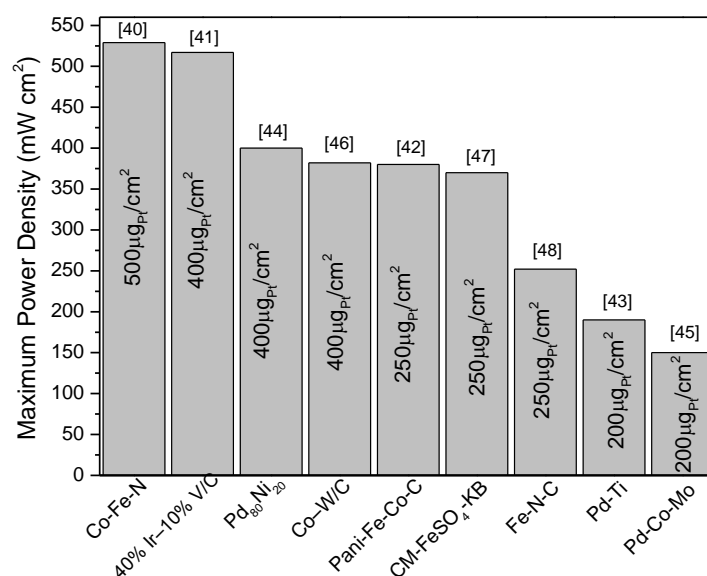
Figure 2.7: Maximum power density (mWcm^{-2}) over different Pt-free cathodes. In the column is reported the Pt amount (μgcm^{-2}) contained in the anode.

The cobalt tungsten Co–W/C treated by ammonia [53] obtained performance of 382 mWcm^{-2} (anode Pt loading: 400 μgcm^{-2}). According to Zelenay *et al.* [54] using cathode catalyst cynamide as a nitrogen source, H$_2$-PEMFC exhibited a maximum power density of 370 mWcm^{-2}. A highly ordered Pt-free Fe–N–C catalyst is synthesized by Tang *et al.* [55] achieving maximum power of the cell 252 mWcm^{-2}.

References

[1]   N.Y. Amponsah, M. Troldborg, B. Kington, I. Aalders, R.L. Hough. Renewable and Sustainable Energy Reviews 39 (2014) 461-475.

[2]   M. Ball, M. Wietschel. International Journal of Hydrogen Energy 34 (2009) 615-627.

[3]   A. Midilli, M. Ay, I. Dincer, M.A. Rosen. Renewable and Sustainable Energy Reviews 9 (2005) 255-271.

[4]   S.M.M. Ehteshami, S.H. Chan. Energy Policy 73 (2014) 103-109.

[5]   P.P. Edwards, V.L. Kuznetsov, W.I.F. David, N.P. Brandon. Energy Policy 36 (2008) 4356-4362.

[6]   L.J.M.J. Blomen, M. N.Mugerwa, Fuel Cell Systems, 1993.

[7]   L. Carrette, K.A. Friedrich, U. Stimming. ChemPhysChem 1 (2000) 162-193.

[8]   C.S. Spiegel. Mc Graw Hill (2007).

[9]   J. Ramírez-Salgado, M.A. Domínguez-Aguilar. Journal of Power Sources 186 (2009) 455-463.

[10]   C.R. Karger, R. Bongartz. Energy Policy 36 (2008) 798-810.

[11]   J.G. Speight, The Chemistry and Technology of Petroleum, Fifth Edition, CRC Press, 2007.

[12]   D. Shekhawat, J.J. Spivey, D.A. Berry, Fuel cells: Technologies for fuel processing, in: Elsevier (Ed.), 2011.

[13]   S.Q. Song, Z.X. Liang, W.J. Zhou, G.Q. Sun, Q. Xin, V. Stergiopoulos, P. Tsiakaras. Journal of Power Sources 145 (2005) 495-501.

[14]   S.D. Knights, K.M. Colbow, J. St-Pierre, D.P. Wilkinson. Journal of Power Sources 127 (2004) 127-134.

[15]   S. Song, P. Tsiakaras. Applied Catalysis B: Environmental 63 (2006) 187-193.

[16]   S.Q. Song, W.J. Zhou, Z.H. Zhou, L.H. Jiang, G.Q. Sun, Q. Xin, V. Leontidis, S. Kontou, P. Tsiakaras. International Journal of Hydrogen Energy 30 (2005) 995-1001.

[17]   C. Lamy, A. Lima, V. LeRhun, F. Delime, C. Coutanceau, J.-M. Léger. Journal of Power Sources 105 (2002) 283-296.

[18]   P. Millet, S. Grigoriev, in: L.M. Gandía, G. Arzamendi, P.M. Diéguez (Eds.), Renewable Hydrogen Technologies, Elsevier, Amsterdam, 2013, pp. 19-41.

[19]   R. Oriňáková, A. Oriňák. Fuel 90 (2011) 3123-3140.

[20]   F. Salvador, J. Montero, M.J. Sánchez-Montero, C. Izquierdo. International Journal of Hydrogen Energy 36 (2011) 7567-7579.

[21]   H.A. Gasteiger, J. Garche, Handbook of Heterogeneous Catalysis, Wiley-VCH Verlag GmbH & Co. KGaA, 2008.

[22]   J.K. Nørskov, J. Rossmeisl, A. Logadottir, L. Lindqvist, J.R. Kitchin, T. Bligaard, H. Jónsson. The Journal of Physical Chemistry B 108 (2004) 17886-17892.

[23]   K. Krischer, E.R. Savinova, Handbook of Heterogeneous Catalysis, Wiley-VCH Verlag GmbH & Co. KGaA, 2008.

[24]   A. Brouzgou, S.Q. Song, P. Tsiakaras. Applied Catalysis B: Environmental 127 (2012) 371-388.

[25]   H.A. Gasteiger, S.S. Kocha, B. Sompalli, F.T. Wagner. Applied Catalysis B: Environmental 56 (2005) 9-35.

[26]   S. Vengatesan, H.J. Kim, S.K. Kim, I.H. Oh, S.Y. Lee, E. Cho, H.Y. Ha, T.H. Lim. Electrochimica Acta 54 (2008) 856-861.

[27]   K.-S. Lee, D.M. Kim. International Journal of Hydrogen Energy 37 (2012) 6272-6276.

[28]   M. Wang, K.-D. Woo, D.-K. Kim. Energy Conversion and Management 47 (2006) 3235-3240.

[29]   J.-l. Shui, C. Chen, J.C.M. Li. Advanced Functional Materials 21 (2011) 3357-3362.

[30]   M. Brodt, R. Wycisk, P.N. Pintauro. Journal of The Electrochemical Society 160 (2013) F744-F749.

[31]   A. Esmaeilifar, S. Rowshanzamir, M.H. Eikani, E. Ghazanfari. Electrochimica Acta 56 (2010) 271-277.

[32]   L. Xiong, A. Manthiram. Electrochimica Acta 50 (2005) 3200-3204.

[33]   N. Ramaswamy, T.M. Arruda, W. Wen, N. Hakim, M. Saha, A. Gullá, S. Mukerjee. Electrochimica Acta 54 (2009) 6756-6766.

[34]   Y.-H. Cho, B. Choi, Y.-H. Cho, H.-S. Park, Y.-E. Sung. Electrochemistry Communications 9 (2007) 378-381.

[35]   M.S. Saha, A.F. Gullá, R.J. Allen, S. Mukerjee. Electrochimica Acta 51 (2006) 4680-4692.

[36]   L. Xiong, A. Manthiram. Electrochimica Acta 50 (2005) 3200-3204.

[37]   E. Antolini, S.C. Zignani, S.F. Santos, E.R. Gonzalez. Electrochimica Acta 56 (2011) 2299-2305.

[38]   J.M. Tang, K. Jensen, M. Waje, W. Li, P. Larsen, K. Pauley, Z. Chen, P. Ramesh, M.E. Itkis, Y. Yan, R.C. Haddon. The Journal of Physical Chemistry C 111 (2007) 17901-17904.

[39]   M. Cavarroc, A. Ennadjaoui, M. Mougenot, P. Brault, R. Escalier, Y. Tessier, J. Durand, S. Roualdᴦ˘s, T. Sauvage, C. Coutanceau. Electrochemistry Communications 11 (2009) 859-861.

[40]   R. Zeis, A. Mathur, G. Fritz, J. Lee, J. Erlebacher. Journal of Power Sources 165 (2007) 65-72.

[41]   D. Gruber, N. Ponath, J. Müller, F. Lindstaedt. Journal of Power Sources 150 (2005) 67-72.

[42]   B. Li, S.H. Chan. International Journal of Hydrogen Energy 38 (2013) 3338-3345.

[43]   M. Mougenot, A. Caillard, P. Brault, S. Baranton, C. Coutanceau. International Journal of Hydrogen Energy 36 (2011) 8429-8434.

[44]   B. Li, J. Qiao, D. Yang, J. Zheng, J. Ma, J. Zhang, H. Wang. Electrochimica Acta 54 (2009) 5614-5620.

[45]   D. Ham, S. Han, C. Pak, S. Ji, S.-A. Jin, H. Chang, J. Lee. Top Catal 55 (2012) 922-930.

[46]   D.J. Ham, C. Pak, G.H. Bae, S. Han, K. Kwon, S.-A. Jin, H. Chang, S.H. Choi, J.S. Lee. Chemical Communications 47 (2011) 5792-5794.

[47]   V. Nallathambi, J.-W. Lee, S.P. Kumaraguru, G. Wu, B.N. Popov. Journal of Power Sources 183 (2008) 34-42.

[48]   J. Qiao, R. Lin, B. Li, J. Ma, J. Liu. Electrochimica Acta 55 (2010) 8490-8497.

[49]   G. Wu, Z. Chen, K. Artyushkova, F.H. Garzon, P. Zelenay. ECS Transactions 16 (2008) 159-170.

[50]   J.L. Fernández, V. Raghuveer, A. Manthiram, A.J. Bard. Journal of the American Chemical Society 127 (2005) 13100-13101.

[51]   J. Zhao, A. Sarkar, A. Manthiram. Electrochimica Acta 55 (2010) 1756-1765.

[52]   V. Raghuveer, A. Manthiram, A.J. Bard. The Journal of Physical Chemistry B 109 (2005) 22909-22912.

[53]   T. Ando, S. Izhar, H. Tominaga, M. Nagai. Electrochimica Acta 55 (2010) 2614-2621.

[54]   H.T. Chung, C.M. Johnston, K. Artyushkova, M. Ferrandon, D.J. Myers, P. Zelenay. Electrochemistry Communications 12 (2010) 1792-1795.

[55]   M. Lei, P.G. Li, L.H. Li, W.H. Tang. Journal of Power Sources 196 (2011) 3548-3552.

CHAPTER 3

Experimental apparatus

&

Experimental techniques

Abstract

This chapter initially indicates an analytical description of the preparation method of the studied electrocatalysts. The method that was used for the preparation of the electrocatalysts is microwave assisted polyol and is referred analytically. Moreover, the experimental apparatus that were used to carry out the experimental measurements of the Fuel Cell and the experimental techniques for the physicochemical and electrochemical characterization of the studied electrocatalysts are given. At first stage their physicochemical characterization was conducted by the techniques of Transmitting Electrode Microscopy (TEM) and X-Ray Diffraction (XRD). Then, their electrochemical characterization towards hydrogen oxidation reaction (HOR) and oxygen reduction reaction (ORR) was conducted by the Cyclic Voltammetry (CV), Chronoamperometry and Rotating Disk Electrode (RDE) methods. Fuel cell performance was studied and examined by electrochemical impedance spectroscopy (EIS), cyclic voltammetry (CV) and potentiodynamic (I-V) techniques.

Contents

List of Figures

3.1 Preparation Method of Electrocatalysts: modified microwave assisted polyol method.

Microwaves are electromagnetic waves with frequencies in the range of 0.3 to 300 GHz. The commonly used frequency for microwave heating is 2.45 GHz. The principle of microwave heating is related to the polar characteristics of molecules. During the microwave heating, polar molecules such as water molecules try to orientate with the electric field. When dipolar molecules try to re-orientate with the rapidly changing alternating electric field, the heat is generated by rotation, friction and collision of molecules. One of the advantages of the microwave heating is rapid volumetric heating, which results in the higher reaction rate and selectivity, reduction in the reaction time often by orders of magnitude and higher yield of the product compared to the conventional heating methods. As a result, the microwave heating opens up the possibility of realizing fast preparation of materials in a very short time, leading to relatively low cost, energy saving and high efficiency for materials production. The microwave energy is found to be more efficient in the selective heating in many processes. These processes are environmentally friendly, requiring less energy than the conventional methods.

Since the first reports of the microwave-assisted organic synthesis in 1986, the microwave heating has received considerable attention as a promising heating method for both organic and inorganic synthesis. The use of microwave heating as an alternative heat source is becoming more and more popular in chemistry and materials science. The microwave heating has received considerable attention as a new promising method for the rapid preparation of inorganic nanostructures in the liquid solvents.

A variety of nanomaterials such as metals, metal oxides, metal sulphides, selenides, tellurides, carbonates organic/inorganic composites have been prepared by the microwave heating method [1]. Nanostructures with various morphologies including spheres,

polygonal plates, sheets, rods, wires, tubes and dendrites were prepared within a few minutes under microwave heating. Morphologies and sizes of metal nanostructures could be controlled by changing various experimental parameters, such as the concentration of metal salt and the chain length of the surfactant, the solvent and the reaction temperature. The heating rate and efficiency of the microwaves strongly depends on the properties of the reaction mixture. When good microwave absorbing solvents are used the results is a very fast heating. Among the typical solvents commonly used in microwave heating, water alcohols and ethylene glycol are ideal solvents and they are commonly used for the preparation of inorganic nanostructures. Ethylene glycol also has a reductive ability.

The microwave-assisted polyol method has been developed for the preparation of inorganic nanostructures such as metals, metal oxides and sulphides. Liu et al. [2] reported the synthesis of spherical metal nanoparticles by the microwave-polyol method. In summary, the heating mechanism of the microwaves is different from the conventional heating. Unlike other heating methods the microwave heating has remarkable advantages such a) higher temperature inside the product than on its surface, b) due to the heating of the material throughout the whole volume the high uniformity of warming is reached as well as more precise temperature regulation, c) shorter reaction time and higher yield of the product and we should point that d) overheating of certain parts (to the overcritical damaging temperature) of the product can be better prevented this way [3].

In the present work the electrocatalysts' preparation procedure was the following: A certain amount of $PdCl_2$/ethyl glycol (EG) or/and second metal salt/EG solution were well mixed with EG in ultrasonic bath, and then carbon powder was added into the solution according to the pre-calculated metal loading. After stirring, 2.0 mol L^{-1} NaOH/EG was added into the solution to adjust the pH value of the above mixture to be more than 12. After further stirring for another 1h, the slurry was pulse microwave heated for several times in a 10s-on/10s-off pulse form and then re-acidified with hydrochloric acid. The

pulse-microwave procedure was adopted in order to avoid the agglomeration of the metal particles at high temperatures. This is due to the fact that continuous microwave can easily cause a quite rapid heating rate for carbon materials. In this process, EG acts not only as dispersant and reducing agent, but also as the microwave additive due to the fact that the dielectric constant (41.4 at 25 °C) and dielectric loss for ethylene glycol are high, and consequently rapid heating takes place under the microwave radiation. The support, carbon (Vulcan XC-72R, Cabot Corp.) is also a microwave-sensitive material, which is believed to play an important role in the acceleration of the metal reduction. Hydrochloric acid was added into the above dispersion system as the sedimentation promoter to accelerate the adsorption of the suspended Pt nanoparticles onto the carbon support. The obtained black solid sample was washed by hot deionized water and dried in a vacuum oven at 80°C for 12 h.

3.2 Physical characterization for Catalyst Activity Evaluation

3.2.1 Transmission Electron Microscopy (TEM) characterization

Transmission electron microscope (TEM) is one of the most powerful techniques to characterize materials with nanometer-scale features. TEM is a tool for exploring the micro- and the nano-world and it can provide information from micron sizes down to atomic scale. It provides a wide range of different imaging modes with the ability to provide information on elemental composition and electronic structure at the ultimate sensitivity, that of a single atom. The TEM uses a high energy electron beam transmitted through a very thin sample (< 50nm) to image and analyze the structure of materials. TEM comprises a variety of methods:

- **Bright Field (BF)/Dark Field (DF)** methods can provide information about size and morphology of particles, can detect crystalline areas, defects, grain boundaries and phases.

- **Electron Diffraction (ED)** is applied to obtain crystallographic information such as lattice parameters, crystal symmetry and orientation.

- **High Resolution Transmission Electron Microscopy (HRTEM)** allows lattice fringe imaging, that can be directly related to the structure (interpretation has to be confirmed by image simulation) and visualization of defects and interfaces at atomic scale resolutions.

TEM enable identification and classification of aggregates, which may include protofibrils, amyloid fibrils containing varying numbers of strands, and amorphous aggregates. In contrast, methods used to quantify fibril production, such as thioflavin-T binding, light scattering, Fourier transform infrared spectroscopy, and circular dichroism spectroscopy, cannot discriminate among different types of β-sheet rich species. Nevertheless, TEM imaging provides no quantitative information about aggregation kinetics or about the concentrations of the observed fibrils. In addition, rare species or aggregates that do not stick to the TEM grids may not be detected. Therefore, TEM can confirm the presence of a particular type of aggregate, but it cannot prove that a type is disallowed.

3.2.2 Basic principles of transmission electron microscopy

The TEM operates on the same basic principles as the light microscope but uses electrons instead of light. Because the wavelength of electrons is much smaller than that of light, the optimal resolution attainable for TEM images is many orders of magnitude better than that from a light microscope. However, in TEM, the transmission of electron beam is highly dependent on the properties of material being examined. Such properties include density, composition, etc. For example, porous material will allow more electrons to pass through while dense material will allow less. As a result, a specimen with a non-uniform density can be examined by this technique. Whatever part is transmitted is projected onto a phosphor screen for the user to see [4].

Working principle

TEM works like a slide projector. A projector shines a beam of light which transmits through the slide. The patterns painted on the slide only allow certain parts of the light beam to pass through. Thus the transmitted beam replicates the patterns on the slide, forming an enlarged image of the slide when falling on the screen.

3.2.3 X-Ray Diffraction Technique

X-ray powder diffraction (XRD) is one of the most powerful techniques for qualitative and quantitative analysis of crystalline compounds. This provides information that cannot be obtained with any other way. The information that can be obtained includes types and nature of present crystalline phases, structural make-up of phases, degree of crystallinity, amount of amorphous content, microstrain and size and orientation of crystallites.

When a material (sample) is irradiated with a parallel beam of monochromatic X-rays, the atomic lattice of the sample acts as a three dimensional diffraction grating causing the X-ray beam to be diffracted to specific angles. The diffraction pattern, that includes position (angles) and intensities of the diffracted beam, provides much information about the sample.

In the present work the X-ray Diffraction (XRD) measurements were carried out by the aid of a D/Max-IIIA (Rigaku Co., Japan) employing Cu K$_\alpha$ ($\lambda = 0.15406$ nm) as the radiation source. The samples were scanned over the range $10° \leq 2\theta \leq 86°$. The peak at 68° (Pd 220) was used for the calculation of crystallites size using the Scherrer formula and Bragg equation [5]:

$$d=n\lambda/2\sin\theta \tag{3.1}$$

where λ is the X-ray wavelength ($\lambda = 1.5418$ Å) and θ is the angle of (111) peaks.

3.3 Electrochemical methods for Catalyst Activity Evaluation

3.3.1 Introduction

Since a fuel cell is an electrochemical device, electrochemical methods are playing roles in characterizing and evaluating the cell and its components such as the electrode, the membrane and the catalyst. The most popular electrochemical characterization methods include potential step, potential sweep, potential cycling, rotating disc electrode, rotating ring-disk electrode and impedance spectroscopy. Some techniques derived from these methods are also used for fuel cell characterization.

An electrochemical reaction involves at least the following steps: transport of the reactants to the surface of the electrode, adsorption of the reactants onto the surface of the electrode and transport of the product(s) from the surface of the electrode. The purpose of the electrochemical characterizations is to determine the details of these steps [6].

The electrochemical characterizations are carried out in various electrochemical cells. There are typically three types of cells: conventional 3-electrode cells, half-cells, and single cells. In those cells, the entity (e.g., catalyst, electrode) to be characterized forms the working electrode, the potential of which or the current passing through which is controlled or monitored. What happens on the working electrode is the sole interest of the investigation. The working electrode and another electrode, called the counter electrode, form a circuit, and the current flowing through this circuit will cause some reaction on the counter electrode as well. However, the investigation has no interest in what happens on the counter electrode, except that the reaction occurring on it should not interfere with the working electrode.

In order to minimize the impact of the solution (or electrolyte) resistance on the potential of the working electrode, a reference electrode is often used to form another circuit with the working electrode. Ideally, this electrode is non-polarizable and maintains a stable potential. There is high input impedance in the voltage measurement equipment, which makes the

current flowing in this circuit very small. Therefore, the impact of the uncompensated electrolyte resistance on the potential of the working electrode is minimized [6].

In the following section is described a brief introduction to techniques, principles and instrumentation. The illustration is limited to low- to medium temperature fuel cells such as the proton exchange membrane (PEM). All electrochemical techniques involve the use of electricity as either an input or an output signal. The function of an electrochemical instrument is to generate an input electrical signal and to measure the corresponding output electrical signal. More details will be given in the discussion below of different types of electrochemical techniques.

3.3.2 Conventional 3-Electrode Cells or Cyclic Voltammetry

Cyclic voltammetry is the most widely used technique for acquiring qualitative information about electrochemical reactions. Cyclic Voltammetry (CV) is an electrochemical technique which measures the current that develops in an electrochemical cell under conditions where voltage is in excess of that predicted by the Nerst equation. CV is performed by cycling the potential of a working electrode, and measuring the resulting current.

3.3.3 The electrochemical Cell

A typical cell design for a cyclic voltammetric experiment is shown in Fig.1. The simplest approach is merely to have the three electrodes immersed in the solution very close. The Luggin capillary further isolates the reference solution from the cell solution. At the outset of the experiment the cell contains solvent, electrolyte, one or more principal electroactive species and possibly added reagents that will undergo reactions with the electrolytic products. Before the experiment, it is necessary to remove dissolved

oxygen, which has a cathodic signal that can interfere with the observed current response. This is normally done by purging the solution with an inert gas such as N_2 or Ar.

The exposed surface of an electronically conducting disk such as glassy carbon, gold, or platinum sealed in an inert material such as glass is the working electrode. A piece of Pt coil or sheet with a surface area much larger than that of the working electrode is used as the counter electrode. The purpose of a larger counter electrode is to assure that the electrochemical reaction occurring on it is fast enough so that it does not impede the electrochemical reaction occurring on the working electrode. The potential of the working electrode is measured against a reference electrode which maintains a constant potential and the resulting applied potential produces an excitation signal. Figure 3.1 depicts the basic structure of a conventional CV.
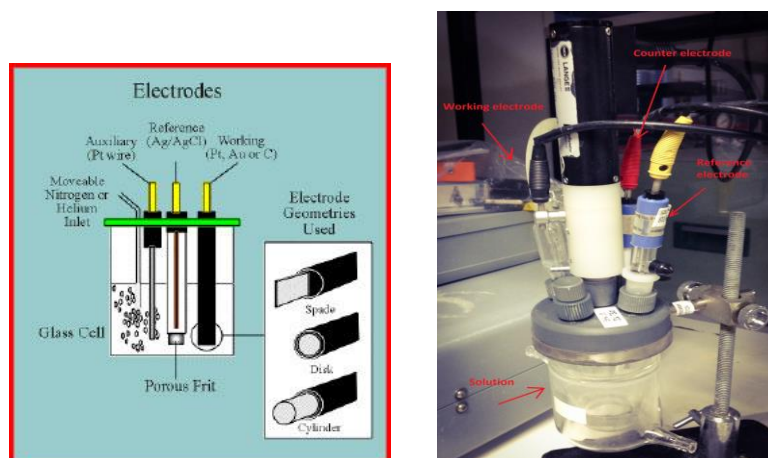

Figure 3.1: Basic structure of cyclic voltammetry.

3.3.4 Experimental apparatus

A typical experimental apparatus contains the electrolyte in a single compartment into all three electrodes are inserted. The electrolytic current (I) flows through the electrolyte between the working (W) and counter (C) electrodes in response to the potential of the working electrode (Figure 2). The electrode potential of interest (E) is that between W and the reference electrode (R). The instrument which controls the E is the potentiostat.

The linear potential sweep is relayed to the potentiostat by a function generator and the waveform shown is a single cycle CV.
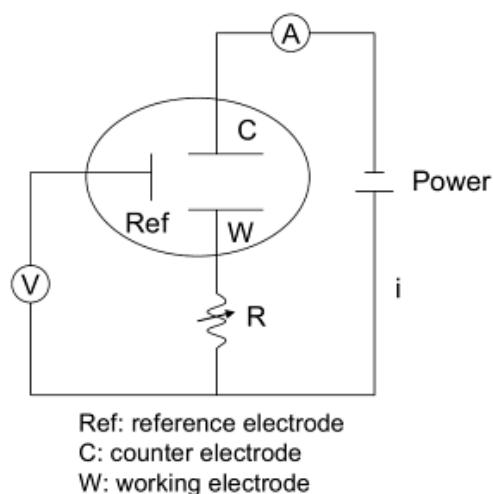

Ref: reference electrode
C: counter electrode
W: working electrode

Figure 3.2: Illustration of the basic circuitry of a potentiostat [6].

A resistance in the electric circuit is used to adjust and maintain the potential of the working electrode. For example, in order to keep the potential of the working electrode constant during a potential step measurement that involves changing current, the resistance (R) of the resistors will be varied so that the voltage drop (iR) on the resistor is the same.

A potentiostat measures the voltage difference between the reference and the working electrode. A potentiostat has extremely high input impedance so that the input current is nearly zero, which enables the reference electrode to keep a constant potential. The current passing through the working and the counter electrodes is determined by measuring the voltage drop through a known resistor according to Ohm's law. When the electronic circuit is slightly modified so that the current is controlled and the corresponding potential of the working electrode is measured, it becomes a galvanostat [6].

Electron transfer plays a fundamental role in governing the pathway of chemical reactions. Yet the speed and size of the electron mean that tracing its movement is difficult using tradition methods such as spectroscopy and synthetic chemistry. Consequently our knowledge of the driving force for many reactions remains elusive.

Electrochemical methods offer the potential to investigate these processes directly by the detection of the electrons involved.

Cyclic voltammetry refers to cycling the potential between a low and high potential value and recording the current in the potential cycling region. The resulting potential versus current plot is called a voltammogram. The sweeping of the potential is carried out linearly, and the sweeping rate can be controlled in a wide range. Most studies are carried out with a potential scanning rate between 1 and 1000 mV s^{-1}. Before the scanning starts, the working electrode is usually held at a potential that does not cause any electrochemical reactions. After the start of the scanning, the potential goes higher (or lower), and when it becomes high (or low) enough to cause the oxidation (or reduction) of an electrochemically active species, an anodic (or cathodic) current appears. The anodic (or cathodic) current increases as the potential increases (or decreases) because the reaction kinetics becomes faster.

A typical electrode reaction involves the transfer of charge between an electrode and a species in solution. The electrode reaction usually referred to as electrolysis, typically involves a series of steps (Figure 3):

Figure 3.3: An electrode reaction

a) Reactant (O) moves to the interface: this is termed mass transport.

b) Electron transfer can then occur via quantum mechanical tunneling between the electrode and reactant close to the electrode (typical tunneling distances are less than 2 nm)

c) The product (R) moves away from the electrode to allow fresh reactant to the surface.

The above electrode steps can also be complicated by:

1) The applied voltage on the electrode. 2) The reactivity of the species. 3) The nature of the electrode surface. 4) The structure of the interfacial region over which the electron transfer occurs.

A typical cyclic voltammogram recorded for a reversible single electrode transfer reaction is shown below. The solution contains only a single electrochemical reactant
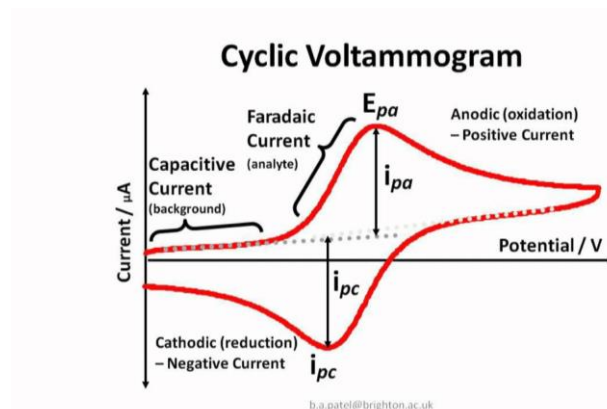

Figure 3.4: A typical cyclic voltammogram for a reversible reaction.

During this reversed potential scan the oxidized (or reduced) form of the electrochemically active species reacts and develops a cathodic (or anodic) peak. The cathodic (anodic) peak is located at a slightly lower (higher) potential than the anodic (cathodic) peak. The cathodic and anodic peaks are of equal height (or, more accurately, equal area), unless there are complications caused by some side chemical or electrochemical processes (Figure 3.4).

Although cyclic voltammetry is very widely used for the initial redox characterization of a molecule (i.e., the redox potentials, and the stability of the different oxidations states) and for qualitative investigation of chemical reactions that accompany electron transfer, there are a number of disadvantages inherent in this technique:

- The effects of slow heterogeneous electron transfer and chemical reactions cannot be separated. If both of these effects are present, then the rate constants for these processes can only be calculated using simulation methods.

- There is a background charging current throughout the experiment of magnitude vC_{dl} (where vC_{dl} is the capacitance of the interface at the working electrode). This restricts the detection limit to about 10^{-5} M. In addition, the ratio of the peak faradaic current to the charging current decreases with increasing n (since i_p is proportional to $v^{1/2}$), and this places an upper limit on the value of n that can be used

In spite of these limitations, cyclic voltammetry is very well suited for a wide range of applications. Indeed, in some areas of research, cyclic voltammetry is one of the standard techniques used for characterization.

3.3.5 Rotating disk electrode technique (RDE)

Hydrodynamic devices use convection to enhance the rate of mass transport to the electrode and can offer advantages over techniques which operate in stagnant solution. The addition of convection to the cell usually results in increased current and sensitivity in comparison to voltammetric measurements performed in stagnant solution. Also the introduction of convection (usually in a manner that is predictable) helps to remove the small random contribution from natural convection which can complicate measurements performed in stagnant solution. Finally, it is possible to vary the rate of reaction at the electrode surface by altering the convection rate in the solution and this can be usefully exploited in mechanistic analysis and electroanalytical applications. In the discussion below a range of traditional and recent developments in the field of hydrodynamic techniques and their potential applications are outlined.

In Figure 3.5 is depicted the rotating disk electrode equipment. In this arrangement solution is brought to the surface by a Teflon disc which rotates in solution. The working electrode (glassy carbon) is embedded in the top face of the Teflon shield.
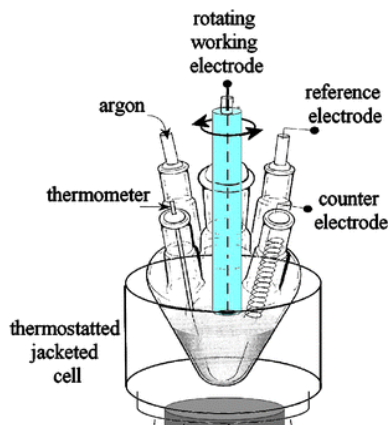
Figure 3.5: Rotating disk electrode equipment. Reprinted from Ref.[7].

When operated at rotation speeds of around 60 Hz (cycles per second) the flow profile to the electrode is laminar and so can be predicted mathematically. The figure below (Fig.3.6) shows the type of flow profile that is developed when a circular object is rotated in solution and how this brings fresh reactant to the surface.
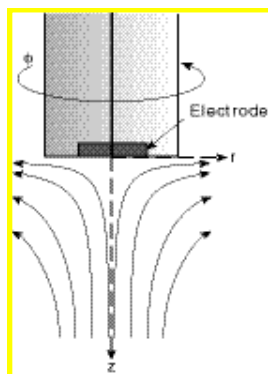

Figure 3.6: Scheme of the flow on working electrode surface. Reprinted from Ref. [8].

A typical voltammetric measurement used with the rotating disc and other hydrodynamic systems is linear sweep voltammetry. The Figure 3.7 shows a set of current voltage curves recorded for a reversible on electron transfer reaction and different rotation speeds. The scan rate used was 1 mV s^{-1} (compared to perhaps 20 mV s^{-1} for conventional cyclic voltammetry) and as can be seen the total current flowing depends upon the rotation speed used.
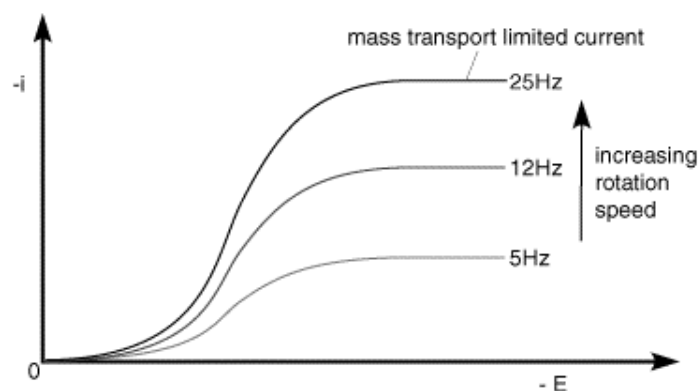
Figure 3.7: Linear sweep voltammetric measurement with RDE. Reprinted from Ref.[8].

This can be understood by returning to the concept of the 'diffusion layer' thickness controlling the flux of material to the surface. As the rotation speed is increased the distance that material can diffuse from the surface before being removed by convection is decreased. This results in a higher flux of material to the surface at higher rotation speeds. The mass transport limited current arises from the fact that the system reaches a steady state and so the current reaches a plateau once the equilibrium at the surface is driven to the products side.

3.3.6 Electro-kinetic analysis

As it is well known, during a reaction the kinetic current density (i_k) is a measure of the rate of charge transfer on the catalyst's surface. More precisely, i_k describes the real kinetics of an electrocatalytic reaction and therefore is directly related to the activity of an electrocatalyst. To determine the catalytic activity of the electrocatalysts, we adopted the Koutecky–Levich analysis where the kinetic current is related to the rotational velocity of the RDE through the following equation:

$$\frac{1}{i} = \frac{1}{i_k} + \frac{1}{i_d}$$

(3.2)

where i is the measured current density, i_k the kinetic current in the absence of mass transfer limitations and i_d the limiting diffusion current density. A plot of i^{-1} vs $\omega^{-1/2}$ at different potentials should be yield straight and parallel lines with intercepts corresponding to the inverse of the real kinetic current. The i_d can be calculated according to the Levich equation:

$$i_d = 0.62nFD^{2/3}v^{-1/6}C\omega^{1/2}$$
(3.3)

Where n is the overall electron transfer number, F the Faraday constant (95485 C/mol), D the diffusion coefficient of H_2 in H_2SO_4 (3.7×10^{-5} cm^2 s^{-1}), v the kinematic viscosity of the electrolyte and C the H_2 concentration in the electrolyte (7.14×10^{-7} mol cm^{-3}).

For RDE data analysis, three non-electrochemical kinetic parameters, such as the diffusion coefficient of H_2, the kinematic viscosity of the electrolyte solution, and the solubility of H_2 must be known accurately. These parameters are all temperature dependent. Their values are also slightly dependent on the electrolyte used.

3.3.7 Chronoamperometry (CA)

Chronoamperometry is an electrochemical technique in which the potential of the working electrode is stepped and the resulting current from faradic processes occurring at the electrode (caused by the potential step) is monitored as a function of time. The analysis of chronoamperometry (CA) data is based on the Cottrell equation, which defines the current-time dependence for linear diffusion control:

$$i = nFACD^{1/2}\pi t^{-1/2}$$
(3.4)

where: n = number of electrons transferred/molecule

F = Faraday's constant (96,500 C mol^{-1})

A = electrode area (cm^2)

D = diffusion coefficient (cm^2 s^{-1})

C = concentration (mol cm^{-3})

At the beginning of the transient experiment the potential of the working electrode is held at Ei (Fig. 3.8a). At t=0 the potential is instantaneously changed to a new value E_1, and corresponding current time response is recorded as shown in Fig. 3.8.
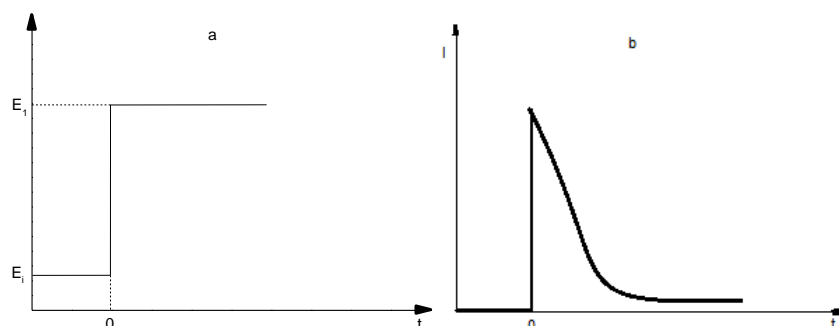

Figure 3.8: The chronoamperometric experiment. a) The potential-time profile applied during experiment, E_i is initial value and E_1 is the potential where no reduction of O occurs or some other potential of interest. b) The corresponding response of the current due to changes of the potential.

It is important, that such an analysis has to be applied over a broad time interval in order to ensure the reliability of results. At short times the current consists of a large non faradaic component due to charging of the double-layer capacitance. Hence, the typical time range of chronoamperometric measurements lies normally in the range from 0.001 to 10 s. However, there are a number of additional instrumental and experimental limitations. For example, current and voltage characteristics of a potentiostat can limit the current maximum and time resolution.

Even though the chronoamperometry is relatively simple technique, there are a number of difficulties, which are related to the interpretation of the current-transient curve. Hence, it is very important to find the possibility of comparative analysis of the chronoamperometric results with the results of cyclic voltammetry and other techniques. This type of comparison will also help to understand the studied system more completely and with better precision.

3.4 Fuel cell system

3.4.1 Experimental apparatus

Figure 3.9 depicts the flowchart of the system of electrochemical measurements of an array anode / electrolyte / cathode. Hydrogen is fed to the anode and oxygen to the cathode. The flows supply controlled by digital mass flowmeters (Brooks Instruments). For safety reasons, shortly after leaving flowmeters hydrogen and oxygen two way valves on / off are mounted in order to control the flow. Thereafter the flows (hydrogen+oxygen) entering the saturator humidity, wherein reactant gases are enriched in water vapor and routed to the fuel cell (Figure 3.9).
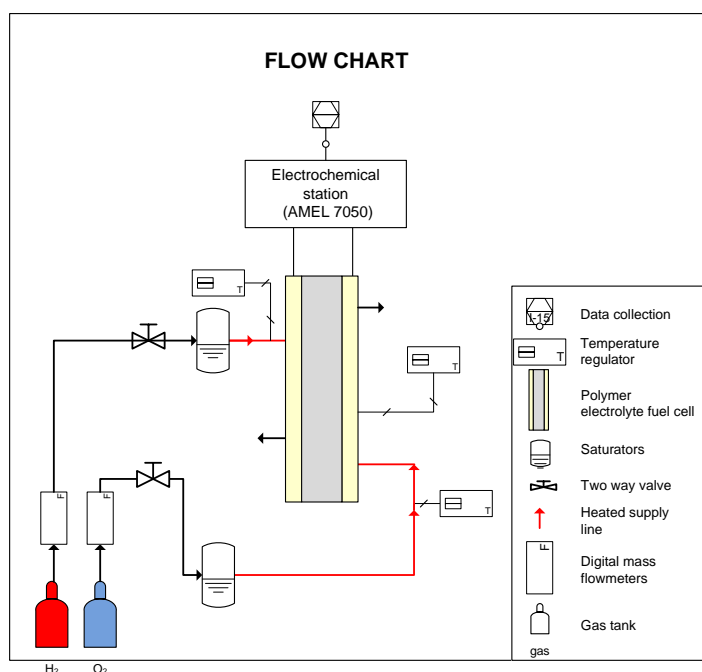

FLOW CHART

Electrochemical station (AMEL 7050)

Data collection
Temperature regulator
Polymer electrolyte fuel cell
Saturators
Two way valve
Heated supply line
Digital mass flowmeters
Gas tank
gas

H₂   O₂

Figure 3.9: Flow chart system

Gaseous reactants need to be enriched in vapor before entering the fuel cell so that the membrane is hydtrate. From the output of the saturation until entering the anode and the cathode of fuel cell supply lines are heated. The temperature of the certain lines must not have large deviation (± 5°C) compared with the temperature of the fuel cell, otherwise large deviation can cause condensation of water vapor within the cell resulting flooding phenomena.

Between each analysis the MEA was allowed to rest for 30 minutes under the OC condition. At the end of this characterization sequence, the first cycle was considered concluded. The procedure was then repeated for a new cycle until almost steady state PEMFC performance was reached. The test was carried out at atmospheric pressure.

It should be pointed out that during the electrochemical experiments, the cell was gradually activated. However, the obtained values from each experimental electrochemical technique give us a good idea about the performance history along the activation procedure.

3.4.2 Polarization Curve

A plot of cell potential against current density under a set of constant operating conditions, known as a polarization curve, is the standard electrochemical technique for characterizing the performance of fuel cells (both single cells and stacks). It yields information on the performance losses in the cell or stack under operating conditions [9]. A steady-state polarization curve can be obtained by recording the current as a function of cell potential or recording the cell potential as the cell current changes. A non-steady-state polarization curve can be obtained using a rapid current sweep. By measuring polarization curves, certain parameters such as the effects of the composition, flow rate, temperature, and RH of the reactant gases on cell performance can be characterized and compared systematically. A sample polarization curve is shown in Figure 3.10. Very often, polarization curves are converted to power density versus current density plots by multiplying the potential by the current density at each point of the curve, also seen in Figure 3.10. Polarization curves provide information on the performance of the cell or stack as a whole. While they are useful indicators of overall performance under specific operating conditions, they fail to produce much information about the performance of individual components within the cell.
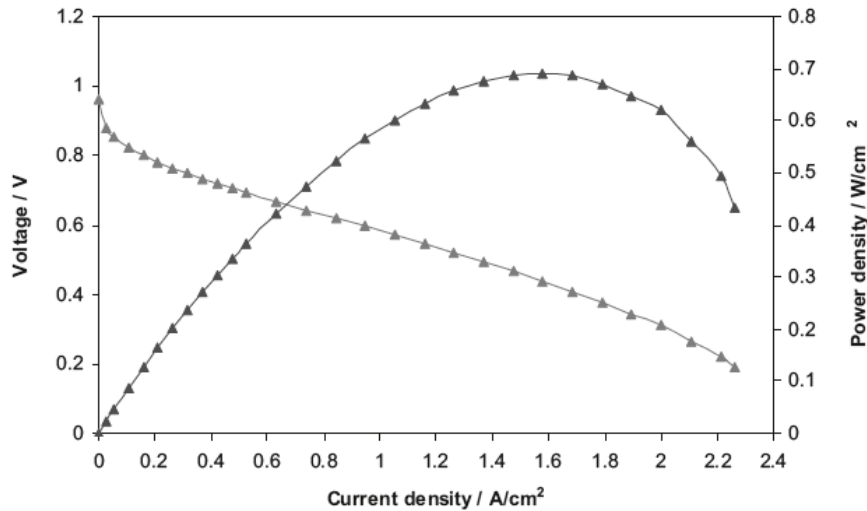
Figure 3.10: A sample fuel cell polarization curve obtained from the diagnostic modeling PEM fuel cell.

They cannot be obtained during normal operation of a fuel cell and take significant time. In addition, they fail to differentiate different mechanisms; for example, flooding and drying inside a fuel cell cannot be distinguished in a single polarization curve. They are also incapable of resolving time-dependent processes occurring in the fuel cell and the stack. For the latter purpose, current interrupt, EIS measurements, and other electrochemical approaches are preferred. These techniques will be introduced in the following sections.

3.4.3 Voltage Loss

The fuel cell voltage losses are classified into three categories: the activation loss (activation polarization), the ohmic loss (ohmic polarization), and the concentration loss (concentration polarization). Plots of voltage drops caused by each of the losses are shown in Figure 3.11. At low current densities (the region of activation polarization), the cell potential drops sharply and the majority of these losses are due to the sluggish kinetics of the ORR. At intermediate current densities (the region of ohmic polarization), the voltage loss caused by ohmic resistance becomes significant and results mainly from resistance to the flow of ions in the electrolyte and resistance to the flow of electrons

through the electrode. In this region, the cell potential decreases nearly linearly with current density, while the activation overpotential reaches a relatively constant value. At high current densities (the region of concentration polarization), mass transport effects dominate due to the transport limit of the reactant gas through the pore structure of the GDLs and electrocatalyst layers, and cell performance drops drastically.
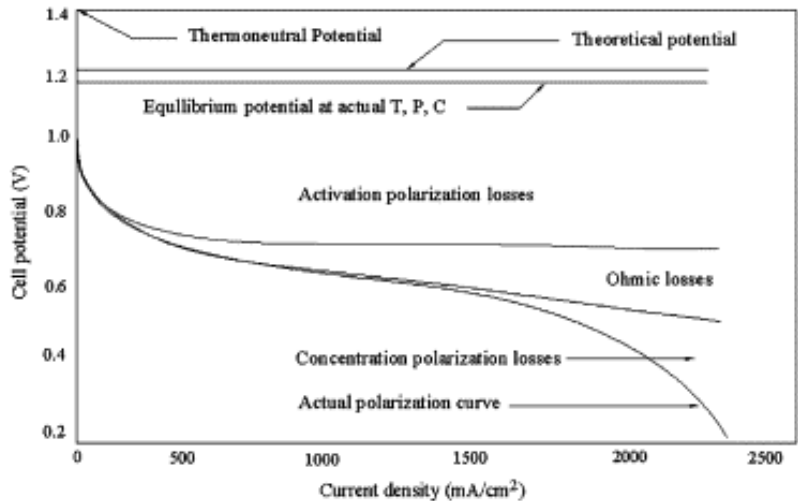

Figure 3.11: Schematic of an ideal polarization curve with the corresponding regions and overpotentials.

The output voltage of a single cell, E_{cell}, can be defined as follows:

$$E_{cell} = E_{OCV} - \Delta E_{act} - \Delta E_{ohmic} \; \Delta E_{con}$$

where E_{cell} is the voltage for a certain operating condition, E_{OCV} represents the fuel cell OCV, ΔE_{act} is the voltage drop associated with the activation of the anode and of the cathode, ΔE_{ohmic} is the ohmic voltage drop associated with the conduction of protons and electrons, and ΔE_{con} is the voltage drop resulting from the decrease in the concentration of oxygen and hydrogen.

3.4.4 Impedance spectroscopy

Electrochemical Impedance spectroscopy (EIS) appears destined to play an important role in fundamental and applied electrochemistry and materials science in the coming years. In a number of respects it is the method of choice for characterizing the electrical

behavior of systems in which the overall system behavior is determined by a number of strongly coupled processes, each proceeding at a different rate [10].

The classical electrochemical techniques present measurements of currents, electrical charges or electrode potentials as functions of time. In contrast, EIS presents the signal as a function of frequency at a constant potential. In spectroscopy, we used to think in terms of the frequency domain (wave number, frequency or some related functions as wavelength) [11].

The advantages of using EIS are numerous. First of all, it provides a lot of useful information that can be further analyzed. In practical applications of cyclic voltammetry, simple information about peak currents and potentials is measured. These parameters contain very little information about the whole process especially when hardware and software is able sampling the current-potential curve producing thousands of experimental points every fraction of mV. EIS contains analyzable information at each frequency [11].

3.4.5 Instrumentation and measurement basics

During an impedance measurement, a frequency response analyzer (FRA) is used to impose a small amplitude AC signal to the fuel cell via the load (Figure 10). The AC voltage and current response of the fuel cell is analyzed by the FRA to determine the resistive, capacitive and inductive behavior - the impedance - of the cell at that particular frequency. Physicochemical processes occurring within the cell – electron & ion transport, gas & solid phase reactant transport, heterogeneous reactions, etc. – have different characteristic time-constants and therefore are exhibited at different AC frequencies. When conducted over a broad range of frequencies, impedance spectroscopy can be used to identify and quantify the impedance associated with these various processes [12].
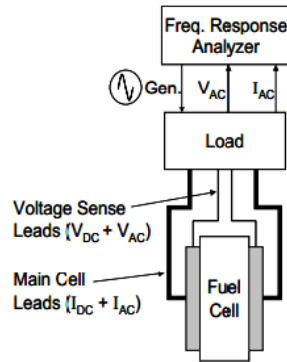
Figure 3.12: Instrumentation for EIS of fuel cells.

Advantages of EIS:

- Measurements can be made under real-world fuel cell operating conditions, e.g., open circuit voltage or under load (DC voltage or current).

- Multiple parameters can be determined from a single experiment.

- Relatively simple electrical measurement that can be automated.

- Can verify reaction models, and characterize bulk and interfacial properties of the system, e.g., membrane resistance and electrocatalysts.

- Measurement is non-intrusive – does not substantially remove or disturb the system from its operating condition.

- A high precision measurement – the data signal can be averaged over time to improve the signal-to-noise ratio.

3.4.6 Equivalent Circuit Modeling

Equivalent circuit modeling of EIS data is used to extract physically meaningful properties of the electrochemical system by modeling the impedance data in terms of an electrical circuit composed of ideal resistors (R), capacitors (C), and inductors (L). Because we are dealing with real systems that do not necessarily behave ideally with processes that occur distributed in time and space, we often use specialized circuit elements. These include the generalized constant phase element (CPE) and Warburg element (ZW). The Warburg element is used to represent the diffusion or mass transport impedances of the cell. An example of a generalized equivalent circuit element for a single cell fuel cell is shown below.
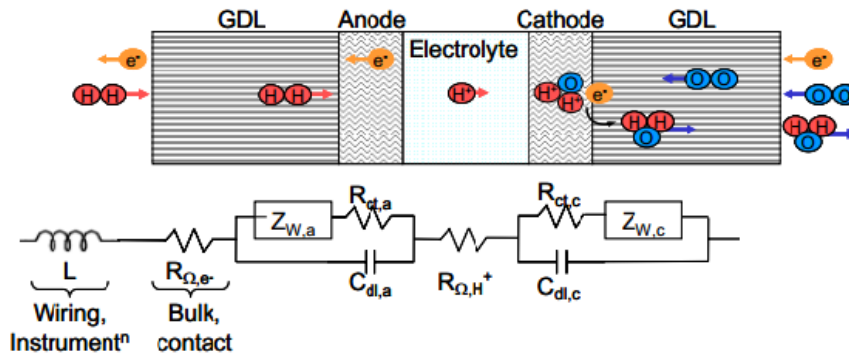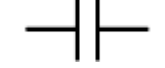
Figure 3.13: Equivalent circuit element for a single cell fuel cell.

In the equivalent circuit analog, resistors represent conductive pathways for ion and electron transfer. As such, they represent the bulk resistance of a material to charge transport such as the resistance of the electrolyte to ion transport or the resistance of a conductor to electron transport. Resistors are also used to represent the resistance to the charge-transfer process at the electrode surface. Capacitors and inductors are associated with space-charge polarization regions, such as the electrochemical double layer, and adsorption/desorption processes at an electrode, respectively.

The defining relation and impedance for ideal bulk electrical elements are shown below.

Resistor	—⋀⋀⋀—	$V = I \times R$	$Z_R = R$
Capacitor	—┤├—	$I = C\dfrac{dV}{dt}$	$Z_C = \dfrac{1}{j\omega C} = -\dfrac{j}{\omega C}$
Inductor	—◠◠◠—	$V = L\dfrac{dI}{dt}$	$Z_L = j\omega L$

3.4.7 Representation of Impedance Data

EIS data for electrochemical cells such as fuel cells are most often represented in Nyquist and Bode plots as shown in Figure 12. Bode plots refer to representation of the impedance magnitude (or the real or imaginary components of the impedance) and phase angle as a function of frequency. Because both the impedance and the frequency often

span orders of magnitude, they are frequently plotted on a logarithmic scale. Bode plots explicitly show the frequency-dependence of the impedance of the device under test.
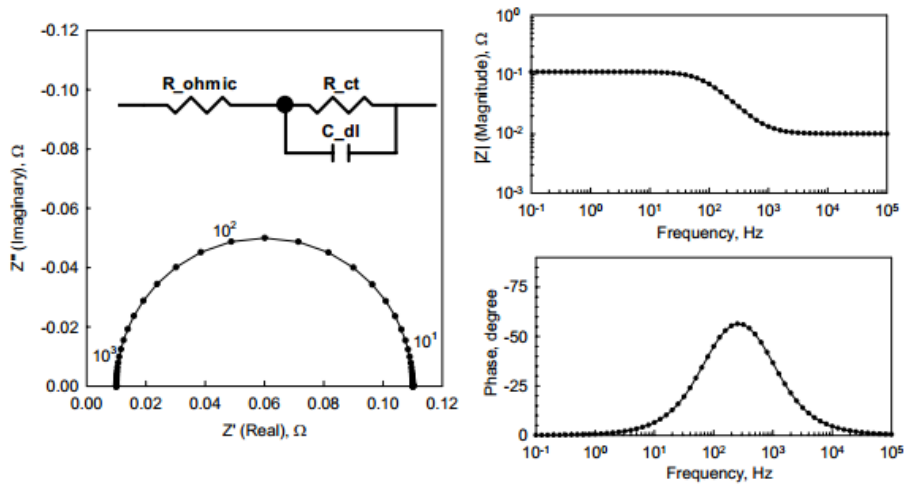

Figure 3.14: Impedance plots for the indicated simple RC circuit where R_{ohmic} = 0.01 Ω, R_{ct} = 0.1 Ω and C_{dl} =0.02 F.

The Nyquist plot is the most usual way of presenting the impedance spectrum. In the imaginary part of the impedance (mostly presented with the negative sign) is plotted against the real part. The plot normally contains of two or more semicircles in different frequency ranges. Although the Nyquist plot is the most common representation in the EIS measurement technique, Bode magnitude (magnitude vs. frequency) and phase (phase vs. frequency) plots have also been used in the past to extract information that cannot be readily obtained from the Nyquist plot. For instance, the local maximum values in the Bode phase plot show the characteristic frequencies which are proportional to the time constants of the processes [13].

References

[1]   S. Song, Y. Wang, P.K. Shen. Journal of Power Sources 170 (2007) 46-49.

[2]   W. Yu, W. Tu, H. Liu. Langmuir 15 (1998) 6-9.

[3]   D.A. Jones, T.P. Lelyveld, S.D. Mavrofidis, S.W. Kingman, N.J. Miles. Resources, Conservation and Recycling 34 (2002) 75-90.

[4]   Atomic World, in: http://www.hk-phy.org/atomic_world/tem/tem02_e.html (Ed.).

[5]   F. Zhu, G. Ma, Z. Bai, R. Hang, B. Tang, Z. Zhang, X. Wang. Journal of Power Sources 242 (2013) 610-620.

[6]   W. Pan, X. Zhang, H. Ma, J. Zhang. The Journal of Physical Chemistry C 112 (2008) 2456-2461.

[7]   A. Vuorema, P. John, A.T. Jenkins, F. Marken. J Solid State Electrochem 10 (2006) 865-871.

[8]   U.o. Cambridge, Department of Chemical Engineering and Biotechnology, http://www.ceb.cam.ac.uk/research/groups/rg-eme/teaching-notes/hydrodynamic-voltammetry.

[9]   J. Wu, X.Z. Yuan, H. Wang, M. Blanco, J.J. Martin, J. Zhang. International Journal of Hydrogen Energy 33 (2008) 1735-1746.

[10]   Evgenij Barsoukov, J.R. Macdonald, Impedance Spectroscopy: Theory, Experiment, and Applications, Wiley, April 2005.

[11]   A. Lasia, Electrochemical Impedance Spectroscopy and Its Applications, Springer, 2014.

[12]   T.E. Springer, T.A. Zawodzinski, M.S. Wilson, S. Gottesfeld. Journal of The Electrochemical Society 143 (1996) 587-599.

[13]   S.M. Rezaei Niya, M. Hoorfar. Journal of Power Sources 240 (2013) 281-293.

Electrocatalytic Activity of Vulcan Supported Pd, Rh and Pd_xRh_y towards HOR and ORR*

Abstract

Carbon-supported (Vulcan XC-72) Pd, Rh, and Pd_xRh_y (20wt.%, x:y=1:1, 3:1, 1:3) electrocatalysts are prepared according a modified pulse-microwave assisted polyol synthesis method and their electrocatalytic activity towards *hydrogen electrooxidation* (HOR) and *oxygen reduction* (ORR) reactions is investigated.

The as-prepared electrocatalysts are physicochemically characterized by Transmission Electron Microscopy (TEM) and X-ray diffraction (XRD). Their electrochemical characterization is carried out by the aid of Cyclic Voltammetry (CV), Rotating Disk Electrode (RDE) and Chronoamperometry (CA) techniques.

It is found that among the as-prepared catalysts, $PdRh_3$ exhibits the highest HOR (i_k=7.6 mA cm^{-2}) and ORR (i_k=5.20 mA cm^{-2}) electrocatalytic activity.

It is also found that the addition even of small amount of Rh (Pd_3Rh-2.7μg cm^{-2}) enhances both Pd's HOR and ORR electrocatalytic activity by 33% and by 53%, respectively.

For the as prepared electrocatalysts, the HOR activity order, in terms of kinetic current density, is found to be as follows: $PdRh_3 \approx PdRh > Rh > Pd_3Rh > Pd$, while a similar trend was found for ORR activity: $PdRh_3 > PdRh > Rh > Pd_3Rh > Pd$.

Contents

List of Figures

List of Tables

4.1 Introduction

Platinum based electrocatalysts, due to its excellent catalytic activity, still remains the most commonly used for both the hydrogen oxidation and oxygen reduction reactions. However, the high cost and the limited resources of platinum are among the main factors that still hinder the commercialization of fuel cells, increasing at the same time the interest of the scientific community towards the exploration of Pt-free electrocatalysts. The last decade, a severe number of research groups world-widely have focused on the investigation of electrocatalysts with small amount or without Pt, for both the hydrogen oxidation reaction (HOR) and the oxygen reduction reaction (ORR) [1-9].

The aforementioned research and development has shot either to commonly-adopted materials, which provide enhanced Pt's utilization coefficient and consequently use of lower content of it, or to Pt-based electrocatalysts with ultra-low-Pt loading [10-12]. A great number of studies have also been devoted to the investigation of Pt combination with another metal such as Pd [13-17], Ru[18, 19], Sn [20], W [20], Au [21], Mo [22], etc.

With the exception of Pt, it has been demonstrated that among pure metals, Pd exhibits relatively high electrocatalytic activity towards both HOR and ORR. This fact combined with the relatively low cost of Pd, makes it an attractive and alternative candidate for the aforementioned reactions [7, 23-28]. However, the use of pure Pd, mostly in terms of electrocatalytic activity, has not totally and successfully replaced the role of Pt [9].

Consequently, to enhance HOR activity, various bi-metallic and tri-metallic Pd alloys such as Pd-Rh [29], Pd–Co [13, 30], Pd–Au [31-33], Pd–Mo [34], Pd–Pt–Ru [15] and Pd-Pt-Rh [35] have been investigated. Nevertheless, the basic electrochemistry of Pd–Rh based electrocatalysts has not been sufficiently explored and only few reports are available in literature [29, 36-38].

According to literature [23] Pd presents higher activity, than any other noble metal and comparable to that of Pt, not only for HOR but also for ORR. Active palladium-based alloys for the ORR in acid medium were presented for first time by Ota *et al.* [39, 40], attracting, nevertheless, less attention than Pt due to its lower activity and stability. However, very recently, Kondo *et al.* [41] proved that the ORR activity of the Pd depends on the orientation of the index plane. More precisely, they proved that the Pd's activity towards ORR has the following order: Pd(100)>>Pd(111)>Pd(110), with the Pd(100) exhibiting 14 times higher activity than Pt.

Except for the pure Pd's plane orientation, it has been shown that its activity can be enhanced by alloying it with a second or a third metal. Binary and ternary Pd–based alloys such as Pd-Ni [42-44], Pd-Cu [44, 45], Pd-Fe [44], Pd-Rh [46], Pd-Ti [47], Pd-Co-Mo [48] and Pd-Co-Au [47] exhibited better electrocatalytic activity for the ORR than pure Pd and in some other cases better than that of pure Pt. Even so, PdRh bi-metallic electrocatalysts have not been studied sufficiently for the oxygen reduction reaction.

In the present work, carbon supported (Vulcan-XC-72R) Pd_xRh_y (20wt%) bimetallic catalysts with different atomic ratios (x:y) were prepared via a modified pulse-microwave assisted polyol method. The as-prepared electrocatalysts were physicochemically characterized using TEM and XRD techniques. Moreover, their electrocatalytic activity towards HOR and ORR was evaluated by the aid of RDE and CV methods and their stability by the chronoamperometric measurement.

4.2   Experimental

4.2.1 Electrocatalysts preparation

The examined electrocatalysts were quickly and easily prepared via a modified pulse-microwave assisted polyol synthesis. In a beaker, the starting precursors ($PdCl_2 \cdot 2H_2O$ and

RhCl$_3$ provided by Strem Chemicals) were well mixed with ethylene glycol (EG) in an ultrasonic bath, and then XC-72R carbon black (Cabot Corporation) was added in the above mixture. After the adjustment of system's pH value to 13, by the drop-wise addition of 1.0 M NaOH/EG, a well-dispersed slurry was obtained with ultrasonic stirring for 60 min. Thereafter, the slurry was microwave-heated in the pulse form 10 s on/10 s off for several times. In order to promote the adsorption of the suspended metal nanoparticles onto the carbon support, hydrochloric acid was adopted as the sedimentation promoter and the solution was re-acidified to a pH value of about 2–4. The resulting black solid sample was filtered, washed and dried at 80°C for 10 h in a vacuum oven [49].

4.2.2 Physicochemical characterization

The X-ray Diffraction (XRD) measurements were carried out by the aid of a D/Max-IIIA (Rigaku Co., Japan) employing Cu Kα (λ = 0.15406 nm) as the radiation source. The samples were scanned in the range of $10° ≤ 2θ ≤ 86°$. Catalysts were also investigated by transmission electron microscopy (TEM) using a Philips CM12 microscope (resolution 0.2 nm), provided with high resolution camera, at an accelerating voltage of 120 kV. Suitable specimens for TEM analyses were prepared by ultrasonic dispersion in i-propylic alcohol adding a drop of the resultant suspension onto a holey carbon supported copper grid. To prevent the agglomeration of carbon supports, the prepared catalyst was diluted in ethanol using ultrasonic water bath for some minutes and dried before TEM analysis.

4.2.3 Electrochemical characterization

All electrochemical measurements were conducted in an electrochemical workstation AMEL 5000 adopting a saturated calomel electrode (SCE) and a Pt wire as reference and counter electrodes, respectively. Cyclic Voltammetry (CV) and Rotating Disc Electrode (RDE) measurements carried out, on a thin film catalyst deposited on a glassy carbon (GC)

disc electrode (working electrode, Ø = 3.0 mm) mounted in an interchangeable RDE holder, into 0.5M H_2SO_4 solution (Carlo Erba, 99%) at room temperature. The electrocatalytic ink was prepared by mixing 1.95 mg of electrocatalyst, 1.8 mL ethanol and 0.2 mL Nafion solution (5 wt%, IonPower, GmbH). Then, the as-prepared ink quantitatively (4 μL) was transferred onto the surface of the GC electrode and was dried to obtain a thin porous layer. For all measurements, the catalyst total loading was maintained at 11 μg cm^{-2}. Before each measurement the solution was deaerated with helium stream for 20 min. Then, hydrogen (or oxygen) gas was supplied until a saturated solution was created. During the experiments the helium (or hydrogen or oxygen) stream was directed above the solution level in order to avoid contact with air as well as keep saturated the solution (inert in case of helium). Before the voltammograms being reproducible, several scans were obtained.

4.3 Results and discussion

4.2.1 Physicochemical measurements

XRD patterns of the as-prepared electrocatalysts are shown in Fig. 4.1. The first peak at 25° is associated with the Vulcan XC-72 support material for all the five samples. The four diffraction peaks appeared at ca. 40°, 48°, 68° and 83° belong to the face-centered cubic (fcc) crystalline Pd and Rh (1 1 1), (2 0 0), (2 2 0), (3 1 1), respectively. As it can be observed there is a peak shift toward higher 2θ values for higher Rh contents, revealing decreased lattice parameters and the high level of alloying. The (1 1 1), plane has the largest intensity among the others planes, which grows with respect to the corresponding peak of the Pd and Rh catalysts, indicating the effect of increased amounts of Rh in the Pd_xRh_x. In Table 4.1 the average lattice parameters and crystallite size values are reported. The above-two parameters were estimated according to Scherrer's equation [50].

As it can be seen, Pd/C has the highest lattice parameter (0.38615 nm) and crystallite size (3.0 nm), while the Rh/C the lowest one (lattice parameter: 0.38456 nm, crystallite size: 2.0 nm). The formed Pd-Rh alloys seem to present lattice parameter values between of the two pure metals, with the following order: PdRh(3:1)/C > PdRh(1:3)/C > PdRh(1:1)/C. Thus, the addition of Rh contracts the lattice parameter of Pd, decreasing also its crystallite size. This modification to the lattice parameter, may affect the hydrogen adsorption properties [35].
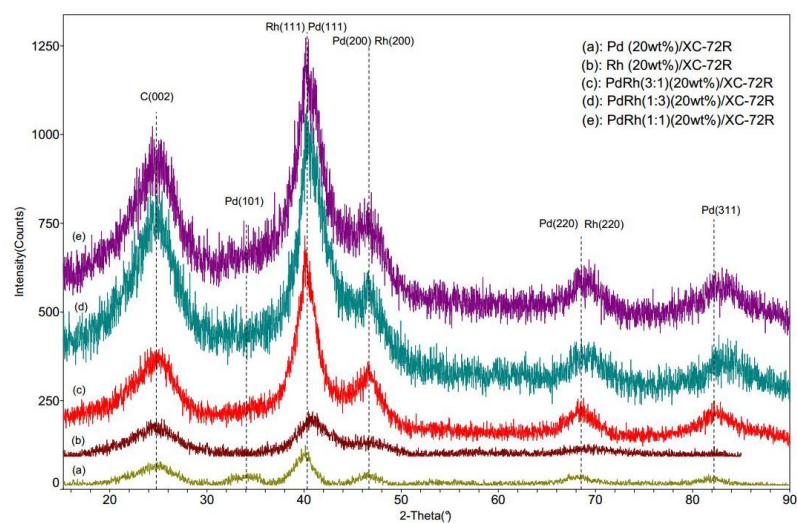
Figure 4.1: X-ray diffraction patterns of (a) Pd, (b) Rh, (c) PdRh(3:1), (d) PdRh(1:3) and (e) PdRh(1:1) bimetallic catalysts prepared with polyol reduction.

TEM images with the respective particle size distribution histogram of Pd/C, Rh/C and Pd_xRh_y catalysts are shown in Fig. 4.2. A remarkably uniform and high dispersion of metal particles on the carbon surface is observed concerning all the examined samples. As it can also be seen (Table 4.1), the mean particle size was in the following order: Pd_3Rh (4.8±0.3nm) > PdRh (4.4±0.3nm) > Pd (4.3±0.3) > $PdRh_3$ (3.5±0.3nm) > Rh (3.3±0.3).
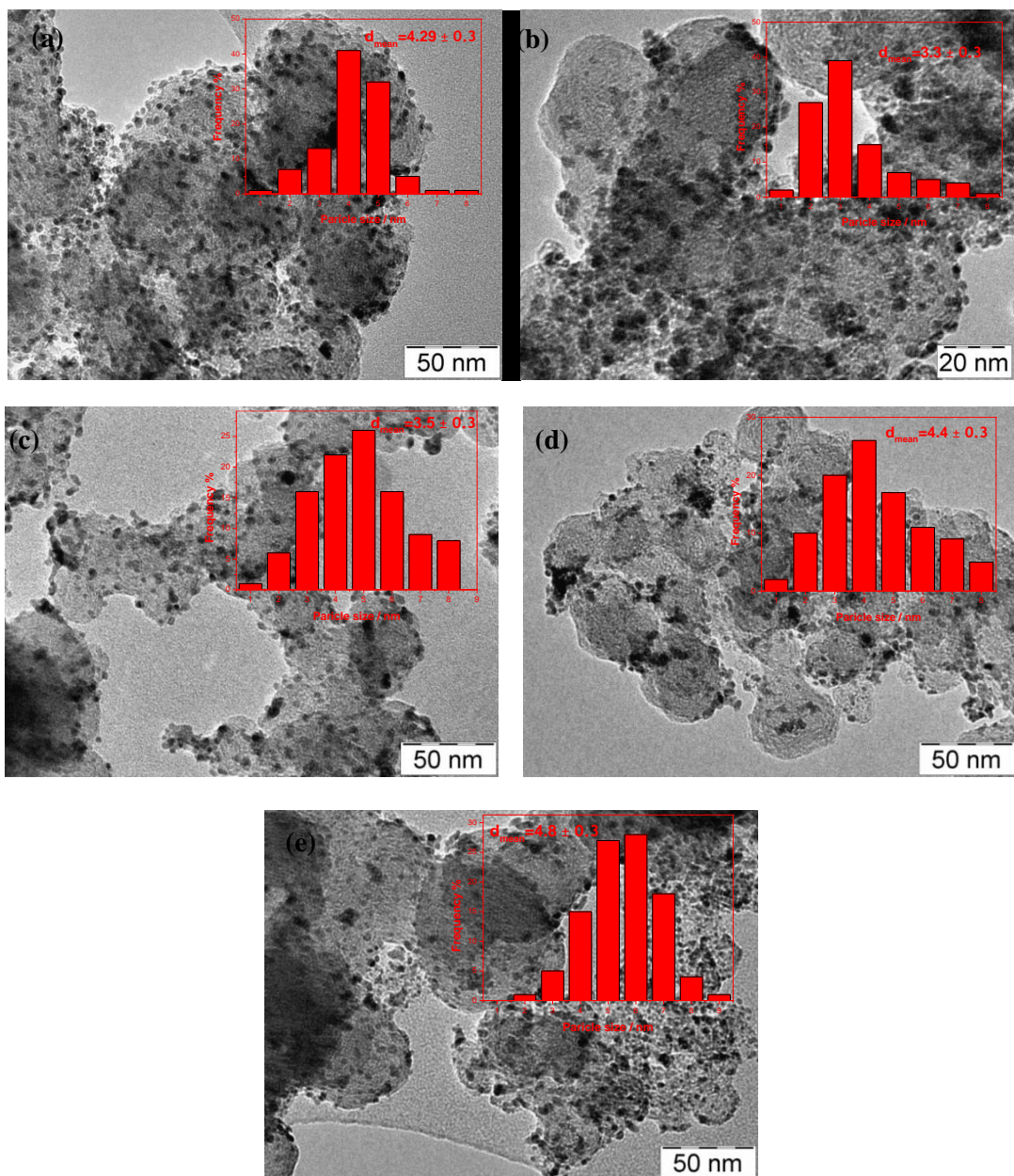
Figure 4.2: TEM images of (a) Pd, (b) Rh, (c) PdRh₃, (d) PdRh, (e)Pd₃Rh

Table 4.1: Physicochemical analysis results.

Electrode (20%wt metal loading)	Lattice Parameter (nm)	Crystallite Size (nm)	Particles Size (nm)
Pd/C	0.38615	3.0	4.3±0.3
Rh/C	0.38456	2.0	3.3±0.3
PdRh(3:1)/C	0.38794	~3.0	4.8±0.3
PdRh(1:1)/C	0.38474	3.5	4.4±0.3
PdRh(1:3)/C	0.38516	2.0	3.5±0.3

4.2.2 Electrochemical catalytic surface area

The voltammetric profiles recorded for Pd, Rh, and Pd_xRh_y alloys obtained in 0.5M H_2SO_4 solution and with a scan rate of 50 mV s^{-1}, are schematically shown in Fig. 4.3. The electrochemical active surface area (ECSA) was estimated by the aid of the following equation [51] taking into account the reduction peak that is observed during the backward scanning:

$$ECSA \left[\frac{m^2}{g} \right] = \frac{Q_H}{Q_{(Pd\ or\ Rh)} \times m_{Pd\ or\ Rh} \times 10}$$

,where $Q_H = (Q_{ads} + Q_{des})/2$ $(\mu C\,cm_{Pt}^{-2})$ represents the average charge extracted from the integration of the adsorption/desorption hydrogen regions of the CV curves, $Q_{Pd} = 420(\mu C\,cm_{Pd}^{-2})$ and $Q_{Rh} = 256(\mu C\,cm_{Rh}^{-2})$ [52] are the specific amount of electricity corresponding to the full coverage of the Pd or Rh surface by one monolayer of oxygen and $m_{Pd(Rh)}$ ($mg\,cm_{electrode}^{-2}$) is the palladium or rhodium loading on the working electrode's surface. The results of the ECSA calculations, for the electrocatalysts used in the present investigation are reported in Table 4.2.

Table 4.2: Cyclic voltammetry analysis.

Electrode (20%wt metal loading)	Pd loading (µg cm^{-2})	Rh loading (µg cm^{-2})	ECSA (m^2 g$^{-1}_{metal}$)
Pd/C	11	0	21.0
PdRh(3:1)/C	8.3	2.7	22.5
PdRh(1:1)/C	5.6	5.4	27.0
PdRh(1:3)/C	2.8	8.2	29.5
Rh/C	0	11	25.6

As it can be noticed, the electrochemical active surface area exhibits the following order: $Pd < Pd_3Rh < Rh/C < PdRh/C < PdRh_3/C$.
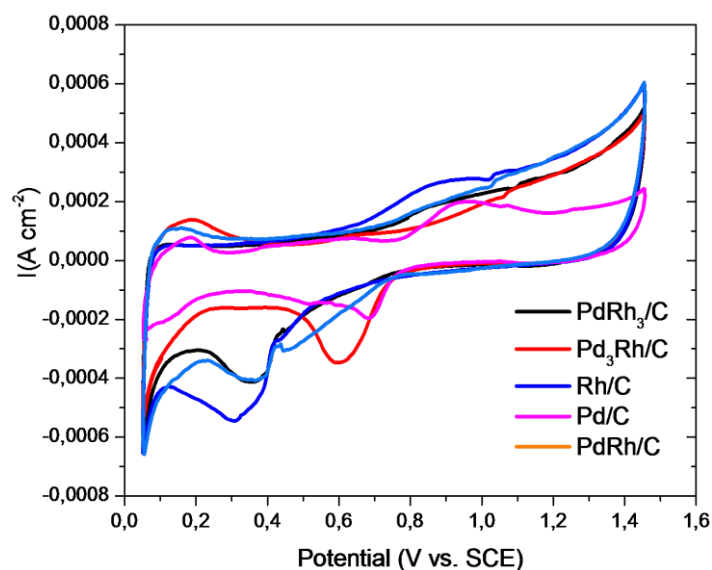
Figure 4.3: Cyclic voltammograms for (a) Pd, (b) Pd₃Rh, c) PdRh and d) PdRh₃ in 0.5 M H₂SO₄, scan rate: 50 mV s⁻¹.

4.2.3 Hydrogen oxidation reaction kinetics

The HOR polarization curves for the Pd, Rh and Pd_xRh_y electrocatalysts are depicted in Fig. 4.4. As it can be distinguished, the oxidation of H_2 over the Pd_xRh_y/C alloys and pure Rh starts at potential values around to 0.01 V (onset potential), while over pure Pd electrocatalyst the HOR's onset potential is higher, ca 0.1V. It can also be seen that, the current continues increasing sharply up to 0.1 V and 0.2 V for the Pd_xRh_y, Rh and pure Pd, respectively. At more positive potentials, transition into the region of hydrogen mass transport controlled current densities starts at approximately 0.15 V. As it was expected, the limiting current increases with the increment of the rotational speed of the electrode [53]. Moreover, the electrochemical behavior of the as prepared Pd_xRh_y electrocatalysts is similar to that of pure Rh. As it is well known, during a reaction the kinetic current density (i_k) is a measure of the rate of charge transfer on the catalyst's surface.
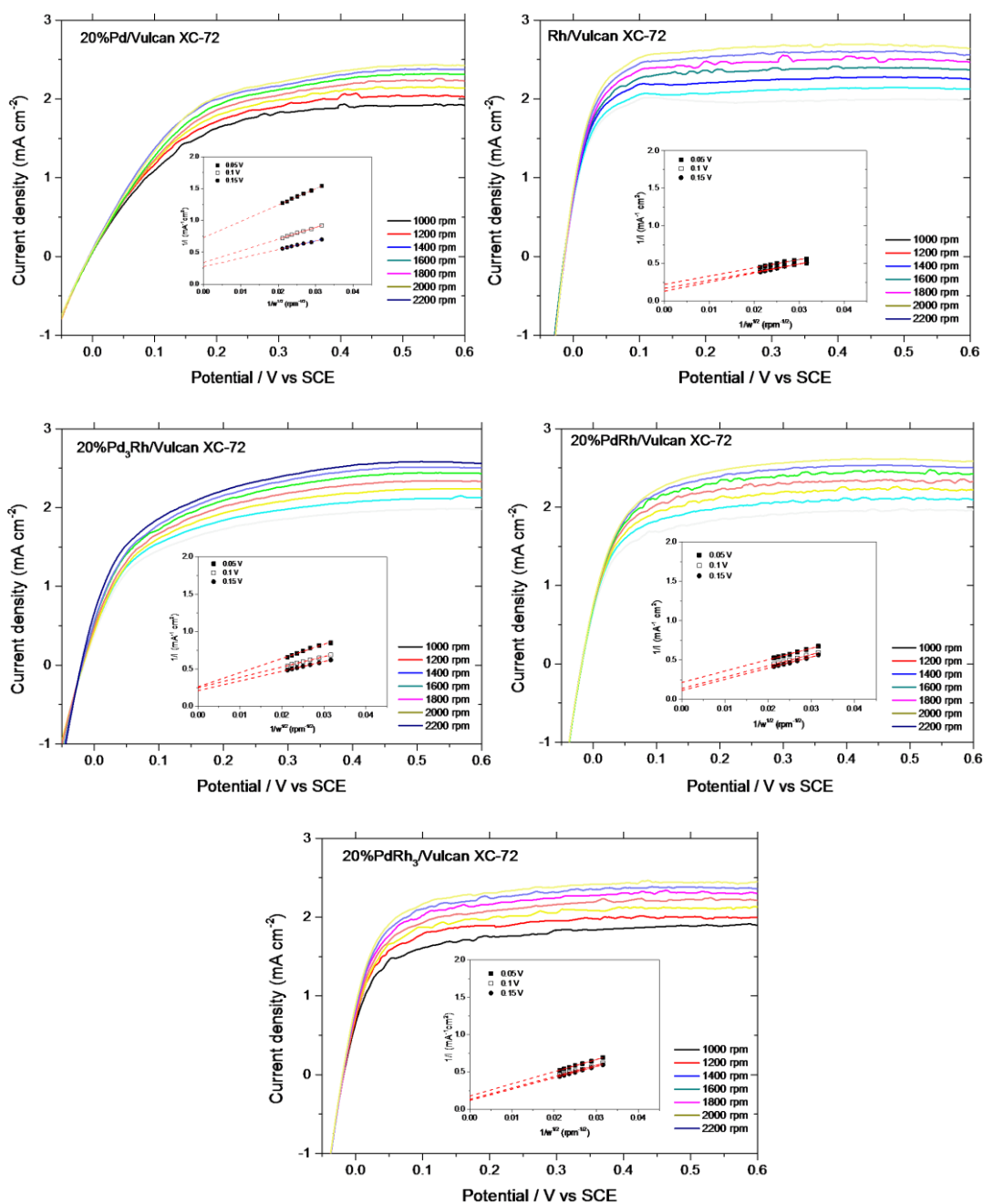
Figure 4.4: RDE curves in H$_2$-saturated 0.5 M H$_2$SO$_4$, scan rate: 5 mV s^{-1}. Insets: Koutecky-Levich plots. The insets are the corresponding Koutecky-Levich plots for the hydrogen oxidation reaction.

More precisely, i_k describes the real kinetics of an electrocatalytic reaction and therefore is directly related to the activity of an electrocatalyst. To determine the catalytic activity of the electrocatalysts, we adopted the Koutecky–Levich analysis [54], where the kinetic current is related to the rotational velocity of the RDE through the following equation:

$$\frac{1}{i} = \frac{1}{i_k} + \frac{1}{i_d}$$

(4.1)

Where i represents the experimental value of the current, i_k the kinetic current in the absence of mass transfer limitations and i_d the diffusion-limited current. The later can be calculated according to the Levich equation:

$$i_d = 0.62nFD^{2/3}v^{-1/6}C\omega^{1/2}$$

(4.2)

where n is the number of theoretically-transferred electrons (=2), F the Faraday constant (95485 C/mol), D the diffusion coefficient of H_2 in the H_2SO_4, v the kinematic viscosity of the electrolyte and C the H_2 concentration in the electrolyte. The kinetic current density was graphically determined ($1/i$ vs. $1/\omega^{1/2}$ - Koutecky-Levich plots).

The insets of Fig. 4.4 provide the Koutecky-Levich plots for the examined Pd_xRh_y, Pd and Rh electrocatalysts, from which the kinetic currents for HOR, at 0.1 V (vs SCE), were extracted. As follows from their analysis, the experimental points have a linear behaviour ensuring the accuracy of i_k determination.

Table 4.3: Kinetic analysis results for hydrogen oxidation reaction.

Electrode (20%wt metal loading)	Tafel slope (mV decade^{-1})	i_o (mA cm^{-2})	i_k (@0.1V) (mA cm^{-2})
Pd/C	80.0	0.32	3.0
PdRh(3:1)/C	120.0	1.24	4.0
PdRh(1:1)/C	230.0	2.56	7.3
PdRh(1:3)/C	180.0	3.00	7.6
Rh/C	210.0	2.58	6.0
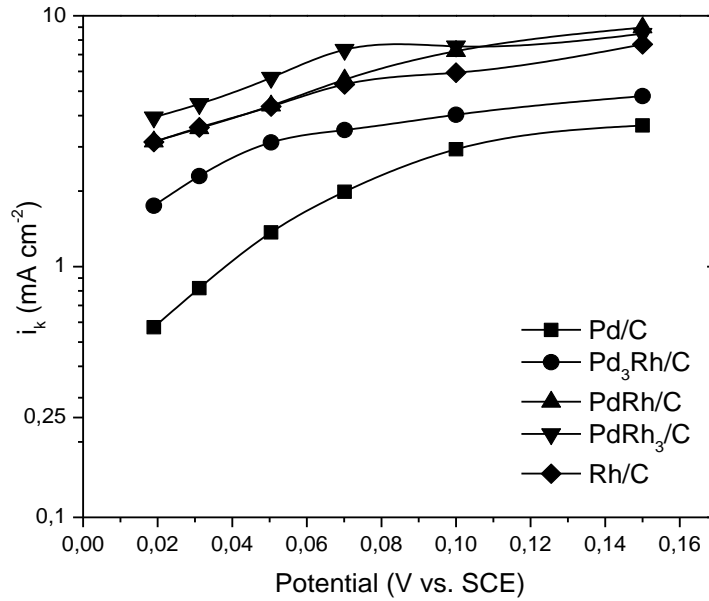
Figure 4.5: Tafel plots for HOR.

The kinetic current density (Fig. 4.5) values (at 0.05 V (vs SCE), 1200 rpm, Table 4.3) were calculated to be 6.0, 7.6, 7.3, 4.0 and 3.0 mA cm^{-2} for Rh, PdRh$_3$, PdRh, Pd$_3$Rh and Pd, respectively. It is obvious that, PdRh and PdRh$_3$ exhibit the highest electrocatalytic activity towards hydrogen electrooxidation and comparable to that of Pt's, as reported in literature (Fig. 4.6) [55, 56]. After that, the kinetic analysis the Tafel-Heyrovsky (mass transfer corrected) plots were also obtained (Fig. 4.5) after the measured currents were corrected for diffusion to obtain the kinetic current [57]

.

$$\log(i_k) = \log(i_o) + (\frac{anF}{2.303RT})\eta \tag{4.3}$$

where $i_k = \dfrac{i \times i_d}{i_d - i}$, as being calculated from the Koutecky-Levich plots.

The slope of Tafel plots (∂log jk/∂E), varies with the electrode potential, lacking an extended linear Tafel region. It is well known that, from the Tafel slope and intercept useful kinetic information can be obtained [58]: i) the exchange current density and ii) the charge transfer coefficient.
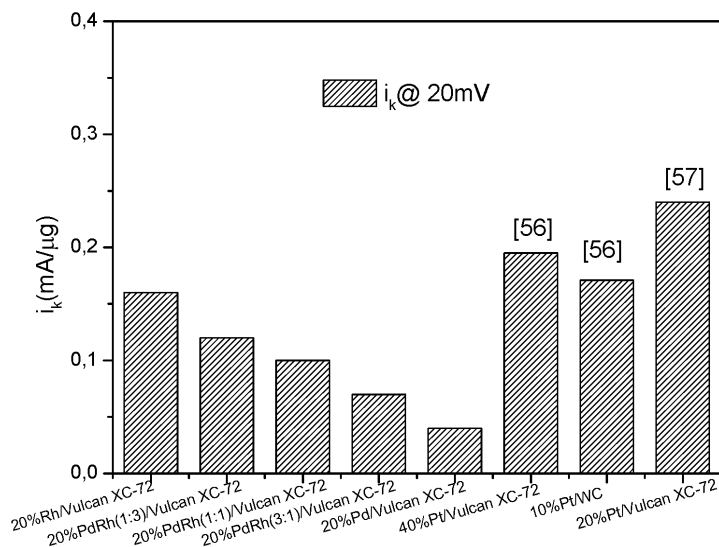
Figure 4.6: Comparison of kinetic current density @0.02V for HOR.

From the kinetic analysis (Table 4.3) it is deduced that Rh's activity predominates over other electrocatalysts, followed by the PdRh and PdRh$_3$. Moreover, from the slope values and in accordance with the literature, the hydrogen oxidation reaction on the as prepared samples, follows the Tafel–Heyrovsky–Volmer mechanism, as with Pt-based electrocatalysts do [23]. Furthermore the exchange current density value measured for Pd is quite close to those reported in literature, 0.29 mA cm^{-2} by Shao et al [23] and 0.22 mA cm^{-2} by Pronkin et al. [58].

Additionally, from the values of the charge transfer coefficient (α), which all were calculated to be close to 0.25, maybe due to the increased overpotential [59]. The charge transfer coefficient represents the fraction of additional energy that goes toward the reaction at the electrode. Also the mass corrected Tafel slopes are calculated and reported in Table 4.3. According to literature [60-62] and the reported slopes the adsorption dissociation of hydrogen on the catalyst surface is the rate determining step (Volmer), taking into consideration the Tafel-Heyrovsky-Volmer mechanism for HOR:

$$H_2 \rightleftharpoons 2H_{ad} : \text{Tafel}$$

$$H_2 \rightleftharpoons H_{ad} + e^- + H^+ : \text{Heyrovsky}$$

$$H_{ad} \rightleftharpoons H^+ + e^- : Volmer$$
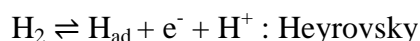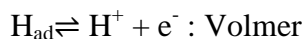
In order to obtain a more thorough understanding about the effect of Rh loading to the activity (to the kinetic and exchange current) of the examined electrocatalysts, Fig.4.7 is given. From this figure it can be deduced that, the increase of the Rh loading strongly enhances the electrocatalytic activity of Pd towards HOR in terms of both exchange current and kinetic density. The increased electrocatalytic activity of PdRh bimetallic electrocatalysts could be attributed to their ability to adsorb more hydrogen than pure Pd, as it has been declared by Żurowski *et al.* [63]. On the other hand, according to Mallen *et al.* [64], the higher (than pure Pd) electrocatalytic activity was measured for pure Rh/C, could be attributed to the fact that Rh, has the same hydrogen binding energy with Pt.
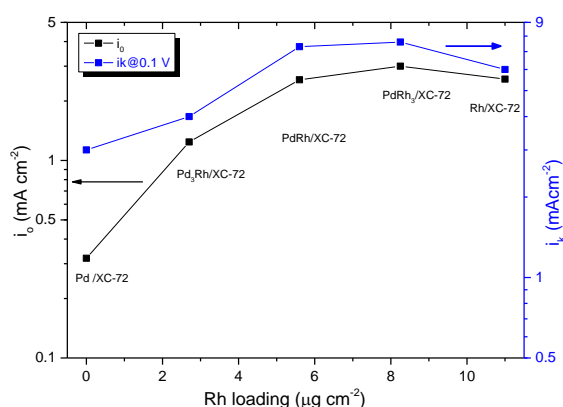
Figure 4.7: Exchange current density and kinetic current density vs. rhodium metal loading for HOR.

4.3.4 Chronoamperometric measurements

The stability of the examined electrocatalysts for hydrogen electrooxidation in 0.5 M H_2SO_4 at 25°C for 1300s was investigated by chronoamperometric measurements, and the results are reported in Fig. 4.8. As can be seen in Fig. 4.8 the $PdRh_3$/Vulcan XC-72 catalyst appears to have the same current decay with PdRh after 200s, however, after 200s $PdRh_3$ show better long term stability. That means that the addition of rhodium hinders pure palladium from leaching, giving higher stability to Pd's electrocatalyst. Furthermore

the chronoamperometric measurements further confirmed pure Rh's, PdRh and PdRh$_3$ enhanced catalytic activity towards hydrogen oxidation reaction.
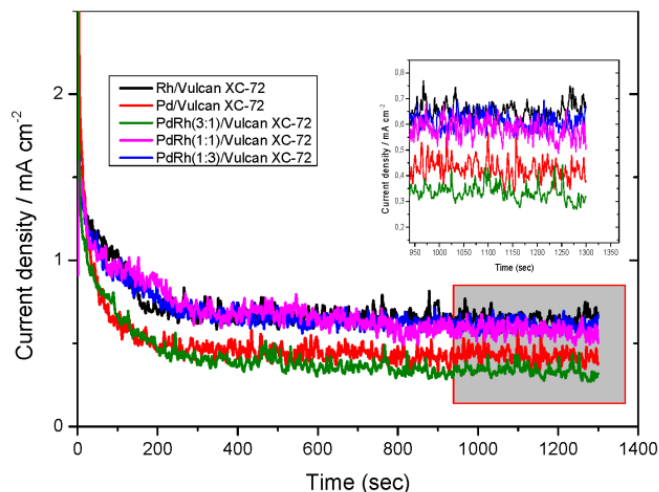
Figure 4.8: Chronoamperometry curves for HOR, in 0.5M H$_2$SO$_4$ for 1300 sec at 0.25V.

4.3.5 Oxygen reduction reaction kinetics

The tests for ORR activity of the electrocatalysts were conducted in oxygen-saturated 0.5 M H$_2$SO$_4$ solution, from 0 to 0.90 V (vs SCE), at different rotation rates (from 500 to 2500 rpm) and at constant sweep rate of 10 mV s^{-1}.
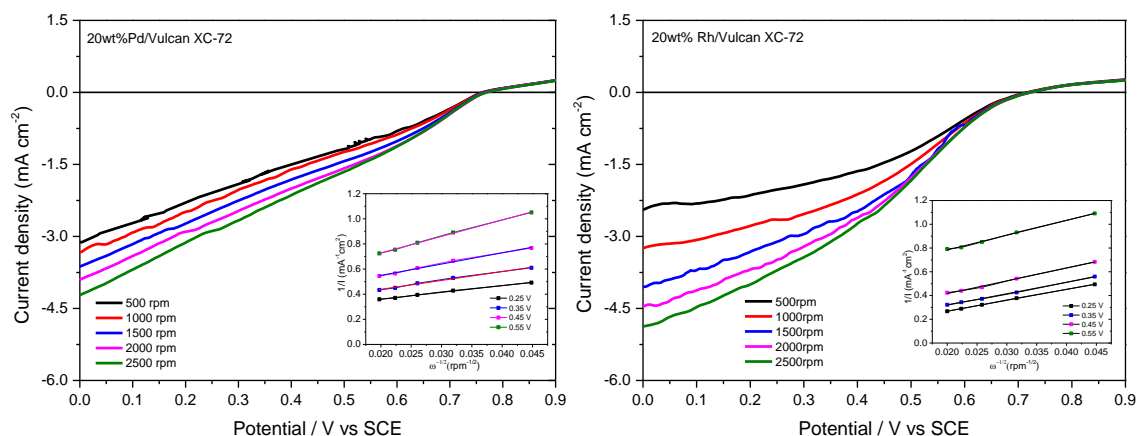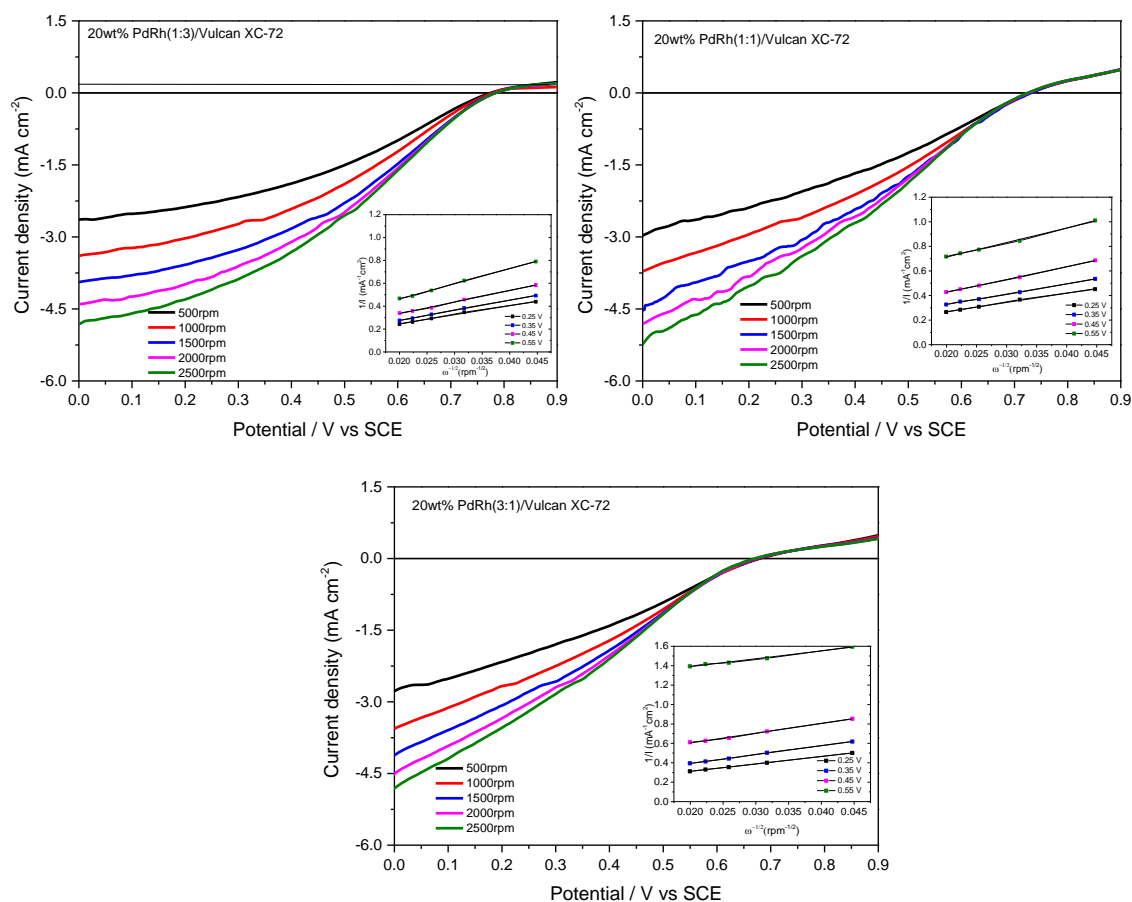
Figure 4.9: RDE curves of (A) Pd, (B)Rh, (C) PdRh₃, (D) PdRh and (E) Pd₃Rh electrodes in O₂-saturated 0.5M H₂SO₄, scan rate: 10 mV s⁻¹.

As it is schematically shown in Fig. 4.9, well-defined limiting currents were observed increasing the rotation rate due to the increased availability of oxygen at the electrodes surface. In each polarization curve three different characteristic regions are displayed: The first region which is observed from 0.9 to 0.65V (*vs* SCE) is the kinetic one, where the kinetic current is independent of the rotation rate. The second one is the mixed control region and it is observed from 0.65 to 0.2 V (*vs* SCE). In this, the current is controlled by both kinetic as well as diffusion-limited processes. Finally in the third region, from 0.2 to 0.0 V (vs SCE) the ORR curve is under mass transport control limited by the diffusion of the dissolved oxygen in the electrolyte [65]. In the last region the polarization curves do not catch a flat plateau; behaviour that can be explained from irreversible electrode processes [66]. Another possible explanation is that the film that was formed on the working electrode

was very thin, due to the low amount of catalytic ink (4μL) that was deposited on it in order to have very low catalyst loading. The onset potential for all the examined samples is observed to be the same, ca 0.7V (vs SCE) and the limiting diffusion currents 4.15, 4.70, 4.79, 4.80 and 4.86 mA cm^{-2} (at 2500 rpm) for the Pd, Pd$_3$Rh, PdRh, PdRh$_3$ and Rh, respectively.

Koutecky–Levich equation (eq.1) was adopted to determine the kinetic parameters of the electrocatalysts: i) the kinetic current density and ii) the number of electrons that take part into the reaction. More precisely, from the intercept of Koutecky-Levich plots (insets of Fig. 4.9) and using Levich equation (4.3), where n is the number of electrons involved in the reaction, F is the Faraday constant (96485 C/mol), D is the diffusion coefficient of O$_2$ in the H$_2$SO$_4$ (1.4×10^{-5} cm^2 s^{-1}), v is the kinematic viscosity of the electrolyte (1.0×10^{-2} cm^{-2} s^{-1}), C is the O$_2$ concentration in the electrolyte (1.1×10^{-6} mol cm^{-3}), are calculated the kinetic current density values and from the slope, the total number of electrons involved in the reaction [67]. Then for further kinetic analysis the Tafel plots (Fig.4.10) were done, from which: i) the exchange current density and ii) Tafel slopes and charge transfer coefficients, are also calculated.
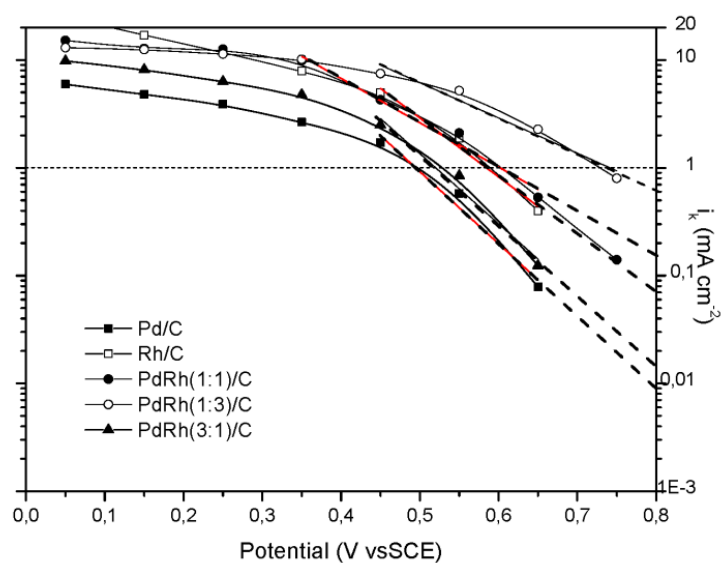
Figure 4.10: Tafel plots for ORR.

The linearity and parallelism of the Koutecky-Levich plots show the first-order kinetics with respect to molecular oxygen (insets of Fig. 4.9). The kinetic current density is proportional to the intrinsic activity of the catalysts and the slopes of the straight lines allow us to estimate the number of electrons involved in the ORR [68]. Except for Pd where the total electrons involved in the reaction are two, for all the others examined electrocatalysts the total electrons are four. A widely accepted method to determine the ORR activity of an electrocatalyst is based on the half-wave potential, which is defined as the potential at which the magnitude of the current is half of the limiting current [65]. According to theory [59], ORR in aqueous solutions occurs mainly by two pathways: the direct 4-electron reduction pathway from O_2 to H_2O, and the 2-electron reduction pathway from O_2 to hydrogen peroxide (H_2O_2). In the present case and from the kinetic analysis for all the examined electrocatalysts the total electrons that are transferred during the oxygen reduction reaction are four.

From Fig. 4.11 it can be deduced that, the addition of the Rh loading to Pd enhances the electrocatalytic activity of Pd towards ORR in terms of both exchange current and kinetic density. The kinetic current density at half-wave potential (0.55 V) is higher for the $PdRh_3$ (5.20 $mAcm^{-2}$), followed by PdRh and Pd (2.10 $mAcm^{-2}$) and by pure Rh (1.89 $mAcm^{-2}$) and finally by the Pd_3Rh (0.89 $mAcm^{-2}$). The addition of specific amount of Rh (>5.4μgcm^{-2}) to pure Pd increases the kinetic current density by 147%. As it is expected pure palladium and high palladium loading (Pd_3Rh) do not enhance the oxygen reduction reaction in comparison with the other electrocatalysts (Rh, PdRh and $PdRh_3$). This is also confirmed by their low reaction rate constant (Table 4.4). Additionally, the obtained Tafel slopes were calculated at a range of ~200mV and are reported in Table 4.4.

Table 4.4: Kinetic analysis results for oxygen reduction reaction.

Electrode (20%wt metal loading)	Tafel slope (mV decade^{-1})	i_o (mA cm^{-2})	i_k (@0.55V) (mA cm^{-2})
Pd/C	131	0.03	0.58
PdRh(3:1)/C	140	0.04	0.89
PdRh(1:1)/C	149	0.21	2.10
PdRh(1:3)/C	110	0.65	5.20
Rh/C	111	0.1	1.87

As it is well known from the theory, for T=298K, α=0.5 and n=1or 2, two slopes have been should be reported: 120mV/decade (n=1) and 60 mV/decade (n=2). From the calculated Tafel slopes (slope=2.303RT/αnF) the electrons, that are involved in the rate determining step, can be estimated [67].

It should be noted that, in the current work, the estimated Tafel slopes (Table 4.4) are very high (in comparison with the value of 120 mVdecade^{-1}), due to the high overpotential. The high overpotential may attributed to mass transport phenomena [69].
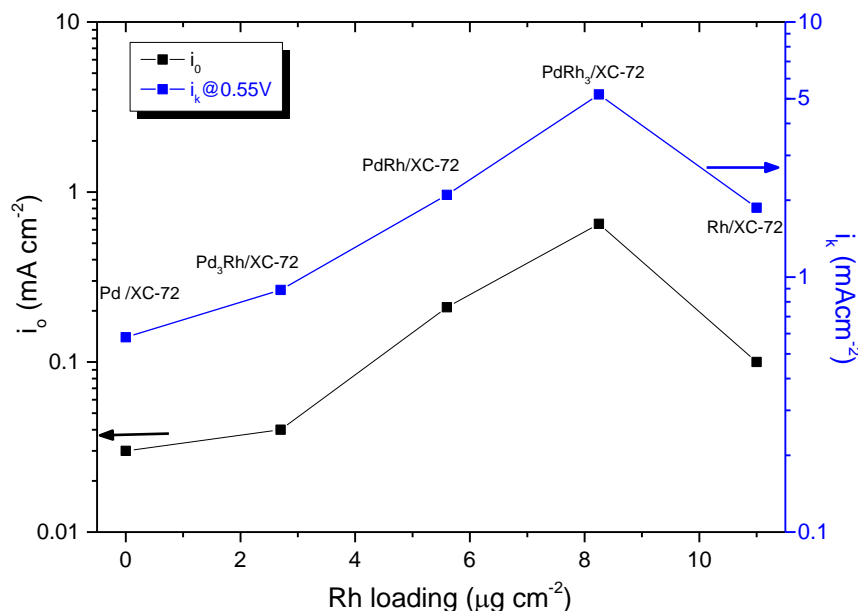
Figure 4.11: Exchange current density and kinetic current density vs. rhodium metal loading for ORR.

4.4 Conclusions

From the analysis of the obtained results the following conclusions can be drawn:

Pd-based electrocatalysts could play a great role to whole or partially replace costly Pt in both anode and cathode compartments, at low temperature H_2-PEMFCs. Pure Rh and Pd–Rh binary alloys show comparable or higher hydrogen oxidation and oxygen reduction activity than pure Pd. The HOR activity order, in terms of kinetic current density, is the following: $PdRh_3$ (7.6 mAcm^{-2}) > PdRh (7.3 mAcm^{-2}) > Rh (6.0 mAcm^{-2}) > Pd_3Rh (4.0 mAcm^{-2}) > Pd (3.0 mAcm^{-2}). Rhodium's enhanced activity towards HOR may is attributed to its high (as Pt's) hydrogen binding energy. However, the higher (than pure Pd) palladium-rhodium bimetallic electrocatalysts' activity is probably due to their ability to adsorb more hydrogen. According to the chronoamperometric results, the addition of rhodium also increases the stability of pure palladium, since it hinders the last from leaching, due to the corrosive environment of the acidic medium. As the kinetic analysis shown, over all the samples the hydrogen oxidation reaction was charge transfer controlled. The ORR activity order at half wave potential, in terms of kinetic current density, is the following: $PdRh_3$ (5.2mAcm^{-2}) > PdRh$\approx$Pd (2.10mAcm^{-2}) > Rh (1.89mAcm^{-2}) > Pd_3Rh (0.89mAcm^{-2}). Consequently, also the addition of a certain amount of rhodium (8.2μgcm^{-2}) significantly enhances the activity of pure palladium. According to the kinetic analysis, all the examined electrocatalysts seem to follow the two-way pathway with four electrons total to be included in the oxygen reduction reaction process.

Summarizing, the addition even of small amounts of Rh (2.7 μg$_{Rh}$ cm^{-2}) as a second metal to Pd (24.5%Rh) contributes to the activity increment towards both the hydrogen oxidation and oxygen reduction reaction by 132% and 80%, respectively. Finally, according to the as-reported results, also pure Rh could be a possible alternative for higher anodic and cathodic catalytic activity, however it's very high cost do not make it appealing for further investigation.

References

[1]   Wolf Vielstich, Arnold Lamm, H.A. Gasteiger, Handbook of Fuel Cells: Fundamentals, Technology, Applications, 4-Volume Set, 2003.

[2]   J.D. Holladay, J. Hu, D.L. King, Y. Wang. Catalysis Today 139 (2009) 244-260.

[3]   H.A. Gasteiger, S.S. Kocha, B. Sompalli, F.T. Wagner. Applied Catalysis B: Environmental 56 (2005) 9-35.

[4]   X. Liu, E.H. Yu, K. Scott. Applied Catalysis B: Environmental 162 (2015) 593-601.

[5]   C. Domínguez, F.J. Pérez-Alonso, M. Abdel Salam, S.A. Al-Thabaiti, A.Y. Obaid, A.A. Alshehri, J.L. Gómez de la Fuente, J.L.G. Fierro, S. Rojas. Applied Catalysis B: Environmental 162 (2015) 420-429.

[6]   S.N. Stamatin, M. Borghei, R. Dhiman, S.M. Andersen, V. Ruiz, E. Kauppinen, E.M. Skou. Applied Catalysis B: Environmental 162 (2015) 289-299.

[7]   E. Antolini. Energy & Environmental Science 2 (2009) 915-931.

[8]   B. Li, Z. Yan, D.C. Higgins, D. Yang, Z. Chen, J. Ma. Journal of Power Sources 262 (2014) 488-493.

[9]   K. Kwon, S.-a. Jin, K.H. Lee, D.J. You, C. Pak. Catalysis Today 232 (2014) 175-178.

[10]   S. Vengatesan, H.J. Kim, S.K. Kim, I.H. Oh, S.Y. Lee, E. Cho, H.Y. Ha, T.H. Lim. Electrochimica Acta 54 (2008) 856-861.

[11]   D. Dang, S. Liao, F. Luo, S. Hou, H. Song, P. Huang. Journal of Power Sources 260 (2014) 27-33.

[12]   A. Brouzgou, S.Q. Song, P. Tsiakaras. Applied Catalysis B: Environmental 127 (2012) 371-388.

[13]   F. Kadirgan, A.M. Kannan, T. Atilan, S. Beyhan, S.S. Ozenler, S. Suzer, A. Yörür. International Journal of Hydrogen Energy 34 (2009) 9450-9460.

[14]   Y.H. Cho, B. Choi, H.S. Park, Y.E. Sung. Electrochemistry Communications 9 (2007) 378-381.

[15]   A.C. Garcia, V.A. Paganin, E.A. Ticianelli. Electrochimica Acta 53 (2008) 4309-4315.

[16]   S.J. Yoo, H.-Y. Park, T.-Y. Jeon, I.-S. Park, Y.-H. Cho, Y.-E. Sung. Angewandte Chemie International Edition 47 (2008) 9307-9310.

[17]   D.C. Papageorgopoulos, M. Keijzer, J.B.J. Veldhuis, F.A. De Bruijn. Journal of the Electrochemical Society 149 (2002) A1400-A1404.

[18]   T. Yamanaka, T. Takeguchi, G. Wang, E.N. Muhamad, W. Ueda. Journal of Power Sources 195 (2010) 6398-6404.

[19]   W.C. Chang, M.T. Nguyen. Journal of Power Sources 196 (2011) 5811-5816.

[20]   M. Götz, H. Wendt. Electrochimica Acta 43 (1998) 3637-3644.

[21]   R. Zeis, A. Mathur, G. Fritz, J. Lee, J. Erlebacher. Journal of Power Sources 165 (2007) 65-72.

[22]   T. Ioroi, N. Fujiwara, Z. Siroma, K. Yasuda, Y. Miyazaki. Electrochemistry Communications 4 (2002) 442-446.

[23]   M. Shao. Journal of Power Sources 196 (2011) 2433-2444.

[24]   P.S. Ruvinsky, S.N. Pronkin, V.I. Zaikovskii, P. Bernhardt, E.R. Savinova. Physical Chemistry Chemical Physics 10 (2008) 6665-6676.

[25]   S. Trasatti. Journal of Electroanalytical Chemistry 39 (1972) 163-184.

[26]   J. Moreira, P. del Angel, A.L. Ocampo, P.J. Sebastián, J.A. Montoya, R.H. Castellanos. International Journal of Hydrogen Energy 29 (2004) 915-920.

[27]   C. Gabrielli, P.P. Grand, A. Lasia, H. Perrot. Journal of the Electrochemical Society 151 (2004) A1937-A1942.

[28]   M.S. Rau, P.M. Quaino, M.R. Gennero de Chialvo, A.C. Chialvo. Electrochemistry Communications 10 (2008) 208-212.

[29]   M. Łukaszewski, A. Czerwiński. Journal of Alloys and Compounds 473 (2009) 220-226.

[30]   V. Di Noto, E. Negro, S. Lavina, S. Gross, G. Pace. Electrochimica Acta 53 (2007) 1604-1617.

[31]   N.A. Maiorova, A.A. Mikhailova, O.A. Khazova, V.A. Grinberg. Russian Journal of Electrochemistry 42 (2006) 331-338.

[32]   T.J. Schmidt, Z. Jusys, H.A. Gasteiger, R.J. Behm, U. Endruschat, H. Boennemann. Journal of Electroanalytical Chemistry 501 (2001) 132-140.

[33]   M. Łukaszewski, K. Kuśmierczyk, J. Kotowski, H. Siwek, A. Czerwiński. Journal of Solid State Electrochemistry 7 (2003) 69-76.

[34]   M. Ura, Y. Haraguchi, F.L. Chen, Y. Sakamoto. Journal of Alloys and Compounds 231 (1995) 436-439.

[35]   M. Łukaszewski, M. Grdeń, A. Czerwiński. Journal of Electroanalytical Chemistry 573 (2004) 87-98.

[36]   M.A. Montero, J.L. Fernández, M.R. Gennero de Chialvo, A.C. Chialvo. Journal of Power Sources 254 (2014) 218-223.

[37]   A. Czerwinski, M. Lukaszewski, A. Zurowski, H. Siwek, S. Obrebowski. Journal of New Materials for Electrochemical Systems 9 (2006) 419-429.

[38]   M. Łukaszewski, A. Czerwiński. Journal of Solid State Electrochemistry 11 (2007) 339-349.

[39]   O. Savadogo, K. Lee, S. Mitsushima, N. Kamiya, K.I. Ota. Journal of New Materials for Electrochemical Systems 7 (2004) 77-83.

[40]   O. Savadogo, K. Lee, K. Oishi, S. Mitsushima, N. Kamiya, K.I. Ota. Electrochemistry Communications 6 (2004) 105-109.

[41]   S. Kondo, M. Nakamura, N. Maki, N. Hoshi. The Journal of Physical Chemistry C 113 (2009) 12625-12628.

[42]   J. Zhao, A. Sarkar, A. Manthiram. Electrochimica Acta 55 (2010) 1756-1765.

[43]   G. Ramos-Sánchez, H. Yee-Madeira, O. Solorza-Feria. International Journal of Hydrogen Energy 33 (2008) 3596-3600.

[44]   X. Wang, N.N. Kariuki, S. Niyogi, M.C. Smith, D.J. Myers, T. Hofmann, Y. Zhang, M. Bär, C. Heske, Bimetallic palladium-base metal nanoparticle oxygen reduction electrocatalysts, ECS Transactions, 2 PART 1 ed., 2008, pp. 109-119.

[45]   X. Wang, N. Kariuki, J.T. Vaughey, J. Goodpaster, R. Kumar, D.J. Myers. Journal of the Electrochemical Society 155 (2008) B602-B609.

[46]   Y. Qi, J. Wu, H. Zhang, Y. Jiang, C. Jin, M. Fu, H. Yang, D. Yang. Nanoscale 6 (2014) 7012-7018.

[47]   J.L. Fernández, V. Raghuveer, A. Manthiram, A.J. Bard. Journal of the American Chemical Society 127 (2005) 13100-13101.

[48]   V. Raghuveer, A. Manthiram, A.J. Bard. Journal of Physical Chemistry B 109 (2005) 22909-22912.

[49]   S. Song, J. Liu, J. Shi, H. Liu, V. Maragou, Y. Wang, P. Tsiakaras. Applied Catalysis B: Environmental 103 (2011) 287-293.

[50]   A.L. Patterson. Physical Review 56 (1939) 978-982.

[51]   D. Chi Linh, P. Thy San, N. Ngoc Phong, T. Viet Quan. Advances in Natural Sciences: Nanoscience and Nanotechnology 4 (2013) 035011.

[52]   T. Langkau, H. Baltruschat. Electrochimica Acta 44 (1998) 909-918.

[53]   R. Escudero-Cid, A.S. Varela, P. Hernández-Fernández, E. Fatás, P. Ocón. International Journal of Hydrogen Energy 39 (2014) 5063-5073.

[54]   J. Durst, A. Siebel, C. Simon, F. Hasche, J. Herranz, H.A. Gasteiger. Energy & Environmental Science 7 (2014) 2255-2260.

[55]   V.M. Nikolic, D.L. Zugic, I.M. Perovic, A.B. Saponjic, B.M. Babic, I.A. Pasti, M.P. Marceta Kaninski. International Journal of Hydrogen Energy 38 (2013) 11340-11345.

[56]   N.R. Elezović, L. Gajić-Krstajić, V. Radmilović, L. Vračar, N.V. Krstajić. Electrochimica Acta 54 (2009) 1375-1382.

[57]   S.J. Yoo, H.-Y. Park, T.-Y. Jeon, I.-S. Park, Y.-H. Cho, Y.-E. Sung. Angewandte Chemie 120 (2008) 9447-9450.

[58]   S.N. Pronkin, A. Bonnefont, P.S. Ruvinskiy, E.R. Savinova. Electrochimica Acta 55 (2010) 3312-3323.

[59]   J. Zhang, PEM Fuel Cell Electrocatalysts and Catalyst Layers: Fundamentals and Applications, Springer, 2008.

[60]   W. Sheng, H.A. Gasteiger, Y. Shao-Horn. Journal of the Electrochemical Society 157 (2010) B1529-B1536.

[61]   D. Pletcher, A First Course in Electrode Processes, Royal Society of Chemistry, 2009.

[62]   T.J. Schmidt, V. Stamenkovic, N.M. Markovic, P.N. Ross Jr. Electrochimica Acta 48 (2003) 3823-3828.

[63]   A. Żurowski, M. Łukaszewski, A. Czerwiński. Electrochimica Acta 51 (2006) 3112-3117.

[64]   M.P. Zum Mallen, W.R. Williams, L.D. Schmidt. Journal of Physical Chemistry 97 (1993) 625-632.

[65]   Y. Sun, Y.-C. Hsieh, L.-C. Chang, P.-W. Wu, J.-F. Lee. Journal of Power Sources 277 (2015) 116-123.

[66]   R.H. Castellanos, A.L. Ocampo, P.J. Sebastian. Journal of New Materials for Electrochemical Systems 5 (2002) 83-90.

[67]   W. Xing, G. Yin, J. Zhang, Rotating Electrode Methods and Oxygen Reduction Electrocatalysts, Elsevier Science, 2014.

[68]   J.J. Salvador-Pascual, S. Citalán-Cigarroa, O. Solorza-Feria. Journal of Power Sources 172 (2007) 229-234.

[69]   S.L. Gojković, S. Gupta, R.F. Savinell. Journal of Electroanalytical Chemistry 462 (1999) 63-72.

Hydrogen oxidation and Oxygen reduction reactions over Pd_xIr_y electrocatalysts for PEMFC application*

Abstract

In the present work, Vulcan XC-72 carbon supported Pd, Ir and Pd_xIr_y (with x:y atomic ratios 3:1, 1:1, 1:3) electrode materials are prepared by a modified pulse microwave-assisted polyol method. The as-prepared catalysts are characterized structurally by X-ray diffraction (XRD) and morphologically by Transmission Electron Microscopy (TEM). Their electrocatalytic properties toward the reactions of Hydrogen Oxidation and Oxygen Reduction (HOR & ORR) are evaluated by cyclic voltammetry (CV) and by rotating disk electrode (RDE) techniques. The electrocatalytic activity of the electrode materials is estimated from the kinetic parameters, such as exchange current and kinetic current density, which are calculated from the experimental results and they are discussed in detail. It is found that exchange and kinetic current densities of Pd toward both HOR and ORR are enhanced after the addition of even small amounts of Ir. According to the results the highest HOR and ORR electrocatalytic activity enhancement is exhibited by PdIr (~100%) and Pd_3Ir (~350%) respectively. The order of electrocatalytic activity over the as prepared electrode materials is found to be $PdIr > PdIr_3 > Pd_3Ir > Pd > Ir$ for HOR and $Pd_3Ir > PdIr > PdIr_3 > Pd > Ir$ for ORR. The extent of alloying and d-band vacancies reveals new insights into the synergistic and antagonistic effects of the Pd_xIr_y electrode materials toward HOR and ORR electrocatalytic activity.

Contents

List of Figures

List of Tables

5.1 Introduction

Since 1999, the year in which Iceland announced its plan to become the first hydrogen-based economy in the next 30–40 years, governments and businesses have begun to seriously consider the hydrogen option. Hydrogen, is an attractive energy carrier and storage medium with high efficiency for developing a low-emission, environmentally benign, clean and sustainable energy system, to help solve the world's energy security and environmental problems [1]. However, numerous technical and infrastructure challenges in the areas of production, distribution, storage and end use must be resolved for hydrogen to play a central role in earth's energy and environment future [2]. One of the major energy conversion devices mainly in terms of efficiency are fuel cells, expected to play a great role in the integration of hydrogen into the economy. Fuel cells are electrochemical engines that directly convert chemical energy to electricity. One of the most developed fuel cells are those based on proton exchange membrane (PEMFCs) electrolytes. However, their commercialization is still hindered because of their high cost, which is in part attributed to their electrocatalysts mostly based on the expensive platinum (Figure 1) extensively adopted because its high activity and high stability.
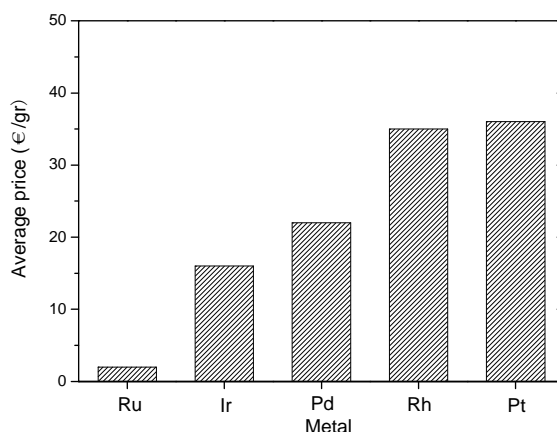
Figure 5.1: The average price in Euro per gram in the last year 2014 [3].

Therefore, in order to improve the catalytic activity, reduce the cost and increase the durability of the catalysts, many attempts have been made to design novel platinum-based

and platinum-free electrocatalysts for *hydrogen oxidation reaction* (HOR) and *oxygen reduction reaction* (ORR). With the exception of Pt, the electrocatalytic activity of Pd is one of the highest among the pure metals for both HOR and ORR. This, combined with the fact that the cost of Pd is about the half of Pt (Figure 1), makes it an attractive alternative [4].

It has been proved, that in acidic environment Pd-based electrocatalysts exhibit better activity than those based on Pt due to high solubility, permeability and selectivity for hydrogen, thus being a suitable membrane material for hydrogen separation [5-7]. Many attempts have been made to incorporate Pd with other elements in order to enhance the HOR activity of pure Pd. Various Pd-based catalysts with novel nanostructures, such as hollow, porous, core/shell, near-surface alloys etc. have been synthesized [8, 9]. Among them were bimetallic, Pt–Pd [10-12], Pd–Ru [13], Pd–Ni [14] and tri-metallic Pd–Pt–Rh [15], Pd-Ru–WO$_x$ [16] catalysts.

The performance of catalysts used for the oxygen reduction reaction (ORR) is one of the most extensively studied subjects in fuel cell research. Meanwhile, between the studied nanocatalysts, Pd bimetallic nanostructures are among the most interesting as cathode materials because of their superior catalytic activity [17, 18]. It has been found that the catalytic activity and stability of Pd based alloys for the ORR is improved by the addition of other elements, which could modify its electronic structure into core–shell type catalyst [19, 20]. Bimetallic combinations such as Pd-Ni [21], Pd-Co [22, 23], Pd-Cu [24-27], Pd-Fe [28, 29] have demonstrated to be the most active catalysts among the investigated ones, because of their moderate interaction with oxygen in acidic media [18].

Additionally, iridium is another metal which belongs to the platinum group (Figure 1) and according to theory [30] it should exhibit almost similar activity as platinum toward HOR and ORR. However, in literature very few studies have been devoted to palladium-iridium bimetallic electrocatalysts for HOR and ORR [31-33].

In the present work the catalytic activity of different Vulcan XC-72 supported Pd, Ir and Pd_xIr_y (where x:y = 3:1, 1:1, 1:3) electrocatalysts was separately tested for the reactions of *hydrogen oxidation* and *oxygen reduction*. The examined electrocatalysts were prepared by a modified pulse-microwave assisted polyol synthesis method. Their corresponding physico-chemical characteristics were obtained by using transmission electron microscopy (TEM) and X-ray diffraction (XRD), while their electrocatalytic activity toward the reactions of hydrogen oxidation and oxygen reduction was measured in acidic environment by cyclic voltammetry (CV) and rotating disk electrode (RDE) techniques.

5.2 Experimental

5.2.1 Electrocatalysts preparation

The 20 wt % Pd_xIr_y supported on Vulcan-XC 72 carbon electrocatalysts were prepared via a modified pulse-microwave assisted polyol synthesis procedure [34]. The primary steps of this synthesis process were: the starting precursors ($PdCl_2$.$2H_2O$ and $IrCl_2$ provided by Strem Chemicals) were added in a beaker with ethylene glycol (EG) and were well mixed in an ultrasonic bath. Then, Vulcan XC-72 carbon black (Cabot Corporation) was added into the above mixture. Consequently, the pH value of the system was adjusted to 13 by the drop-wise addition of 1.0 M NaOH/EG and a well-dispersed slurry was obtained with ultrasonic stirring for 60 min. Thereafter, the slurry was microwave-heated in the pulse form 10 s on/10 s off, for several times. In order to promote the adsorption of the suspended metal nanoparticles onto the carbon support, hydrochloric acid was adopted as the sedimentation promoter and the solution was re-acidified with a pH value of about 2–4. The obtained black solid sample was filtered,

washed and dried at 80°C for 10 h in a vacuum oven [35]. For the sake of comparison 20 wt% Pd/Vulcan XC-72 and 20wt% Ir/Vulcan XC-72 was similarly prepared.

5.2.2. Physicochemical characterization

The X-ray Diffraction (XRD) measurements were carried out with the aid of a D/Max-IIIA (Rigaku Co., Japan) employing Cu Kα ($\lambda = 0.15406$ nm) as the radiation source at 40 kV and 40 mA. Catalysts were investigated by TEM using a Philips CM12 microscope (resolution 0.2 nm), provided with high resolution camera, at an accelerating voltage of 120 kV. Suitable specimens for TEM analyses were prepared by ultrasonic dispersion in i-propylic alcohol adding a drop of the resultant suspension onto a holey carbon supported grid.

5.2.3 Electrochemical characterization

All the electrochemical measurements were carried out by the aid of an electrochemical workstation AMEL 5000, in a three-electrode model cell 497 (AMEL) with a mercury/mercury oxide ($Hg/HgCl_2$) (0.098 V vs. SCE) and platinum wire as the reference electrode and counter electrode, respectively.

A thin catalyst film was deposited onto a glassy carbon disk surface with a diameter of 3.0 mm. More precisely, a mixture containing 1.95 mg of electrocatalyst, 1.8 mL ethanol and 0.2 mL Nafion solution (5 wt %, Dupont Company) was ultrasonicated for 40 min to obtain a well-dispersed ink. The catalyst ink was then quantitatively (4 µL) transferred by the aid of a microsyringe onto the surface of the glassy carbon electrode and dried under infrared lamp to obtain a catalyst thin film. All the experiments were conducted using an aqueous solution containing 0.5 mol L^{-1} H_2SO_4 (Carlo Erba, 96%) at 25°C.

Before each experiment, the solution was bubbled for 30 min with high-purity N_2 in order to remove the dissolved oxygen. Moreover, before each measurement, each catalyst was applied under continuous potential cycling until stable electrochemical signals were

received. Each measurement started after several scans were performed and until reproducible voltammograms were obtained. The scanning potential was ranging from 0.0 to 1.2 V (vs. SCE) at a sweeping rate of 20 mVs^{-1}. For the ORR experiment, the electrolyte was saturated with oxygen, with a potential range from 0.9 to 0 V (vs. SCE) and a scan rate of 10 mV s^{-1}. For all measurements, the total catalyst loading was maintained at 11 μg cm^{-2}, while before each measurement the glassy carbon electrode was carefully cleaned by firmly pressing and moving it on a papery vessel containing a viscous deionized water solution of alumina.

5.3 Results and Discussion

5.3.1 Physicochemical characterization

In Fig. 5.2 the XRD patterns of the as prepared Pd, Ir and Pd$_x$Ir$_y$ catalysts are schematically shown. It can be distinguished that, except the characteristic peak of Vulcan XC-72 at 24.5°, the 2θ values of four more peaks at 40.07°, 46.53°, 68.19∘ and 82.02°, that correspond to face-centered cubic (fcc) crystalline Pd (1 1 0), (1 1 1), (2 0 0), (2 2 0) and (3 1 1), respectively are also shown. The highest intensity of peak from (1 1 1) plane indicates that this is the most exposed face of the Pd$_x$Ir$_y$/C nanoparticles. The peak position of (1 1 1) plane of Pd$_x$Ir$_y$/C electrocatalysts is between the Pd/C's and Ir/C's peaks position. In addition, no characteristic peaks related to Ir were observed, further supporting that a Pd-Ir alloy has been formed via insertion of Ir into Pd lattice. When the atomic ratio of Ir is decreased, the 2θ values of four peaks of Pd are also decreased. For example, the 2θ values of the four peaks of Ir and PdIr$_3$ catalysts are 40.06°, 46.91°, 67.89° and 84.09°, respectively (Fig. 5.2, curve e and d) and they are 39.04°, 45.51°, 66.55° and 82.00°, respectively, for the PdIr and Pd$_3$Ir catalyst (Fig. 5.2, curve c, b) [36]. Table 1 lists the crystallite sizes and the corresponding lattice parameters calculated using

the Scherrer formula and Bragg equations, respectively [37]. All the examined catalysts have crystallite sizes ranged between~3.5-4.0 nm.
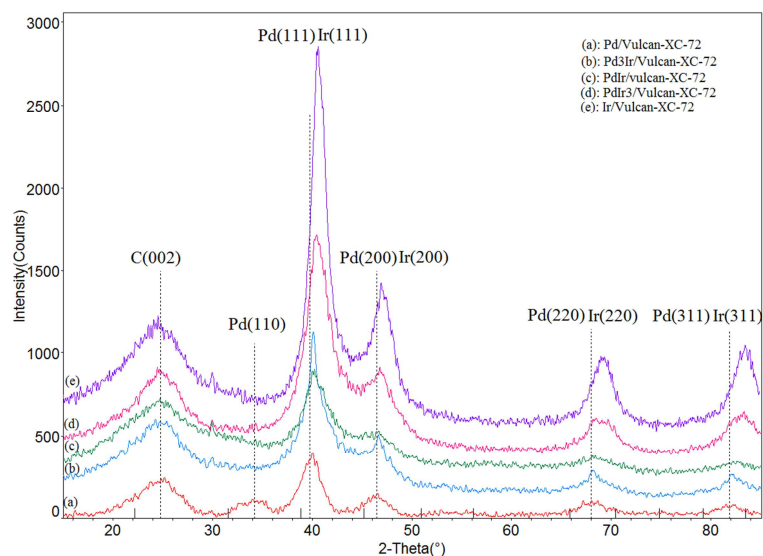
Figure 5.2: XRD patterns of Vulcan XC-72 supported: (a) Pd, (b) Pd₃Ir, (c) PdIr, (d) PdIr₃ and (e) Ir.

Table 5.1: Results obtained from the physicochemical characterization

Electrocatalyst	Lattice Parameter (nm)	Crystallite Size (nm)	Internal distance (nm)	Particles Size (±0.3nm)
Pd	0.38615	3.00	0.18701	4.30
Ir	0.38448	3.50	0.16655	5.70
Pd₃Ir	0.38843	3.50	0.16835	4.50
PdIr	0.38810	3.00	0.16812	4.40
PdIr₃	0.38503	4.00	0.16688	5.30

The mean size of the nanoparticles and their structure were further evaluated by the aid of TEM. The TEM micrographs with the respective particle size distribution histogram of the as-examined electrocatalysts are depicted in Fig. 5.3. It can be observed that, for Pd, Pd₃Ir and PdIr the metallic nanoparticles are homogenously dispersed on the carbon support with narrow size distribution in the supported catalyst. Ir and PdIr₃ have non-spherical morphologies and some larger aggregates were observed, but the amount of particles is few. One hundred particles were randomly measured to obtain the particle size distribution. The average particle sizes of the as prepared catalysts are reported in Table 5.1.
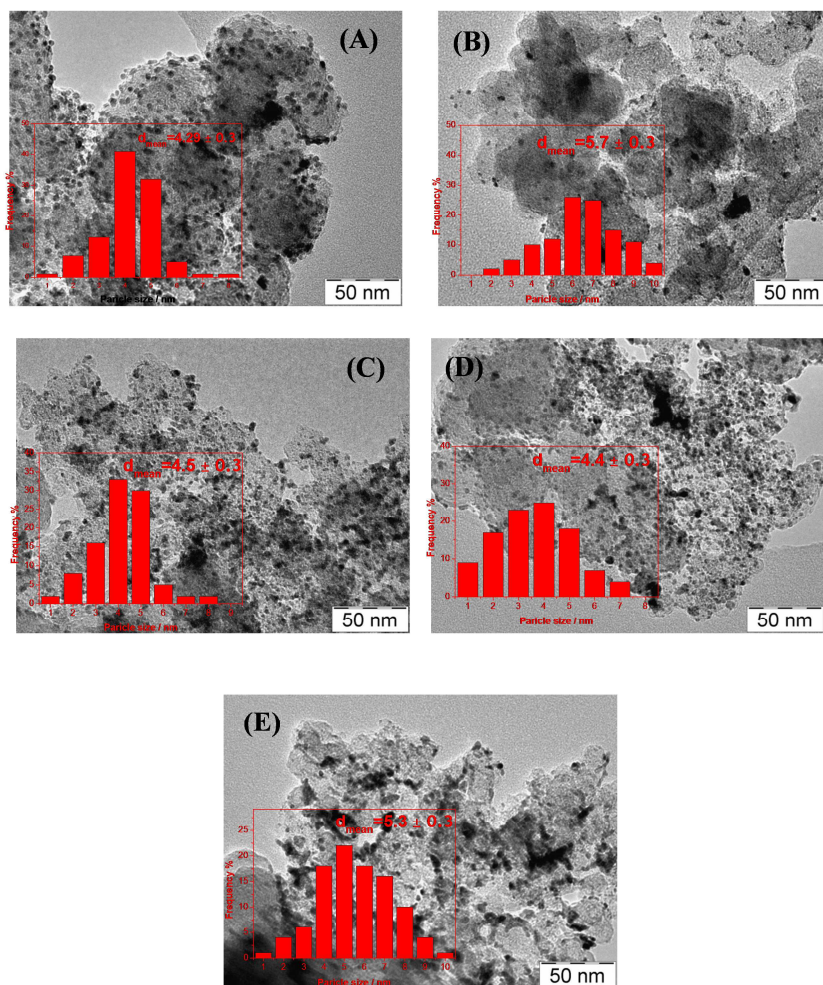
Figure 5.3: TEM images and corresponding of (A) Pd/ Vulcan XC-72, (B) Ir/Vulcan XC-72, (C) Pd$_3$Ir/Vulcan XC-72, (D) PdIr/Vulcan XC-72, (E) PdIr$_3$/Vulcan XC-72.

5.3.2 Electrochemical characterization

5.3.2.1 Cyclic voltammetry - Electrochemical active surface area

The cyclic voltammograms of Vulcan (XC-72) supported Pd, Ir, and Pd$_x$Ir$_y$ catalysts in 0.5M H$_2$SO$_4$ aqueous solution are depicted in Fig. 5.4. The broad peaks appearing between 0.0 and 0.2 V are due to the adsorption and desorption of atomic hydrogen at the surface of polycrystalline Pd in acidic media. As distinguished, for Ir and Pd$_3$Ir electrocatalysts are shifted to more positive potential values (ca.0.4V) [38]. The differences in position and shape of hydrogen peaks may be caused by a weaker adsorption of hydrogen on Pd.
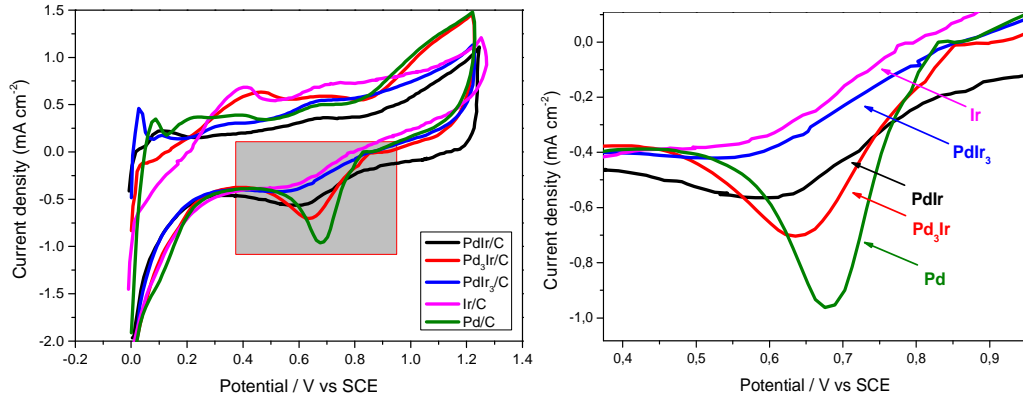
Figure 5.4: Cyclic voltammograms of the as prepared electrocatalysts in 0.5M H_2SO_4 with a scan rate of 50 mV s^{-1}.

A first estimation of the electrochemical reaction effectiveness can be achieved by the aid of the *electrochemical surface area* (ECSA), according to the following equation [39]:

$$ECSA\ \left[\frac{m^2}{g}\right] = \frac{Q_H}{Q_{(Pd\ or\ Ir)} \times m_{Pd\ or\ Ir} \times 10} \tag{5.1}$$

where Q_H ($\mu C cm^{-2}_{Pd}$) is the integrated charge on the PdO peak, Q_{Pd} ($= 420\ \mu C cm^{-2}_{Pd}$) and Q_{Ir} ($= 210\ \mu C cm^{-2}_{Ir}$) [40] are the specific amount of electricity corresponding to the full coverage of the Pd or Ir surface by one monolayer of oxygen ($\mu C cm^{-2}$) and $m_{Pd(Ir)}$ ($mg cm^{-2}_{electrode}$) is the palladium or iridium loading on the working electrode's surface. In the case of Pd-based electrocatalysts the hydrogen adsorption/desorption on Pd is overlapped by hydrogen adsorption/dissolution, with the ECSA of the as-prepared catalysts to be calculated by the charge consumed during the reduction of PdO_x at the backward scan. The consumed charge for a Pd monolayer oxide reduction is kept 0.420 $mC cm^{-2}$. The estimated ECSA are reported in Table 5.2.

Table 5.2: Cyclic voltammetry analysis.

Electrocatalyst	Pd loading ($\mu g\ cm^{-2}$)	Q_H ($mC\ cm^{-2}$)	ECSA ($m^2\ g^{-1}$)$_{Pd}$
Pd/ Vulcan XC-72	11	2.5	21.0
Pd$_3$Ir/ Vulcan XC-72	6.9	2.3	42.0
PdIr/ Vulcan XC-72	3.9	1.4	38.0
PdIr$_3$/ Vulcan XC-72	1.7	0.8	32.0
Ir/ Vulcan XC-72	0	0.7	30.0

In this study, for Vulcan (XC-72) supported Pd it is found an ECSA of 21 $m^2g_{Pd}^{-1}$, which is consistent with the value reported in literature [28]. According to the estimated ECSA values, as the Ir loading increases in the electrocatalyst, the number of surface active metal sites is decreased (consistent with larger particles). The specific ECSA of Pd_3Ir is 42 m^2g^{-1}, which is the highest measured among the as-prepared electrocatalysts. This could be ascribed to the relatively small particle sizes of the electrocatalyst's structure, as it can be distinguished from the TEM micrographs.

5.3.2.2 Hydrogen oxidation reaction (HOR)

Hydrogen oxidation reaction (HOR) has been extensively studied on Pt surfaces [41]. There are three elementary reaction steps for HOR on a Pt surface, based on the Tafel–Heyrovsky–Volmer mechanism [42]:

$$H_2 \leftrightarrows H_{ad} + H_{ad} \qquad \text{Tafel reaction} \qquad (1)$$

$$H_2 \leftrightarrows H_{ad} + H^+ + e^- \qquad \text{Heyrovsky reaction} \qquad (2)$$

$$H_{ad} \rightleftarrows H^+ + e^- \qquad \text{Volmer reaction} \qquad (3)$$

The most accepted mechanism for the hydrogen oxidation reaction (HOR) on polycrystalline metals in acidic media includes two steps: the 1st step, which involves the adsorption of molecular hydrogen on a surface active metal site either by the dissociation of hydrogen molecules into adsorbed atoms (Tafel process) or by the dissociation into ion and adsorbed atom (Heyrovsky process) and the 2nd step, which includes charge transfer procedure (Volmer process) [43].

Since the electronic properties of Pd are very similar to those of Pt, the HOR on Pd surfaces may follow the same pathways proposed for Pt [19]. The HOR polarization curves are depicted in Fig. 5.5. As it can be distinguished, the oxidation of H_2 over the Pd_xIr_y/C alloys and pure Ir/C starts at potential values around to 0.01 V (onset potential), while over pure Pd/C electrocatalyst the HOR's onset potential is higher, ca 0.1 V. At

more positive potentials, transition into the region of hydrogen mass transport controlled current densities starts at approximately 0.15 V for the PdIr/C, PdIr₃/C and Ir/C, while for the Pd/C and Pd₃Ir/C starts at 0.2V. As it was expected, the limiting current increases with the increment of the rotational speed of the electrode [44].
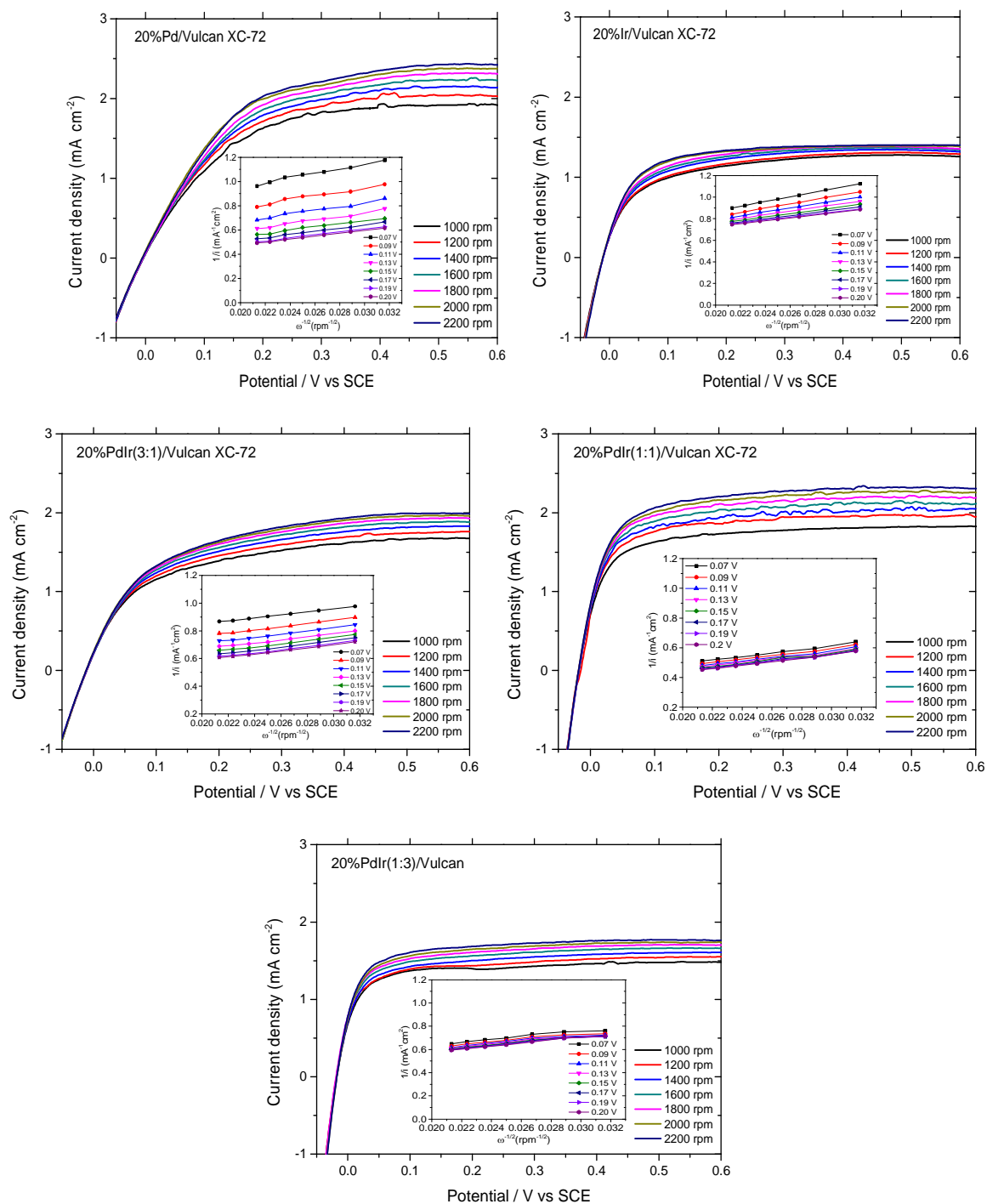
Figure 5.5: RDE curves in H_2-saturated 0.5 M H_2SO_4 at 5 mVs^{-1} for the examined electrocatalysts. The insets are the corresponding Koutecky-Levich plots for the hydrogen oxidation reaction.

As known, the kinetic current density (i_k) is a measure of the rate of charge transfer on the catalyst's surface, describing the real kinetics of an electrocatalytic reaction and therefore is directly related to the electrocatalyst's activity. To determine the catalytic activity of the electrocatalysts, the Koutecky–Levich analysis [39, 45] has been adopted, where the kinetic current is related to the rotational velocity of the RDE through the following equation:

$$\frac{1}{i} = \frac{1}{i_k} + \frac{1}{i_d}$$

(5.2)

In Eq. 5, i is the measured current density, i_k the kinetic current in absence of mass transfer limitations and i_d the diffusion current density. The later (i_d) can be calculated according to the Levich equation:

$$i_d = 0.62 nFD^{2/3} v^{-1/6} C\omega^{1/2}$$

(5.3)

Where n represents the number of theoretically-transferred electrons (=2), F the Faraday constant (95485 C/mol), D the diffusion coefficient of H_2 in H_2SO_4 (3.7×10^{-5} cm^2 s^{-1}), v the kinematic viscosity of the electrolyte and C the H_2 concentration in the electrolyte (7.14×10^{-7} mol cm^{-3}).

In the insets of Fig.5.5 the respective Koutecky-Levich plots are depicted at different potential values. The intercept of each line corresponds to the inverse of the intrinsic kinetic current value, i_k (according to eq.5), while from the slope the number (*n*) of the transferred electrons can be calculated. More specifically, the Koutecky-Levich plots are provided for the examined Pd_xIr_y, Pd and Ir electrocatalysts. From the plots the kinetic currents for HOR, at different potential values (vs SCE), were extracted. As follows from their analysis, the experimental points exhibit a linear behaviour ensuring the accuracy of *n* and i_k determination. In Table 5.3 the calculated kinetic current density values at 0.07V

are reported. According to them, for 1:1, Pd:Ir ratio the highest kinetic current density is exhibited, while for 3:1, the lowest one.

Table 5.3: Kinetic parameters of the examined electrocatalysts for HOR

Electrode (20%wt metal loading)	Tafel slope (mV decade^{-1})	i_o (mA cm^{-2})	i_k (@0.07V) (mA cm^{-2})
Pd/ Vulcan XC-72	80.0	0.35	2.50
Pd$_3$Ir/Vulcan XC-72	95.0	0.70	2.80
PdIr/ Vulcan XC-72	120	1.60	4.70
PdIr$_3$/ Vulcan XC-72	50.0	1.00	3.50
Ir/ Vulcan XC-72	71.0	0.20	1.40

Once the kinetic currents for different potential and for all the examined catalysts were calculated, a more thorough kinetic analysis is performed by the aid of the Tafel equation [46] which describes the relationship between overpotential and current density:

$$\log(i_k) = \log(i_o) + (\frac{anF}{2.303RT})\eta \tag{5.4}$$

As known, from Tafel's analysis (intercept and slope) useful kinetic information to measure the electrochemical activity of an electrode material can be obtained [47]: i) the exchange current density (i_o) and ii) the charge transfer coefficient. Exchange current density is analogous to the rate constant used in chemical kinetics, and a high i_o value often translates into a fast electrochemical reaction. On the other hand from the kinetic point of view a smaller Tafel slope is desirable (for smaller overpotential values). Moreover, according to literature [41], the slope values and the hydrogen oxidation reaction are well described by the Tafel–Heyrovsky–Volmer mechanism. In Fig. 5.6 the Tafel plots are depicted. It is obvious that, among the investigated samples, PdIr/C exhibits the highest electrocatalytic activity towards hydrogen electrooxidation. Furthermore, according to the theoretical prediction and the calculated Tafel slopes (around and higher than 60 mVdecade^{-}

[1], Table 5.3), the results are well described by the Tafel-Volmer mechanism Eqs (3) & (4), with the Volmer to be the rate determining step [48]).
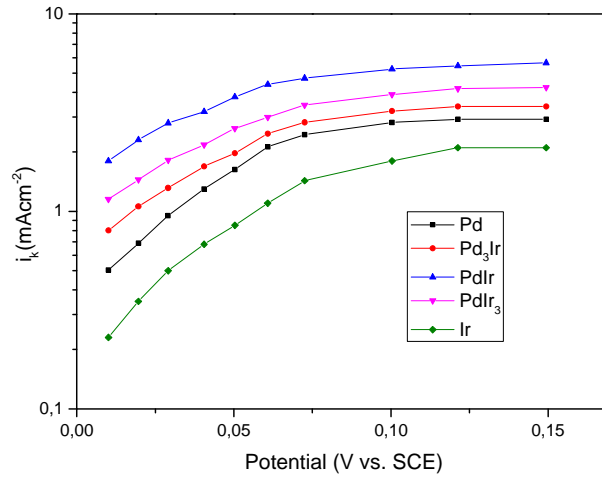
Figure 5.6: Tafel plots for HOR.

The effect of Ir loading to Pd on the HOR electrocatalytic activity (on both kinetic and exchange current) of the examined electrodes materials is schematically shown in Fig. 5.7. As it can be seen, the increase of the Ir loading enhances the electrocatalytic activity of Pd, towards HOR, exhibiting a maximum for the case of PdIr, for which the values of exchange and kinetic current density reaches 1.6 and 4.7 mA cm^{-2}, respectively.
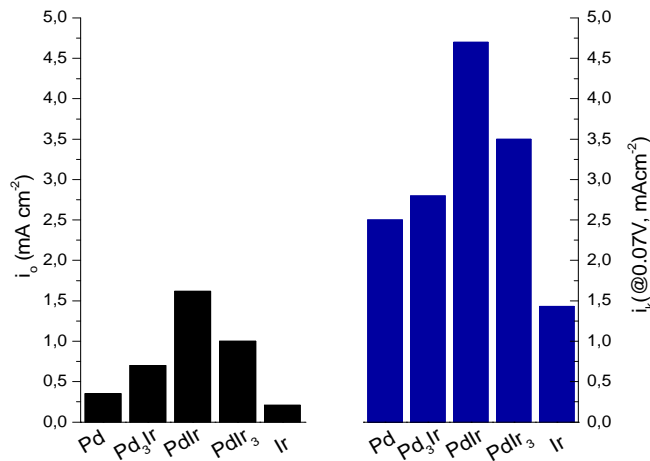
Figure 5.7: Exchange current density and kinetic current density vs iridium metal loading for HOR.

As it has been reported in literature [49], the electrocatalytic hydrogen oxidation reaction over bimetallic palladium-iridium electrocatalysts is affected by the Pd/Ir ratio. More precisely, alloys HOR catalytic activity of the Pd_xIr_y catalysts is correlated to iridium's d-band vacancy

exhibiting volcano type dependence between exchange current density and Pd percentage as well as between the exchange current density and d-band vacancy. This volcano type behavior is attributed to the fact that HOR activity is given by the strength of the Ir-H bond interaction, which depends on the position of the Ir d-band states relevant to the Fermi level. The "extent" of d-band vacancy could affect the "extent" of the electrocatalytic activity of the as prepared electrode materials [49]. The same volcano behavior is observed also for our samples (Fig. 5.7), with the sample contained 50%Pd (PdIr) to exhibit the highest exchange current density. Consequently, the decrement of activity for the $PdIr_3$ it may can be attributed to the further "extent" of Ir's d-band vacancy and to the higher binding of adsorbates.

5.3.2.3. Oxygen reduction reaction kinetics

The ORR activities of Pd/C, Ir/C and Pd_xIr_y/C electrocatalysts were tested in aqueous O_2-saturated 0.5 M H_2SO_4 solution under different rotation rates (from 500 to 2500rpm) at a scan rate of 10 mV s^{-1} (Fig. 5.8).
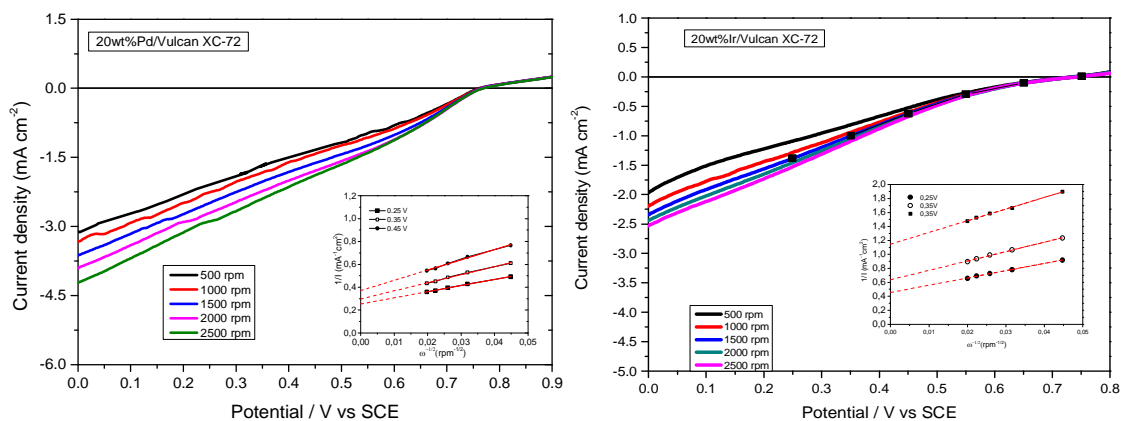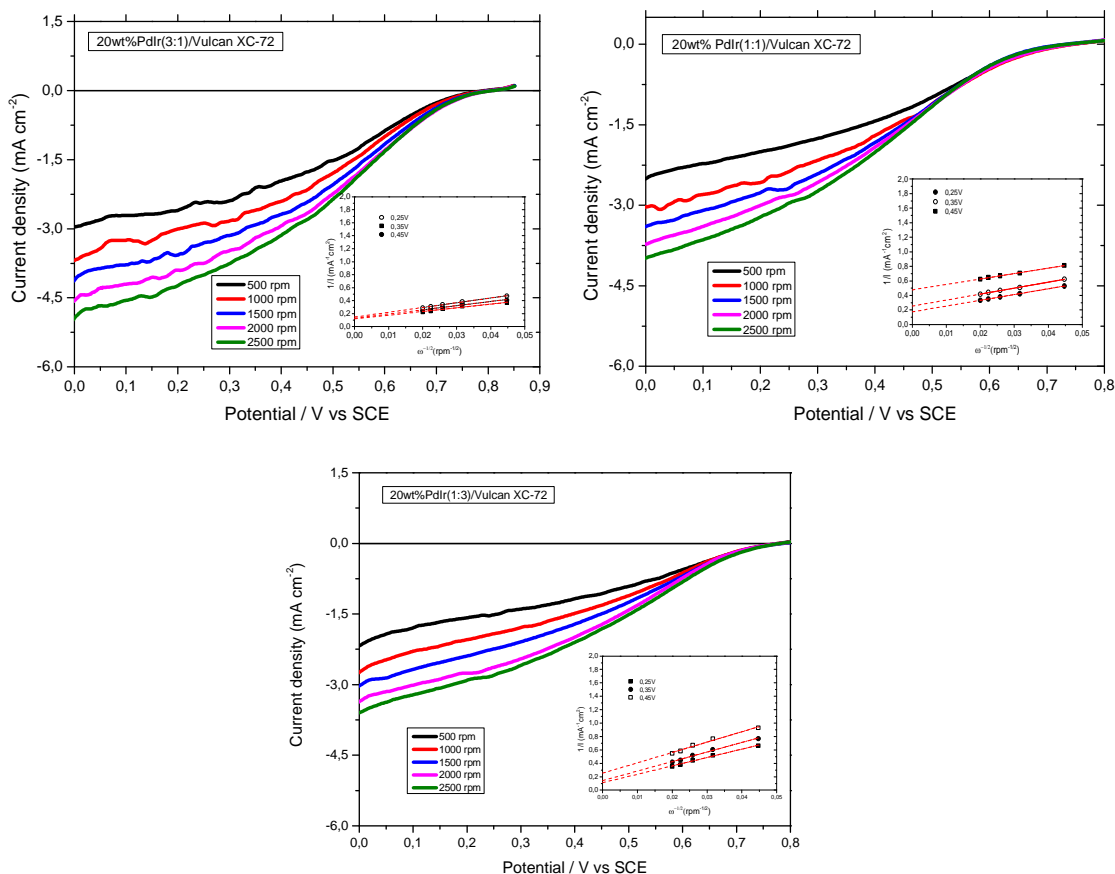
Figure 5.8: Potential curves for ORR on examined electrocatalysts at different rotation rates, in 0.5 M H_2SO_4 electrolyte. Inset: Koutecky–Levich plots at various electrode potentials.

As it can be seen from Fig. 5.8, the ORR curve can be distinguished in three regions: i) the kinetic region (0.6–0.8 V), ii) the mix-controlled region (0.2–0.6 V) and iii) the diffusion region (0.0–0.2 V). At approximately 0.7–0.8 V vs SCE, current values do not change with increasing rotation rate, suggesting the domination of the electron-transfer kinetics in this potential range. In the potential range of 0.0–0.2 V, the currents depend on the rotation rate and display well-defined limiting currents (plateau), indicating that the currents are controlled by the rate of O_2 diffusion from the solution's bulk to the catalyst-electrode surface. In the potential range between 0.7 and 0.2 V, both molecular oxygen mass transfer (diffusion) and electron transfer kinetics contribute to the current. The improved ORR rate obtained with Pd_3Ir was mainly attributed to Pd enrichment on the

surface and the result was consistent with its high ECSA and oxide reduction charge observed in the cyclic voltammogram for this catalyst.

From the experimental results (Figs 5.8) and by the aid of Koutecky–Levich analysis (Eqs 5 & 6), as in the case of HOR reported above, have been determined the kinetic parameters of the electrocatalysts: i) the kinetic current density and ii) the number of electrons transferred during the reaction. More precisely, from the intercept of Koutecky-Levich plots (straight lines in the insets of Figs 5.8), at electrode potentials of 0.25, 0.35 and 0.45 V (vs. SCE), the kinetic current density values were calculated, while from their slope the number of electrons involved in the ORR has been identified. In Fig. 9 the transferred electron number (n), for all tested catalysts and for two different potential values are reported.
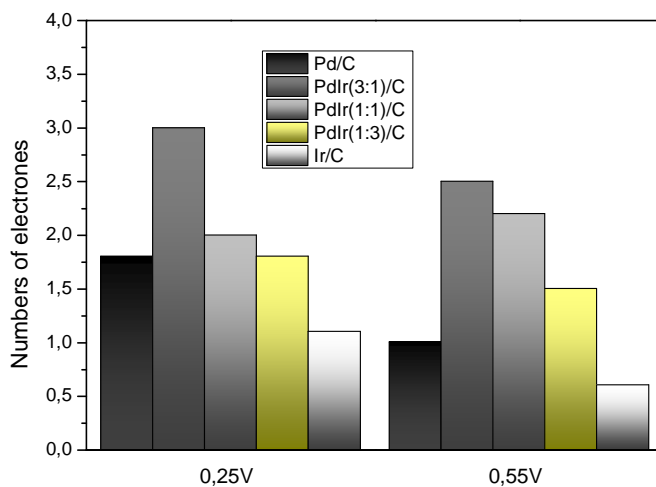
Figure 5.9: Electron transfer numbers (n) during the ORR on the prepared catalysts at 0.25 and 0.55V.

The ORR is a multi-electron reaction, consisting of elementary steps and different reaction intermediates. During ORR two main reactions usually occur on the catalyst surface, as it is described in equations (8) and (9):

$$O_2 + 2H^+ + 2e \rightarrow H_2O_2 \qquad\qquad \text{(5.5)}$$

$$H_2O_2 + 2H^+ + 2e \rightarrow 2H_2O \qquad\qquad \text{(5.6)}$$

Hydrogen peroxide is the intermediate species when ORR proceeds via the two-electron pathway [50]. The electron transfer number for the Pd/C catalyst is 1.8, therefore it could be said that hydrogen peroxide is the main product in Pd/C-catalyzed ORR. For the Pd_3Ir catalyst the value of electron transfer number varies from 2.5 to 3, indicating that the ORR occurs following an approximate 4-electron pathway where O_2 is directly reduced to H_2O [51]. The direct ORR pathway via a 4-electron transfer is desirable rather than the 2-electron transfer pathway, which may negatively affect the stability of the catalysts [52]. Based on Tafel equation (eq.7) and the Tafel plots that are depicted in Fig. 5.10: i) the exchange current density and ii) Tafel slopes are calculated (Table 5.4). For all the catalysts Tafel slopes are estimated at ~120 mVdecade^{-1} As it is known a Tafel slope value of 120 mV indicates that the first electro n transfer is the rate-determining step: $O_2 + e^- \rightleftarrows O_{2,ads}$[53].
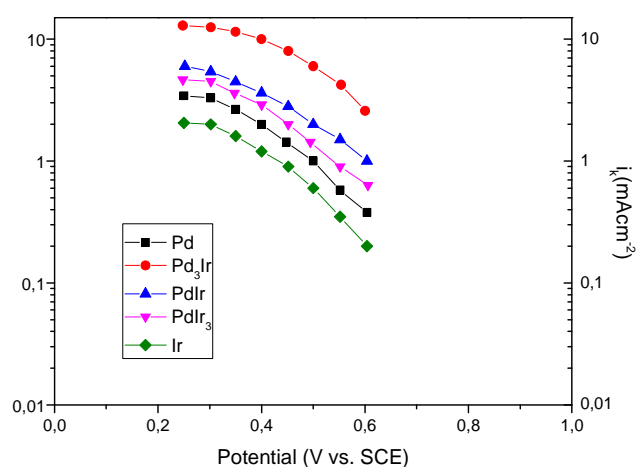
Figure 5.10: Tafel plots for ORR.

As it can be seen, pure iridium exhibits a relatively low ORR electrocatalytic activity as compared with other electrocatalysts. Birss, V.I *et al.* [54] reported that despite the fact that pure Ir possesses low activity towards ORR, it owes a promoting action in alloys.

Table 5.4: Kinetic parameters of the examined electrocatalysts for ORR

Electrode (20%wt metal loading)	i_o (mA cm^{-2})	Tafel slope (mV decade^{-1})	i_k (@0.35V) (mA cm^{-2})
Pd/ Vulcan XC-72	0.01	131	2.65
Pd$_3$Ir/Vulcan XC-72	0.1	140	11.50
PdIr/ Vulcan XC-72	0.06	110	4.40
PdIr$_3$/ Vulcan XC-72	0.02	129	3.60
Ir/ Vulcan XC-72	0.005	111	1.60

A schematic representation of the effect of Ir loading on the exchange current density and the kinetic current is depicted in Fig. 5.11. It can be clearly seen that the addition of Ir to Pd, positively affects the values of both exchange current density and kinetic current density, exhibiting a volcano-type dependence on the Pd:Ir atomic ratio.
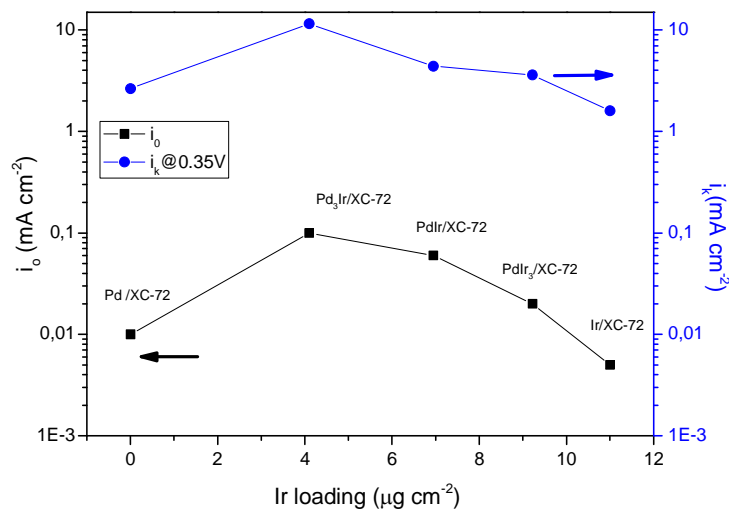
Figure 5.11: Exchange current density and kinetic current density vs iridium metal loading for ORR.

As in similar cases reported in literature [31], the observed volcano behaviour could partly be attributed to electronic reasons. More precisely, the addition of Ir to Pd increase the extent of Pd's d-vacancy, increasing in the oxygen π electrons donation to the surface of Pd, enhancing consequently oxygen adsorption and weakening of the O-O bonds. Another reason could also be attributed to the fact that Ir atoms exposed to the catalyst

surface are likely to be covered by OH_{ads} at more negative potentials than Pd, because the onset potential of the OH_{ads} region for Ir is more negative than that for Pd (Fig.4). Thus, the Ir atoms could predominantly be covered by OH_{ads} at the first stage of the OH_{ads} formation, leaving more Pd sites free for the ORR, which may partly lead to the enhanced kinetics of the Pd-Ir alloys [31].

Therefore, according to the generally accepted four-electron transfer mechanism of oxygen reduction it seems that the O-O bond breaking and the O–H bond formation take easier place at lower Ir loading. It seems that this loading of Ir is enough for binding the oxygen strongly and the OH modestly so that OH removal from the catalyst surface by water elimination to be also reasonably facile [55].

5.4 Conclusions

Platinum free, Vulcan XC-72 carbon supported Pd_xIr_y, Pd and Ir catalysts with relatively high nanoparticles dispersion were successfully synthesized by the aid of a pulse-microwave assisted polyol method. Based on the experimental results, it could be concluded that the use of the above synthesis method is an effective way to get carbon supported electrocatalysts with high dispersion in a short time and with low cost. According to the electrochemical results obtained in the present work, it seems that in all cases the addition of Ir enhances the electrocatalytic activity of Pd toward hydrogen oxidation and oxygen reduction reaction. In both cases a volcano-type exchange current density dependence on Ir-loading is observed. The maximum value: for HOR was measured over PdIr (1.6 $mAcm^{-2}$), while for ORR was measured over Pd_3Ir (0.1 $mAcm^{-2}$). A similar behavior has been also observed for the kinetic current density vs Ir-loading. The lower values have been observed for pure iridium and pure palladium. From the K–L plots, the ORR the electron transfer number ~2 and believed to occur mainly via 2-electron transfer except for Pd_3Ir which the electron transfer number ~4.

As it can be concluded from the exchange current density values, measured for the as prepared electrode materials and under the same experimental conditions, the hydrogen oxidation reaction is 1-3 magnitudes faster than the oxygen reduction reaction. It seem that both HOR & ORR electrocatalytic activity of the as prepared electrode materials could be attributed to the extent of d-band vacancy and the Pd_xIr_y interatomic distance. From the obtained results, it is believed that PdIr and Pd_3Ir could be considered as promising (cheaper than Pt) anode and cathode electrocatalysts respectively for hydrogen fed PEM fuel cells.

References

[1]   X. Deng, H. Wang, H. Huang, M. Ouyang. Int. J. Hydrogen Energy 35 (2010) 6475-6481.

[2]   F. Kreith, R. West. J Energy Resour Technol 126 (2004) 249-257.

[3]   S. Song, J. Liu, J. Shi, H. Liu, V. Maragou, Y. Wang, P. Tsiakaras. Appl. Catal., B 103 (2011) 287-293.

[4]   A. Brouzgou, S.Q. Song, P. Tsiakaras. Appl. Catal., B 127 (2012) 371-388.

[5]   J. Shu, B.P.A. Grandjean, A. Van Neste, S. Kaliaguine. Can. J. Chem. Eng. 69 (1991) 1036-1060.

[6]   S. Yun, S. Ted Oyama. J. Membr. Sci. 375 (2011) 28-45.

[7]   O. Hatlevik, S.K. Gade, M.K. Keeling, P.M. Thoen, A.P. Davidson, J.D. Way. Sep. Purif. Technol. 73 (2010) 59-64.

[8]   X.W. Lou, L.A. Archer, Z. Yang. Adv. Mater. 20 (2008) 3987-4019.

[9]   H.P. Liang, H.M. Zhang, J.S. Hu, Y.G. Guo, L.J. Wan, C.L. Bai. Angew. Chem. Int. Ed. 43 (2004) 1540-1543.

[10]   A. Czerwiński, M. Grdeń, M. Łukaszewski. J. Solid State Electrochem. 8 (2004) 411-415.

[11]   Y.-H. Cho, Y.-H. Cho, J.W. Lim, H.-Y. Park, N. Jung, M. Ahn, H. Choe, Y.-E. Sung. Int. J. Hydrogen Energy 37 (2012) 5884-5890.

[12]   A.u. Rehman, S.S. Hossain, S.u. Rahman, S. Ahmed, M.M. Hossain. Appl. Catal., A 482 (2014) 309-317.

[13]   S.K. Gade, M.K. Keeling, A.P. Davidson, O. Hatlevik, J.D. Way. Int. J. Hydrogen Energy 34 (2009) 6484-6491.

[14]   D.J. Ham, C. Pak, G.H. Bae, S. Han, K. Kwon, S.A. Jin, H. Chang, S.H. Choi, J.S. Lee. Chem. Commun. 47 (2011) 5792-5794.

[15]   M. Łukaszewski, M. Grdeń, A. Czerwiński. J. Electroanal. Chem. 573 (2004) 87-98.

[16]   K. Kwon, S.-a. Jin, K.H. Lee, D.J. You, C. Pak. Catalysis Today 232 (2014) 175-178.

[17]   H. Lee, S.E. Habas, G.A. Somorjai, P. Yang. J. Am. Chem. Soc. 130 (2008) 5406-5407.

[18]   J.J. Salvador-Pascual, S. Citalán-Cigarroa, O. Solorza-Feria. J. Power Sources 172 (2007) 229-234.

[19]   M. Shao. J. Power Sources 196 (2011) 2433-2444.

[20]   M. Shao, P. Liu, J. Zhang, R. Adzic. J. Phys. Chem. B 111 (2007) 6772-6775.

[21]   G. Ramos-Sánchez, H. Yee-Madeira, O. Solorza-Feria. Int. J. Hydrogen Energy 33 (2008) 3596-3600.

[22]   E. Antolini, S.C. Zignani, S.F. Santos, E.R. Gonzalez. Electrochim. Acta 56 (2011) 2299-2305.

[23]   W. Wang, D. Zheng, C. Du, Z. Zou, X. Zhang, B. Xia, H. Yang, D.L. Akins. J. Power Sources 167 (2007) 243-249.

[24]   D.C. Martínez-Casillas, G. Vázquez-Huerta, J.F. Pérez-Robles, O. Solorza-Feria. J. Power Sources 196 (2011) 4468-4474.

[25]   X. Wang, N. Kariuki, J.T. Vaughey, J. Goodpaster, R. Kumar, D.J. Myers. J. Electrochem. Soc. 155 (2008) B602-B609.

[26]   C. Xu, Y. Zhang, L. Wang, L. Xu, X. Bian, H. Ma, Y. Ding. Chem. Mater. 21 (2009) 3110-3116.

[27]   N.N. Kariuki, X. Wang, J.R. Mawdsley, M.S. Ferrandon, S.G. Niyogi, J.T. Vaughey, D.J. Myers. Chem. Mater. 22 (2010) 4144-4152.

[28]   M.H. Shao, K. Sasaki, R.R. Adzic. J. Am. Chem. Soc. 128 (2006) 3526-3527.

[29]   M.R. Tarasevich, G.V. Zhutaeva, V.A. Bogdanovskaya, M.V. Radina, M.R. Ehrenburg, A.E. Chalykh. Electrochim. Acta 52 (2007) 5108-5118.

[30]   O.T. Holton, J.W. Stevenson. Platinum Metals Review 57 (2013) 259.

[31]   T. Ioroi, K. Yasuda. J. Electrochem. Soc. 152 (2005) A1917-A1924.

[32]   C.-H. Wang, H.-C. Hsu, K.-C. Wang. J. Colloid Interface Sci. 427 (2014) 91-97.

[33]   T. Ioroi, N. Kitazawa, K. Yasuda, Y. Yamamoto, H. Takenaka. J. Electrochem. Soc. 147 (2000) 2018-2022.

[34]   S. Song, Y. Wang, P.K. Shen. J. Power Sources 170 (2007) 46-49.

[35]   S. Song, J. Liu, J. Shi, H. Liu, V. Maragou, Y. Wang, P. Tsiakaras. Applied Catalysis B: Environmental 103 (2011) 287-293.

[36]   X. Wang, Y. Tang, Y. Gao, T. Lu, J. Power Sources, 2008, pp. 784-788.

[37]   V. Radmilovic, H.A. Gasteiger, P.N. Ross. J. Catal. 154 (1995) 98-106.

[38]   D.J. You, S.-a. Jin, K.H. Lee, C. Pak, K.H. Choi, H. Chang. Catalysis Today 185 (2012) 138-142.

[39]   D. Chen, P. Cui, H. He, H. Liu, J. Yang. J. Power Sources 272 (2014) 152-159.

[40]   E. Abu Irhayem, H. Elzanowska, A.S. Jhas, B. Skrzynecka, V. Birss. J. Electroanal. Chem. 538–539 (2002) 153-164.

[41]   P.M. Quaino, J.L. Fernández, M.R. Gennero de Chialvo, A.C. Chialvo. J. Mol. Catal. A: Chem. 252 (2006) 156-162.

[42]   C. Gabrielli, P.P. Grand, A. Lasia, H. Perrot. J. Electrochem. Soc. 151 (2004) A1937-A1942.

[43]   B.E. Conway, B.V. Tilak. Electrochim. Acta 47 (2002) 3571-3594.

[44]   R. Escudero-Cid, A.S. Varela, P. Hernández-Fernández, E. Fatás, P. Ocón. Int. J. Hydrogen Energy 39 (2014) 5063-5073.

[45]   J. Durst, A. Siebel, C. Simon, F. Hasche, J. Herranz, H.A. Gasteiger. Energy Environ Sci 7 (2014) 2255-2260.

[46]   W. Sheng, H.A. Gasteiger, Y. Shao-Horn. J. Electrochem. Soc. 157 (2010) B1529-B1536.

[47]   D.L. Langhus. J. Chem. Educ. 76 (1999) 1069.

[48]   R.M. Mello, E.A. Ticianelli. Electrochim. Acta 42 (1997) 1031-1039.

[49]   A. Wieckowski, J. Norskov, S. Gottesfeld, Fuel Cell Science: Theory, Fundamentals, and Biocatalysis, Wiley, 2011.

[50]   C.M. Sánchez-Sánchez, A.J. Bard. Anal. Chem. 81 (2009) 8094-8100.

[51]   S.-S. Li, J.-N. Zheng, A.-J. Wang, F.-L. Tao, J.-J. Feng, J.-R. Chen, H. Yu. J. Power Sources 272 (2014) 1078-1085.

[52]   S.J. Han, H.J. Jung, J.H. Shim, H.-C. Kim, S.-J. Sung, B. Yoo, D.H. Lee, C. Lee, Y. Lee. J. Electroanal. Chem. 655 (2011) 39-44.

[53]   M. Macia, J. Campina, E. Herrero, J. Feliu. J. Electroanal. Chem. 564 (2004) 141-150.

[54]   P.G. Pickup, V.I. Birss. J. Electroanal. Chem. Interf. Electrochem. 240 (1988) 185-199.

[55]   H.I. Karan, K. Sasaki, K. Kuttiyiel, C.A. Farberow, M. Mavrikakis, R.R. Adzic. ACS Catalysis 2 (2012) 817-824.

An Investigation of WC Stability during the Preparation of Pt@WC/OMC via a Pulse Microwave Assisted Polyol Method*

Abstract

In the present work, the tungsten carbide (WC) stability during the preparation of Pt@WC/OMC (Ordered Mesoporous Carbon) electrocatalysts, via a pulse microwave-assisted polyol method, is investigated by the aid of X-ray diffraction and thermogravimetric method. More precisely, OMC self-supported Tungsten Carbide (WC/OMC) is successfully synthesized by combing the hydrothermal process with a hard template method and its stability is step by step checked during the preparation process of the Pt@WC/OMC electrocatalyst by the pulse microwave-assisted polyol method. It is found that the strong alkaline and acid environment has a relatively small but not serious effect on the stability of WC. It is also found that in absence of Pt precursor, microwave irradiation itself also has a small effect on the stability of WC, while once Pt precursor is introduced into the system more than half of the initial WC disappeared or is oxidized. To avoid this process, Pt@WC/OMC-MM is obtained by mechanically mixing (MM) of the as prepared WC/OMC and Pt@C. Moreover, the electrochemical results of methanol oxidation reaction how that the content of WC has an obvious effect on Pt's activity towards MOR, with the best performance in the case of $Pt_{20}WC_{22}/OMC$-MM.

Chapter 6: An Investigation of WC Stability during the Preparation of Pt@WC/OMC via a Pulse Microwave Assisted Polyol Method

127

Contents

Chapter 6: An Investigation of WC Stability during the Preparation of Pt@WC/OMC via a Pulse Microwave Assisted Polyol Method

128

List of Figures

Chapter 6: An Investigation of WC Stability during the Preparation of Pt@WC/OMC via a Pulse Microwave Assisted Polyol Method

129

6.1 Introduction

Tungsten carbide (WC), since Levy *et al.* [1] demonstrated its catalytic properties similar to Pt, has been proved to be a very promising alternative electrocatalyst [2-6] for fuel cell application. The special characteristics of tungsten carbide (WC) in electrocatalysis, such as the excellent tolerance to CO and H_2S [7-9], the desirable synergetic effect on Pt's activity towards the electrooxidation of both hydrogen [10] and methanol [11-14], as well as towards the oxygen reduction reaction [15-21], have already been recognized. These properties make WC an interesting and an attractive low-cost electrocatalyst alternative. Moreover, WC exhibits good stability in both acidic and alkaline media, under different electrochemical conditions [22-27].

The corresponding investigations on WC stability in variable harsh conditions, such as strong base or acid environment [24], high temperature [23] and potential cycling [28], have been carried out. On the other hand, it is known that WC alone is inactive or less active to the electrochemical reactions [29]. For this reason, Pt-based particles are always deposited on WC or on carbon supported WC, leading to an increased electrochemical activity through the synergetic effect [4, 29]. Recently, Zheng *et al.* [3] reported that WC/OMC composites were active and exhibited very close performance to Pt for methanol electrooxidation reaction (MOR). Additionally, Lu *et al.* [2] indicated that WC not only played the role of support in Pt-based electrocatalysts, but also it constituted an active phase for MOR.

In any case, during the supported catalyst preparation process, in order to deposit and

Chapter 6: An Investigation of WC Stability during the Preparation of Pt@WC/OMC via a Pulse Microwave Assisted Polyol Method

130

reduce the metal precursors, alkaline environment (or other deposition agents) and high temperature are always required [31-33]. Furthermore, in the colloid method for catalysts preparation, acid is needed to destroy the colloid and thus accelerate the deposition of metal particles [34, 35]. Obviously, the general catalysts preparation process always involves wild conditions, which could lead to the instability of WC, in the case that it is adopted as the supporting materials. The microwave-assisted polyol method is one of the most desirable techniques for preparing supported Pt-based catalysts, because of the fast (~2 min) and efficient reduction of the metal precursors to metal atoms [36-41].

The main advantages of this method derive from the microwave heating itself, which include: i) speeding up (minutes instead of hours), ii) high efficiency, iii) high uniformity, and iv) precise temperature regulation and control. The as-referred typical preparation process, as shown in Fig. 6.1, involves strong alkaline environment for metal precursor deposition and strong acid environment for destroying the colloid, and thus promoting the metal particles to settle onto the supported materials.
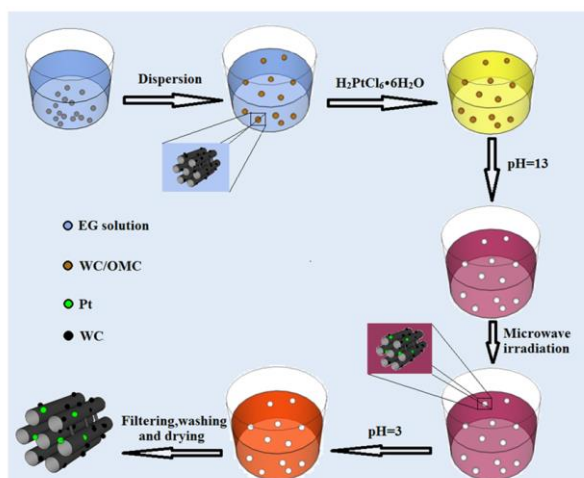
Figure 6.1: The schematic procedure for Pt@WC/OMC preparation through a pulse microwave assisted polyol method.

Chapter 6: An Investigation of WC Stability during the Preparation of Pt@WC/OMC via a Pulse Microwave Assisted Polyol Method

131

Additionally, in order for the metal ions to be completely reduced, high temperature (here in the form of pulse microwave irradiation) is required, especially in the case that ethylene glycol is used as the reducing agent.

In the present investigation, the stability of the as-prepared (via the combination of a hydrothermal process and a hard template method) *ordered mesoporous carbon self-supported tungsten carbide* (WC/OMC) composites is step by step systematically studied during the preparation process of Pt@WC/OMC via a pulse microwave-assisted polyol method.

6.2 Experimental

6.2.1 Synthesis of WC/OMC composites

WC/OMC sample was prepared by combing the hydrothermal reaction and the hard template method with ammonium metatungstate (AMT) as the tungsten precursor, glucose as the carbon source and the ordered mesoporous silica (SBA-15) as the hard template, respectively. The preparation details have been previously described [14].

6.2.2 Preparation of electrocatalysts

The Pt@WC/OMC-MP (Microwave-Polyol method) catalyst with a Pt loading of 20 wt.% was prepared by a pulse microwave-assisted polyol method [42]. The preparation procedure, as shown in Fig. 6.1, can be described in details as follows. The as-prepared WC/OMC as the supporting materials was well mixed with *ethylene glycol* (EG) in an ultrasonic bath and then an appropriate amount of $H_2PtCl_6 \cdot 6H_2O$ dissolved in EG was

Chapter 6: An Investigation of WC Stability during the Preparation of Pt@WC/OMC via a Pulse Microwave Assisted Polyol Method

132

added into the mixture. After the pH value of the above mixture was adjusted to 13 by the dropwise addition of 1.0 mol L^{-1} NaOH/EG solution, the well-dispersed slurry was obtained with magnetic stirring for another 1 h. Thereafter, the slurry was microwave-heated in the pulse form of 10 s-ON/10 s-OFF for several times. After reaction, 1.0 mol L^{-1} HCl solution was added to accelerate the deposition process of metal particles. Finally, the resulting sample was filtered, washed with abundant hot water ($\geq 90^{o}C$) until no chloride anion was detected by 1.0 mol L^{-1} $AgNO_3$ solution in the filtrate and then dried at $80^{o}C$ overnight in a vacuum oven.

In order to control WC content in the catalyst and compare with the activity of Pt@WC/OMC-MP, mechanical mixing method was adopted to obtain Pt@WC/OMC-MM (Mechanical Mixing) with different WC content. Pt@C catalysts were prepared by a pulse microwave-assisted polyol method. Then, the as-prepared Pt@C catalysts were mixed with the as-prepared WC/OMC by grinding for 2 h and then stirring in EG for 24 h. Next, the resulting sample was filtered, washed and then dried at $80^{o}C$ overnight in a vacuum oven. Finally, $Pt_{20}@WC_{17}$/OMC-MM, $Pt_{20}@WC_{22}$/OMC-MM and $Pt_{20}@WC_{27}$/OMC-MM were obtained ($Pt_x@WC_y$/OMC-MM, here the subscript is the weight percent and MM means the sample was obtained by mechanical mixing).

6.2.3 Physico-chemical characterization of WC/OMC

The low-angle and wide-angle *X-ray diffraction* (XRD) patterns were recorded on a D-MAX 2200 VPC diffractometer using Cu K_{α} radiation (30 kV, 30 mA). N_2 adsorption-desorption measurements were carried out using a Micromeritics ASAP 2010

Chapter 6: An Investigation of WC Stability during the Preparation of Pt@WC/OMC via a Pulse Microwave Assisted Polyol Method

133

analyzer at 77 K. The BET surface area (S_{BET}) and the mesopores volume (V_{mes}) were determined by the BET theory and Barrett-Joyner-Halenda (BJH) method, respectively. The *transmission electron microscopy* (TEM) investigations were performed by a JEOL TEM-2010 (HR) operating at 120 kV. *X-ray photoelectron spectroscopy* (XPS) characterization was performed by an ESCALAB 250.

6.2.4 Stability investigation of WC/OMC

In order to check the stability of the as-prepared WC/OMC (WC/OMC-0), the corresponding WC/OMC samples were treated through the following process without (a) or with (b) Pt precursor: i) immersion in alkaline EG solution (pH=13.0) for 3 h (WC/OMC-1a and WC/OMC-1b), ii) after immersion in alkaline EG solution, microwave irradiation in the pulse mode of 10 s-ON/ 10 s-OFF for 5 times (WC/OMC-2a and WC/OMC-2b), iii) after the above two steps, immersion in acidic solution (pH=2.0) for 3 h (WC/OMC-3a and WC/OMC-3b). For the sake of clarification, the above treatment process is illustrated in Fig. 6.2. For the determination of WC content in the WC/OMC composite material, *thermogravimetric* (TG) experiments were carried out with a Netzsch TG-209 analyzer in air with a flow rate of 20 mL min^{-1} and a temperature ramp of 10°C min^{-1}.

Chapter 6: An Investigation of WC Stability during the Preparation of Pt@WC/OMC via a Pulse Microwave Assisted Polyol Method

134
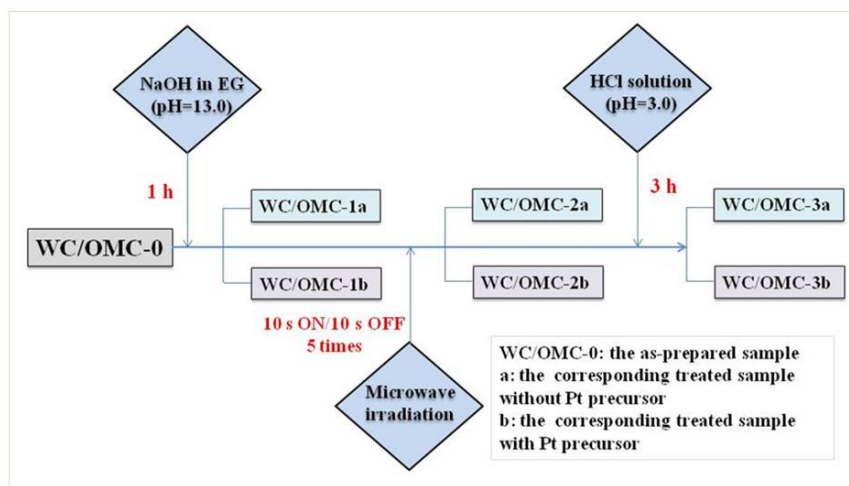
Figure 6.2: The treated WC/OMC samples in the same procedure for the supported Pt catalyst preparation by the pulse microwave assisted polyol method.

6.2.5 Electrochemical characterization

All the electrochemical measurements were conducted on an AUT84480 instrument in a three-electrode cell with a *saturated calomel electrode* (SCE) and a Pt foil (1.0 cm×1.0 cm) as the reference and counter electrode, respectively. The thin catalyst film was prepared onto the glassy carbon disk surface with a diameter of 0.5 cm. Typically, a mixture containing 5.0 mg electrocatalyst, 1.80 mL ethanol and 0.20 mL Nafion solution (5 wt.%, density: 0.874 g mL^{-1}@25°C, DuPont, USA) was ultrasonicated for 10 min and then stirred for 40 min to obtain a well-dispersed ink. The catalyst ink (10 μL) was then quantitatively transferred onto the surface of the glassy carbon disk electrode and dried under infrared lamp to obtain a catalyst thin film. The Pt loading was maintained to be 25.5 μg$_{Pt}$cm^{-2}. It should be noted that all the potential was referred to the SCE without specification.

Chapter 6: An Investigation of WC Stability during the Preparation of Pt@WC/OMC via a Pulse Microwave Assisted Polyol Method

135

6.3 Results and discussion

6.3.1 Physicochemical characterization

The corresponding physico-chemical properties of the as-prepared WC/OMC are shown in Fig. 6.3. The respective diffraction peaks at 31.4^o, 35.6^o, and 48.4^o in the wide angle XRD correspond to (001), (100) and (101) facets of WC (Fig. 6.3A), indicating that WC has been successfully synthesized. As seen from the low-angle XRD patterns of WC/OMC (the inset of Fig. 6.3B), WC/OMC exhibits an intense diffraction peak (10), demonstrating the formation of a highly ordered 2D hexagonal mesostructure [43, 44]. This can be further verified by the parallel arranged channels observed from the TEM image (the inset of Fig. 6.3B). Typical IV nitrogen adsorption/desorption isotherms with distinct hysteretic loop (Fig. 6.3B) indicate the mesoporous structure of WC/OMC. The BET surface area and mesopore volume of WC/OMC are 409 m^2 g^{-1} and 0.47 cm^3 g^{-1}, respectively. Obviously, the WC/OMC has a high enough specific surface area to load metal particles with high dispersion. The pore size distribution through the BJH method clearly displays a unimodal, narrow pore size distribution with a peak pore diameter at about 5.0 nm for WC/OMC. Based on the above results, it is obvious that the ordered mesoporous WC/OMC composites have been successfully synthesized through combing the hydrothermal reaction and the hard template method.

Chapter 6: An Investigation of WC Stability during the Preparation of Pt@WC/OMC via a Pulse Microwave Assisted Polyol Method

136
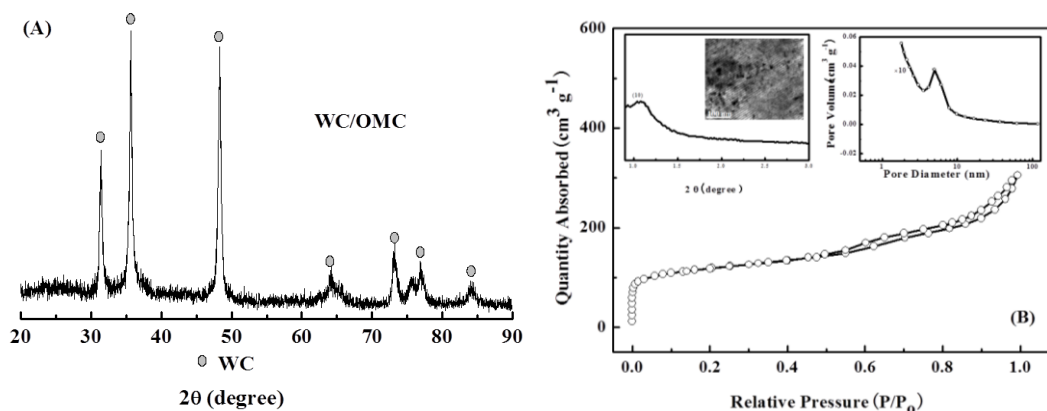
Figure 6.3: (A) XRD patterns of WC/OMC sample, and (B) its N_2 adsorption-desorption isotherms and the corresponding BJH pore size distribution and low-angle XRD patterns and TEM images of WC/OMC sample (inset of B).

Thermogravimetric analysis has already been adopted to determine the Pt content in carbon and nitrogen doped carbon supported Pt catalysts by using the weight of the final products PtO_2 [45, 46]. TG is also tentatively used to quantify WC content in the WC/OMC composite material in the present work. In order to achieve this purpose, it should be to know what the final product of WC/OMC is after TG measurement. For this issue, the as-prepared WC/OMC was heat-treated under air at a flow rate of 20 mL min^{-1}, with temperature ramped from room temperature to 900 ^{o}C at 10 ^{o}C min^{-1}, which were the same operation parameters as those of TG analysis.

The XRD results shown in Fig. 6.4A clearly indicate that the main products of the heat-treated WC/OMC under the same TG operation conditions are WO_3, with little WO_{3-x}. For the further check of the final state of the sample after TG operation, XPS for the products of the heat-treated WC/OMC under the same conditions of TG operation was also collected. As shown in Fig. 6.4B, the W_{4f} spectra can be deconvoluted into two pairs of doublets ($W_{4f5/2}$ and $W_{4f7/2}$). The strong peaks located at 35.91 ev and 38.06 eV

Chapter 6: An Investigation of WC Stability during the Preparation of Pt@WC/OMC via a Pulse Microwave Assisted Polyol Method

137

are corresponding to WO_3 oxidation state, while the weak peaks located at 35.41 ev and

37.56 eV are corresponding to $WO_{2.5}$ oxidation state [13, 47-49].
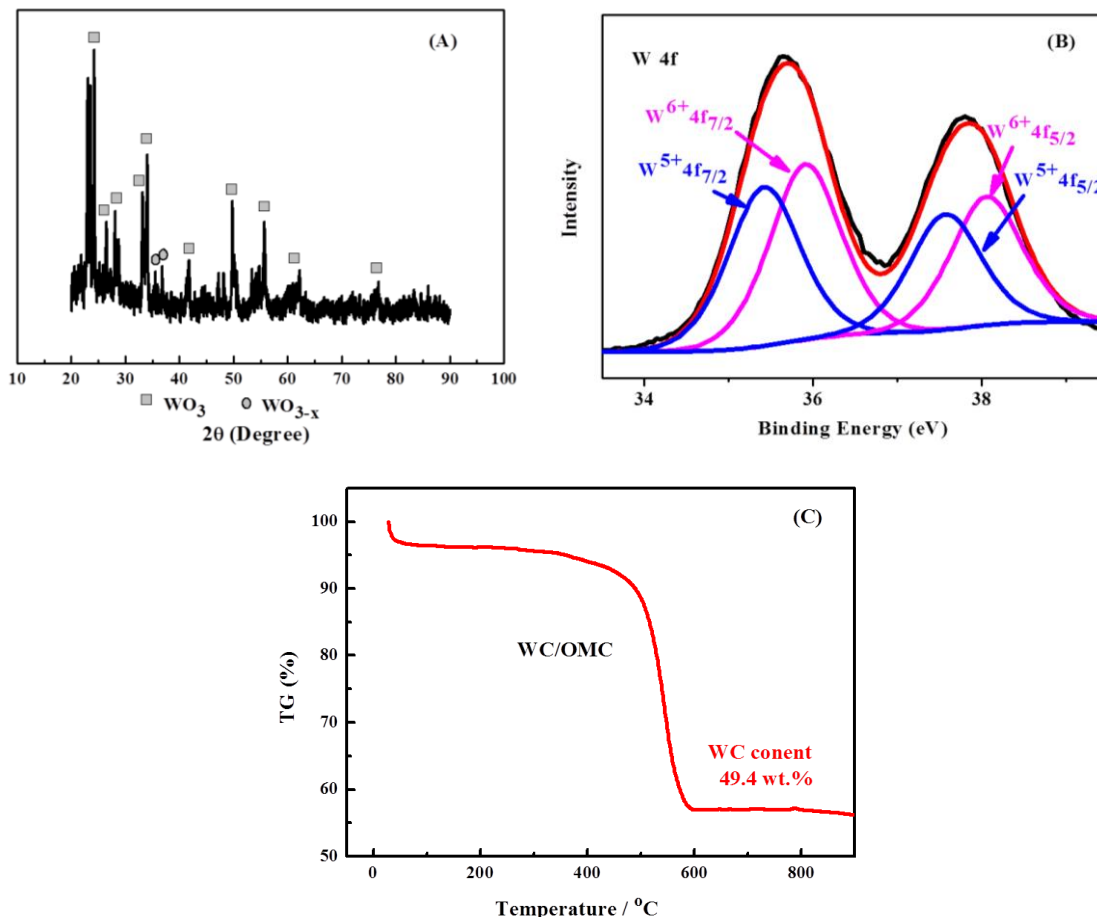
Figure 6.4: (A) XRD and XPS (B) of the heat-treated WC/OMC sample under the same operation conditions as those of TG test and (C) the thermogravimetric curves of the as-prepared WC/OMC for WC quantitative determination.

Considering the much bigger atomic weight of W (184) than that of O (16) and much

lower content of WO_{3-x} with respect to that of WO_3, even if the WC content

determination is just based on WO_3 as the only residue in TG analysis, the measurement

error can be neglected. As it can be seen from Fig. 6.4C, setting the weight of the

anhydrous material to be 100 wt.%, with WO_3 as the final product for the calculation

basis, the content of WC in the as-prepared WC/OMC is 49.4 wt.%. Based on the above

discussion, TG analysis can be used for the determination of WC content in the WC/OMC

Chapter 6: An Investigation of WC Stability during the Preparation of Pt@WC/OMC via a Pulse Microwave Assisted Polyol Method

138

composite material and then for its stability investigation during its supported Pt catalysts preparation through the pulse microwave assisted polyol method.

6.3.2 Investigation of WC/OMC stability

In order to investigate the stability of WC/OMC in the catalyst preparation process through the pulse microwave assisted polyol method, in each step which could affect the stability of WC (Fig. 6.2), the sample was filtered, washed, dried and then evaluated.
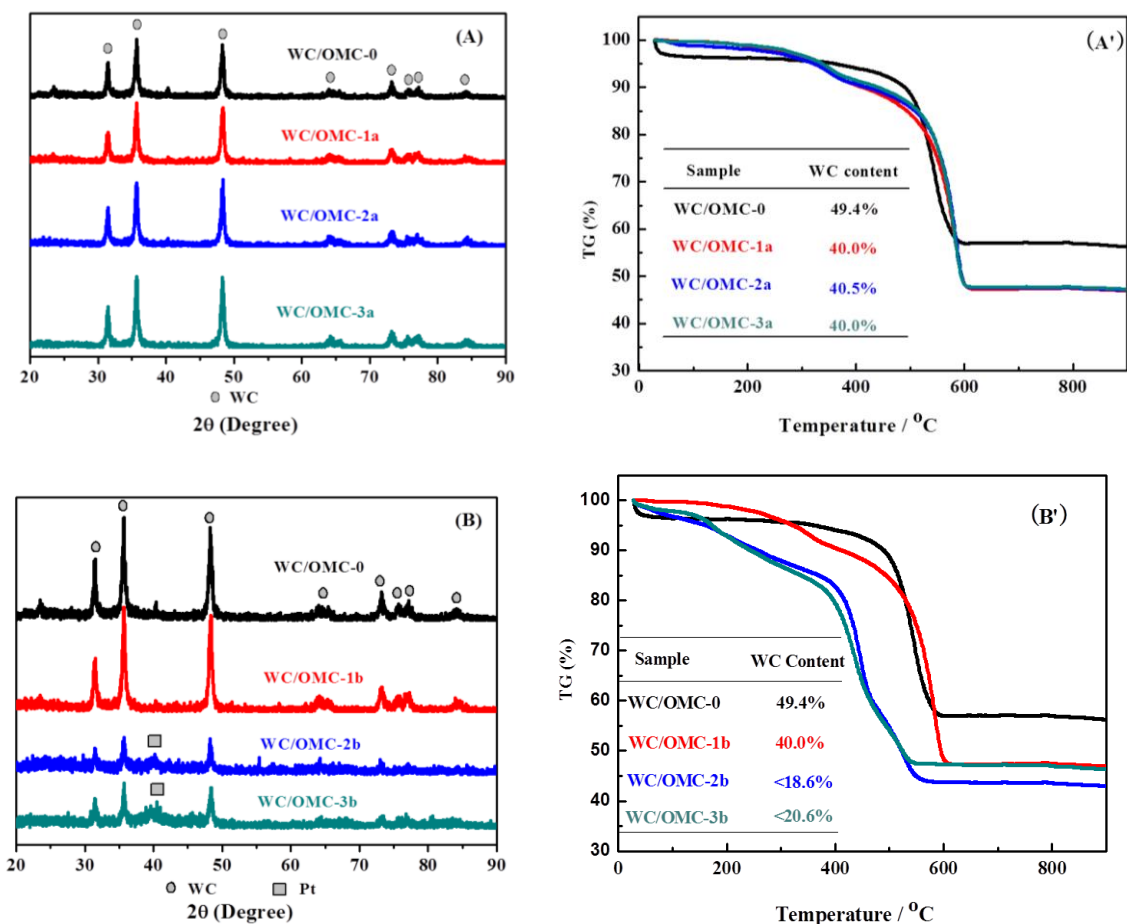
Figure 6.5: (A, B) XRD and (A', B') TG thermogravimetric curves of the treated WC/OMC samples as shown in Fig. 6.2.

The wide-angle XRD patterns of treated WC/OMC samples (Fig. 6.5A) reveal that the diffraction peaks of WC still maintain in the catalyst preparation process in the absence of

Pt precursor. While, in the presence of Pt precursor, the diffraction peak intensity of WC becomes obviously weaker after microwave irradiation (Fig. 6.5B).

To further explore the possible reasons, TG was carried out to quantify WC content in the sample. As shown in Fig. 6.5A',in the case of without Pt precursor, WC loss is almost similar, from the initial 49.4 wt.% to about 40 wt.%, even WC/OMC-0 was treated through all the catalyst preparation process. This phenomenon indicates not only alkaline or acidic environmental but also the microwave irradiation has a little effect on WC stability in absence of Pt precursor. While, in the presence of Pt precursor, before microwave irradiation, the WC loss is similar to the previous case. On the other hand, once microwave irradiation is provided, WC loss becomes significant, from 49.4 wt.% to less than 20 wt.% (Fig. 6.5B'). With the further treatment by acid, no further WC loss happens. This indicates that the existence of Pt can induce the dissolution or oxidation of WC in the microwave irradiation process. One can easily infer that the step of microwave irradiation in the presence of Pt precursor during the catalysts preparation process is the most serious parameter that leads to WC loss. Here it is worth noting that if the catalysts were prepared through the pulse microwave assisted polyol method, in the Pt@WC/OMC sample, W can be found in the form of WC and WO_3, which could be seen from the XPS results shown in Fig. 6.6. Obviously, part of WC has been oxidized into WO_3 during Pt@WC/OMC cattalyst preparation. So, based on TG method, the real WC content in Pt@WC/OMC should be less than the calculated value.

Chapter 6: An Investigation of WC Stability during the Preparation of Pt@WC/OMC via a Pulse Microwave Assisted Polyol Method

140
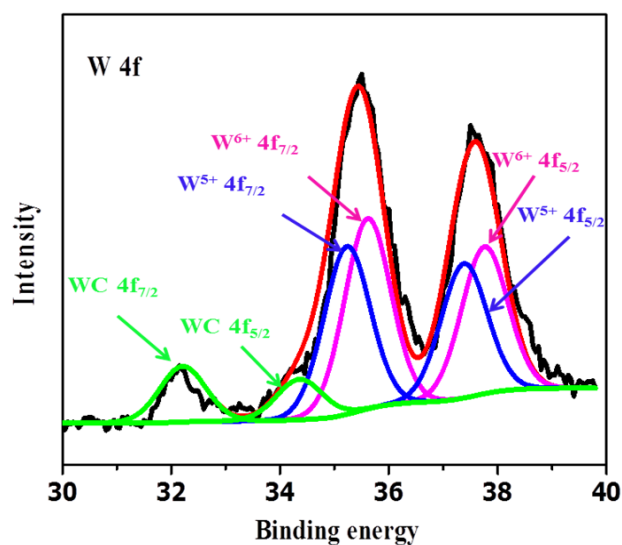
Figure 6.6: Deconvoluted W$_{4f}$ spectra in the Pt@WC/OMC sample prepared by the pulse microwave assisted polyol method.

6.3.3 Electrochemical characterization: methanol electrooxidation reaction

Considering the issue of WC loss in the catalyst preparation process and the contributing effect of WC on Pt's electrocatalytic activity, in order to take good advantage of the synergetic effect of WC, the as-prepared WC/OMC-0 was mechanically mixed with the as-prepared Pt/C to obtain Pt$_{20}$@WC$_{22}$/OMC (denoted as Pt$_{20}$@WC$_{22}$/OMC-MM). Pt$_{20}$@WC$_{21}$/OMC-MP (here the subscript 21 is the calculated WC weight percent from TG results, while the real WC content should be less than 21 wt.% as discussed above) was prepared through the normal pulse microwave assisted polyol method as the counterpart. Both were tested for MOR and the results are shown in Fig. 6.7.

Chapter 6: An Investigation of WC Stability during the Preparation of Pt@WC/OMC via a Pulse Microwave Assisted Polyol Method

141
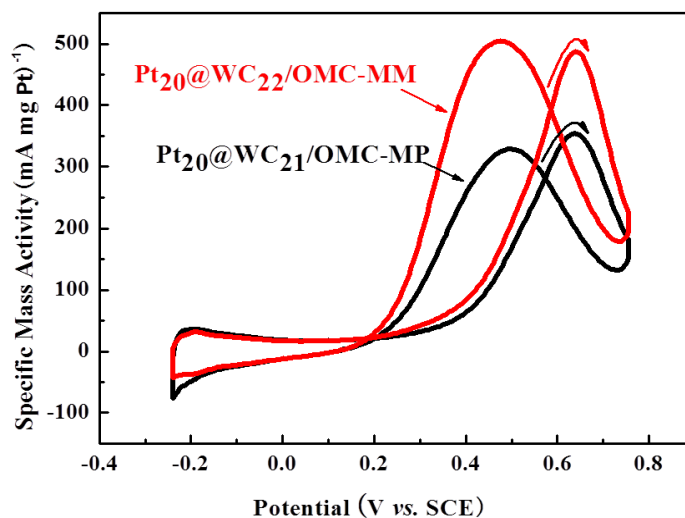
Figure 6.7: **Cyclic voltammograms of methanol electrooxidation on Pt$_{20}$@WC$_{22}$/OMC-MM and Pt$_{20}$@WC$_{21}$OMC-MP in 0.5 mol L^{-1} H$_2$SO$_4$+1.0 mol L^{-1} CH$_3$OH solution. Scan rate: 50 mV s^{-1}.**

Not only the onset potential but also the specific mass activity on Pt$_{20}$@WC$_{22}$/OMC-MM is superior to those on Pt$_{20}$@WC$_{21}$/OMC-MP. In more details, the peak value of the specific mass activity of the Pt$_{20}$@WC$_{22}$/OMC-MM is about 488 mA mg$_{Pt}$$^{-1}$, much higher than the corresponding value (354 mA mg$_{Pt}$$^{-1}$) of the–Pt$_{20}$@WC$_{21}$/OMC-MP. Our present results have a comparable result to that (410 mA mg$_{Pt}$$^{-1}$) on Pt supported on WO$_3$/OMC [50]. This could be attributed to the decreased crystallization of WC due to part of WC dissolution and WO$_3$ existence, produced from the oxidation of WC during the preparation of Pt$_{20}$@WC$_{21}$/OMC-MP. This can be clearly seen from the weaker diffraction peaks for WC in Pt$_{20}$@WC$_{21}$/OMC-MP with respect to those in Pt$_{20}$@WC$_{22}$/OMC-MM (Fig. 6.8). One might further conclude that the content of WC can affect the activity of Pt@WC/OMC to some extent.

Chapter 6: An Investigation of WC Stability during the Preparation of Pt@WC/OMC via a Pulse Microwave Assisted Polyol Method

142
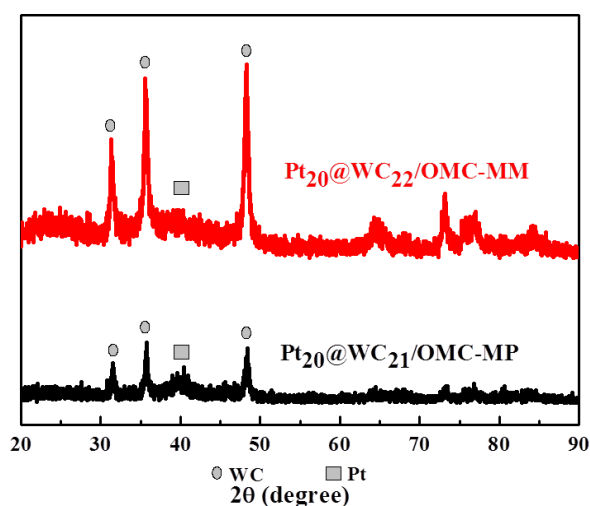
Figure 6.8: XRD patterns of the Pt$_{20}$@WC$_{22}$/OMC-MM and Pt$_{20}$@WC$_{21}$/OMC-MP samples.

For the further optimization of WC content in the catalysts, different Pt@WC/OMC-MM catalysts with the same Pt loading but different WC content (Pt$_{20}$@WC$_{17}$/OMC-MM, Pt$_{20}$@WC$_{22}$/OMC-MM and Pt$_{20}$@WC$_{27}$/OMC-MM) were prepared and evaluated for MOR. The CV results for MOR (Fig. 6.9A) clearly indicate that Pt$_{20}$@WC$_{22}$/OMC outperforms the other two samples, with a higher electrocatalytic peak current (488 mA mg$_{Pt}^{-1}$). This behavior could be due to the bigger electrochemical surface area in the case of Pt$_{20}$@WC$_{22}$/OMC-MM. This can be clearly seen from the obviously bigger reduction peak of platinum oxide, shown in Fig. 6.9B. Moreover, the lower MOR performance on Pt$_{20}$@WC$_{27}$/OMC-MM could be due to the amount of WC which has low efficiency of synergistic effect [51]. Furthermore, in the case of high WC content, because of its high density, it is difficult to prepare the well-dispersed catalyst ink and the catalyst particles are accessible to settle. In this way, the catalyst thin film could be not so good compared with the others, and thus probably leading to the inferior performance.

Chapter 6: An Investigation of WC Stability during the Preparation of Pt@WC/OMC via a Pulse Microwave Assisted Polyol Method

143
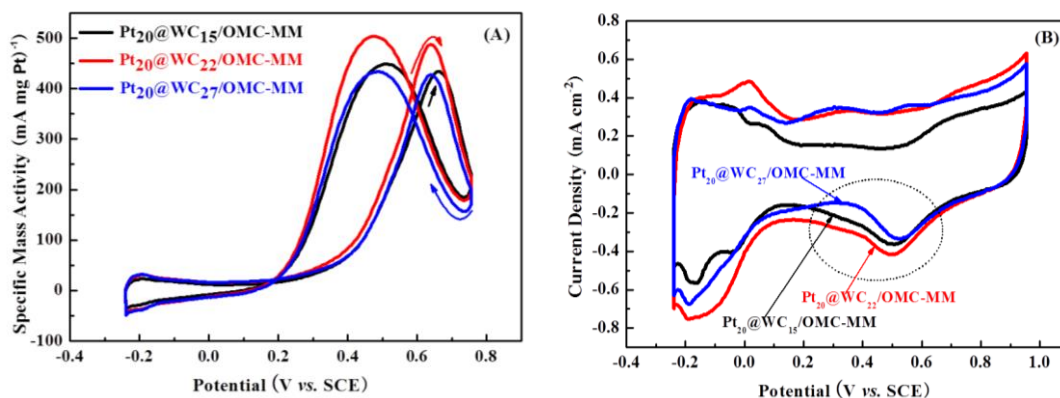
Figure 6.9: (A) Cyclic voltammograms of methanol electrooxidation on Pt$_{20}$@WC$_{15}$OMC, Pt$_{20}$@WC$_{22}$/OMC and Pt$_{20}$@WC$_{27}$/OMC obtained through mechanically mixing WC/OMC and Pt@C in 0.5 mol L^{-1} H$_2$SO$_4$+1.0 mol L^{-1} CH$_3$OH solution (Scan rate: 50 mV s^{-1}) and **(B)** in 0.5 mol L^{-1} H$_2$SO$_4$ (Scan rate: 20 mV s^{-1}).

As far as the Pt$_{20}$@WC$_{17}$/OMC-MM is concerned, probably it has lower WC content, resulting in weaker synergistic effect on Pt, so its mass activity for MOR is lower than that on Pt$_{20}$@WC$_{22}$/OMC-MM. For all electrocatalysts, the backward specific mass peak current density presents the same value with the respective forward peak (I$_{forward}$/I$_{backward}$≈1), indicating their good tolerance to the formed intermediates as well as good activity towards MOR [3, 52].

6.4 Conclusions

In the present work, the stability of WC during the WC/OMC supported Pt-based catalysts preparation process through a pulse microwave-assisted polyol method was investigated by XRD technique and TG method. In summary, the following conclusions can be drawn: Acidic or alkaline environment during the above-mentioned catalysts preparation process has a little impact on WC stability. Microwave irradiation in the presence of Pt precursor can significantly lower the stability of WC. This finding is of vital importance to realize that WC is seriously unstable during the specific catalysts

Chapter 6: An Investigation of WC Stability during the Preparation of Pt@WC/OMC via a Pulse Microwave Assisted Polyol Method

144

preparation process.

The degree of crystallization and content of WC could obviously affect the activity of Pt towards methanol electrooxidation reaction. In order to maximize the synergistic effect of WC supported electrocatalysts, it is necessary and important to identify and then avoid or improve the operation parameters affecting WC stability not only during the application of WC but also during catalysts preparation process.

Chapter 6: An Investigation of WC Stability during the Preparation of Pt@WC/OMC via a Pulse Microwave Assisted Polyol Method

145

References

[1] R.B. Levy, M. Boudart, Science 181 (1973) 547-549.

[2] J.L. Lu, Z.H. Li, S.P. Jiang, P.K. Shen, L. Li, J. Power Sources 202 (2012) 56-62.

[3] H. Zheng, Z. Chen, Y. Li, C.a. Ma, Electrochim. Acta 108 (2013) 486-490.

[4] W. Zhu, A. Ignaszak, C. Song, R. Baker, R. Hui, J. Zhang, F. Nan, G. Botton, S. Ye, S. Campbell, Electrochim. Acta 61 (2012) 198-206.

[5] A. Brouzgou, S.Q. Song, P. Tsiakaras, Appl. Catal. B: Environ. 127 (2012) 371-388.

[6] H. Lv, T. Peng, P. Wu, M. Pan, S. Mu, J. Mater. Chem. 22 (2012) 9155-9160.

[7] J.B. Christian, S.P.E. Smith, M.S. Whittingham, H.D. Abruña, Electrochem. Commun. 9 (2007) 2128-2132.

[8] M.K. Jeon, H. Daimon, K.R. Lee, A. Nakahara, S.I. Woo, Electrochem. Commun. 9 (2007) 2692-2695.

[9] D.R. McIntyre, G.T. Burstein, A. Vossen, J. Power Sources 107 (2002) 67-73.

[10] Y. Kimmel, D. Esposito, R. Birkmire, J. Chen, Int. J. Hydrogen Energy 37 (2012) 3019-3024.

[11] Y. Wang, S. Song, P.K. Shen, C. Guo, C.M. Li, J. Mater. Chem. 19 (2009) 6149-6153.

[12] Y. Wang, C. He, A. Brouzgou, Y. Liang, R. Fu, D. Wu, P. Tsiakaras, S. Song, J. Power Sources 200 (2012) 8-13.

[13] R. Ganesan, J.S. Lee, Angew. Chem. Int. Ed. 117 (2005) 6715-6718.

[14] Z.-Y. Wu, P. Chen, Q.-S. Wu, L.-F. Yang, Z. Pan, Q. Wang, Nano Energy 8 (2014) 118-125.

[15] Y. Wang, S. Song, V. Maragou, P.K. Shen, P. Tsiakaras, Appl. Catal. B: Environ. 89 (2009) 223-228.

[16] V.M. Nikolic, D.L. Zugic, I.M. Perovic, A.B. Saponjic, B.M. Babic, I.A. Pasti, M.P. Marceta Kaninski, Int. J. Hydrogen Energy 38 (2013) 11340-11345.

[17] G. Zhong, H. Wang, H. Yu, F. Peng, Fuel Cells 13 (2013) 387-391.

[18] X. Ma, H. Meng, M. Cai, P.K. Shen, J. Am. Chem. Soc. 134 (2012) 1954-1957.

[19] S. Yin, M. Cai, C. Wang, P.K. Shen, Energy Environ. Sci. 4 (2011) 558-563.

Chapter 6: An Investigation of WC Stability during the Preparation of Pt@WC/OMC via a Pulse Microwave Assisted Polyol Method

146

[20] H. Lv, S. Mu, N. Cheng, M. Pan, Appl. Catal. B: Environ. 100 (2010) 190-196.

[21] H. Lv, N. Cheng, T. Peng, M. Pan, S. Mu, J. Mater. Chem. 22 (2012) 1135-1141.

[22] C.J. Barnett, G.T. Burstein, A.R.J. Kucernak, K.R. Williams, Electrochim. Acta 42 (1997) 2381-2388.

[23] H. Chhina, S. Campbell, O. Kesler, J. Power Sources 164 (2007) 431-440.

[24] M.B. Zellner, J.G. Chen, Catal. Today 99 (2005) 299-307.

[25] A. Serov, C. Kwak, Appl. Catal. B: Environ. 90 (2009) 313-320.

[26] E.C. Weigert, D.V. Esposito, J.G. Chen, J. Power Sources 193 (2009) 501-506.

[27] M. Shao, B. Merzougui, K. Shoemaker, L. Stolar, L. Protsailo, Z.J. Mellinger, I.J. Hsu, J.G. Chen, J. Power Sources 196 (2011) 7426-7434.

[28] H. Chhina, S. Campbell, O. Kesler, J. Power Sources 179 (2008) 50-59.

[29] R. Ganesan, D.J. Ham, J.S. Lee, Electrochem. Commun. 9 (2007) 2576-2579.

[30] Y. Hara, N. Minami, H. Matsumoto, H. Itagaki, Appl. Catal. A: Gen. 332 (2007) 289-296.

[31] J. Regalbuto, Catalyst Preparation: Science and Engineering, Taylor & Francis, 2006.

[32] D.W. McKee, F.J. Norton, J. Phys. Chem. 68 (1964) 481-489.

[33] A.S. Aricò, Z. Poltarzewski, H. Kim, A. Morana, N. Giordano, V. Antonucci, J. Power Sources 55 (1995) 159-166.

[34] Z. Zhou, S. Wang, W. Zhou, G. Wang, L. Jiang, W. Li, S. Song, J. Liu, G. Sun, Q. Xin, Chem. Commun. (2003) 394-395.

[35] W.J. Zhou, S.Q. Song, W.Z. Li, G.Q. Sun, Q. Xin, S. Kontou, K. Poulianitis, P. Tsiakaras, Solid State Ionics 175 (2004) 797-803.

[36] Z. Liu, J.Y. Lee, W. Chen, M. Han, L.M. Gan, Langmuir 20 (2003) 181-187.

[37] S. Song, Y. Wang, P.K. Shen, J. Power Sources 170 (2007) 46-49.

[38] S. Komarneni, D. Li, B. Newalkar, H. Katsuki, A. Bhalla, Langmuir 18 (2002) 5959-5962.

[39] W. Chen, J. Zhao, J.Y. Lee, Z. Liu, Mater. Chem. Phys. 91 (2005) 124-129.

[40] W.-X. Chen, J.Y. Lee, Z. Liu, Mater. Lett. 58 (2004) 3166-3169.

[41] W.X. Chen, J.Y. Lee, Z. Liu, Chem. Commun. (2002) 2588-2589.

Chapter 6: An Investigation of WC Stability during the Preparation of Pt@WC/OMC via a Pulse Microwave Assisted Polyol Method

147

[42] S. Song, J. Liu, J. Shi, H. Liu, V. Maragou, Y. Wang, P. Tsiakaras, Appl. Catal. B: Environ. 103 (2011) 287-293.

[43] R. Ryoo, S.H. Joo, M. Kruk, M. Jaroniec, Adv. Mater. 13 (2001) 677-681.

[44] Y. Meng, D. Gu, F. Zhang, Y. Shi, H. Yang, Z. Li, C. Yu, B. Tu, D. Zhao, Angew. Chem. Int. Ed. 117 (2005) 7215-7221.

[45] F. Su, Z. Tian, C. Poh, Z. Wang, S. Lim, Z. Liu, J. Lin, Chem. Mater. 22 (2009) 832-839.

[46] C. He, Y. Liang, R. Fu, D. Wu, S. Song, R. Cai, J. Mater. Chem. 21 (2011) 16357-16364.

[47] A. Mozalev, V. Khatko, C. Bittencourt, A.W. Hassel, G. Gorokh, E. Llobet, X. Correig, Chem. Mater. 20 (2008) 6482-6493.

[48] M.B. Zellner, J.G. Chen, Surf. Sci. 569 (2004) 89-98.

[49] J. Luthin, C. Linsmeier, Surf. Sci. 454-456 (2000) 78-82.

[50] J. Zeng, C. Francia, C. Gerbaldi, V. Baglio, S. Specchia, A.S. Aricò, P. Spinelli, Electrochim. Acta 94 (2013) 80-91.

[51] Z. Yan, G. He, M. Cai, H. Meng, P.K. Shen, J. Power Sources 242 (2013) 817-823.

[52] J. Wu, Y. Xu, M. Pan, W. Ma, H. Tang, Chin. Sci. Bull. 54 (2009) 1032-1036.

Chapter 6: An Investigation of WC Stability during the Preparation of Pt@WC/OMC via a Pulse Microwave Assisted Polyol Method

148

Carbon supported Ultra-low Pt (Pd$_x$Pt$_y$) electrocatalysts preparation, characterization and H$_2$-PEMFC performance

Abstract

In the present manuscript very low-platinum electrocatalysts, Pd$_{97}$Pt$_3$/C, Pd$_{98}$Pt$_2$/C, Pd$_{99}$Pt$_1$/C and pure Pd/C are prepared, physicochemically as well as electrochemically characterized and they are tested in a single hydrogen proton exchange membrane fuel cell. The electrocatalysts are prepared via a modified pulse-microwave assisted polyol method and they are physicochemically characterized with techniques of X-ray diffraction (XRD) and transmission electron microscopy (TEM). Moreover, the as prepared electrocatalysts are electrochemically characterized by the aid of the techniques of cyclic voltammetry (CV) and rotating disk electrode (RDE). According to the experimental results, all the as-prepared PdPt bimetallic electrocatalysts exhibit much higher activity towards HOR than pure Pd.

Among the investigated electrocatalysts Pd$_{98}$Pt$_2$/C presented the highest electrocatalytic activity. Moreover, Pd$_{97}$Pt$_3$/C and Pd$_{98}$Pt$_2$/C electrocatalysts are examined as anode electrode in a single hydrogen proton exchange membrane fuel cell. As expected, along with the temperature increase from 30 to 80°C, the power density increases for the Pd$_{98}$Pt$_2$/C anode.

However, for the Pd$_{97}$Pt$_3$/C a further increase in the temperature from 70 to 80°C results in a slight decay of power density. According to the electrochemical impedance measurements the decay of the power density may attributed to the decrement of membrane conductivity.

Chapter 7: Carbon supported Ultra-low Pt (PdxPty) electrocatalysts preparation, characterization and H2-PEMFC performance

149

Contents

Chapter 7: Carbon supported Ultra-low Pt (PdxPty) electrocatalysts preparation, characterization and H2-PEMFC performance

150

List of Figures

List of Tables

Chapter 7: Carbon supported Ultra-low Pt (PdxPty) electrocatalysts preparation, characterization and H2-PEMFC performance

151

7.1 Introduction

Today, after many years of research [1], *Hydrogen Fueled Proton Exchange Membrane Fuel Cells* (H$_2$-PEMFCs) have achieved much progress for their wide potential commercial applications. H$_2$-PEMFCs are the smallest and lightest of the designs at present, making them the choice mainly for transportation applications, like automobiles and trucks. H$_2$-PEMFCs also, among the other fuel cells, have the lowest operating temperatures, and this means faster start-up time for the internal chemical reactions. On the other hand, they need pure hydrogen to operate and up-to-date, they run typically with only 30% efficiencies, having also a high cost [2]. Among the total cost the electrode represents 40%, with 1.7% due to platinum as the active catalysts [3]. Reducing cost and improving durability are the most two significant challenges for the commercialization of H$_2$-PEMFCs. Ongoing research has been focused on identifying and developing new materials that will reduce the cost and extend the life of fuel cell different components including membranes, electrocatalysts, bipolar plates and membrane electrode assemblies. More precisely, for electrocatalysts the most addressed technical barriers are to:

- Reduce precious metal loading of electrocatalysts

- Increase the specific and mass activities of electrocatalysts

- Increase the durability and stability of electrocatalysts with cycling

In addition, the U.S. Department of Energy (DOE) has set long-term goals for PEMFC performance in a 50 kW stack with the catalyst loading of 0.05 mg cm^{-2} or less at the cathode. Furthermore, the target includes less than 200 mg of Pt$_{total}$ per kW (higher than 5Mw μg_{Pt}^{-1}) at cell voltages higher than 0.65 V. In our previous review work [1] we have identified that the most active electrocatalysts (>5 mWμg_{Pt}^{-1}) for hydrogen oxidation reaction (HOR) are bimetallic Pd-Pt ones. In an attempt to reduce the catalyst loading, the

Chapter 7: Carbon supported Ultra-low Pt (PdxPty) electrocatalysts preparation, characterization and H2-PEMFC performance

152

international research community has identified Pd as the best non-platinum electrocatalyst, with comparable, but a little lower electrocatalytic activity than Pt. Meanwhile, doping Pd electrocatalyst with a very small amount of Pt has been proved to significantly enhance the electrocatalytic activity at pure Pd, indicating activity higher than pure Pt. Cho *et al.* [4] synthesized and tested PdPt catalyst with an atomic ratio of 19:1 and applied it in a H_2-PEMFC. The single PEMFC using PdPt/C as the anode electrocatalyst exhibited a high performance comparable to that with a commercial Pt/C anode electrocatalyst. This result indicates that Pd-based electrocatalysts can be used as an anode electrocatalyst in PEMFC with a very small amount of Pt (just about 5 at.%). Additionally, Antolini *et al.* [5] decreased Pt loading by adopting carbon supported $Pd_{96}Pt_4$ and Pt as anode and cathode catalysts, respectively. They found that the fuel cell performance was only slightly lower than the conventional PEMFC with Pt/C catalysts at both electrodes.

In the present work, carbon (Vulcan XC-72®) supported $Pd_{97}Pt_3$, $Pd_{98}Pt_2$, $Pd_{99}Pt_1$ and pure Pd electrocatalysts are prepared via a modified-pulse microwave assisted polyol method and are examined for HOR. Additionally then $Pd_{97}Pt_3$/C and $Pd_{98}Pt_2$/C are also tested in a single H_2-PEMFC as anode electrocatalyst with commercial Pt/C as cathode electrocatalyst.

7.2 Experimental

7.2.1 Materials

Vulcan XC-72R (Cabot Corporation) carbon powder was used as the support material. $PdCl_2$ and $H_2PtCl_6{\cdot}6H_2O$ were the corresponding metal precursors. All aqueous solutions were prepared by ultrapure water (18.2 MΩ cm Millipore–MilliQ) during catalyst preparation. Ethanol (>99% purity) (Sigma Aldrich) and Nafion® (5 wt.%, Dupont Company) were used for catalyst ink preparation.

Chapter 7: Carbon supported Ultra-low Pt (PdxPty) electrocatalysts preparation, characterization and H2-PEMFC performance

153

7.2.2 Electrocatalysts preparation

Pd_xPt_y (x:y=97:3, 98:2 and 99:1) with different Pd/Pt molar ratios supported on Vulcan-XC72 carbon (the metal loading was kept at 20 wt.% for all the catalysts) were prepared by a modified pulse-microwave assisted polyol synthesis procedure [6]. Briefly, in a beaker, the starting metal precursors ($PdCl_2$ and $H_2PtCl_6 \cdot 6H_2O$) were well mixed with *ethylene glycol* (EG) in an ultrasonic bath, and then XC-72 R carbon black (Cabot Corporation) was added into the above mixture. After the pH value of the system was adjusted to be more than 10 by the drop-wise addition of 1.0 M NaOH/EG, a well-dispersed slurry was obtained with ultrasonic stirring for 60 min. Thereafter, the slurry was microwave-heated in the pulse form of 10s-on/10-s-off for several times. In order to promote the adsorption of the suspended metal nanoparticles onto the carbon support, hydrochloric acid was adopted as the sedimentation promoter and the solution was re-acidified with a pH value of about 4. The resulting black solid sample was filtered, washed and dried at 80°C for 12 h in a vacuum oven.

7.2.3 Fabrication of membrane electrode assembly (MEA)

A Toray carbon paper (Toray TGP-H-060, Toray Industries Inc.) was used as the anode and cathode backing layer. Carbon black ink containing Vulcan XC-72R carbon black and polytetrafluoroethylene (PTFE, Aldrich) was painted onto the backing layer to form a microporous layer. The carbon black loading was about 1.0 mg cm^{-2} and the PTFE content in the microporous layer was 40 wt. %. To fabricate the anode catalyst layer, the Pd_xPt_y/C catalyst and Nafion$^®$ solution was ultrasonically suspended in water and then brushed onto the microporous layer at 70 ^{o}C. The resulting loading of the Pd_xPt_y/C catalyst was 1.6 ± 0.1 mg cm^{-2} and the Nafion content was 10 wt. %. And then, a Nafion solution was sprayed onto the surface of the anode catalyst layer with a dry ionomer loading of about 0.5 mg cm^{-2}. In all cases, an identical cathode catalyst layer was

Chapter 7: Carbon supported Ultra-low Pt (PdxPty) electrocatalysts preparation, characterization and
H2-PEMFC performance

154

prepared by the same procedure as that described above. The resulting Pt/C (40 wt%, Tanaka Kikinzoku Kogyo K. K.) loading was 1.6 ± 0.1 mg cm^{-2} and the Nafion content was the same as in the anode catalyst layer. Finally, the anode and cathode (2.5 cm $\times$ 2.5 cm) were placed onto each side of a Nafion NRE-212 membrane (Aldrich) and hot-pressed at 135 ^{o}C and 1 MPa for 3 min to form the MEA. The membrane is used as received without any treatment.

7.2.4 Physicochemical characterization

The X-ray diffraction (XRD) patterns were recorded on a D-MAX 2200 VPC diffractometer using Cu Kα radiation (30 kV, 30 mA). The transmission electron microscopy (TEM) investigations were carried out on a JEOL TEM-2010 (HR) at 120 kV to determine the size and surface morphology of the catalyst particles. Before the measurements, the catalysts were uniformly dispersed in ethanol solution using an ultrasonic water bath and then dried onto carbon coated copper grid.

7.2.5 Electrochemical measurements

Cyclic voltammetry (CV) and rotating disk electrode (RDE) studies were carried out to estimate the electrochemical active surface area and to characterize the activity of the as-prepared electrocatalysts for the HOR and ORR. The performance of the electrocatalysts was also evaluated using a commercial fuel cell test system (Fuel Cell Technologies Inc.), with a single test rig of 5.0 cm^2 active geometric area. Polarization studies were conducted at various cell temperatures with humidified hydrogen and oxygen gas reactants at an atmospheric pressure.

Chapter 7: Carbon supported Ultra-low Pt (PdxPty) electrocatalysts preparation, characterization and H2-PEMFC performance

155

7.2.6 Cyclic voltammetry and rotating disk electrode measurements (HOR&ORR)

All electrochemical measurements were conducted in an electrochemical workstation AMEL 7050 adopting a saturated calomel electrode (SCE) and a Pt wire as reference and counter electrodes, respectively. CV and RDE- measurements were carried out, on a thin film catalyst coated on a glassy carbon (GC) disk electrode (working electrode, d= 3.0 mm) mounted in an interchangeable RDE holder, in 0.5 mol L^{-1} H$_2$SO$_4$ aqueous solution (Carlo Erba, 99%) at room temperature. The electrocatalytic ink was prepared by mixing 2.0 mg of electrocatalyst, 1.8 mL ethanol and 0.2 mL Nafion solution (5 wt.%, IonPower, GmbH). Then, the as-prepared catalyst ink was quantitatively (4.0 μL) transferred onto the surface of the GC electrode and was dried to obtain a thin porous layer. For all measurements, the total catalyst loading was maintained at 11 μg cm^{-2}. Before each measurement, the solution was bubbled with high-purity nitrogen for 30 min to remove the dissolved oxygen in the solution. For the activity evaluation for HOR, hydrogen gas was supplied to the electrolyte more than 30 min to obtain a H$_2$-saturated solution. During the experiments the N$_2$ (or hydrogen) stream was directed provided above the solution level in order to avoid contact with air as well as keep saturated the solution (inert in case of nitrogen). Before the voltammograms being reproducible, several scans were carried out.

7.2.7 Single fuel cell test

Initially, it should be pointed out that before the electrochemical experiments, the cell was activated with the method of cyclic voltammetry. During the activation process, the pipe temperatures for both the anode and cathode sides were at room temperature. Activation was carried out under reference conditions (λ_{Air} = 20cc, λ_{H2}=100cc) for 1000 cycles, from 0 to 1V, at 150mV/sec scan rate [7].

Chapter 7: Carbon supported Ultra-low Pt (PdxPty) electrocatalysts preparation, characterization and H2-PEMFC performance

156

Then the CV was performed on a two-electrode MEA with a potentiostat (AMEL 7050) at 50 mV s^{-1} from 0 to 1.0 V in order to estimate the electrochemical active surface area of the MEA. In this configuration, the anode serves as both the counter and reference electrodes, while the cathode as the working electrode. The fuel cell cathode and anode were supplied with 20 mL min^{-1} H$_2$ and 100 mL min^{-1} N$_2$, respectively. The cell working temperature was controlled to be 25 ^{o}C.

The single cell polarization experiments were carried out at different working temperatures of 30, 40, 50, 60, 70 and 80°C at an atmospheric pressure. Before entering the cell, the reactant gases, pure hydrogen (80 mL min^{-1}) and oxygen (40 mL min^{-1} O$_2$), were saturated with steam water contained in glassy humidifiers under controlled temperature (the same with the cell for relative humidity 100%).

7.2.8 In situ electrochemical impedance spectroscopy (In situ-EIS)

Electrochemical impedance spectroscopy (EIS) can evaluate the internal property of electrodes, such as ohmic resistance, charge transfer resistance and mass transfer resistance in the catalyst layer and constant phase element of the catalyst layer capacitance. Consequently, alternative impedance (AC) measurements were carried out using a MaterialsM 520 frequency response analyzer (AMEL) coupled to 7050 AMEL electrochemical station. The AC signal had an amplitude of 10 mV and the frequency range was from 1 mHz to 100 kHz, covered with 10 points per decade. Impedance spectra at different temperatures were recorded at 0.6 V and at open circuit voltage (OCV). For the measurements at OCV conditions symmetrical feeding to anode and cathode H$_2$/H$_2$ (80 mLmin^{-1}) was used, while for the measurements at 0.6 V, H$_2$ (80 mLmin^{-1}) and O$_2$ (40 mLmin^{-1}) was fed to the anode and the cathode respectively. Using the values of the high frequency resistance, cell potentials were corrected for the ohmic drop.

Chapter 7: Carbon supported Ultra-low Pt (PdxPty) electrocatalysts preparation, characterization and H2-PEMFC performance

157

7.3 Results and Discussion

7.3.1 Physicochemical characterization

The diffraction peaks of Pd_xPt_y/C catalysts at about 40∘, 46∘, 68∘ and 81∘ are attributed to the (1 1 1), (2 0 0), (2 2 0) and (3 1 1) planes of the face center cubic (fcc) structure of the PdPt alloys.
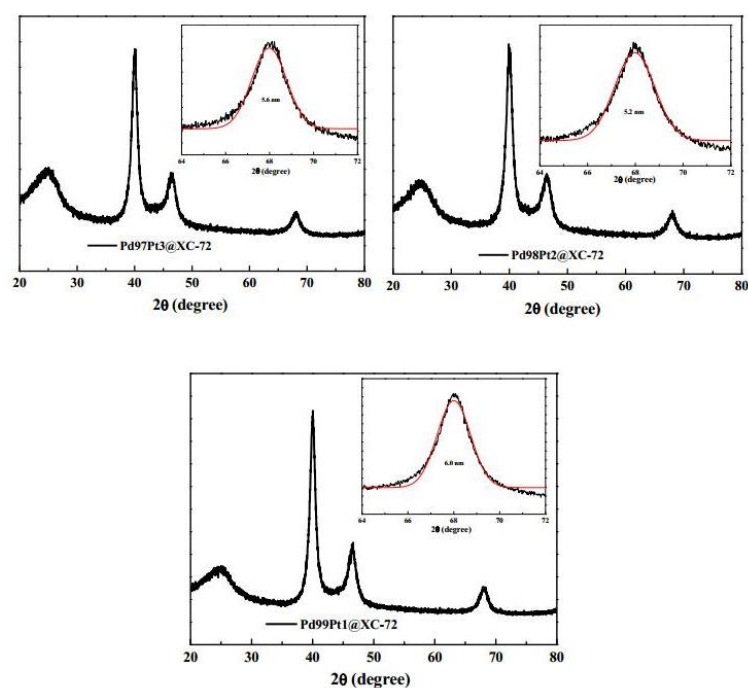
Figure 7.1: XRD results. Insets: crystallite size.

From the XRD results the crystallite size is calculated (inset of Fig.7.1) 5.6, 5.2 and 6.0nm for the $Pd_{97}Pt_3$/C, $Pd_{98}Pt_2$/C and $Pd_{99}Pt_3$/C, respectively. Moreover from the TEM images (Fig.7.2), the smallest nanoparticles and the most homogenously distributed are observed for the $Pd_{98}Pt_2$/C, ~5.0nm. Then the $Pd_{97}Pt_3$/C follows with ~5.5nm nanoparticles size and finally the $Pd_{99}Pt_1$/C with ~6.0nm nanoparticles size and inhomogeneous distribution.

Chapter 7: Carbon supported Ultra-low Pt (PdxPty) electrocatalysts preparation, characterization and H2-PEMFC performance

158
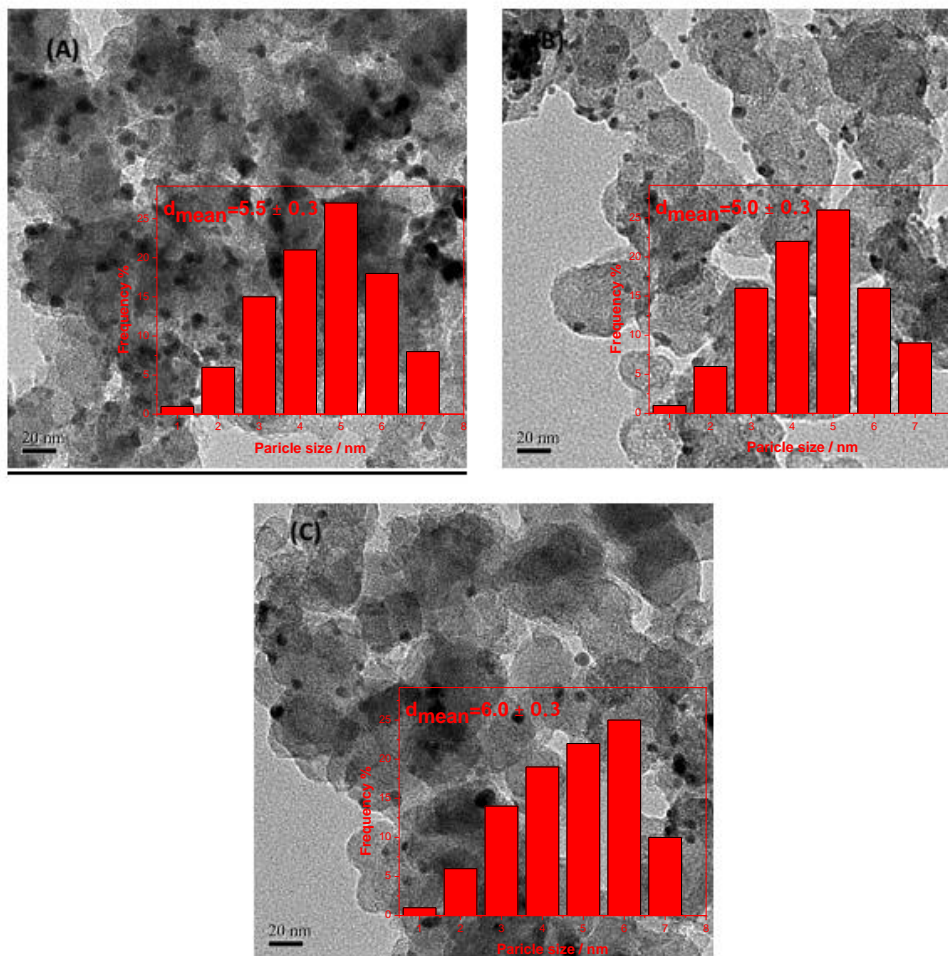
Figure 7.2: TEM images of Pd$_{97}$Pt$_3$/Vulcan-XC72 (A), Pd$_{98}$Pt$_2$/Vulcan-XC72 (B), Pd$_{99}$Pt$_1$/Vulcan-XC72 (C).

7.3.2 Electrochemical characterization

7.3.2.1 Cyclic voltammetry and estimated electrochemical active surface area

CVs were recorded at 50 mV s^{-1} in 0.5M aqueous H$_2$SO$_4$ solution for estimating the electrochemical active surface areas (ECSA) as it is shown in Fig. 7.3. As it is observed, when the concentration of one metal is increased relative to another, then the behavior of the surface begins to resemble the bulk features of the predominant metal [8]. Considering this issue, the estimation of the ECSA for Pd-rich catalysts is based on the reduction peak during the backward scanning in CV results.

Chapter 7: Carbon supported Ultra-low Pt (PdxPty) electrocatalysts preparation, characterization and H2-PEMFC performance

159
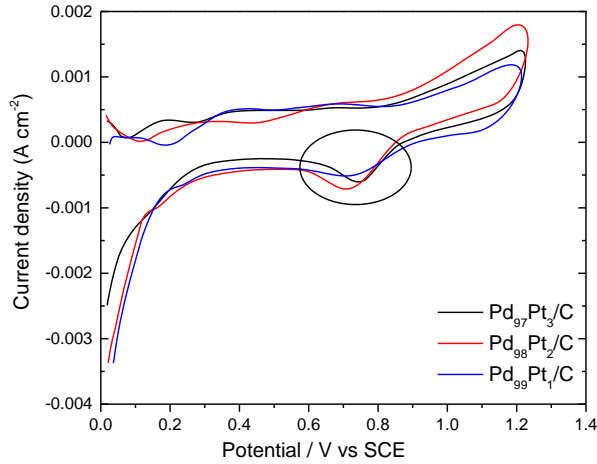
Figure 7.3: Cyclic voltammetry measurements, in 0.5M H₂SO₄, at room temperature with scan rate 50 mVs⁻¹.

The ECSA values are calculated by determining the columbic charge (Q) for the reduction of palladium oxide peak for the indicated area with the cycle in Fig. 7.3.

$$ECSA \left[\frac{m^2}{g}\right] = \frac{Q_o}{Q_{Pd} \times m_{Pd} \times 10} \tag{7.1}$$

where Q_o represents the charge of reduction peak for palladium oxide, Q_{Pd} =420 $\mu C\ cm_{Pd}^{-2}$ is the specific columbic charge corresponding to the full coverage of the Pd surface by one monolayer of oxygen ($\mu C\ cm^{-2}$), and m_{Pd} ($mg\ cm_{electrode}^{-2}$) is the Pd loading on the working electrode. For Pd₉₇Pt₃/C (10.4 $\mu g_{Pd}\ cm^{-2}$), Pd₉₈Pt₂/C (10.6 $\mu g_{Pd}\ cm^{-2}$) and Pd₉₉Pt₁/C (10.8 $\mu g_{Pd}\ cm^{-2}$), their respective ECSA is estimated to be 38.6, 45.2 and 29.8 cm² mg⁻¹_Pd, respectively. The electrochemical active surface area of pure Pd/C was estimated 21 cm²mg⁻¹_Pd.

7.3.2.2   Electrocatalytic activity - HOR

Typical RDE polarization curves for the examined electrocatalysts in H₂-saturated 0.5M aqueous H₂SO₄ solution are plotted in Fig. 7.4. At Pd₉₈Pt₂/C and Pd₉₉Pt₁/C, a small shoulder for E<0.1 V is observed, which becomes more intense as the Pd loading increases (at Pd₉₉Pt₁/C). This formation of shoulder could be attributed to the current associated with the slow desorption of absorbed hydrogen, which in turn may can be attributed to the slow scan rate [9].

Chapter 7: Carbon supported Ultra-low Pt (PdxPty) electrocatalysts preparation, characterization and H2-PEMFC performance

160
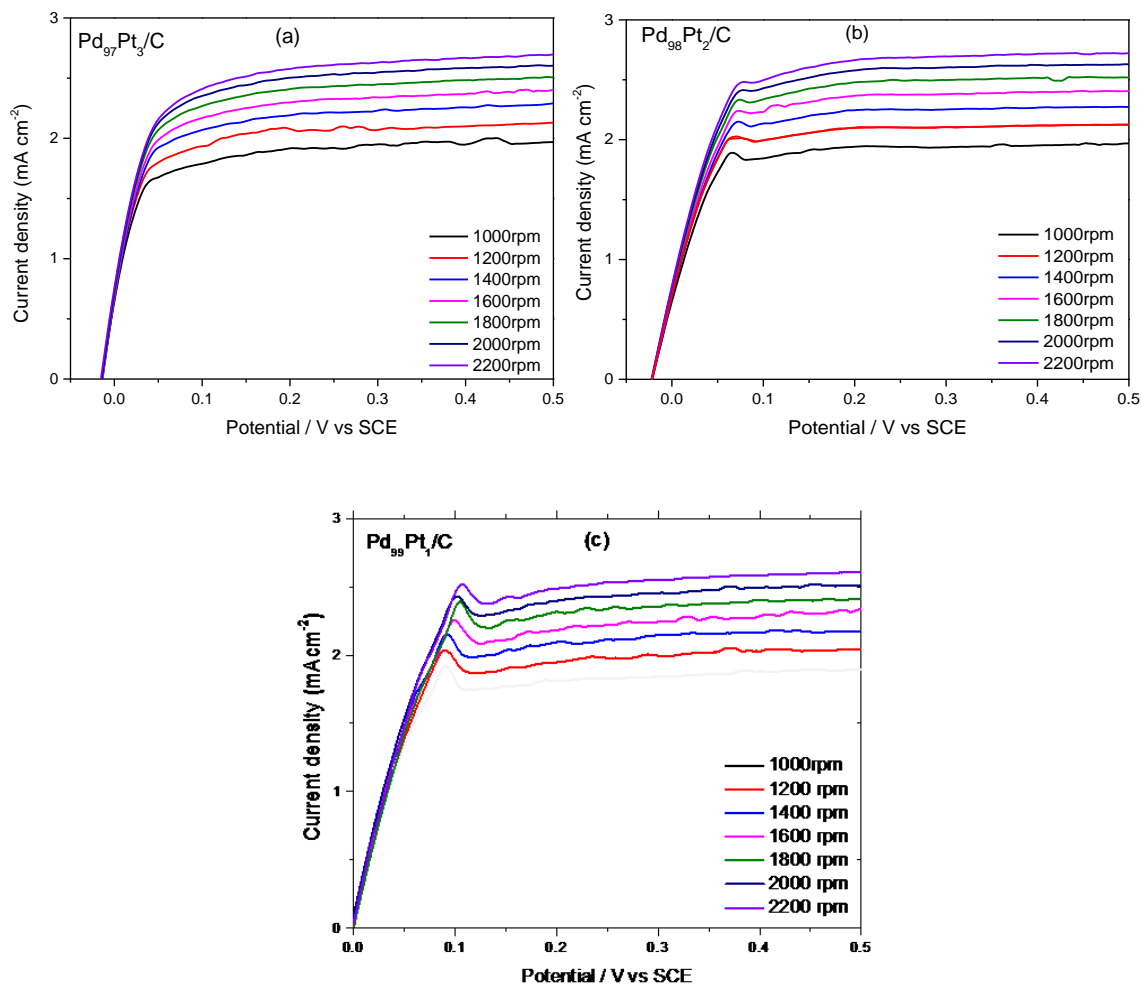
Figure 7.4: RDE polarization curves for HOR in H₂ saturated 0.5 M H₂SO₄ aqueous solution, at a scan rate of 10 mV s⁻¹ at room temperature.

The kinetic parameters can be analyzed on the basis of the Koutecky-Levich equation:

$$\frac{1}{J} = \frac{1}{J_L} + \frac{1}{J_K} = \frac{1}{B\omega^{1/2}} + \frac{1}{J_K}$$

(7.2)

, where $B = 0.62nFD^{2/3}v^{-1/6}C$, n is the number of theoretically-transferred electrons (n=2), F the Faraday constant (96485 C mo⁻¹l), D the diffusion coefficient of H₂ in the H₂SO₄ aqueous solution, v the kinematic viscosity of the electrolyte and C the H₂ concentration in the electrolyte. According to the Koutecky-Levich equation, the kinetic current density (J_K) for different potential values can be obtained from the intercepts of the Koutecky-Levich plots that are depicted in Fig. 7.5.

Chapter 7: Carbon supported Ultra-low Pt (PdxPty) electrocatalysts preparation, characterization and H2-PEMFC performance

161
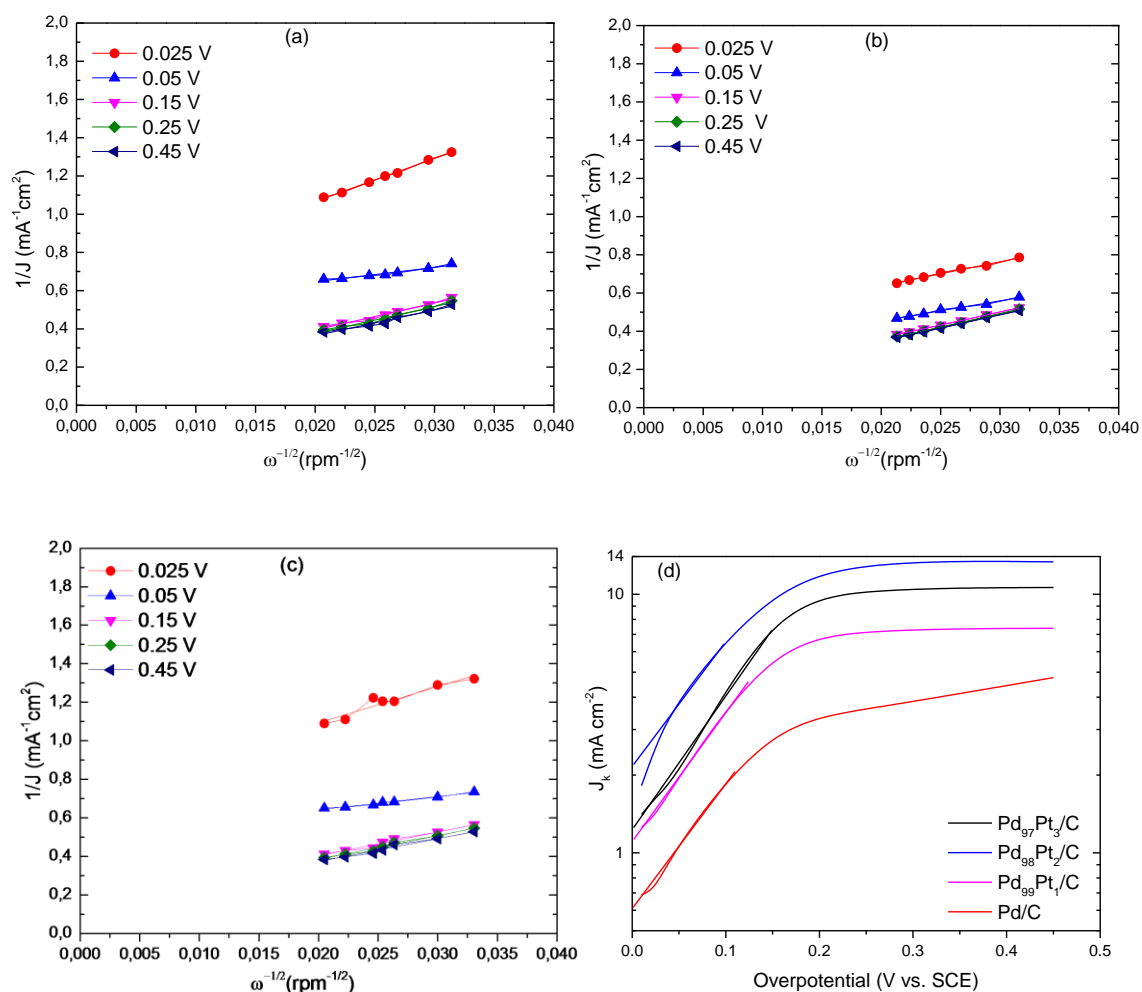
Figure 7.5: Koutecky-Levich plots for the Pd₉₇Pt₃/C (a), Pd₉₈Pt₂/C (b), Pd₉₉Pt₁/C (c), Tafel-Heyrovsky-Volmer plots for the as-examined electrocatalysts (d).

The respective Tafel- Heyrovsky-Volmer plots are depicted for each catalyst separately in Fig. 7.5(d). To compare the catalytic activity of the electrocatalysts the exchange current density (J_o) as well as the charge transfer coefficient are calculated, according to the Tafel-Heyrovsky-Volmer equation [10]:

$$\log(J_k) = \log(J_o) + (\frac{anF}{2.303RT})\eta \tag{7.3}$$

,where J_k :the kinetic current density, calculated from the Koutecky-Levich plots, J_o : the exchange current density, a : the charge transfer coefficient, n: the electron number involved in the reaction (n=2), R: gas constant (R=8.314 J mol⁻¹ K⁻¹), T: the temperature in Kelvin (T=298 K), F: Faraday constant (F=96485 C mol⁻¹), and η the overpotential.

Chapter 7: Carbon supported Ultra-low Pt (PdxPty) electrocatalysts preparation, characterization and H2-PEMFC performance

162

As it is observed, non-zero intercepts indicate that the rate of electron transfer is sufficiently slow to act as a limiting factor [11]. To better compare the catalytic activity of the examined electrocatalysts, the kinetic and exchange current density values in terms of Pd loading are depicted in Fig. 7.6. In all potential values, a volcano behavior is obtained in the plots of current density for HOR and the degree of Pd loading, indicate that two factors (electronic effect and lattice effect) may underlie the alloying effect [12]. The addition of small amounts of Pt to pure Pd electrocatalyst significantly enhances the activity of Pd. This contributing effect becomes sounder at higher potential values. More precisely, at 0.45 V, when the ratio Pd:Pt is 99:1, the kinetic current density is calculated *ca.* 8 mA cm^{-2}. Increasing a little Pt loading (Pd$_{98}$Pt$_2$/C), an intense increment to *ca.* 14 mA cm^{-2} is observed. Similarly, Cho *et al.*[4] found that with the addition of a little amount (5 at.%) of Pt to the Pd electrocatalyst, the electrocatalytic activity towards HOR was enhanced. In the present work, with the addition of only 2 at.%, it is observed also a great enhancement of activity.
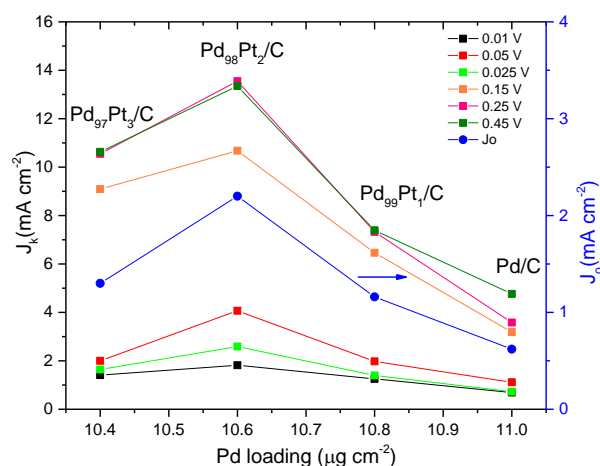
Figure 7.6: Dependence of exchange current density (J$_0$) and kinetic current density (J$_k$) on Pd loading.

Chapter 7: Carbon supported Ultra-low Pt (PdxPty) electrocatalysts preparation, characterization and H2-PEMFC performance

163

7.4 Single Fuel Cell Test

7.4.1 Electrochemical Active Surface Area (ECSA)

The electrochemical characterization of MEA was *in-situ* performed, with the anode to serve as both the counter and reference electrodes and the cathode as the working electrode. Before the measurements activation procedure of MEA took place. The main reason for a MEA activation procedure is to properly humidify both the Nafion electrolyte in the catalyst layer and the Nafion® electrolyte membrane of the MEA that was dried during the assembly process. More precisely, it has been proved that the initial performance of a new MEA with Nafion electrolyte bonded electrodes usually could be improved after the activation, as the electrolyte contained in the electrodes needs hydration to ensure the passage of hydrogen ions. Moreover, the MEA activation has an advantageous effect on the catalyst, such as removal of impurities introduced during the fabrication process of MEA, activation of a catalyst that does not participate in the reaction, and creation of a transfer passage for reactants to the catalyst [13, 14]. The obvious increment in ECSA from 22 m^2/g to 50 m^2/g proves that MEA activation process could provide the catalyst layer with the more transfer passages for hydrogen ions, and thus with a bigger electrochemical active surface area.

7.4.2 Effect of temperature

The power density and polarization curves for single H_2-O_2 PEMFC with $Pd_{97}Pt_3$/C or $Pd_{98}Pt_2$/C as anodes at different temperatures from 30^oC to 80^oC are respectively shown in Figs. 7.7 (A) and (B). In the first case it is observed that the power density increases until 70^oC, exhibiting 93 mW cm^{-2} (or 0.14 mW μg^{-1}_{Pt}), while at 80^oC power density decays to 75 mW cm^{-2} (0.11 mW μg^{-1}_{Pt}). It is noted that the values are referred to the corrected cell potential.

Chapter 7: Carbon supported Ultra-low Pt (PdxPty) electrocatalysts preparation, characterization and
H2-PEMFC performance

164
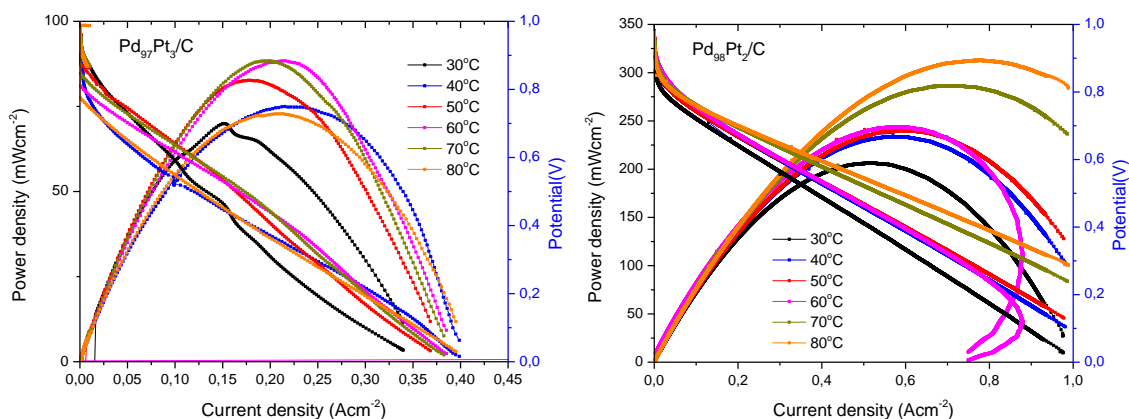
Figure 7.7: Power density and polarization curves at different cell temperature from 30-80°C for: Pd₉₇Pt₃/C//Nafion (NRE212)//Pt/C (A) and Pd₉₈Pt₂/C//Nafion(NRE212)//Pt/C (B).

On the other hand, in the case of $Pd_{98}Pt_2/C$ anode, the maximum power density is observed at 80^oC, reaching $311 mWcm^{-2}$ (or $0.44 mW\mu g^{-1}_{Pt,total}$, $697\mu g_{Pt,total}cm^{-2}$). The exhibited value is far away from the target of $5mW\mu g^{-1}_{Pt,total}$, meaning that further improvement on catalysts' and MEA's preparation method should be taken into future consideration. In order to evaluate the electrochemical behaviour of the as-examined electrocatalysts more thorough during H_2-PEMFC operation, electrochemical impedance measurements were conducted as it is described in the next sub-section.

7.4.3 Electrochemical impedance analysis

In Scheme 1 a typical impedance plot (Nyquist plot) for a membrane electrode assembly is depicted. In a Nyquist plot (Scheme 1), the intersection of the impedance data with the real part of the axis at the high frequency end gives the ohmic (or high frequency or electrolyte) resistance (R_{el}). The ohmic resistance depends on the conductivity of the electrolyte and the geometry of the electrode. The ohmic resistance is the sum of the contributions from uncompensated contact resistance and the ohmic resistance of cell components such as the membrane, catalyst layer, backing layer and end plates.

Chapter 7: Carbon supported Ultra-low Pt (PdxPty) electrocatalysts preparation, characterization and H2-PEMFC performance

165
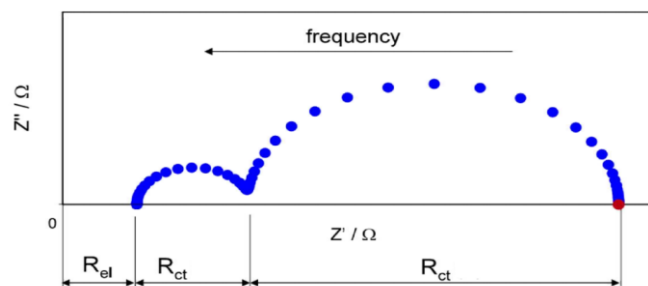
Scheme 1. A typical impedance plot for a membrane electrode assembly.

However, the dominating contribution is from the membrane proton resistance and so it is called electrolyte resistance [15]. Additionally, the intersection of the impedance data with the real part of the axis at the low frequency end gives the sum of the polarization (charge transfer) resistance (R_p) and the ohmic resistance (R_{el}) [16]. Thus, the diameter of the kinetic loop (semi-circle) corresponds to the charge transfer resistance for the hydrogen oxidation (the first arc) and oxygen reduction reactions (the second arc) (Scheme 1). Usually, at the very low frequencies there is a third arc which corresponds to mass transport process.

Fig. 7.8 shows the Nyquist plots of the impedance data for H_2/O_2 (H_2: 80 mL min^{-1}, O_2: 40 mL min^{-1}) feeding, 100% relative humidity, at 0.6 V, at different temperatures from 30 to 80°C, with $Pd_{97}Pt_3$/C as anode. More precisely, symbols are used to depict the experimental results and line to fit the experimental results according to the equivalent circuit depicted in Fig. 7.8 (B).

According to our impedance results (Fig. 7.8(A)), all curves are characterized by a complete semi-circle typical of a kinetic control associated with the oxygen reduction reaction [17], without the anode semi-circle to be so evident. This can be explained by the fact that the anode reaction (hydrogen oxidation) is much faster than the cathode one (oxygen reduction). Moreover, as it is shown there are no observed mass transport limitations (semi-circles at very low frequencies).

Chapter 7: Carbon supported Ultra-low Pt (PdxPty) electrocatalysts preparation, characterization and H2-PEMFC performance

166
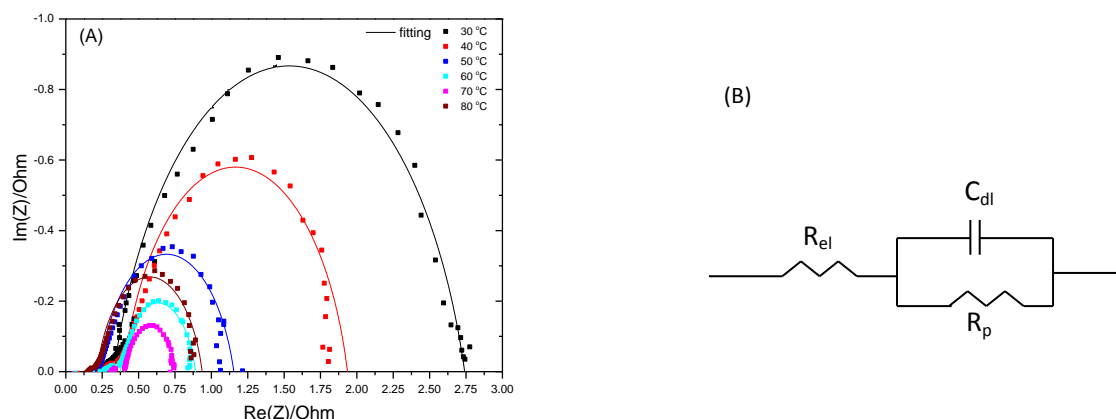
Figure 7.8: MEA impedance plots with H_2/O_2 feeding (H_2: 80 mLmin-1, O_2: 40 mLmin-1), from 1 mHz– 100 kHz . Ac:10mV at 0.6 V at different temperatures of 30-80oC, at atmospheric pressure (A), Nyquist equivalent circuit (B).

Analyzing the impedance data as summarized in Table 1, the electrolyte resistance decreases from 0.24 Ohm to ~0.06 Ohm, when the temperature increases from 30^oC to 80^oC. The resistance decrement is reasonable since with the temperature increment proton conductivity increases. However, at 70^oC an increment of electrolyte resistance at 0.12 Ohm (Fig.7.8 and Table 1), it is observed.

Consequently, explaining the polarization behavior of MEA; from Fig. 7.8(A) it is shown that as the temperature value increases, until 70^oC, the ohmic losses are reduced, since with the temperature increment the proton conductivity is enhanced (R_p is reduced to 0.64Ohm). On the other hand the performance loss at 80^oC, is mainly attributed to the low charge transfer due to the adsorbed molecules, as it will be discussed below.

Table 7. 1: Electrochemical impedance analysis results for H_2/O_2 fuel cell at 0.6V.

T (^oC)	C_{dl}(mF)	R_{el} (Ohm)	R_p (Ohm)
30	184	0.24	2.49
40	183	0.12	1.81
50	214	0.10	1.05
60	239	0.08	0.81
70	242	0.12	0.64
80	215	0.06	0.87

From Table 7.1 it is shown that the polarization resistance from 30 to 70^oC, decreases from 2.49 to 0.64 Ohm, indicating the convenience of the charge transfer as the

Chapter 7: Carbon supported Ultra-low Pt (PdxPty) electrocatalysts preparation, characterization and H2-PEMFC performance

167

temperature increases. More precisely, the charge transfer arc (kinetic loop or polarization resistance) decreases, as the temperature increases from 30 to 70°C, while at 80°C, the kinetic loop increases again. That means that the temperature increment up to 70°C accelerates charge transfer and when the temperature is 80°C, the charge transfer slows down. The results are consistent with the fuel cell performance at different temperature values (Fig.7.7). The lowest fuel cell's performance can be mostly attributed to the slow charge transfer than to the proton conductivity, as it can be deduced from the results reported also in Table 7.2.

EIS experimental data have to be interpreted by the aid of an equivalent electric circuit model. This is a combination of electric and electrochemical elements selected to simulate the response of the electrochemical system to the imposition of the excitation signal. Diffusive phenomena at the interface electrode/electrolyte are essential for the correct operation of a fuel cell, as they are part of the charge transfer reaction, and could give a contribution to the total impedance [18]. Anode, cathode and electrolyte should be considered as three electric circuits connected in series, however the polymeric membrane is generally treated as a resistor (electrolyte resistance, Rel), while being the anode reaction (hydrogen oxidation) very faster than the cathode (oxygen reduction), the electric circuit of the anode can be neglected and the elements R_{ct} and C_{dl} are referred only to the cathode [19]. On the basis of the above considerations, and taking into account that no indication of mass transfer control is observed in EIS spectra, the quantitative analysis of experimental data reported in Fig. 7.8 was effected by the equivalent circuit shown in Scheme 1.

The basic equivalent circuit that represents the fuel cell operation is the Randles circuit, where C_{dl} is the double layer capacitance of the catalyst surface, R_{el} describes the movement within a conducting media and illustrates the sum of contribution from contact resistance

Chapter 7: Carbon supported Ultra-low Pt (PdxPty) electrocatalysts preparation, characterization and H2-PEMFC performance

168

between components and high frequency resistance of the cell components, and R_p is the resistance that occurs when electrons transfer at the electrode/electrolyte interface [20]. The double layer capacitance is the highest (242 mF, Table 1) at 70°C, where it is observed the highest fuel cell performance and the lowest charge transfer resistance.

Accordingly, identical gas feeds (H_2/H_2) (or symmetrical gas feeding, SYM) in both anode and cathode compartments, 80 mL min^{-1}, from 30°C to 80°C was used to investigate more thoroughly characteristics of the anodic electrocatalyst ($Pd_{97}Pt_3/C$) [21]. This technique gives more kinetic information, providing a specified qualitative and quantitative analysis of the fuel cell system as well as leading to a better understanding on performance [17]. The reactions occurring in each electrode when the fuel cell is symmetrical fed with hydrogen are the following:

$$H_2 \rightarrow 2H^+ + 2e^- \text{ (anodic reaction)}$$

$$2H^+ + 2e^- \rightarrow H_2 \text{ (cathodic reaction)}$$

Chapter 7: Carbon supported Ultra-low Pt (PdxPty) electrocatalysts preparation, characterization and H2-PEMFC performance

169
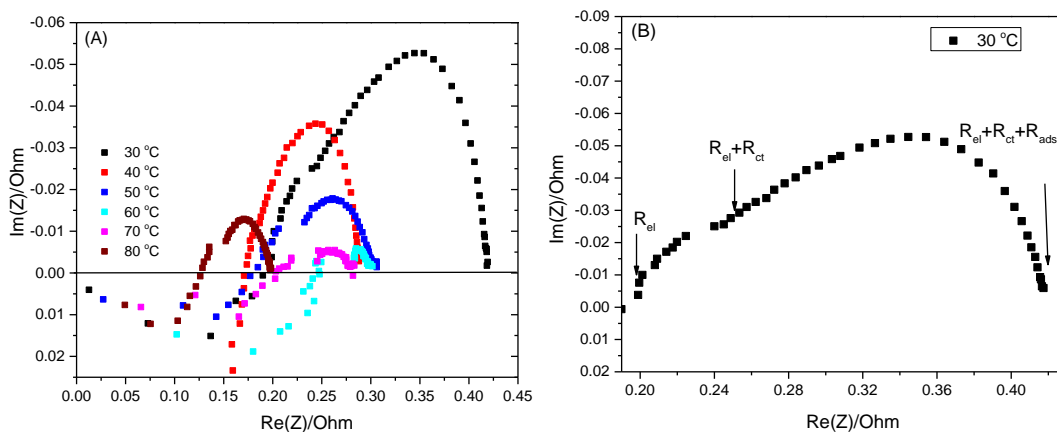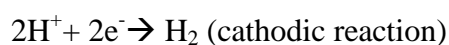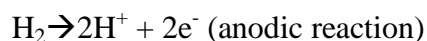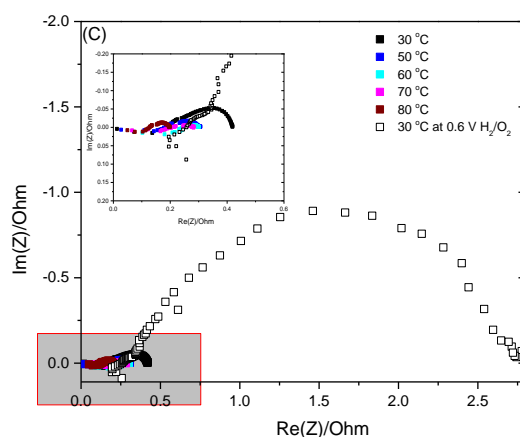
Figure 7.9: Membrane electrode assembly impedance plots with H_2/H_2 feeding (H_2: 80 mLmin^{-1}), from 1 mHz– 100 kHz. Ac:10mV at OCV from 30-80°C, at atmospheric pressure (A), Impedance plot of 30 °C (from Fig.(A)) at a higher magnification (B), comparison of impedance plots of H_2/H_2 and H_2/O_2 (from Fig.(A)) (C).

Fig.7.9 (A) presents typical Nyquist impedance plots for a symmetrical feeding H_2 fuel cell at OCV, at different temperatures from 30 to 80°C. Fig. 7.9 (B) gives a zoom option of the experimental impedance plot at 30°C from Fig.7.9(A), in order to form an opinion about the shape of the semi-circles. While Fig.7.9(C) compares the resistance of anode (H_2/H_2 feeding) with the total MEA resistance (attributed to cathode, H_2/O_2 feeding). In contrast to the H_2/O_2 feeding, in the case of H_2/H_2 feeding, two inter-overlapped semi-circles are observed; one small at high frequencies and a larger at medium frequencies. At very low frequencies there is no observed loop.

Table 7.2: Electrochemical impedance analysis at different temperature values.

T (°C)	R_{el} (Ohm)	R_{ct} (Ohm)	R_{ads} (Ohm)
30	0.20	0.05	0.12
40	0.17	0.02	0.10
50	0.18	0.05	0.08
60	0.25	0.03	0.01
70	0.20	0.05	0.03
80	0.13	0.02	0.05

Chapter 7: Carbon supported Ultra-low Pt (PdxPty) electrocatalysts preparation, characterization and H2-PEMFC performance

170

As it can be observed from the data analysis (Table 7.2) at high frequency values, the electrolyte (membrane) resistance does not increase linearly with the temperature increment. The R_{el} is around 0.13-0.20 Ohm for all the temperature values. Comparing the results of the estimated R_{el} under H_2/H_2 and H_2/O_2 feeding from Table 1 and Table 2, respectively, it is obvious that when reaction takes place and there is production of water at cathode, the membrane is more hydrated and the R_{el} is much lower. Except for 30°C, where the water production is not favored a lot due to the low temperature and so the electrolyte resistance is almost 0.20 Ohm in both cases (H_2/H_2 and H_2/O_2). As the temperature increases, the diameter of the charge transfer and adsorption species loops decreases.

In Fig. 7.9 (C), where the H_2/O_2 (at 30°C) and H_2/H_2 (from 30 to 80°C) are given, it can be deduced that the anode contributes a little to the total impedance, at all temperature values. Consequently, the impedance from the H_2/O_2 operation is attributed totally to slow ORR at the cathode.

7.5 Conclusions

According to the experimental results and the kinetic analysis, the addition of a little amount of Pt to pure Pd electrocatalyst enhances electrocatalytic activity towards HOR and ORR. More precisely, the exchange current density for HOR was calculated to has the following order: $Pd_{98}Pt_2$/C(2.2 mA cm^{-2})>$Pd_{97}Pt_3$/C(1.3mA cm^{-2})>$Pd_{99}Pt_1$/C(1.16 mA cm^{-2})>Pd/C (0.62 mA cm^{-2}), presenting a volcano-type dependence on Pd loading. Among the examined electrocatalysts $Pd_{98}Pt_2$/C and $Pd_{97}Pt_3$/C exhibited better activity for HOR at room temperature. However, the increase of temperature favors electrooxidation reactions. For this reason in this work the $Pd_{97}Pt_3$/C and $Pd_{98}Pt_2$/C, tested as anode electrode in a single hydrogen fuel cells, using commercial Pt/C as cathode electrode. The total Pt loading was only 657 μg_{Pt} cm^{-2}. Increasing the temperature value from 30° to 70°C,

Chapter 7: Carbon supported Ultra-low Pt (PdxPty) electrocatalysts preparation, characterization and H2-PEMFC performance

171

the power density increased from 75 to 98 mW cm^{-2}. However, further temperature increment to 80°C had a negative effect on fuel cell performance, decreasing the power density at *ca.* 75 mWcm^{-2}. According to electrochemical impedance measurements this decay can be attributed to the lower membrane conductivity as well as to the slow oxygen reduction reaction kinetics. Consequently, Pd can replace at the most percentage the platinum electrocatalyst.

Chapter 7: Carbon supported Ultra-low Pt (PdxPty) electrocatalysts preparation, characterization and H2-PEMFC performance

172

References

[1]   A. Brouzgou, S.Q. Song, P. Tsiakaras. Applied Catalysis B: Environmental 127 (2012) 371-388.

[2]   F. Barbir, PEM Fuel Cells: Theory and Practice, Academic Press, 2012.

[3]   H. Tsuchiya, O. Kobayashi. International Journal of Hydrogen Energy 29 (2004) 985-990.

[4]   Y.-H. Cho, B. Choi, Y.-H. Cho, H.-S. Park, Y.-E. Sung. Electrochemistry Communications 9 (2007) 378-381.

[5]   E. Antolini, S.C. Zignani, S.F. Santos, E.R. Gonzalez. Electrochimica Acta 56 (2011) 2299-2305.

[6]   S. Song, Y. Wang, P.K. Shen. Journal of Power Sources 170 (2007) 46-49.

[7]   Jong-Mun Jang, Gu-Gon Park, Y.-J. Sohn, S.-D. Yima, C.-S. Kima, T.-H. Yang. Journal of Electrochemical Science and Technology 2 (2011) 131-135.

[8]   C.-C. Chen, C.-L. Lin, L.-C. Chen. Electrochimica Acta.

[9]   A. Czerwiński, M. Grdeń, M. Łukaszewski. Journal of Solid State Electrochemistry 8 (2004) 411-415.

[10]   S.J. Yoo, H.-Y. Park, T.-Y. Jeon, I.-S. Park, Y.-H. Cho, Y.-E. Sung. Angewandte Chemie International Edition 47 (2008) 9307-9310.

[11]   S.N. Pronkin, A. Bonnefont, P.S. Ruvinskiy, E.R. Savinova. Electrochimica Acta 55 (2010) 3312-3323.

[12]   A. Wieckowski, J. Norskov, S. Gottesfeld, Fuel Cell Science: Theory, Fundamentals, and Biocatalysis, in: Wiley (Ed.), 2011.

[13]   M. Zhiani, S. Majidi, M.M. Taghiabadi. Fuel Cells 13 (2013) 946-955.

[14]   J.-M. Jang, G.-G. Park, Y.-J. Sohn, S.-D. Yim, C.-S. Kim, T.-H. Yang. Journal of Electrochemical Science and Technology 2 (2011) 131-135.

[15]   X.Z. Yuan, C. Song, H. Wang, J. Zhang, Electrochemical Impedance Spectroscopy in PEM Fuel Cells: Fundamentals and Applications, Springer, 2009.

[16]   B. Li, J. Qiao, D. Yang, J. Zheng, J. Ma, J. Zhang, H. Wang. Electrochimica Acta 54 (2009) 5614-5620.

[17]   X. Yuan, H. Wang, J. Colin Sun, J. Zhang. International Journal of Hydrogen Energy 32 (2007) 4365-4380.

[18]   P.M. Gomadam, J.W. Weidner. International journal of energy research 29 (2005) 1133-1151.

Chapter 7: Carbon supported Ultra-low Pt (PdxPty) electrocatalysts preparation, characterization and H2-PEMFC performance

173

[19]   F. Migliardini, P. Corbo. Int. J. Electrochem. Sci 8 (2013) 11033-11047.

[20]   G. Mousa, F. Golnaraghi, J. DeVaal, A. Young. Journal of Power Sources 246 (2014) 110-116.

[21]   S.-J. Seo, J.-J. Woo, S.-H. Yun, H.-J. Lee, J.-S. Park, T. Xu, T.-H. Yang, J. Lee, S.-H. Moon. Physical Chemistry Chemical Physics 12 (2010) 15291-15300.

Chapter 7: Carbon supported Ultra-low Pt (PdxPty) electrocatalysts preparation, characterization and H2-PEMFC performance

174

Water Electrolysis: A Brief literature review

&

Electrocatalytic activity of Platinum free (Pd-based) electrocatalysts towards hydrogen evolution reaction (HER)

Abstract

The main subjects of this chapter are:

A) A brief summary of the fundamentals of water electrolysis and the available electrolyzers' technology. Moreover, the state-of-the-art for the PEM electrolysis technologies, establishing PEM electrolysis as a commercially viable hydrogen production solution.

B) The fabrication and investigation the electrochemical behavior of cathode catalysts appropriate for medium- temperature proton exchange membrane (PEM) water electrolysis (WE). The electrochemical characterizations were performed using cyclic voltammetry (CV), linear sweep voltammetry (LSV) and electrochemical impedance spectroscopy (EIS). The results show that incorporation of Ir and Rh in Pd as a binder in construction of the electrode, improve the electrocatalytic behavior of palladium for proton reduction.

Chapter 8: Water Electrolysis: A brief literature review & Electrocatalytic activity of Pd-based electrocatalysts towards hydrogen evolution reaction (HER)

175

Contents

Chapter 8: Water Electrolysis: A brief literature review & Electrocatalytic activity of Pd-based electrocatalysts towards hydrogen evolution reaction (HER)

176

List of Figures

List of Tables

Chapter 8: Water Electrolysis: A brief literature review & Electrocatalytic activity of Pd-based electrocatalysts towards hydrogen evolution reaction (HER)

177

8.1   Introduction

Hydrogen must be produced by means of an energy input, and to date, hydrogen is mainly produced by steam reforming natural gas or other fossil fuels, such as propane, gasoline, diesel, methanol, or ethanol [1, 2]. This is achieved in a processing device called a reformer in which water vapor at high temperature ($\sim$700−1100 °C) is reacted with a fossil fuel, in the presence of a metal-based catalyst (usually nickel). However, steam reforming of fossil fuels produces low purity hydrogen with a high concentration of carbonaceous species such as carbon monoxide. More importantly, steam reforming does not relieve dependencies on scarce fossil fuels or reduce their pollutants, ultimately, not contributing to the establishment of a "carbon-balanced" energy matrix. One of the promising approaches to produce high-quality hydrogen ($\approx$100% hydrogen) is by splitting water using electricity (water electrolysis) [3].

Water electrolysis is one of the most promising methods for hydrogen production. Electrolysis technologies are developed and successfully integrated into renewable and hydrogen energy based system [4]. Electrolysis is less efficient than a direct chemical path but offers virtually no pollution or toxic byproducts if the electric current is generated using renewable energy (wind, solar, geothermal and hydropower) thus making it a very plausible option if the efficiency could be increased [3, 5]. The currently established technologies for producing hydrogen require significant improvements in their technical and economic performance (efficiency and costs) if hydrogen is to be produced for energy use.

Electrolyzers dissociate water into hydrogen and oxygen gasses by passing an electrical current through the water. Electrolysis is not a renewable method because it depends on the source of the electricity used in the electrolysis. If electricity can be provided by any renewable energy source such as, geothermal, solar, wind energy

Chapter 8: Water Electrolysis: A brief literature review & Electrocatalytic activity of Pd-based electrocatalysts towards hydrogen evolution reaction (HER)

178

sources, the electrolysis generates renewable hydrogen and oxygen. The reaction with the thermodynamic energy values is described in Eq. (8.1):

$$H_2O_{(l)} + 237.2 kJ\ mol^{-1} + 48.6 kJ \rightarrow H_2 + \tfrac{1}{2}O_2 \qquad (8.1)$$

$$\underbrace{\phantom{237.2 kJ\ mol^{-1}}}_{\text{Electricity}} \quad \underbrace{}_{\text{Heat}}$$
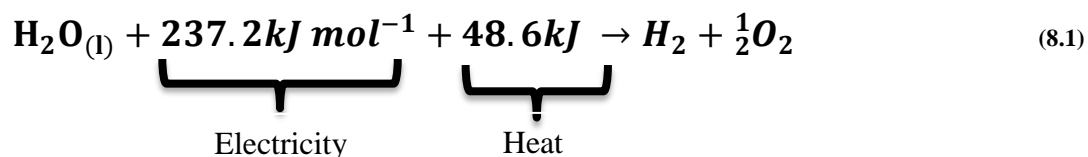
There are two main distinct water electrolyzer technologies: i) alkaline electrolysers (AE) and ii) acid water electrolyzers. Among acid electrolyzers, proton exchange membrane (PEM) electrolyzer being the solid acid membranes is mostly preferred due to ease of handling and safety. There are considerable fundamental differences between these electrolyzer technologies, but in each case the net chemical effect remains the same (i.e. dc electricity + $H_2O \rightarrow 2H_2 + O_2$) and by definition a water electrolyzer always produces hydrogen at twice the volumetric rate as oxygen. Table 8.1 provides a summary of their key attributes [6].

Table 8.1: Types of Electrolyzers

Type	Alkaline	PEM
Electrolyte	Sodium or potassium hydroxide	Solid polymer membrane (usually nafion)
Transport mechanism	Hydroxyl ion, $OH^-_{(aq)}$	Hydrogen ion (proton) H^+
Electrode catalyst	Nickel based	Platinum/Iridium
Working Temperature	$40\text{-}90^o$	$50\text{-}100^o$
Cell voltage (V)	1.8–2.4	1.8–2.2
Power density (mW cm^{-2})	<1	<4.4
Current density (mA cm^{-2})	0.2–0.4	0.6–2.0

Chapter 8: Water Electrolysis: A brief literature review & Electrocatalytic activity of Pd-based electrocatalysts towards hydrogen evolution reaction (HER)

179

Alkaline electrolyzers are the most commonly used electrolyzers in the industry. By using alkaline electrolyzer 99% purity hydrogen can be obtained, but only with usage of another purification unit. This because of high electrolyte vapor alkaline electrolyzer suffers from corrosion and only 25-30% weight KOH solution issued as an electrolyte. The efficiency of hydrogen production reaches up to ~80%. Alkaline electrolyzer is the most effective on low current densities; i.e.ca. 0.3 Amp/cm^2. On the other hand, the lifetime of the electrolyzer is short and is not durable at high temperatures due to highly corrosive electrolyte.

Proton exchange membrane (PEM) water electrolysis is considered as an attractive process to accelerate the transition to the hydrogen economy and to develop a hydrogen infrastructure network (development of hydrogen re-filling stations for automotive applications using electric power stations at night hours and/or renewable energy sources) [7]. Compared to the more conventional alkaline process, PEM water electrolysis offers a number of significant technical advantages for the production of electrolytic-grade hydrogen: higher operating security offering the possibility of producing compressed gases (>200 bar) for direct storage with no compressor, higher gas purity (>99.99% for hydrogen) with no soda, and long time performance without maintenance. However, the main drawback of this technology, which still postpones applications in the industry, is its prohibitive cost, which comes mainly from the use of noble metals as electrocatalysts. Typically, platinum is used at cathodes for the hydrogen evolution reaction (HER) and iridium (metal or oxides) is used at anodes for the oxygen evolution reaction (OER). These noble metals are required (i) because they yield the best catalytic activity for the HER and the OER in acidic media (typical conversion efficiencies >80% are commonly obtained at 1 A cm^{-2}) and (ii) because of the strong acidity of the solid electrolyte, which would cause the corrosion of non-noble metals. To reduce the cost of PEM cells, different approaches can

Chapter 8: Water Electrolysis: A brief literature review & Electrocatalytic activity of Pd-based electrocatalysts towards hydrogen evolution reaction (HER)

180

be followed: (i) a reduction in Pt and Ir loadings (in state-of-the-art electrolyzers, 2–5 mgcm^{-2} black Pt and Ir are commonly used), (ii) the use of less expensive noble metals such as Pd and Rh or (iii) the development of alternative low-cost electrocatalysts based on non-noble metals and molecular chemistry [8].

8.1.1 Proton Exchange Membrane (PEM) Electrolyzer

The concept of PEM technology (a zero-gap cell using a proton-conducting solid polymer electrolyte) was proposed half a century ago, at the dawn of the US space program, when new energy management devices operating in a zero-gravity environment were needed. At that time, the concept was first used to develop H_2/O_2 fuel cells and later, water electrolyzers. Almost fifty years later, there are still a lot activities on this technology which is still considered as a key process for transforming zero-carbon electricity sources into the supply of zero-carbon hydrogen and oxygen for miscellaneous end-uses [5].

Basically water is a reactant and products are hydrogen and oxygen. PEM electrolyzer consists of membrane electrode assembly (MEA) which is composite material containing solid electrolyte coated with catalysts on each side (it is the medium where the electrolysis reaction occurs), gas diffusion layer and electric current collectors.

The reaction medium is the surfaces of the MEA of the electrolyzer. The electrolyte of PEM is a solid perfluorinated membrane (Nafion membrane) which is the electrically nonconductive and also physical barrier to both hydrogen and oxygen gases but protons pass through the membrane. Both sides of the membrane are coated with noble metals. In water electrolysis liquid or gaseous water is fed to the anodic compartment where it is oxidized producing oxygen and protons, i.e.:

$$H_2O \rightarrow \tfrac{1}{2}O_2 + 2H^+ + 2e^- \tag{8.2}$$

Chapter 8: Water Electrolysis: A brief literature review & Electrocatalytic activity of Pd-based electrocatalysts towards hydrogen evolution reaction (HER)

181

Oxygen evolves in the gaseous phase, whereas the electrons circulate in the external circuit and protons cross-over the membrane, reaching the cathodic compartment where they are reduced by the electrons coming from the external circuit, thus producing hydrogen, as follows:

$$2H^+ + 2e^- \rightarrow H_2 \qquad (8.3)$$

This corresponds to the overall decomposition of water into hydrogen and oxygen:

$$H_2O \rightarrow H_2 + \tfrac{1}{2}O_2 \qquad (8.4)$$

with $\Delta H = 286$ kJ and $\Delta G = 237$ kJ under standard conditions.

This reaction need external energy ($\Delta H > 0$), coming from the external electrical power sources. The corresponding theoretical cell voltage can be calculated from ΔG, i.e. $E_{cell} = \Delta G/2F$, giving $E_{cell} = 1.23$ V for water electrolysis. The schematic view of the PEM water electrolyzer is shown in figure 8.1.
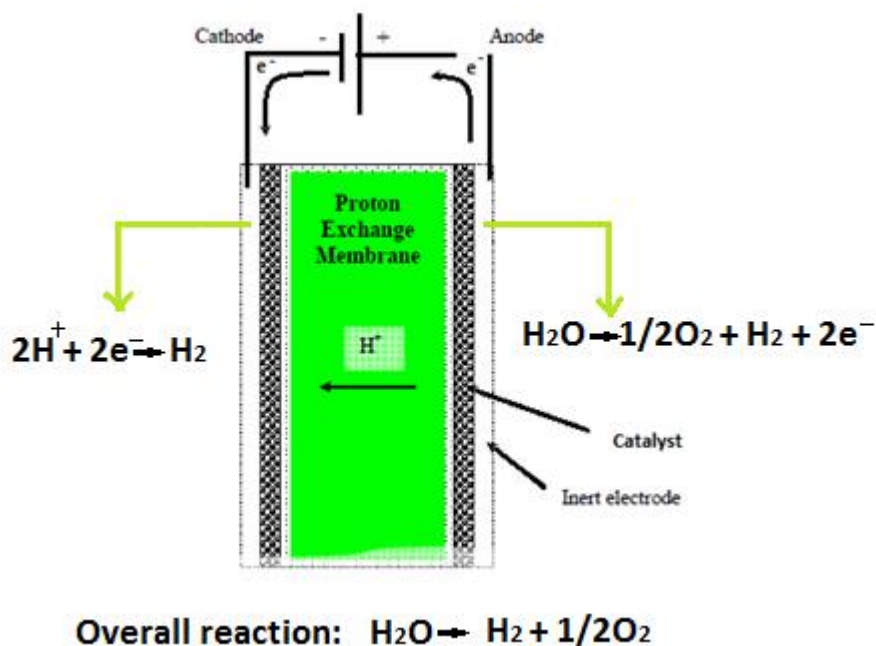
Figure 8.1: Schematic of the Operating Principle of a PEM Electrolyzer.

Chapter 8: Water Electrolysis: A brief literature review & Electrocatalytic activity of Pd-based electrocatalysts towards hydrogen evolution reaction (HER)

182

8.1.2 Thermodynamics and kinetics

The minimum potential difference which must be applied between the two electrodes of an electrolyzer is thermodynamically defined in terms of change of the reaction Gibbs free energy **(3)**

$$E = -\frac{\Delta G}{nF} \tag{8.5}$$

Where

$$\Delta G = \mu_{H2} + 1/2\mu_{O2} - \mu_{H2O} \tag{8.6}$$

μ is chemical potential and ΔG is the Gibbs free energy at standard conditions (25°C and atmospheric pressure) **(3)** from equations **(4)** and **(5)** (Nernst equation):

$$E^{rev} = -\frac{\Delta G^0}{nF} - \frac{RT}{2F} ln(\frac{P_{H2}P_{O2}}{aH_2O}) \tag{8.7}$$

Where n the number of electrons involved, F is Faraday's number (F=96487 C/mol), P is partial pressure and α is the activity. E^{rev} measures the difference between the reversible potentials of the anode and the cathode (equilibrium cell voltage) which is the lowest potential that must be applied for the reaction to happen. Under standard conditions at 25^oC and water in liquid form, $\Delta G^o=237,178\frac{kJ}{mol^{-1}}$, the E^{rev} is calculated to be 1.229V. Equation (8.7) shows that E^{rev} is increased by an increase in partial pressure. Moreover, E^{rev} is decreased by increasing temperature therefore thermodynamics suggests that the best conditions for operating in case of saving energy would be at high temperatures and low pressures if water remains in liquid state since at very high temperature (steam water electrolysis) the benefit of E^{rev} is quite clear.

The energy balance for the cell is to be referred to the enthalpy by the following equation [9]:

$$\Delta G=\Delta H- T\Delta S \tag{8.8}$$

Chapter 8: Water Electrolysis: A brief literature review & Electrocatalytic activity of Pd-based electrocatalysts towards hydrogen evolution reaction (HER)

183

where ΔH is the enthalpy a measure for the energy required to break and form molecular bonds and to bring reactants and products into their reference states and ΔS is the entropy of the reaction. The formation equation for ΔG at different temperatures can be expressed as:

$$\Delta G(T) = -295.6 - 0.033 \cdot T \cdot \ln T + 2.81 \cdot 10^{-6} \cdot T^2 - 12.77 \cdot T^{-1} + 0.38 \cdot T \text{ (kJ/mole)}$$

8.2 Electrode reactions in PEM water electrolysis

8.2.1 The hydrogen evolution reaction (HER)

The hydrogen evolution reaction (HER) is the main reaction in the water electrolysis and has been widely studied on various metals, alloys and oxide films [10]. Noble metals are considered as the best candidates for the HER in acidic media [10, 11] due to their best catalytic activity and the low corrosion resistance of non-noble metals such as Ni, Co, Fe in acidic media. Among noble metals, platinum (Pt) is regarded as an ideal catalyst for electrochemical production of hydrogen, but its high cost and scarce resource definitely limit its extensive application in HER [12]. An approach to explain the particular role of platinum as an electrocatalyst for anodic hydrogen oxidation and cathodic hydrogen evolution is correlating by the catalytic activity of different metals for this reaction and the strength of the adsorption enthalpy of hydrogen on these metals in Figure 8.2 [13]. The electrochemical activity of the hydrogen evolution reaction (HER) on different metals can be compared using the energy of the chemisorbed H to the active sites. The standard potential of H_2 is by definition zero. As a first approximation the electrochemical activity of HER on different metals can be compared by a so-called "Vulcano-plot", where $\log(i_0)$ is related to the bond energy for cathodic release of hydrogen H at a given overpotential (kcal/mole). A "Vulcano-plot" as shown in Figure 8.2 it can be seen that the metals of intermediate bond-strength energy is the most active towards the HER represented by the noble metals [13].

Chapter 8: Water Electrolysis: A brief literature review & Electrocatalytic activity of Pd-based electrocatalysts towards hydrogen evolution reaction (HER)

184
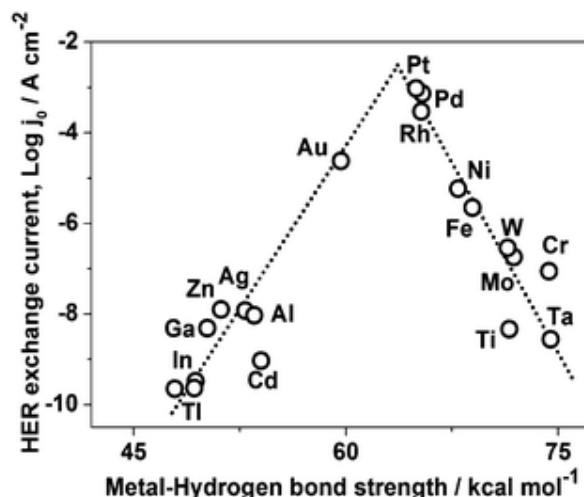
Figure 8.2: Volcano type correlation of catalytic activity of different metals for hydrogen evolution reactions in acid solutions [14].

For the metals of low bond-strength on the left side of the curve discharge of H with lower bond strengths the interaction between adsorbate and metal is too low to allow for an effective activation of the H-H bond.

In most of the early studies, researchers used platinum black as a standard catalyst on the cathode side (HER). Later on, due to the experience on the development of catalysts for PEM fuel cells, researchers started to use platinum nanoparticles supported on carbon black (Pt/C) from different manufacturers (ETEK/BASF, Tanaka, and Johnson & Matthey) as their standard catalysts for the HER. However, despite the lower platinum loadings compared to the anode side loading, the cathode catalyst still represents a considerable portion of the total system cost, especially if degradation or corrosion of the carbon support occurs.

Today, loadings for the cathode side range between 0.5 and 1mg cm^{-2} and further reductions will always be desired, with the potential of reaching values below 0.2 mg cm^{-2}. Since 2005, few studies exist attempting to reduce the platinum loadings, improve catalysts utilization (homogeneity, particle size), and potentially substitute (creating the so-called platinum free catalysts). When studying the cathode catalyst, due to the

Chapter 8: Water Electrolysis: A brief literature review & Electrocatalytic activity of Pd-based electrocatalysts towards hydrogen evolution reaction (HER)

185

dominance of the OER, experimentation is usually done in a liquid electrolyte half-cell or three electrode apparatus to isolate the contribution of only the cathode.

8.2.2. The oxygen evolution reaction (OER)

Among the two half-reactions of water electrolysis, the OER is the most demanding [15]. The OER involves the formation of a double O-O bond from two water molecules with the simultaneous release of four protons and four electrons [16]. The four protons and four electrons are then combined in the overall two-electron, two-proton process of the HER. Since it is generally accepted that electron transfers at the interface occur one electron at a time, the OER is more kinetically demanding in as much as four (vs two for the HER) charge equivalents must be stored and cumulatively discharged toward a productive O-O bond forming reaction. In addition, the OER is the first step of water splitting. For these reasons, the OER is viewed by consensus to be the key to water splitting.

Iridium and ruthenium based oxides have been preferred as anode catalysts [17, 18] because of their low anodic overvoltage for the oxygen-evolution reaction (OER) at high current densities and in the case of iridium oxide long term stability. Although iridium oxide is a very good choice of catalyst in terms of stability and overpotential, this material poses a significant cost challenge on a large-scale deployment of water electrolysis. For PEM electrolysis cells a decrease in the precious metal IrO_2 or RuO_2 catalyst loading to ultra-low levels by the development and processing of improved electrochemically active and durable electrocatalysts would significantly decrease the overall capital costs. So other metal oxides such as Co-based oxide, Ni-based oxide, Ni-Co oxide and Mn-based oxide have been developed [19-22].

To summarize, the reaction rate of oxygen evolution is determined by the material properties of the surface species at the electrode. The volcano plot in figure 8.3 compares the

Chapter 8: Water Electrolysis: A brief literature review & Electrocatalytic activity of Pd-based electrocatalysts towards hydrogen evolution reaction (HER)

186

catalytic activity of different oxides. Here, the electrocatalytic activity (measured as anodic overpotential) is related to the enthalpy for the oxides to form a higher oxidation state from a lower oxidation state. This could be directly related to the M-O bond strength [23].
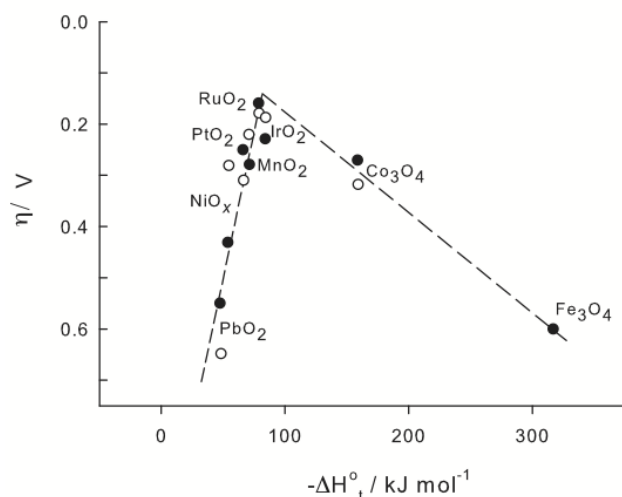
Figure 8.3: Volcano-plot of electrocalalytic activity of different oxides in acidic (open spheres) and alkaline (filled spheres) solutions.

The reaction will most likely happen at a surface defect, or an active site, so the reaction rate will also depend on the number of available sites. The number of active sites is given by the surface area of the catalyst. To get a larger area with the same amount of noble metal, the particle size should to be small.

As previously discussed, Ir (IrO_2) is generally recognized as the state-of-the-art for the OER in PEM electrolysis. Ru (RuO_2) is more active than Ir (IrO_2), but the problems related to instability (corrosion) limit its use. Until the early 1990s PEM electrolysis publications concentrated mainly on the use and understanding of Ru and Ir catalysts, and their alloys, for the OER. With the aim of improving efficiency, stability, and reducing the costs, researchers in the following years began trying different catalyst alternatives for the OER. The first approaches were concentrated on mixing IrO_2 with a cheaper "diluent" forming a solid solution with less expensive and more durable materials that could be easily manufactured. This would considerably reduce the capital costs. In 1995, De Pauli and Trasatti [24] prepared mixed oxide layers of SnO_2 and IrO_2 which were

Chapter 8: Water Electrolysis: A brief literature review & Electrocatalytic activity of Pd-based electrocatalysts towards hydrogen evolution reaction (HER)

187

electrochemically characterized in a liquid acidic regime. They found that with only 10% Ir, the surface of the SnO_2 was almost fully saturated with Ir.

Currently, Kunta et al. successfully identifies nanostructured fluorine doped IrO_2 thin film (IrO_2:F) as a promising anode electrocatalyst with the ability to significantly improve the electrocatalytic performance and electrochemical stability [25]. It has been reported [26-28] that mixed oxides obtained by the addition of cheaper oxides such as SnO_2, Ta_2O_5, Nb_2O_5, TiO_2 to active electrocatalyst IrO_2 and/or RuO_2 (e.g. IrO_2–SnO_2, RuO_2–SnO_2, IrO_2–Ta_2O_5, IrO_2–SnO_2–Nb_2O_5 etc.) would reduce the cost of the noble metal loading while maintaining the catalytic activity and electronic conductivity similar to the pure noble metal oxide and improve the corrosion property of noble metal oxide electrocatalysts. The IrO_2-Ta_2O_5 system is one of the most promising catalysts in different electrochemical industries where O_2 evolution is the main anodic reaction. Ta_2O_5 is mixed with IrO_2 mainly to improve the service life of the latter, which is the active catalyst and most expensive component [29].

Comparison with base SnO_2 and binary SnO_2 + IrO_2 materials evidences the superior properties of the ternary mixtures and the key role of tantalum (even at low molar fraction) expanding the surface area, improving the electronic conductivity, increasing the charge storage capacitance and promoting the surface enrichment of iridium [30].

Chapter 8: Water Electrolysis: A brief literature review & Electrocatalytic activity of Pd-based electrocatalysts towards hydrogen evolution reaction (HER)

188

8.3 Electrocatalytic activity of Pd-based electrocatalysts towards hydrogen evolution reaction (HER)

8.3.1 Introduction

Platinum-based catalysts are effective and stable for both hydrogen oxidation reaction (HOR) and hydrogen evolution reaction (HER) under acidic conditions as it is found in a polymer electrolyte fuel cell or electrolyzer. While platinum is the most extensively used noble metal for catalysis at different areas, its high price is a major restriction factor on its utility as an electrocatalyst [31]. Much effort has been devoted to minimize the Pt loading and to achieve optimum performance [32-37].

Palladium (Pd), which resembles Pt in many respects, seems to be the most obvious substitute for Pt as HER catalyst due to its excellent catalytic capabilities and a relatively abundant resource [38]. Palladium and its alloys are classical materials that received significant interest in the recent years [39] due to their superior catalytic performance towards various chemical and electrochemical reactions such as catalysis, hydrogen storage [40] and sensors [41]. Pd-based alloys, on the other hand, offer a class of attractive materials for studying metal hydrides because of the high solubility and permeability of hydrogen compared to pure Pd as well as the reduced cost if cheaper metals are added [42]. Surface modification and alloying are applicable for improvement of electrocatalytic performance of Pd catalysts towards HER [43, 44]. Pd alloying with other metals could change the electronic structure (electronic effect), crystal lattice dimensions (geometric effect), and elastic properties of pure Pd. Pd based has already been widely used as the catalyst for HER in alkaline media [45-48], but in acid media there are few reports.

Chapter 8: Water Electrolysis: A brief literature review & Electrocatalytic activity of Pd-based electrocatalysts towards hydrogen evolution reaction (HER)

189

In this paper, the electrocatalytic activity of different PdRh and PdIr nanostructures prepared via a modified pulse-microwave assisted polyol method, was studied toward hydrogen evolution reaction in acid solution and compared with pure Pd. The electrochemical and catalytic behaviors were investigated using cyclic voltammetry (CV), linear sweep voltammetry (LSV) and electrochemical impedance spectroscopy (EIS).

8.3.2 Electrocatalysts preparation

The examined electrocatalysts were quickly and easily prepared via a modified pulse-microwave assisted polyol synthesis. In a beaker, the starting precursors ($PdCl_2 \cdot 2H_2O$ and $RhCl_3$ provided by Strem Chemicals) were well mixed with ethylene glycol (EG) in an ultrasonic bath, and then XC-72R carbon black (Cabot Corporation) was added in the above mixture. After the adjustment of system's pH value to 13, by the drop-wise addition of 1.0 M NaOH/EG, a well-dispersed slurry was obtained with ultrasonic stirring for 60 min. Thereafter, the slurry was microwave-heated in the pulse form 10 s on/10 s off for several times. In order to promote the adsorption of the suspended metal nanoparticles onto the carbon support, hydrochloric acid was adopted as the sedimentation promoter and the solution was re-acidified to a pH value of about 2–4. The resulting black solid sample was filtered, washed and dried at 80°C for 10 h in a vacuum oven [49]. For the sake of comparison 20 wt% Pd/Vulcan XC-72, 20wt% Rh/Vulcan XC-72 and 20wt% Ir/Vulcan XC-72 was similarly prepared.

The thin catalyst film was deposited onto a glassy carbon disk surface with a diameter of 3.0 mm. More precisely, a mixture containing 1.95 mg electrocatalyst, 1.8 mL ethanol and 0.2 mL Nafion solution (5 wt. %, Dupont Company) was ultrasonicated for 40 min to obtain a well-dispersed ink. The catalyst ink was then quantitatively (4 μL) transferred onto the surface of the glassy carbon electrode and dried under infrared lamp to obtain a catalyst thin film.

Chapter 8: Water Electrolysis: A brief literature review & Electrocatalytic activity of Pd-based electrocatalysts towards hydrogen evolution reaction (HER)

190

8.3.3 Physicochemical measurements

All of the prepared electrodes were analyzed by XRD and the resultant diffraction patterns were shown in Fig. 8.4.
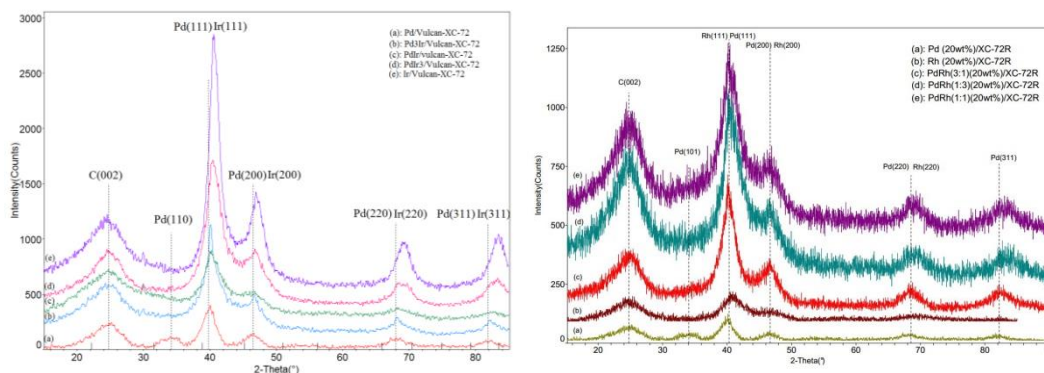
Figure 8.4: The XRD patterns of (A) Pd_xIr_y, (B) Pd_xRh_y catalysts

In Fig. 8.4 the XRD patterns of the as prepared Pd, Ir, Rh, Pd_xIr_y and Pd_xRh_y catalysts are schematically presented. As it can be seen except the characteristic peak of Vulcan XC-72 at 24.5°, the 2θ values of four more peaks at 40.07°, 46.53°, 68.19° and 82.02°, that correspond to face-centered cubic (fcc) crystalline Pd (1 1 0), (1 1 1), (2 0 0), (2 2 0) and (3 1 1), respectively are shown. The highest intensity of peak from (1 1 1) plane indicates that this is the most exposed face of the Pd_xIr_y/C nanoparticles. The peak position from (1 1 1) plane of Pd_xIr_y/C binary electrocatalysts is between the Pd/C and Ir/Cs' peaks position. In addition, no characteristic peaks related to Ir were observed, further supporting that Pd-Ir alloy has been formed via insertion of Ir into Pd lattice. Moreover, it is observed that the peaks of the Pd planes in the binary Pd_xIr_y/C catalysts are higher and sharper than that of the Pd and the Pd(1 1 0) has been disappeared, indicating the formation of alloy. Table 8.2 lists the crystallite sizes and the corresponding lattice parameters calculated using the Scherrer formula and Bragg equations, respectively [50]. All the examined catalysts have almost the same crystallite size (~3.5-4.0nm).

Chapter 8: Water Electrolysis: A brief literature review & Electrocatalytic activity of Pd-based electrocatalysts towards hydrogen evolution reaction (HER)

191

Furthermore, the insertion of iridium to palladium seems to contract the crystal, since the internal distance of the Pd_xIr_y binary electrocatalysts is smaller than pure Pd's.

Table 8.2: Physicochemical analysis results.

Electrode (20%wt metal loading)	Lattice Parameter (nm)	Crystallite Size (nm)	Particles Size (nm)
Pd	0.38615	3.0	4.3±0.3
Rh/C	0.38456	2.0	3.3±0.3
PdRh(3:1)	0.38794	~3.0	4.8±0.3
PdRh(1:1)	0.38474	3.5	4.4±0.3
PdRh(1:3)	0.38516	2.0	3.5±0.3
Ir	0.38448	3.5	5.7±0.3
PdIr(3:1)	0.38843	3.5	4.5±0.3
PdIr(1:1)	0.38810	3.0	4.4±0.3
PdIr(1:3)	0.38503	4.0	5.3±0.3

The (1 1 1), plane has the largest intensity among the others planes, which grows with respect to the corresponding peak of the Pd and Rh catalysts, indicating the effect of increased amounts of Rh in the Pd_xRh_y. As it can be seen from Table 8.2, Pd/C has the highest lattice parameter (0.38615 nm) and crystallite size (3.0 nm), while the Rh/C the lowest one (lattice parameter: 0.38456 nm, crystallite size: 2.0 nm). The formed Pd-Rh alloys seem to present lattice parameter values between of the two pure metals, with the following order: PdRh(3:1)/C > PdRh(1:3)/C >PdRh(1:1)/C. Thus, the addition of Rh contracts the lattice parameter of Pd, decreasing its crystallite size.

TEM images with the respective particle size distribution histogram of Pd/C, Rh/C and Pd_xRh_y catalysts are shown in Fig. 8.5. A remarkably uniform and high dispersion of metal particles on the carbon surface is observed concerning all the examined samples. As it can also be seen (Table 8.2), the mean particle size was in the following order: Pd_3Rh (4.8±0.3nm) > PdRh (4.4±0.3nm) > Pd (4.3±0.3) > $PdRh_3$ (3.5±0.3nm) > Rh (3.3±0.3).

Chapter 8: Water Electrolysis: A brief literature review & Electrocatalytic activity of Pd-based electrocatalysts towards hydrogen evolution reaction (HER)

192
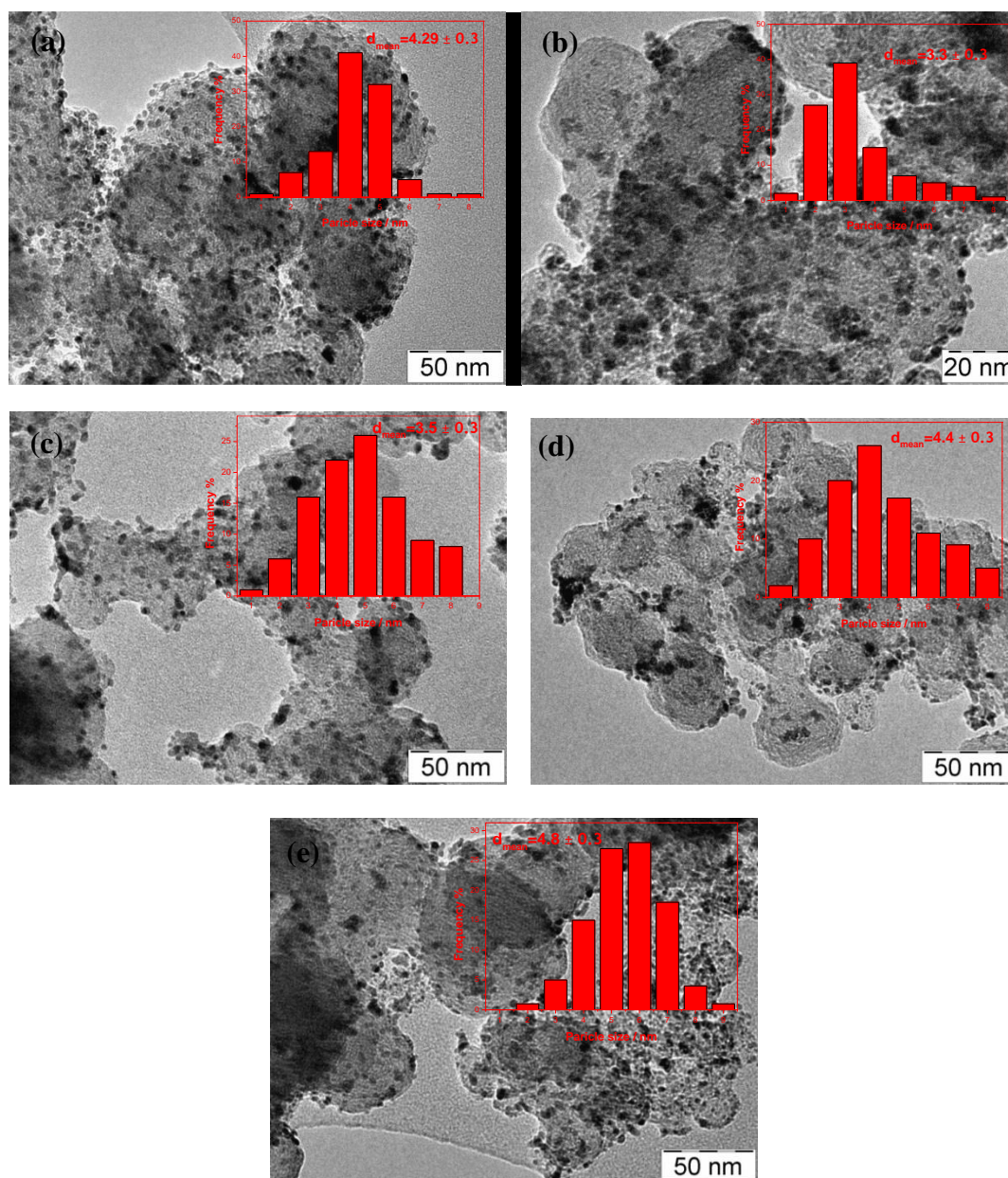
Figure 8.5: TEM images of (a) Pd, (b) Rh, (c) PdRh₃, (d) PdRh, (e)Pd₃Rh

From Fig.8.6 it can be observed that, for Pd, Pd_3Ir and PdIr the metallic nanoparticles are homogenously dispersed on the carbon support with narrow size distribution in the supported catalyst. Ir and $PdIr_3$ have non-spherical morphologies and some larger aggregates were observed, but the amount of particles is few. One hundred particles were randomly measured to obtain the particle size distribution.

Chapter 8: Water Electrolysis: A brief literature review & Electrocatalytic activity of Pd-based electrocatalysts towards hydrogen evolution reaction (HER)

193
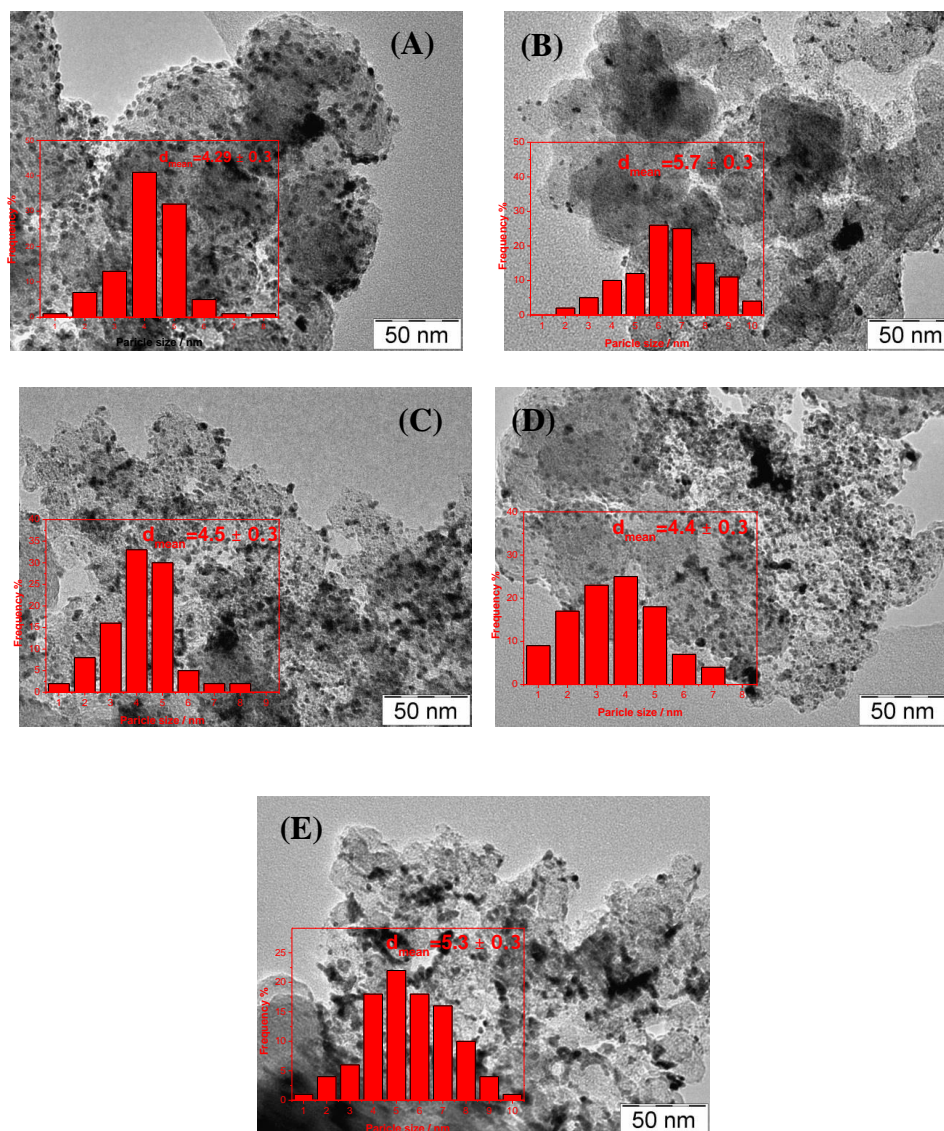
Figure 8.6: TEM images and corresponding of (A) Pd/ Vulcan XC-72, (B) Ir/Vulcan XC-72, (C) Pd₃Ir/Vulcan XC-72, (D) PdIr/Vulcan XC-72, (E) PdIr₃/Vulcan XC-72

8.3.4 Electrochemical characterization

All electrodes were characterized by cyclic voltammetry (CV) tests. CV curves were recorded in the potential range of -400 to +800 mV in Helium purged electrolyte (Fig.1). In the cathodic scan, as the high current caused by hydrogen absorption dominates and covers the adsorption processes [51]. In the anodic scan, a broad peak due to the desorption of hydrogen appears between -300 and 0.0mV on the Pd alloys electrodes.

Chapter 8: Water Electrolysis: A brief literature review & Electrocatalytic activity of Pd-based electrocatalysts towards hydrogen evolution reaction (HER)

194

When the Ir, Rh content of the alloy was increased from (3:1) to (1:3) the integrated peak intensity for the hydrogen desorption/oxidation (i.e. the discharge) significantly increased.
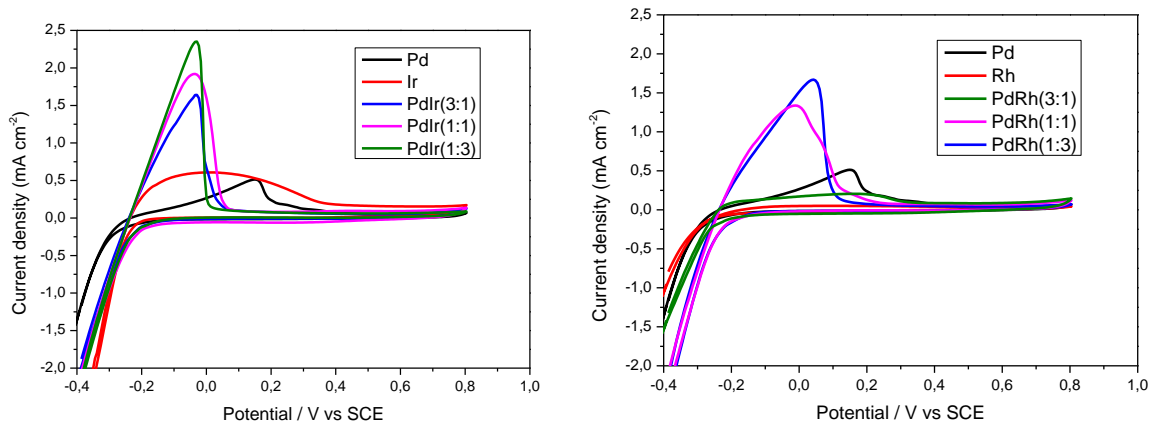
Figure 8.7: Cyclic voltammograms recorded for different compositions in 0.5M H$_2$SO$_4$ solution at a scan rate of 50 mV s^{-1}.

For pure Pd the amount of hydrogen desorption decreased. A similar behavior was observed for the desorption of hydrogen of Ir, appeared between -300 and 400 mV which is also decreased and for Rh which is no hydrogen desorption and absorption. For HER in acidic media, there are three major pathways reported in literature. These include the Volmer (electrochemical hydrogen adsorption) mechanism where hydronium ion (H$_3$O$^+$) is reduced to an adsorbed hydrogen atom atom H (ads) Eq. (10) (which later generates molecular hydrogen gas). The Heyrovsky mechanism (electrochemical hydrogen desorption) in which the hydronium is reduced along with adsorbed hydrogen atoms to generate molecular hydrogen directly Eq. (11) and the Tafel mechanism (chemical desorption) in which adsorbed atoms (already reduced) form molecular hydrogen Eq. (12) [52]:

$$H_3O^+ + e^- \rightarrow H_{ads} + H_2O \tag{8.9}$$

$$H_{ads} + H_3O^+ + e^- \rightarrow H_2 + H_2O \tag{8.10}$$

$$H_{ads} + H_{ads} \rightarrow H_2 \tag{8.11}$$

The linear potential sweep curves for HER are illustrated in Figure 8.8. This is a systematic and effective method to investigate the electrochemical activity of

Chapter 8: Water Electrolysis: A brief literature review & Electrocatalytic activity of Pd-based electrocatalysts towards hydrogen evolution reaction (HER)

195

electrocatalysts [53]. These curves were recorded from 0.2 to -0.8 Vs. SCE at sweep rate of 1mV s^{-1} in 0.5M H$_2$SO$_4$. In the linear potential sweep curves, the cathodic peak current that appears from -0.2 V is due to the reduction of adsorbed hydrogen which is then followed by absorption and hydrogen evolution currents [54]. It should be noted that at a higher scan rate (50 mV s^{-1}) absorption current dominates and overlaps with the adsorption current [51] (Figure 8.5). However, at the scan rate of 1 mV s^{-1} the adsorption peak was separated because absorption current was not so high to cover the adsorption current.
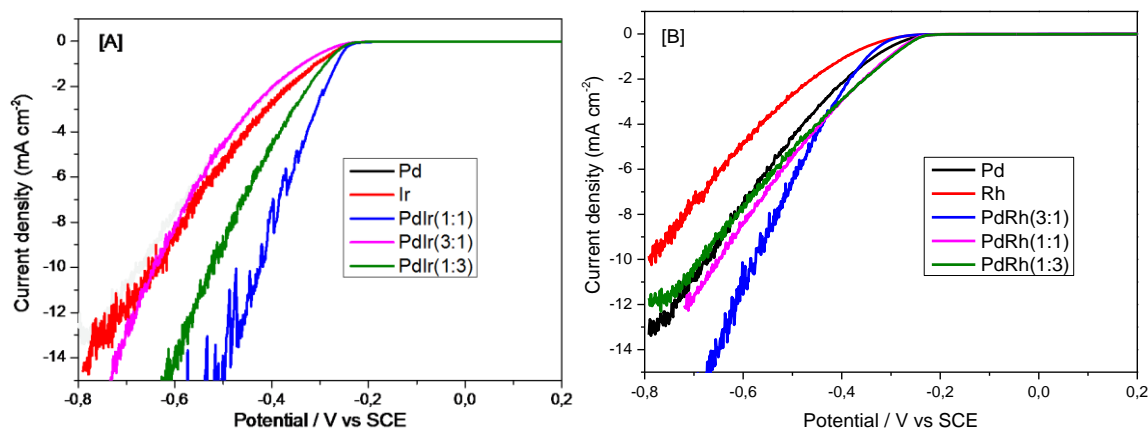
Figure 8.8: Linear potential sweep curves recorded for different compositions in 0.5M H$_2$SO$_4$ solution at a scan rate of 1 mV s^{-1}.

As clearly represented in Figure 8.6A the Pd nanoparticles are more inactive towards the HER and the Ir nanoparticles show a higher HER activity than the Pd nanoparticles. When PdIr alloys are used, the overpotential for the HER shifts to the more positive values than when pure Pd is present. The overpotential for the HER for the PdIr (1:1) shifts to the more positive values compared to all other cases and exhibits the best HER performance. Ir is active toward the HER and needs overpotential of 640 mV to afford current density of 10 mA cm^{-2}. However, the extent of the positive shift was decreased with increasing the Ir content to PdIr(1:3). Similar processes were observed for current of adsorption peak for Rh (Figure 8.8B). Rh nanoparticles are more inactive than Pd towards the HER, however PdRh alloys shifts to more positive values than pure Pd and pure Rh.

Chapter 8: Water Electrolysis: A brief literature review & Electrocatalytic activity of Pd-based electrocatalysts towards hydrogen evolution reaction (HER)

196

In all cases of PdRh alloys need overpotential of 440mV to afford current density of 4 mA cm^{-2}. These results indicate that the presence of both Ir and Rh improves the electrocatalytic activity of the Pd nanoparticles towards the HER.

Fundamental understanding of these special activities is still not well established. Nevertheless, it is believed that the change of the lattice constant and electronic structure of Pd with the addition of Ir or Rh, improves the electrocatalytic activity of Pd nanoparticles towards hydrogen adsorption [54].

In order to investigate the electrocatalytic activity of the prepared catalytic coatings, Tafel linear polarization measurements were made, and the corresponding electrochemical parameters (Tafel slope, transfer coefficient, exchange current density) were derived from the recorded curves [55]. Fig. 8.9 shows the Tafel curves recorded in 0.5M H$_2$SO$_4$ on all the coatings investigated and the calculated kinetic parameters for the HER are listed in Table 8.3.
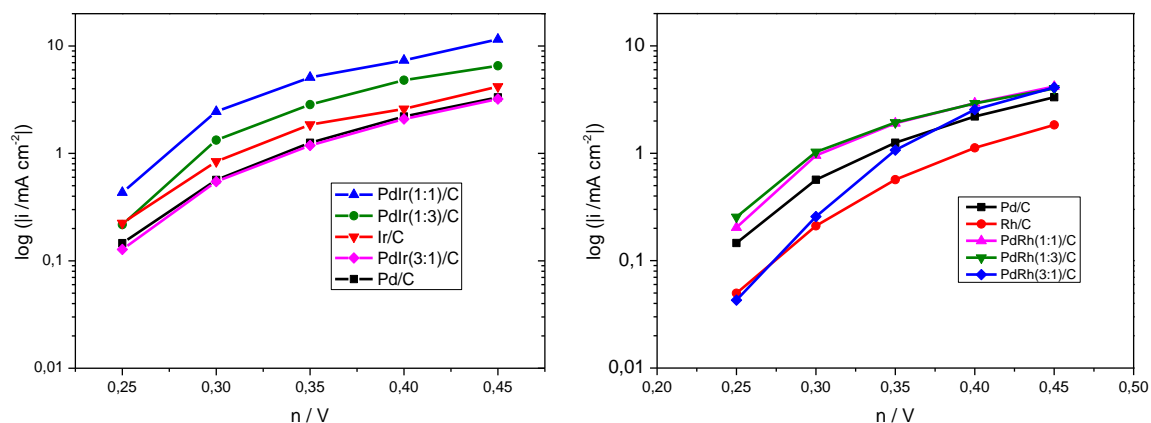
Figure 8.9: Tafel plots for HER

The inherent measure of activity for the HER is the Tafel slope and a lower Tafel slope implies fast kinetics. The Tafel curve recorded on Fig. 8.9 described using the Tafel equation:

$$\log(i) = \log(i_0) + \left(\frac{anF}{2.303RT} \right) n \qquad \textbf{(8.12)}$$

Chapter 8: Water Electrolysis: A brief literature review & Electrocatalytic activity of Pd-based electrocatalysts towards hydrogen evolution reaction (HER)

197

where η(V) represents the applied overpotential, i (A cm^{-2}) the resulting (measured) current, F the Faraday constant (95485 C/mol), R is the gas constant (8.31451 J mol^{-1} K^{-1}), 1-α the cathodic transfer coefficient [56] and the exchange current density i_o (A cm^{-2}) from the intersection point of Tafel plots with the abscissa (log i_o).

The transfer coefficient 1−α was calculated using the Butler-Volmer equation for the limiting case of high overpotential, from the Tafel slope b. According to the Butler − Volmer equation, a low charge transfer coefficient 1−α is unfavorable for HER kinetics, but as it will be seen below this effect may be offset and exceeded by the consistent increase of the exchange current density i_o. The geometrical interpretation of the transfer coefficient led to the idea that 1-a represents a measure of the activated complex coordinate in the electric field of the metal-solution interface.

L.A. Khanova and L.I. Krishtalik have proved that on gold, in sulphuric acid solution, Tafel plots present two distinct slopes. The smaller, obtained at low overpotential, corresponds to the HER controlled by desorption of the hydrogen atoms, while the larger one is due to the mechanism in which the charge transfer is slow step of the cathodic process [57]. Therefore, in order to determine kinetic parameters that characterize the charge transfer, Tafel slopes were plotted for a limiting domain of high overpotentials.

The observed Tafel slopes for different Pd$_x$Ir$_y$ and Pd$_x$Rh$_y$ electrodes are ranging from 97 to 209 mV/dec (Table 1). The estimated Tafel slopes are more than the expected theoretical value for the HER with the Volmer step (120 mV/dec) as the rate determing step (rds) except the Rh catalyst [58]. It should be noticed that obtained Tafel slopes are higher in comparison with theoretical value, probably due to the fact that electrode surface is covered with thin film of oxides, which causes additional potential drop [59].

Chapter 8: Water Electrolysis: A brief literature review & Electrocatalytic activity of Pd-based electrocatalysts towards hydrogen evolution reaction (HER)

198

Table 8.3: Kinetic analysis results for hydrogen evolution reaction

Electrode (20%wt metal loading)	Tafel slope b (mV decade^{-1})	i_o (mA cm^{-2})	1-a
Pd/C	148.0	0.01	0.58
PdIr(3:1)/C	173.0	0.01	0.60
PdIr(1:1)/C	209.0	0.10	0.68
PdIr(1:3)/C	179.0	0.03	0.60
Ir/C	163.0	0.02	0.56
PdRh(3:1)/C	148.0	0.01	0.58
PdRh(1:1)/C	179.0	0.03	0.60
PdRh(1:3)/C	201.0	0.05	0.66
Rh/C	97.0	0.005	0.42

8.3.5 Electrochemical impedance analysis

In order to investigate the effect of reduction treatment, we carried out electrochemical impedance spectroscopy (EIS) in 0.5M H_2SO_4. The electrochemical impedance spectroscopy (EIS) is a powerful technique to study the electrode/electrolyte interface and frequently employed to investigate the HER. Nyquist plots (Z ″ imaginary versus Z ′ real part of the impedance), measured at an overpotential of −250 mV on the PdRh and PdIr electrodes are shown in Fig. 8.10. Two semicircles were observed in Nyquist for most of the catalysts in Figure 8.10A, B.

The semicircle at high frequencies is attributed to the hydrogen adsorption on the electrode surface (hydrogen adsorption resistance - R_{ad}) while the second semicircle at low frequencies represents the HER kinetic (charge transfer process) [58]. Fig. 8.10C, presents the equivalent circuit compatible with the experimental impedance measurements. In this electrical equivalent circuit Rs is the solution resistance, Rct and Rad are the charge transfer resistance for HER and hydrogen adsorption resistance. CPE is constant phase element. The electrical parameters provided are presented in Table 8.4.

Chapter 8: Water Electrolysis: A brief literature review & Electrocatalytic activity of Pd-based electrocatalysts towards hydrogen evolution reaction (HER)

199
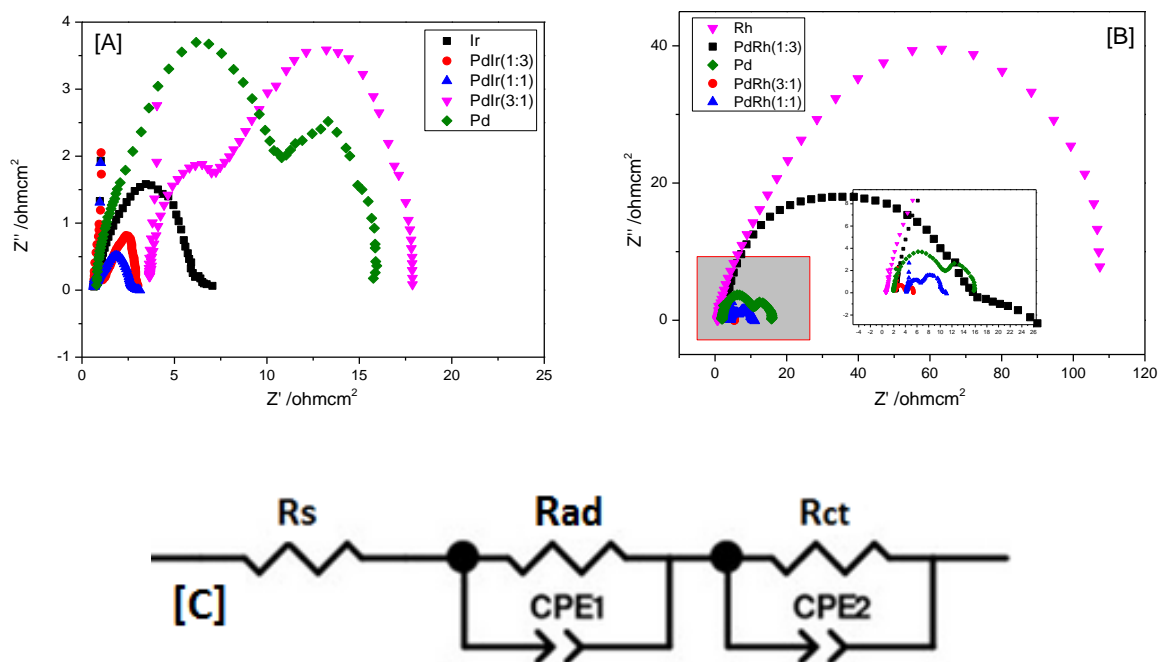
Figure 8.10: Nyquist plots for different alloys at 0.35 V in 0.5M H_2SO_4.

The constant phase elements (CPE) in the scheme represent the capacitances due to hydrogen adsorption and charge transfer processes. The electrical parameters provided by CNLS fitting are presented in Table 8.4. It can be seen that for both PdIr and PdRh alloys hydrogen adsorption resistance (R_{ad}) decreased with increasing the Ir and Rh content, respectively.

Table 8.4: Equivalent circuit parameters obtained by fitting EIS experimental data for Pd_xRh_y and Pd_xIr_y alloys.

Electrode (20%wt metal loading)	R_s (Ohm cm^{-2})	R_{ct} (Ohm cm^{-2})	R_{ad} (Ohm cm^{-2})	CPE$_1$	CPE$_2$
Pd	2.4	5	8.6	0.00080	0.0318
PdIr(3:1)	4.0	10.9	3.0	0.00046	0.0231
PdIr(1:1)	1.0	0.3	1.7	0.26601	33.4901
PdIr(1:3)	4.0	1.4	0.2	0.01431	0.22693
Ir	1.0	2.4	1.2		
PdRh(3:1)	2.7	1.8	0.8		
PdRh(1:1)	4.6	4.3	2.1	0.00370	0.0586
PdRh(1:3)	2.9	27.5	1.2	0.00035	0.2797
Rh	1.0	105.8	0.6	0.00362	0.4560

Chapter 8: Water Electrolysis: A brief literature review & Electrocatalytic activity of Pd-based electrocatalysts towards hydrogen evolution reaction (HER)

200

8.4 Conclusion

The results show that the incorporation of Rh and Ir in Pd, improve the electrocatalytic behavior of pure palladium. The linear polarization curves obtained in diluted sulfuric acid solution have shown a marked depolarization for the HER in the increased addition of Ir and Rh content of the alloy. These results were ascribed to a catalytic effect of Rh and Ir content in Pd on the HER. The catalytic effect of the examined electrocatalysts on HER was compared using the kinetic parameters that characterize the electrode process. Exchange current density i_o and charge transfer coefficient 1–α were determined by the Tafel slope method. Among the different tested compositions of PdRh and PdIr, PdIr (1:1) and PdRh(1:3) showed the best electrocatalytic behavior toward HER.

The electrochemical impedance data confirmed the catalytic effect of incorporation of Rh and Ir in Pd on the HER, as indicated by the decrease of the charge transfer resistance. The lowest charge transfer resistances have been obtained for PdIr(1:1), which are in good agreement with the highest values of the exchange current densities. Analyzing the values of the exchange current density it can be concluded, that addition of Ir enhances noticeably the electrocatalytic activity of Pd, towards HER. More precisely, toward HER following the order: PdRh3 ≈ PdRh > Rh > Pd3Rh > Pd exhibiting for the case of PdIr exchange current density 0.65mA cm^{-2}.

Based on the results obtained in this study we considered that PdIr codeposits is promising electrocatalyst for hydrogen generation which is a prerequisite for further investigation as cathodes in PEM.

Chapter 8: Water Electrolysis: A brief literature review & Electrocatalytic activity of Pd-based electrocatalysts towards hydrogen evolution reaction (HER)

201

References

[1]   M. Ni, D.Y.C. Leung, M.K.H. Leung. International Journal of Hydrogen Energy 32 (2007) 3238-3247.

[2]   J.R. Rostrup-Nielsen, J. Sehested, J.K. Nørskov, Advances in Catalysis, Academic Press, 2002, pp. 65-139.

[3]   C.-J. Winter. International Journal of Hydrogen Energy 34 (2009) S1-S52.

[4]   F. Barbir. Solar Energy 78 (2005) 661-669.

[5]   P. Millet, N. Mbemba, S.A. Grigoriev, V.N. Fateev, A. Aukauloo, C. Etiévant. International Journal of Hydrogen Energy 36 (2011) 4134-4142.

[6]   M. Carmo, D.L. Fritz, J. Mergel, D. Stolten. International Journal of Hydrogen Energy 38 (2013) 4901-4934.

[7]   S.A. Grigoriev, V.I. Porembsky, V.N. Fateev. International Journal of Hydrogen Energy 31 (2006) 171-175.

[8]   O. Pantani, E. Anxolabéhère-Mallart, A. Aukauloo, P. Millet. Electrochemistry Communications 9 (2007) 54-58.

[9]   J. Lipkowski, P. N.Ross, Electrocatalysis, Wiley- VCH, Canada, 1998.

[10]   C.C. Văduva, N. Vaszilcsin, A. Kellenberger, M. Medeleanu. International Journal of Hydrogen Energy 36 (2011) 6994-7001.

[11]   J. Cheng, H. Zhang, H. Ma, H. Zhong, Y. Zou. Electrochimica Acta 55 (2010) 1855-1861.

[12]   J.B. Raoof, R. Ojani, S.A. Esfeden, S.R. Nadimi. International Journal of Hydrogen Energy 35 (2010) 3937-3944.

[13]   S. Trasatti. Journal of Electroanalytical Chemistry and Interfacial Electrochemistry 39 (1972) 163-184.

[14]   D. Pletcher, R.S.o. Chemistry, A First Course in Electrode Processes, Royal Society of Chemistry, 2009.

[15]   R. Eisenberg, H.B. Gray. Inorganic Chemistry 47 (2008) 1697-1699.

[16]   F. Liu, J.J. Concepcion, J.W. Jurss, T. Cardolaccia, J.L. Templeton, T.J. Meyer. Inorganic Chemistry 47 (2008) 1727-1752.

[17]   M.V. ten Kortenaar, J.F. Vente, D.J.W. Ijdo, S. Müller, R. Kötz. Journal of Power Sources 56 (1995) 51-60.

[18]   S. Gottesfeld, S. Srinivasan. Journal of Electroanalytical Chemistry 86 (1978) 89-104.

Chapter 8: Water Electrolysis: A brief literature review & Electrocatalytic activity of Pd-based electrocatalysts towards hydrogen evolution reaction (HER)

202

[19]   M. Musiani. Chemical Communications (1996) 2403-2404.

[20]   S. Chen, T. Zhai, X.H. Lu, M.Z. Zhang, Z.Y. Li, C.W. Xu, Y. Tong. International Journal of Hydrogen Energy 37 (2012) 13350-13354.

[21]   L. Trotochaud, J.K. Ranney, K.N. Williams, S.W. Boettcher. Journal of the American Chemical Society 134 (2012) 17253-17261.

[22]   L. Trotochaud, S.L. Young, J.K. Ranney, S.W. Boettcher. Journal of the American Chemical Society 136 (2014) 6744-6753.

[23]   S. Trasatti. Electrochimica Acta 29 (1984) 1503-1512.

[24]   C.P. De Pauli, S. Trasatti. Journal of Electroanalytical Chemistry 396 (1995) 161-168.

[25]   K. Kadakia, M.K. Datta, P.H. Jampani, S.K. Park, P.N. Kumta. Journal of Power Sources 222 (2013) 313-317.

[26]   E. Mayousse, F. Maillard, F. Fouda-Onana, O. Sicardy, N. Guillet. International Journal of Hydrogen Energy 36 (2011) 10474-10481.

[27]   A. Marshall, B. Børresen, G. Hagen, M. Tsypkin, R. Tunold. Electrochimica Acta 51 (2006) 3161-3167.

[28]   K. Kadakia, M.K. Datta, O.I. Velikokhatnyi, P. Jampani, S.K. Park, P. Saha, J.A. Poston, A. Manivannan, P.N. Kumta. International Journal of Hydrogen Energy 37 (2012) 3001-3013.

[29]   R. Otogawa, M. Morimitsu, M. Matsunaga. Electrochimica Acta 44 (1998) 1509-1513.

[30]   S. Ardizzone, C.L. Bianchi, G. Cappelletti, M. Ionita, A. Minguzzi, S. Rondinini, A. Vertova. Journal of Electroanalytical Chemistry 589 (2006) 160-166.

[31]   Y.-X. Huang, X.-W. Liu, X.-F. Sun, G.-P. Sheng, Y.-Y. Zhang, G.-M. Yan, S.-G. Wang, A.-W. Xu, H.-Q. Yu. International Journal of Hydrogen Energy 36 (2011) 2773-2776.

[32]   P. Los, A. Rami, A. Lasia. Journal of Applied Electrochemistry 23 (1993) 135-140.

[33]   Q. Han, K. Liu, J. Chen, X. Wei. International Journal of Hydrogen Energy 28 (2003) 1207-1212.

[34]   Y.M. Wu, W.S. Li, X.M. Long, F.H. Wu, H.Y. Chen, J.H. Yan, C.R. Zhang. Journal of Power Sources 144 (2005) 338-345.

[35]   S.M.A. Shibli, V.S. Dilimon. International Journal of Hydrogen Energy 32 (2007) 1694-1700.

Chapter 8: Water Electrolysis: A brief literature review & Electrocatalytic activity of Pd-based electrocatalysts towards hydrogen evolution reaction (HER)

203

[36]   F. Rosalbino, G. Borzone, E. Angelini, R. Raggio. Electrochimica Acta 48 (2003) 3939-3944.

[37]   M. Wu, P.K. Shen, Z. Wei, S. Song, M. Nie. Journal of Power Sources 166 (2007) 310-316.

[38]   A.N. Simonov, P.A. Pyrjaev, P.A. Simonov, B.L. Moroz, S.V. Cherepanova, D.A. Zyuzin, V.I. Bukhtiyarov, V.N. Parmon. Journal of Molecular Catalysis A: Chemical 353–354 (2012) 204-214.

[39]   D.-j. Guo, H.-l. Li. Electrochemistry Communications 6 (2004) 999-1003.

[40]   H.-P. Liang, N.S. Lawrence, L.-J. Wan, L. Jiang, W.-G. Song, T.G.J. Jones. The Journal of Physical Chemistry C 112 (2007) 338-344.

[41]   P. Zhou, Z. Dai, M. Fang, X. Huang, J. Bao, J. Gong. The Journal of Physical Chemistry C 111 (2007) 12609-12616.

[42]   A. Safavi, E. Farjami. Journal of Molecular Catalysis A: Chemical 350 (2011) 91-96.

[43]   M. Shao. Journal of Power Sources 196 (2011) 2433-2444.

[44]   F. Al-Odail, A. Anastasopoulos, B. Hayden. Top Catal 54 (2011) 77-82.

[45]   T. Green, D. Britz. Journal of Electroanalytical Chemistry 412 (1996) 59-66.

[46]   M. Smiljanić, I. Srejić, B. Grgur, Z. Rakočević, S. Štrbac. Electrochimica Acta 88 (2013) 589-596.

[47]   J.J. Podestá, R.C.V. Piatti, A.J. Arvia. International Journal of Hydrogen Energy 20 (1995) 111-122.

[48]   N. Tateishi, K. Yahikozawa, K. Nishimura, Y. Takasu. Electrochimica Acta 37 (1992) 2427-2432.

[49]   S. Song, J. Liu, J. Shi, H. Liu, V. Maragou, Y. Wang, P. Tsiakaras. Applied Catalysis B: Environmental 103 (2011) 287-293.

[50]   V. Radmilovic, H.A. Gasteiger, P.N. Ross. Journal of Catalysis 154 (1995) 98-106.

[51]   S. Chen, B.D. Adams, A. Chen. Electrochimica Acta 56 (2010) 61-67.

[52]   X. Cao, Y. Han, C. Gao, Y. Xu, X. Huang, M. Willander, N. Wang. Nano Energy 9 (2014) 301-308.

[53]   L.A. Kibler. ChemPhysChem 7 (2006) 985-991.

[54]   M. Łukaszewski, K. Klimek, A. Żurowski, T. Kędra, A. Czerwiński. Solid State Ionics 190 (2011) 18-24.

Chapter 8: Water Electrolysis: A brief literature review & Electrocatalytic activity of Pd-based electrocatalysts towards hydrogen evolution reaction (HER)

204

[55]   E. Navarro-Flores, Z. Chong, S. Omanovic. Journal of Molecular Catalysis A: Chemical 226 (2005) 179-197.

[56]   H.H. Bauer. Journal of Electroanalytical Chemistry 16 (1968) 419-432.

[57]   L.A. Khanova, L.I. Krishtalik. Journal of Electroanalytical Chemistry 660 (2011) 224-229.

[58]   A. Safavi, S.H. Kazemi, H. Kazemi. Fuel 118 (2014) 156-162.

[59]   B. Baranowski, S. Zaginaichenko, D. Schur, V. Skorokhod, A. Veziroglu, Carbon Nanomaterials in Clean Energy Hydrogen Systems, Springer, 2008.

Chapter 8: Water Electrolysis: A brief literature review & Electrocatalytic activity of Pd-based electrocatalysts towards hydrogen evolution reaction (HER)

205

Conclusions and Future Work

This very last part summarizes the results of the research done in the framework of the present PhD dissertation. At the same time some outlooks for further continuation of this research are provided.

Fuel cells, which directly convert a fuel's chemical energy into electricity by electrochemical reactions, are a key enabling technology for the transition to a hydrogen-based economy. Of several different types under development, a polymer electrolyte fuel cell (PEMFC) is generally recognized as a future power source for zero-emission vehicles. To become commercially viable, however, PEFCs must address several technological and economic challenges. The high cost of catalysts due to the exclusive use of platinum and platinum-based catalysts in fuel cell electrodes is one such challenge.

With the exception of Pt, it has been demonstrated that among pure metals, Pd exhibits relatively high electrocatalytic activity towards both HOR and ORR. Preparation method is also a very important parameter for catalysts' preparation as it affects their properties (lattice parameter, diameter of nanoparticles, catalysts dispersion on the support). In the present PhD dissertation was chosen a modified microwave assisted polyol method.

The metal content in the catalysts is a very important parameter for comparing their activity. Consequently, carbon-supported (Vulcan XC-72) Pd, Rh, and Pd_xRh_y (20wt.%, x:y=1:1, 3:1, 1:3) electrocatalysts are prepared according a modified pulse-microwave

assisted polyol synthesis method and their electrocatalytic activity towards *hydrogen electrooxidation* (HOR) and *oxygen reduction* (ORR) reactions is investigated. Physicochemical characterizations were carried out with the XRD and TEM measurements. When a second metal is adopted with palladium a further decrease in the particle size of the catalysts could give higher activity, and this part of work is under investigation. In general the mean particle size such as extracted from XRD and TEM results of the prepared electrocatalysts is ~3nm. Furthermore, according to the electrochemical results the addition of Rh can increase the activity of Pd towards hydrogen oxidation and oxygen reduction in acid medium with $PdRh_3$/C to exhibit the highest activity. Finally, by chronoamperometric measurements, it was found rhodium hinders pure palladium from leaching, giving higher stability to Pd's electrocatalyst.

The results for the Pd_xIr_y (with x:y atomic ratios 3:1, 1:1, 1:3) showed that the optimum for hydrogen electrooxidation exhibited for PdIr and for oxygen reduction for Pd_3Ir. HOR electrocatalytic activity of Pd-Ir alloy electrodes showed volcano type dependence on exchange current density, and the dependence on alloy composition revealed the principal role of the electronic effect of Ir–Pd alloys in HOR and ORR. The results imply that the high activity of the Pd_xIr_y catalysts in HOR and ORR, relies heavily on the electronic structure of Ir, which is made favorable by Pd spontaneously adsorbed hydrogen gas in the electrocatalytic process. More important and from a practical perspective, we showed that it is possible to design electrocatalysts that does not contain platinum but can surpass the activity of pure platinum.

The study of $Pd_{97}Pt_3$/C, $Pd_{98}Pt_2$/C, $Pd_{99}Pt_1$/C and pure Pd/C for the hydrogen oxidation (HOR) with the rotating electrode technique showed a volcano-type dependence on Pd loading with the exchange current density following the order: $Pd_{98}Pt_2$/C (2.2 mA cm^{-2}) >$Pd_{97}Pt_3$/C(1.3mA cm^{-2})>$Pd_{99}Pt_1$/C(1.16 mA cm^{-2})>Pd/C (0.62 mA cm^{-2}). Among the

examined electrocatalysts $Pd_{98}Pt_2/C$ and $Pd_{97}Pt_3/C$ are tested in a single hydrogen proton exchange membrane fuel cell as anodes electrodes using commercial Pt/C as cathode electrode. The single cell polarization experiments were carried out at different working temperatures of 30, 40, 50, 60, 70 and 80°C at an atmospheric pressure. The total Pt loading was only 657 μg_{Pt} cm^{-2}. Increasing the temperature value from 30° to 70°C, the power density increased from 75 to 98 mW cm^{-2}. However, further temperature increment to 80°C had a negative effect on fuel cell performance, decreasing the power density at *ca.* 75 mWcm^{-2}.

The water electrolysis is one of the large-scale industrial methods for hydrogen production. The hydrogen evolution reaction (HER) is the main reaction in the water electrolysis and has been widely studied on various metals, alloys and oxide films. The objective of the present work is to bring down the high materials' cost of the electrolysis system using different compositions of Pd based catalysts. The results demonstrated that the incorporation of Rh and Ir in Pd towards the HER improves the electrocatalytic behavior of pure palladium. Among the different tested compositions of PdRh and PdIr, PdIr (1:1) showed the best electrocatalytic behavior toward HER.

The results of the present study have been published in refereed journals and international conferences, providing some more information about hydrogen electrooxidation reaction in acid media over Pd-based electrocatalysts. The recognition of some efficient anode and cathode electrocatalysts which constitutes the first step of design and development of a fuel cell has been accomplished. However, the following issues must be taken into account in the future: i) optimization of the preparation method for forming nanoparticles with lower diameter, for hydrogen PEM fuel cells.